Forschungszentrum Karlsruhe
in der Helmholtz-Gemeinschaft

Wissenschaftliche Berichte
FZKA 6890

Contributions to the 28th International Cosmic Ray Conference, Tsukuba, Japan, 2003 by Forschungszentrum Karlsruhe, Institut für Kernphysik, Institut für Prozessdatenverarbeitung und Elektronik and Universität Karlsruhe, Institut für Experimentelle Kernphysik

J. Blümer, R. Engel, A. Haungs (Editors)

Institut für Kernphysik

September 2003

Forschungszentrum Karlsruhe

in der Helmholtz-Gemeinschaft

Wissenschaftliche Berichte

FZKA 6890

Contributions to the 28th International Cosmic Ray Conference, Tsukuba, Japan, 2003

by

Forschungszentrum Karlsruhe,

Institut für Kernphysik,

Institut für Prozessdatenverarbeitung und Elektronik

and

Universität Karlsruhe,

Institut für Experimentelle Kernphysik

Johannes Blümer, Ralph Engel, Andreas Haungs (Editors)

Institut für Kernphysik

Forschungszentrum Karlsruhe GmbH, Karlsruhe

2003

Impressum der Print-Ausgabe:

Als Manuskript gedruckt

Forschungszentrum Karlsruhe GmbH
Postfach 3640, 76021 Karlsruhe

Mitglied der Hermann von Helmholtz-Gemeinschaft
Deutscher Forschungszentren (HGF)

ISSN 0947-8620

ABSTRACT

This volume is a compilation of the contributions of the Forschungszentrum Karlsruhe, Institut für Kernphysik and Karlsruhe University, Institut für Experimentelle Kernphysik to the biannual International Cosmic Ray Conference 2003 (ICRC 2003). It gives an up-to-date summary of the corresponding scientific activities of the aforementioned institutes, focussing on two experiments, **KASCADE-Grande** and the **Pierre Auger Observatory**, the physics of air showers and their simulation using CORSIKA, and cosmic ray phenomenology. Many of the contributions are the product of close collaboration with other national (e.g. Siegen, Wuppertal, Bonn) and international (e.g. from Poland, Italy, Romania, Russia, Great Britain, US) universities and institutes.

KASCADE (**KA**rlsruhe **S**hower **C**ore and **A**rray **De**tector) is a multi-detector set-up on the site of the Forschungszentrum Karlsruhe. The different detector systems allow the reconstruction of a large set of observables for each single event that can be used as redundant information for the analyses. The main aim of the experiment is the determination of the primary energy spectrum and mass composition of cosmic rays in the knee region, i.e. at primary energies of 100 TeV - 100 PeV. The results establish the fact that the knee is dominated by light primaries, whereas the flux of heavy primaries shows no kink in the investigated energy region. The extension of KASCADE to **KASCADE-Grande** for measurements of cosmic rays in the energy region of 100 PeV to 1 EeV is completed now. Results of recent analyses of KASCADE data and an overview of the capabilities of the extended detector set-up are given.

The **Pierre Auger Observatory** is presently being set-up in Argentina's Mendoza Province. It will consist of a 3000 km^2 array of water Cherenkov tanks and fluorescence detectors. The Auger experiment is designed to measure cosmic rays of ultra-high energies above 10 EeV to investigate the energy spectrum, type and origin of these elusive particles. The Karlsruhe research groups are mainly involved in the construction of components of the fluorescence detectors, including their electronics. Reports of the first data taken during a test run are given and underline the unique capabilities of the Auger observatory. Many contributions discuss data analysis aspects ranging from the reconstruction of lateral shower profiles over fluorescence signal calculations to various treatments of the air Cherenkov light background.

Recent additions and improvements of the **CORSIKA** (**CO**smic **R**ay **Si**mulation for **K**ascade and **A**uger) simulation package are reported, in particular investigations of the extrapolation of the interaction models to energies and phase space regions beyond the reach of accelerators and the tests of its validity. Other articles discuss the development of new simulation techniques, called hybrid simulations, combining analytical with Monte Carlo methods. Hybrid techniques allow a much faster simulation of extensive air showers, which is of importance mainly for the simulation of very high primary energies.

In addition to the collaboration works of the KASCADE-Grande and Auger groups the many individual cosmic ray related contributions are also included in this volume. They cover a wide range, including first measurements of radio emission in high-energy air showers at KASCADE-Grande, results of experiments concerning cosmic rays of lower energies (CAPRICE, TRACER), and simulation studies for the atmospheric neutrino problem.

Beiträge zur 28th International Cosmic Ray Conference (ICRC), Tsukuba, Japan, 2003
des Forschungszentrums Karlsruhe, Institut für Kernphysik
und Institut für Prozessdatenverarbeitung und Elektronik,
und der Universität Karlsruhe, Institut für experimentelle Kernphysik

ZUSAMMENFASSUNG

Der vorliegende Bericht fasst Beiträge zur zweijährlich stattfindenden internationalen Konferenz zur kosmischen Strahlung (ICRC 2003) zusammen, die von den herausgebenden Instituten des Forschungszentrums und der Universität Karlsruhe in enger Zusammenarbeit mit weiteren nationalen (z.B. Siegen, Wuppertal, Bonn) und internationalen (z. B. aus Polen, Italien, Rumänien, Russland, Armenien, Großbritannien, USA) Universitäten und Instituten entstanden sind. Die wissenschaftlichen Aktivitäten konzentrieren sich dabei auf den instrumentellen Status und die physikalischen Möglichkeiten der neuen Luftschauer-Experimente **KASCADE-Grande** und **Pierre-Auger-Projekt,** sowie Ergebnisse aus Analysen der Daten von **KASCADE** und Weiterentwicklungen des Luftschauer-Simulationsprogrammes **CORSIKA**. Ergänzt wird der Bericht durch eine ganze Reihe von weiteren Beiträgen zu relevanten Themenbereichen.

KASCADE (**KA**rlsruhe **S**hower **C**ore and **A**rray **De**tector) ist ein Multi-Detektor Aufbau auf dem Gelände des Forschungszentrums Karlsruhe. Die unterschiedlichen Detektorsysteme erlauben die Rekonstruktion einer großen Anzahl von Observablen pro Ereignis. Das Hauptziel des Experimentes ist die Bestimmung des primären Energiespektrums und der Elementzusammensetzung der kosmischen Strahlung im Energiebereich des ‚Knie' (100 TeV – 100 PeV). Die Ergebnisse beweisen nun, dass das Knie durch die leichte primäre Komponente dominiert wird und das Spektrum der schweren Teilchen kein Knie im untersuchten Energiebereich aufweist. Die Erweiterung des KASCADE-Experiments zu **KASCADE-Grande,** um die kosmische Strahlung im Energiebereich von 100 PeV bis 1 EeV zu messen, ist nun abgeschlossen; über die Kapazitäten des Aufbaus wird berichtet.

Das **Pierre-Auger-Observatorium** wird momentan in Argentinien aufgebaut und besteht aus einem 3000 km^2 großen Array aus Wasser-Cherenkov-Tanks und Fluoreszenzdetektoren. Das Auger-Experiment wird Herkunft und Typ der höchstenergetischsten kosmischen Teilchen über 10 EeV messen. Die Karlsruher Forschungsgruppen leisten einen signifikanten Anteil an der Konstruktion und der Elektronik der Fluoreszenzteleskope. Die Beiträge in diesem Bericht widmen sich ersten Daten-Analysen beider Detektorkomponenten sowie Untersuchungen zur Fluoreszens- und Cherenkov-Lichterzeugung in der Luftschauerentwicklung.

Über Erweiterungen und Verbesserungen des **CORSIKA** (**CO**smic **R**ay **Si**mulation for **K**ascade and **A**uger) Programms wird berichtet. Speziell die Extrapolation der Physik der hadronischen Wechselwirkungen zu höchsten Energien und ihr Test ist relevant für die Auswertung der Luftschauerdaten. Berichtet wird auch über Neuentwicklungen auf dem Gebiet von Simulationsprogrammen, sogenannten Hybrid-Programmen, die durch Verbindung von analytischen und Monte-Carlo-Methoden eine wesentlich schnellere Simulation der Luftschauerentwicklung ermöglichen, was vor allem bei hohen Primärenergien an Bedeutung gewinnt.

Zusätzlich zu den kollaborativen Arbeiten an den KASCADE-Grande und Auger Experimenten werden relevante Themen zur kosmischen Strahlung diskutiert. Dies beinhaltet sowohl erste Messungen von Radioemission in hochenergetischen Luftschauern bei KASCADE-Grande, als auch Ergebnisse und Simulationsstudien von Experimenten zur kosmischen Strahlung niedererer Energien (CAPRICE, TRACER) und Simulationsstudien zum atmosphärischen Neutrino Problem.

CONTENTS

The KASCADE-Grande Experiment

A. Haungs[2], T. Antoni[1], W.D. Apel[2], F. Badea[1,a], K. Bekk[2], A. Bercuci[2,a], M. Bertaina[3], H. Blümer[1,2], H. Bozdog[2], I.M. Brancus[4], M. Brüggemann[5], P. Buchholz[5], C. Büttner[1], A. Chiavassa[3], P. Doll[2], R. Engel[2], J. Engler[2], F. Feßler[2], P.L. Ghia[6], H.J. Gils[2], R. Glasstetter[7], D. Heck[2], J.R. Hörandel[1], A. Iwan[8], K-H. Kampert[7], H.O. Klages[2], Y. Kolotaev[5], G. Maier[2], H.J. Mathes[2], H.J. Mayer[2], J. Milke[2], C. Morello[6], M. Müller[2], G. Navarra[3], R. Obenland[2], J. Oehlschläger[2], S. Ostapchenko[1,c], M. Petcu[4], S. Plewnia[2], H. Rebel[2], M. Roth[1], H. Schieler[2], J. Scholz[2], T. Thouw[2], G.C. Trinchero[6], H. Ulrich[2], S. Valchierotti[3], J. van Buren[2], W. Walkowiak[5], A. Weindl[2], J. Wochele[2], J. Zabierowski[8], S. Zagromski[2]

(1) Institut für Exp. Kernphysik, Universität Karlsruhe, 76021 Karlsruhe, Germany
(2) Institut für Kernphysik, Forschungszentrum Karlsruhe, 76021 Karlsruhe, Germany
(3) Dipartimento di Fisica Generale dell'Università, 10125 Torino, Italy
(4) National Institute of Physics and Nuclear Engineering, 7690 Bucharest, Romania
(5) Fachbereich Physik, Universität Siegen, 57068 Siegen, Germany
(6) Instituto di Fisica dello Spazio Interplanetario, CNR, 10133 Torino, Italy
(7) Fachbereich Physik, Universität Wuppertal, 42097 Wuppertal, Germany
(8) Soltan Institute for Nuclear Studies, 90950 Lodz, Poland
[a] *on leave of absence from (4)*
[b] *on leave of absence from Moscow State University, 119899 Moscow, Russia*

Abstract

A scintillator array (Grande) of large collecting area (700m x 700m) has been set up at Forschungszentrum Karlsruhe in Germany to operate jointly with the existing KASCADE multi-detector experiment. The enlarged EAS experiment provides comprehensive observations of cosmic rays in the primary energy range of 0.1 PeV to 1 EeV, i.e. a full coverage of the primary energy region around the knee. Status and capabilities of the KASCADE-Grande experiment are presented.

1. Introduction

The major goal of KASCADE-Grande is the observation of the 'iron-knee' in the cosmic-ray spectrum at around 100 PeV (Fig. 1), which is expected following recent KASCADE observations where the positions of the knees of individual mass groups suggest a rigidity dependence (Roth, Ulrich et al. [8]). The reconstruction of the energy spectra of various mass groups over the large energy range accessible with KASCADE-Grande will provide a comprehensive picture of the physics around the knee. Additionally, the validity of hadronic interaction mod-

pp. 1–4

els used in CORSIKA Monte Carlo simulations of ultra-high energy air showers will be tested with KASCADE-Grande. Investigations of radio emission in high-energy air showers will be performed with a further upgrade of the experimental set-up by installing an array of broad-band antennas provided by the LOPES collaboration [7].

2. The Set-Up

The existing multi-detector experiment KASCADE [1], which takes data since 1996, was recently extended to KASCADE-Grande by installing a large array of 37 stations consisting of $10\,\mathrm{m}^2$ scintillation detectors each, with an average spacing of 137 m. The scintillators were taken from the former EAS-TOP experiment. The stations comprise 16 photo-multipliers each providing a high dynamic range from 1/3 to 30000 charged particles per station for the reconstruction of particle densities and timing measurements. The signals are amplified and shaped inside the Grande stations, and after transmission to a central DAQ station digitalized in peak sensitive ADCs (Chiavassa et al. [3]).
Parallel to the standard DAQ the Grande array will be equipped with FADCs and a continuous data sampling using a ring-buffer system to store the full history of energy deposit at the stations, improving significantly the energy and time measurements.
KASCADE-Grande provides an effective area of more than $0.5\,\mathrm{km}^2$ and operates jointly with the existing KASCADE detectors. Grande is electronically subdivided in 18 hexagons of 6 outer and one central station. Grande is readout and jointly analyzed with KASCADE for showers fulfilling at least one 7-fold coincidence in a hexagonal cluster. The joint measurements are ensured by an additional cluster (Piccolo) close to the center of KASCADE-Grande for trigger purposes. Piccolo consists of $8 \times 10\,\mathrm{m}^2$ stations equipped with plastic scintillators. The trigger conditions at Piccolo can be chosen as a double multiplicity trigger ($> n$ of 8 huts and $> m$ of 48 electronic channels). The expected trigger efficiency for Piccolo with $n = 2, m = 4$ is shown in Fig. 4. The efficiency is calculated by Monte Carlo simulations for the acceptance region shown as circle in Fig. 3.
While the Grande detectors are sensitive to charged particles, the original KASCADE detectors measure the electromagnetic component, the muonic and the hadronic components separately. The 252 KASCADE stations covering an area of $200 \times 200\,\mathrm{m}^2$ consist of unshielded liquid scintillators above shielded plastic scintillators [1]. This enables to reconstruct the lateral distributions of muons and electrons separately on an event-by-event basis. Further muon detector systems at an underground tunnel and at the Central Detector of KASCADE allow to investigate the muon component of EAS at four different threshold energies. A liquid ionisation hadron calorimeter with more than 44000 electronic channels in 9 layers reconstructs the hadronic core of air showers.

Table 1. Compilation of the KASCADE-Grande detector components.

Detector	Particles	sensitive area [m^2]
Grande	charged	370
Piccolo	charged	80
KASCADE array e/γ	electrons	490
KASCADE array μ	muons ($E_\mu^{\rm thresh} = 230\,{\rm MeV}$)	622
MTD	muons ($E_\mu^{\rm thresh} = 800\,{\rm MeV}$)	3×128
Trigger Plane	muons ($E_\mu^{\rm thresh} = 490\,{\rm MeV}$)	208
MWPCs/LSTs	muons ($E_\mu^{\rm thresh} = 2.4\,{\rm GeV}$)	3×129
Calorimeter	hadrons ($E_h^{\rm thresh} = 10 - 20\,{\rm GeV}$)	9×304

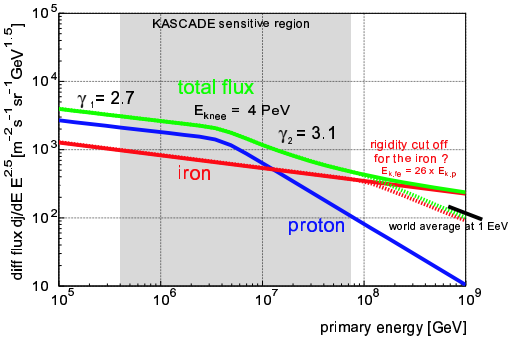

Fig. 1. Motivation for the extension of KASCADE to KASCADE-Grande: Is there also a knee at the spectrum of EAS induced by heavy primaries?

Fig. 2. Antennas for the measurement of radio emission in air showers are set-up at the KASCADE experiment.

Recently first 10 antennas with a large bandwidth (40-80 MHz) for the detection of radio emission in air showers were installed at the KASCADE site (see Fig. 2). Together with the LOPES collaboration KASCADE-Grande is calibrating the amount of the radio emission in high-energy air showers.

3. Capabilities of KASCADE-Grande

Like in KASCADE the concept of KASCADE-Grande is the measurement of as many as possible observables of air showers to perform multi-parameter analyses to disentangle the three-fold problem of determining the primary energy and mass reconstruction and the understanding of hadronic interaction mechanisms in the atmosphere.

Basic shower observables like the core position, angle-of-incidence, or total number of charged particles will be provided by the Grande stations. A core position resolution of $\approx 15\,{\rm m}$ and an angle resolution of $\approx 0.5^\circ$ will be reached by the present set-up. The estimation of energy and mass of the primary particles will be based on a combined investigation of the charged particle, electron and muon components measured by the detector arrays of Grande and KASCADE (Glasstet-

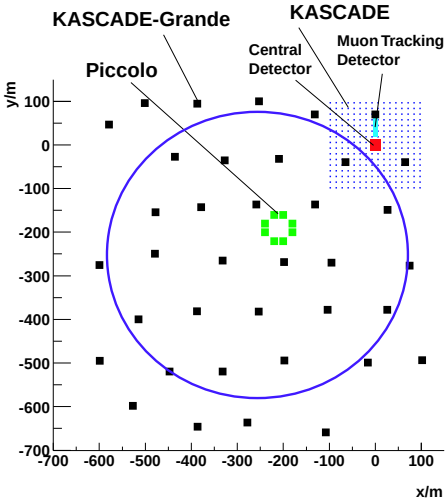

Fig. 3. Layout of the multi-detector experiment KASCADE-Grande.

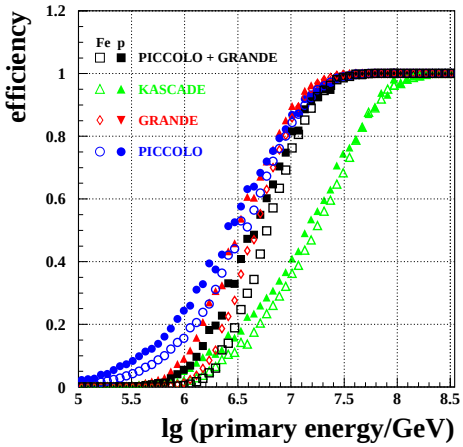

Fig. 4. Simulated trigger efficiency for different trigger sources of KASCADE-Grande for showers inside the area of a circle as shown at Fig. 3.

ter et al. [4]). A common fit to the energy deposits with the relative muon to electron ratio as additional free parameter enables a resolution of electron and muon numbers in the order of 15% and 25%, respectively, for primary energies of 100 PeV.

Additional sensitivity for composition estimates and interaction model tests is provided by muon density measurements at different muon energy thresholds (Haungs et al. [5]), by muon arrival time measurements (Brancus et al. [2]), by the analysis of muon angles-of-incidences (Zabierowski et al. [9]), and by measurements of the hadronic shower core (e.g. Iwan et al. [6]).

Acknowledgment: The authors are indebted to the members of the engineering and technical staff of the KASCADE-Grande collaboration, who contribute with enthusiasm and engagement to the experiment. KASCADE-Grande is supported by the Ministry for Research and Education of the Federal Republic of Germany, the INFN and the Ministero per l'Universita e la Ricerca of Italy, the Polish State Committee for Scientific Research and the Romanian National Academy for Science, Research and Technology.

References

1. Antoni T. et al. - KASCADE Coll. 2003, submitted to Nucl.Instr.Meth. A
2. Brancus I.M. et al. 2003 Proc.28th ICRC, Tsukuba, these proceedings
3. Chiavassa A. et al. 2003 Proc.28th ICRC, Tsukuba, these proceedings
4. Glasstetter R. et al. 2003 Proc.28th ICRC, Tsukuba, these proceedings
5. Haungs A. et al. 2003 Proc.28th ICRC, Tsukuba, these proceedings
6. Iwan A. et al. 2003 Proc.28th ICRC, Tsukuba, these proceedings
7. LOPES collaboration 2003 http://www.mpifr-bonn.mpg.de/staff/hfalcke/LOPES/
8. Roth M., Ulrich H. et al. 2003 Proc.28th ICRC, Tsukuba, these proceedings
9. Zabierowski J. et al. 2003 Proc.28th ICRC, Tsukuba, these proceedings

KASCADE-Grande: the Grande Array

A. Chiavassa[3], T. Antoni[1], W.D. Apel[2], F. Badea[1,a], K. Bekk[2], A. Bercuci[2,a], M. Bertaina[3], H. Blümer[1,2], H. Bozdog[2], I.M. Brancus[4], M. Brüggemann[5], P. Buchholz[5], C. Büttner[1], P. Doll[2], R. Engel[2], J. Engler[2], F. Feßler[2], P.L. Ghia[6], H.J. Gils[2], R. Glasstetter[7], A. Haungs[2], D. Heck[2], J.R. Hörandel[1], A. Iwan[8], K-H. Kampert[7], H.O. Klages[2], Y. Kolotaev[5], G. Maier[2], H.J. Mathes[2], H.J. Mayer[2], J. Milke[2], C. Morello[6], M. Müller[2], G. Navarra[3], R. Obenland[2], J. Oehlschläger[2], S. Ostapchenko[1,c], M. Petcu[4], S. Plewnia[2], H. Rebel[2], M. Roth[1], V. Scherini[9], H. Schieler[2], J. Scholz[2], T. Thouw[2], G.C. Trinchero[6], H. Ulrich[2], S. Valchierotti[3], J. van Buren[2], W. Walkowiak[5], A. Weindl[2], J. Wochele[2], J. Zabierowski[8], S. Zagromski[2]

(1) Institut für Exp. Kernphysik, Universität Karlsruhe, 76021 Karlsruhe, Germany

(2) Institut für Kernphysik, Forschungszentrum Karlsruhe, 76021 Karlsruhe, Germany

(3) Dipartimento di Fisica Generale dell'Università, 10125 Torino, Italy

(4) National Institute of Physics and Nuclear Engineering, 7690 Bucharest, Romania

(5) Fachbereich Physik, Universität Siegen, 57068 Siegen, Germany

(6) Instituto di Fisica dello Spazio Interplanetario, CNR, 10133 Torino, Italy

(7) Fachbereich Physik, Universität Wuppertal, 42097 Wuppertal, Germany

(8) Soltan Institute for Nuclear Studies, 90950 Lodz, Poland

(9) Sciences and Advanced Technologies Department A. Avogadro University, Alessandria, Italy

[a] *on leave of absence from (4)*

[b] *on leave of absence from Moscow State University, 119899 Moscow, Russia*

The KASCADE-Grande experiment is starting data taking at Forschungszentrum Karlsruhe, Germany, with the aim of extending the energy range of KASCADE up to $E_0 \sim 10^{18}$ eV. The new experiment is based on the KASCADE facilities, and two new arrays: Grande and Piccolo, with the respective aims of realizing a large acceptance area and a compact interface triggering system. The characteristics of Grande its performances concerning the dynamic range and timing measurements are presented.

1. Introduction

The purpose of the KASCADE-Grande experiment is to investigate the range of the primary energy spectrum between 10^{16} and 10^{18} eV that, in the hypothesis of a knee occuring at constant rigidity, includes the change of slope of the iron component of primary cosmic rays. The search for this feature of the primary spectrum, the reconstruction of primary cosmic ray composition and studies of hadronic interactions at these energies are the main aims of the experiment. In this paper the status of the new arrays are described. A description of the project and of its characteristics can be found in [1]; a discussion of the reconstruction

pp. 1–4

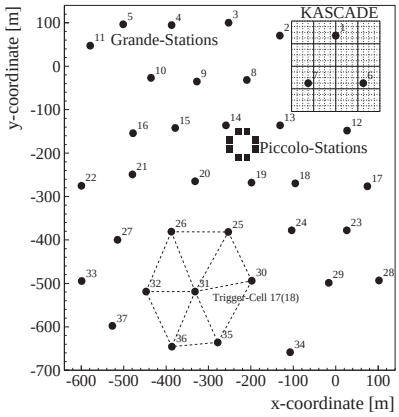

Fig. 1. Layout of the KASCADE - Grande experiment. The dashed lines show one of the cluster used for triggering the Grande array.

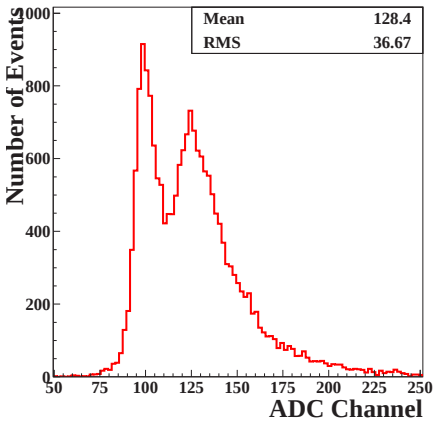

Fig. 2. Single particle spectrum measured in one of the Grande stations.

capabilities of the array is presented in [2].

2. The Grande Array

The Grande array is located at Forschungszentrum Karlsruhe around the KASCADE detectors, made of 37 stations with a mutual distance of 130 m placed in a hexagonal grid covering an area of 0.5 km^2 (figure 1). Each detector has a total surface of 10 m^2 segmented into 16 plastic scintillators 80×80 cm^2 and 4 cm thickness (from the former EAS-TOP experiment [3]). All scintillators are seen by photomultipliers (Philips XP3462, HG, High Gain, in the following) whose signals are summed and used for timing and low particle density measurements ($\sim$ 1.6 pC/m.i.p., at mixer's output). The four central ones are viewed by a second photomultiplier of the same type working at a lower gain (LG, 0.08 pC/m.i.p.), used for highest particle density measurements.

The analog signals of both the HG and LG photomultipliers are fed into two shaping amplifiers (CAEN N442). The charge integrating preamplifier has a decay time of 20 μs, its output is processed by a shaper, with peak time of 8 μs. The gains of different channels are set in order to measure from 0.3 m.i.p. up to $\sim 3 \times 10^4$ m.i.p.. This is obtained through two outputs for HG signals, 25 and 2.5 mV/pC respectively, and one for LG signals, 5 mV/pC. The three outputs are tuned to cover the following particle ranges: from 1 to $\sim$ 200 m.i.p. (*a)*), from $\sim$ 10 up to $\sim$ 2000 m.i.p. (*b)*) and from $\sim$ 200 m.i.p. up to $\sim 3 \times 10^4$ m.i.p. (*c*). The peak height is read, at the end of a 700 m long cable, through a peak ADC (CAEN V785, 12 bits, 8 V full scale).

Detector calibration is performed measuring the single particle spectrum (on ADC scale *a)*) from each station (figure 2), the ADC scales *b)* and *c)* are calibrated using run time data. Figures 3 and 4 show the correlations between ADC scale *b)* and *a)* and scale *c)* and *b)* measured in one station during a $\sim$ 60 hours long data taking. The result of this procedure, i.e. the particle number spectrum measured in one station, is shown in figure 5, which also shows the ranges where the different ADC scales overlap. The detectors m.i.p. spectrum is continuously monitored (to account for possible day-night effects a spectrum is produced every 10 hours).

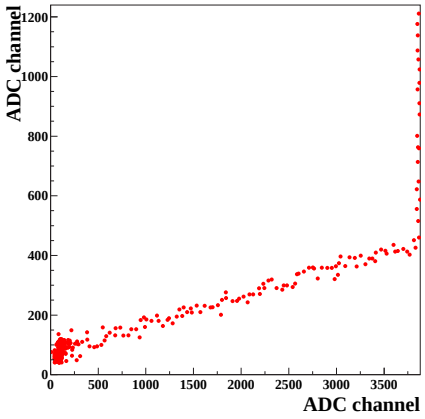

Fig. 3. Correlation of the ADC scales *b)* vs. *a)*

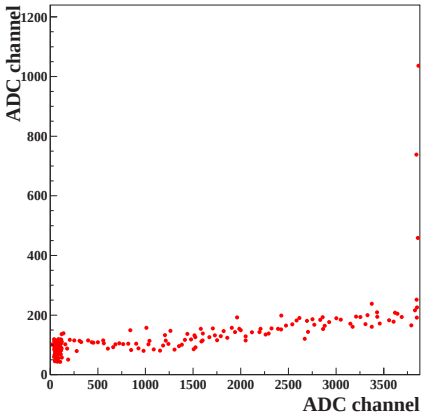

Fig. 4. Correlation of the ADC scales *c)* vs. *b)*

Timing is measured through a TDC CAEN V767 which allows to open a time window around a trigger signal provided by the OR of the 18 clusters. All firing times from all detectors inside a window of $\pm$ 5 μs around the trigger are measured. The time resolution between signals of the same channel is 300 ns. The TDC step is 0.78 ns/channel. Timing and triggering signals from stations are generated by a double threshold discriminator: the lower one is used for timing (set at $\sim$ 0.1 m.i.p.) and the higher one for triggering ($\sim$ 0.3 m.i.p.).

The Grande array is triggered by both the Piccolo array and internally. For the internal trigger the detectors are divided in clusters of hexagonal shape, with six stations surrounding a central one. The minimum trigger requirement is the fourfold coincidence of a central and three neighbouring stations in one hexagon. The array is thus divided into 18 interconnected clusters, the trigger rate is $\sim$ 5 Hz. The event rate of a sevenfold coincidence (i.e. a whole cluster) is 0.4–0.5 Hz. Figure 5 shows the distribution of the event rate as a function of the number of clusters fired. It can be noticed that there is an event every $\sim$ 10 minutes where all clusters have triggered.

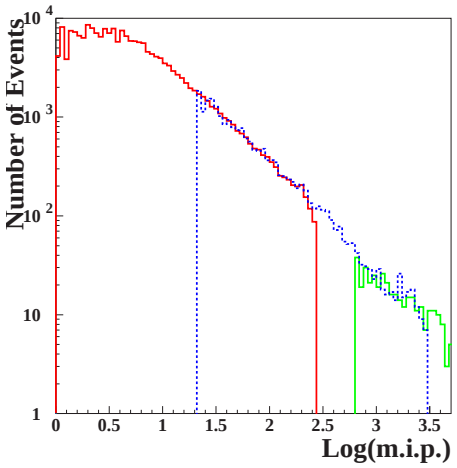

Fig. 5. Particle number spectrum measured in a 60 hours long data taking.

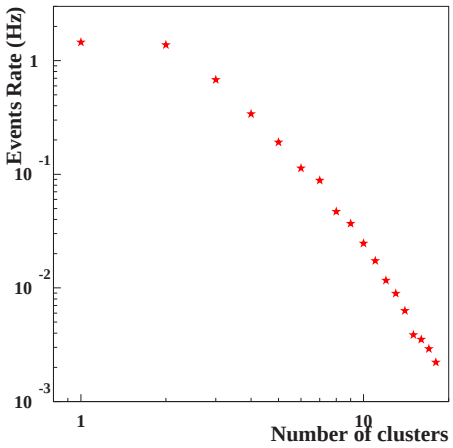

Fig. 6. Event rate vs. number of clusters triggered.

3. The Piccolo Array

Piccolo is a compact array of 8 stations on a squared grid at 25 m distance from each other. Its main task is to provide a fast external trigger to Grande and all the KASCADE detectors allowing to record coincident events with all the detectors of KASCADE-Grande. Each Piccolo station is equipped with 12 scintillator plates, 310 $\times$ 30 cm^2 organized in 6 modules, each read out by two photomultipliers. The trigger condition, optimized with Monte Carlo simulations, is the coincidence of at least 5 modules distributed in at least 4 different stations.

4. Conclusions

The status of the Grande and Piccolo arrays of the KASCADE-Grande experiment has been presented, both are ready for data acquisition and their simultaneous operation will begin in June 2003. In three years of data taking about 250 events with energy $> 10^{18}$ eV are expected.

1. Bertaina M. et al. 2001, Proc. 27^{th} ICRC (Hamburg), 792; Haungs A. et al. 2003, Proc. 28^{th} ICRC (Tsukuba), these proceedings; Kampert K.H. et al. 2003, Nucl. Phys. B (Proc. Suppl.) In Press.
2. Glasstetter R. et al. 2003, Proc. 28^{th} ICRC (Tsukuba), these proceedings.
3. Aglietta M. et al. 1988, Nucl. Instr. and Meth. A 277, 23.

Shower Reconstruction Performance of KASCADE-Grande

R. Glasstetter[7], T. Antoni[1], W.D. Apel[2], F. Badea[1,a], K. Bekk[2], A. Bercuci[2,a], M. Bertaina[3], H. Blümer[1,2], H. Bozdog[2], I.M. Brancus[4], M. Brüggemann[5], P. Buchholz[5], C. Büttner[1], A. Chiavassa[3], P. Doll[2], R. Engel[2], J. Engler[2], F. Feßler[2], P.L. Ghia[6], H.J. Gils[2], A. Haungs[2], D. Heck[2], J.R. Hörandel[1], A. Iwan[8], K-H. Kampert[7], H.O. Klages[2], Y. Kolotaev[5], G. Maier[2], H.J. Mathes[2], H.J. Mayer[2], J. Milke[2], C. Morello[6], M. Müller[2], G. Navarra[3], R. Obenland[2], J. Oehlschläger[2], S. Ostapchenko[1,c], M. Petcu[4], S. Plewnia[2], H. Rebel[2], M. Roth[1], H. Schieler[2], J. Scholz[2], T. Thouw[2], G.C. Trinchero[6], H. Ulrich[2], S. Valchierotti[3], J. van Buren[2], W. Walkowiak[5], A. Weindl[2], J. Wochele[2], J. Zabierowski[8], S. Zagromski[2]

(1) Institut für Exp. Kernphysik, Universität Karlsruhe, 76021 Karlsruhe, Germany
(2) Institut für Kernphysik, Forschungszentrum Karlsruhe, 76021 Karlsruhe, Germany
(3) Dipartimento di Fisica Generale dell'Università, 10125 Torino, Italy
(4) National Institute of Physics and Nuclear Engineering, 7690 Bucharest, Romania
(5) Fachbereich Physik, Universität Siegen, 57068 Siegen, Germany
(6) Instituto di Fisica dello Spazio Interplanetario, CNR, 10133 Torino, Italy
(7) Fachbereich Physik, Universität Wuppertal, 42097 Wuppertal, Germany
(8) Soltan Institute for Nuclear Studies, 90950 Lodz, Poland
[a] *on leave of absence from (4)*
[b] *on leave of absence from Moscow State University, 119899 Moscow, Russia*

Abstract

KASCADE-Grande extends the former KASCADE experiment by a large area scintillator array (0.5 km^2) for the detection of the charged component of extensive air showers. Its goal is to reconstruct the primary energy and composition of cosmic rays up to energies of 10^{18} eV thereby allowing a detailed investigation of the expected iron-knee. Knowing the shower core and size as well as its direction from the Grande array the KASCADE detectors allow the determination of the muon number above different energy thresholds. We present the accuracy of the shower reconstruction methods based on CORSIKA simulations. Implications to the discrimination power of the obtained parameters with respect to the nature of the primary particles will be considered.

1. Introduction

The measurement of the particles of extensive air showers (EAS) requires a surface detector spread over a large area because of the decreasing primary particle flux and a large dynamic range for the detection of the enormous density ranges of the secondary particles. Both requirements are not fulfilled with the former KASCADE experiment at the site of the Forschungzentrum Karlsruhe [2] if the primary energy exceeds ≈100 PeV. An increasing amount of the array

pp. 1–4

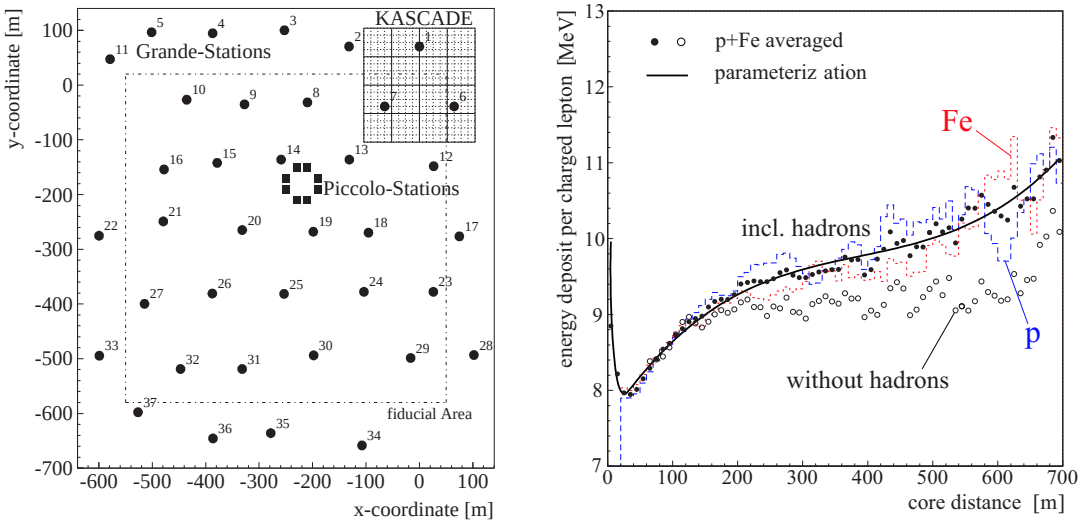

Fig. 1. Layout of the KASCADE-Grande experiment (left) and average energy deposit of an extensive air shower per Grande station (right, p+Fe, 100 PeV, 22°).

detectors shows ADC overflows which reduces the reconstruction accuracy and only a few hundred showers have been measured so far by KASCADE.

To overcome these limitations KASCADE has been extended by 37 new stations equipped with the former EAS-Top [1] scintillation detectors (Fig. 1, left). Each detector station contains a segmented 4 cm thick scintillator with a total detection area of 10 m^2. The stations are distributed over an area of 700×700 m^2 in a hexagonal grid with an average distance of 137 m (see [4, 5] for details).

2. Shower Reconstruction

The energy deposit of shower particles in a scintillation detector is dominated by ionization losses of shower electrons and muons. Therefore with a single Grande array detector it is only possible to reconstruct the combined number of these charged leptons. However, within EASs an additional contribution stems from the conversion of the shower gamma component as well as from hadrons.

To take these effects into account a so-called *Lateral Energy Correction Function* (LECF) is used which gives the average energy deposit per charged lepton at a given core distance. Such a curve has been derived from detailed GEANT3 [3] detector simulations and is plotted in Fig. 1 (right) for 100 PeV proton and iron showers with 22° zenith angle. The showers were generated with the Monte Carlo (MC) code CORSIKA (V6.014) using the QGSJET model [6]. The difference between the two primary particle types p and Fe is not significant and therefore a suitable parameterization is fitted to the average deposits.

After applying this correction to the calibrated detector signals the density distribution of the charged leptons is described by an appropriate lateral distri-

bution function (LDF) to get the core position and a first guess for the shower size. Since the NKG function used in the KASCADE reconstruction is not sufficient to describe the densities for KASCADE-Grande distances, a polynomial approximation with a scaling radius r_0 was chosen:

$$\varrho(r) = C \cdot \frac{N_{tot}}{2\pi r_0^2} \cdot 10^{\,c_1 x + c_2 x^2 + c_3 x^3} \text{ with } x = \lg \frac{r}{r_0} \tag{1}$$

The normalization parameter C and the form parameters c_i have been adjusted to average CORSIKA lateral distributions for the different particle types ($\sigma < 1\%$). Since these parameters are not independent from r_0 one has to fix the scaling radius in this step. For the charged lepton, electron, and muon LDFs the values 90 m, 70 m, and 310 m respectively are chosen in correspondence to the RMS radius of these distributions.

After the adjustment of the functional form the LDFs are fitted to single shower measurements just by varying r_0 and N_{tot} as well as the core position in a log-likelihood approach assuming Poissonian fluctuations for the particle numbers.

To deduce the shower direction the average arrival time probabilities $P_e(t)$ and $P_\mu(t)$ from CORSIKA are used to get the correct dependence of the arrival time t of the first of n particles on the total detected particle number n. This probability $P_1(t)$ can be described by:

$$P_1(t) = n \cdot P(t) \left[\int_t^\infty P(\tau) d\tau\right]^{n-1} \text{ with } P(t) = \frac{\varrho_e P_e(t) + \varrho_\mu P_\mu(t)}{\varrho_e + \varrho_\mu} \tag{2}$$

Because shower muons arrive earlier at the observation level than the electrons, this formalism offers the advantage to get an additional information on the mass of the primary particles from the arrival times. The probability density $P_1(t)$ is used directly in a log-likelihood minimization to get the shower direction. Because of its strong correlation with the detected number of particles it can even be combined with the LDF minimization which depends on the angle anyway.

After the determination of core position and shower direction the muon number is derived from the KASCADE array muon detectors by fitting the appropriate muon LDF with fixed slope parameter because of the limited radial range. Taken into account this muon LDF it is possible to use again the Grande array data (now with the electron LDF) to get the shower electron number instead of the charged lepton number.

3. First Results

Fully simulated 100 PeV proton and iron showers (22°) have been scattered over the Grande area 10 times each and tracked through the detector MC (400 showers total). Because of misreconstructed core positions a fiducial area of 600×600 m^2 around the center of the Grande array was chosen and the reconstructed electron scaling radii $r_{0,e}$ were restricted to 20 m$< r_{0,e} <$200 m. The

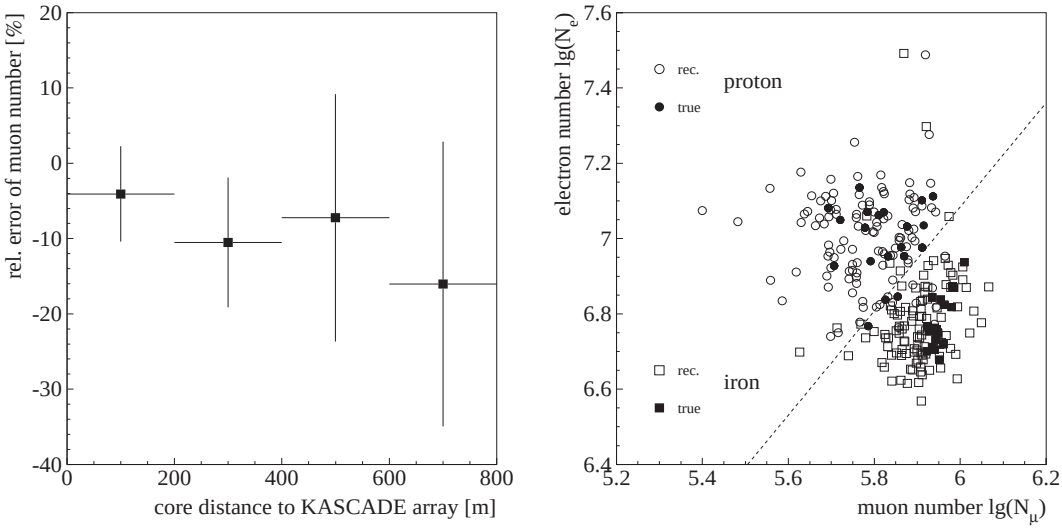

Fig. 2. Systematic (squares) and statistic (bars) errors of the muon number as function of the core distance to the KASCADE array (left) and the distribution of the reconstructed shower sizes (right) for proton resp. iron showers (100PeV, 22°).

reconstruction accuracy of the shower core position and direction has been estimated to 4 m (13 m) and 0.18° (0.32°) with 68% (95%) confidence level.

The statistical uncertainty of the shower sizes are around 15% both for the total number of electrons and muons and so in the same order of magnitude as the intrinsic shower fluctuations in that energy range. The systematic uncertainty depends strongly on the radial range of the data and the chosen LDF. Especially for the muon size both uncertainties are a function of the distance of the KASCADE array to the shower core as can be seen in Fig. 2 (left). This may be optimized by choosing either the muon number for a fixed radial range or the muon density at a fixed radius as reconstructed muon parameter.

Fig. 2 (right) shows the distribution of the reconstructed shower sizes compared to the simulated ones. It can be seen that at least the two extreme primaries proton and iron are distinguishable. The misclassification probability due to the plotted line of constant masses ($\ln A \approx \frac{\ln 56}{2}$) is below 10% for both primaries.

Acknowledgment: This work has been funded by the Ministry for Education and Research of the Federal Republic of Germany.

1. Aglietta M. et al. 1988, Nucl. Instr. & Meth., A277, 23
2. Antoni T. et al. 2003, Nucl. Instr. & Meth. A, submitted
3. Brun R. et al. 1987, CERN report DD/EE/84/1
4. Chiavassa A. et al. 2003, Proc. 28th ICRC, these proceedings
5. Haungs A. et al. 2003, Proc. 28th ICRC, these proceedings
6. Heck D. et al. 1998, Forschungszentrum Karlsruhe, Report FZKA 6019

Muon Density Measurements as Probe of the Muon Component of Air-Shower Simulations

A. Haungs[2], T. Antoni[1], W.D. Apel[2], F. Badea[1,a], K. Bekk[2], A. Bercuci[2,a], M. Bertaina[3], H. Blümer[1,2], H. Bozdog[2], I.M. Brancus[4], M. Brüggemann[5], P. Buchholz[5], C. Büttner[1], A. Chiavassa[3], P. Doll[2], R. Engel[2], J. Engler[2], F. Feßler[2], P.L. Ghia[6], H.J. Gils[2], R. Glasstetter[7], D. Heck[2], J.R. Hörandel[1], A. Iwan[8], K-H. Kampert[7], H.O. Klages[2], Y. Kolotaev[5], G. Maier[2], H.J. Mathes[2], H.J. Mayer[2], J. Milke[2], C. Morello[6], M. Müller[2], G. Navarra[3], R. Obenland[2], J. Oehlschläger[2], S. Ostapchenko[1,c], M. Petcu[4], S. Plewnia[2], H. Rebel[2], M. Roth[1], H. Schieler[2], J. Scholz[2], T. Thouw[2], G.C. Trinchero[6], H. Ulrich[2], S. Valchierotti[3], J. van Buren[2], W. Walkowiak[5], A. Weindl[2], J. Wochele[2], J. Zabierowski[8], S. Zagromski[2]

(1) Institut für Exp. Kernphysik, Universität Karlsruhe, 76021 Karlsruhe, Germany

(2) Institut für Kernphysik, Forschungszentrum Karlsruhe, 76021 Karlsruhe, Germany

(3) Dipartimento di Fisica Generale dell'Università, 10125 Torino, Italy

(4) National Institute of Physics and Nuclear Engineering, 7690 Bucharest, Romania

(5) Fachbereich Physik, Universität Siegen, 57068 Siegen, Germany

(6) Instituto di Fisica dello Spazio Interplanetario, CNR, 10133 Torino, Italy

(7) Fachbereich Physik, Universität Wuppertal, 42097 Wuppertal, Germany

(8) Soltan Institute for Nuclear Studies, 90950 Lodz, Poland

[a] *on leave of absence from (4)*

[b] *on leave of absence from Moscow State University, 119899 Moscow, Russia*

Abstract

The KASCADE experiment measures local muon densities of EAS in the knee region at various core distances for different muon energy thresholds. Expectations of detailed Monte Carlo simulations including various combinations of high-energy and low-energy hadronic interaction models in the frame of the CORSIKA code are compared with the data. This allows a comprehensive test of the simulated muon energy spectra for various Monte Carlo codes in the primary energy range of $10^{14} - 10^{16}$ eV for KASCADE and of $10^{16} - 10^{18}$ eV for KASCADE-Grande.

1. Introduction

The validity of hadronic interaction models used as generators of Monte Carlo simulations is an important subject in context of EAS analyses. A cooperation between present and future accelerator experiments and cosmic-ray investigations is aspired for tests, but also by cosmic-ray measurements there appear possibilities to probe the validity of the models [11]. In the present paper we endeavor to analyze local muon densities in high energy air-showers for two

pp. 1–4

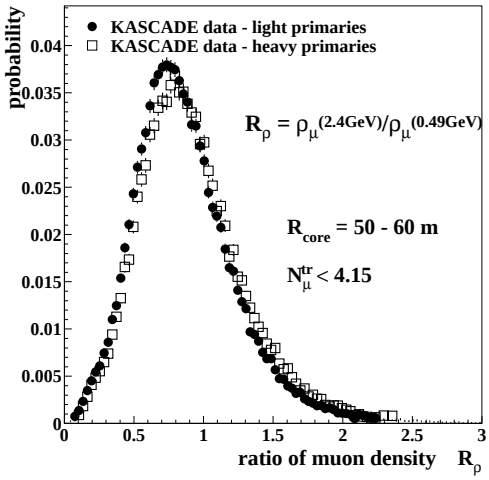

Fig. 1. Examples of the distribution of the ratio of local muon densities measured by KASCADE.

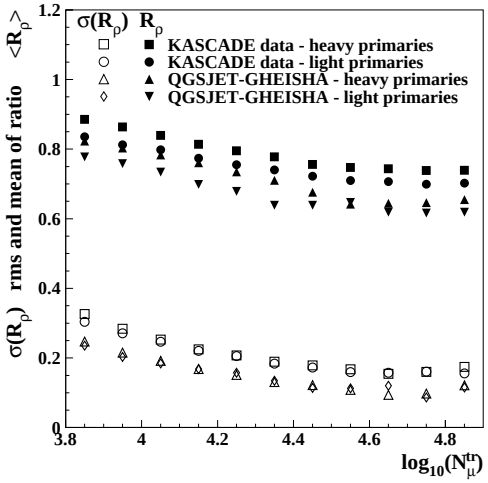

Fig. 2. Mean and width of the muon density ratio distributions vs. N_μ^{tr} for measurements and simulations.

different muon energy thresholds. Therewith the consistency of the simulations with respect to the muon energy spectrum and systematic features of different Monte Carlo models can be revealed. Analyzing KASCADE data, the local muon densities were used to reconstruct the primary energy spectrum of cosmic rays in the energy range of 1 to 10 PeV [1]. A systematic inconsistency were found by using the two different muon thresholds for transforming the measured local muon density spectrum in the primary energy spectrum with help of Monte Carlo simulation procedures. To proceed a more direct comparison between measured and simulated data with respect to the muon energy spectrum, in the present paper the ratio R_ρ of the local muon densities estimated on an event-by-event basis is used. With the extension of KASCADE to KASCADE-Grande [6] this kind of analysis can be continued and applied on data of higher primary energies, where systematic validity checks of the models are even more important, as no accelerator data will exist in next decades at energies above 100 PeV, but the models will be used for interpretations of the data of giant air-shower experiments.

2. Measurements at KASCADE

The local muon density of the EAS is measured with two separate detector set-ups of the KASCADE central detector which is placed in the geometrical center of the KASCADE detector array. A setup of 32 large multiwire proportional chambers (MWPC) is installed in the basement of the building and enables the estimation of the muon density $\rho_\mu^\star$ for each single EAS. The total absorber corresponds to a threshold for muons of 2.4 GeV. The second muon detection system is a layer of 456 plastic scintillation detectors in the third gap of the central

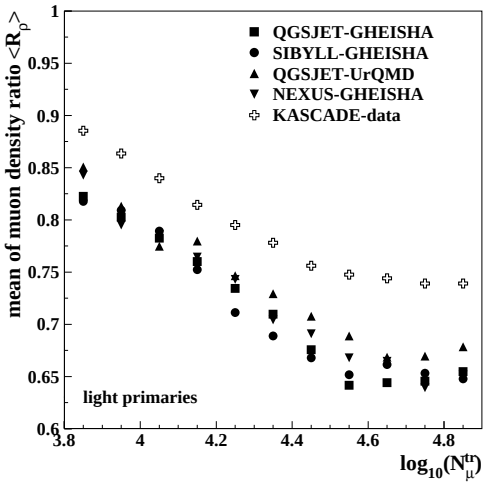

Fig. 3. Comparison of $\langle R_\rho \rangle$ for different model combinations with KASCADE data.

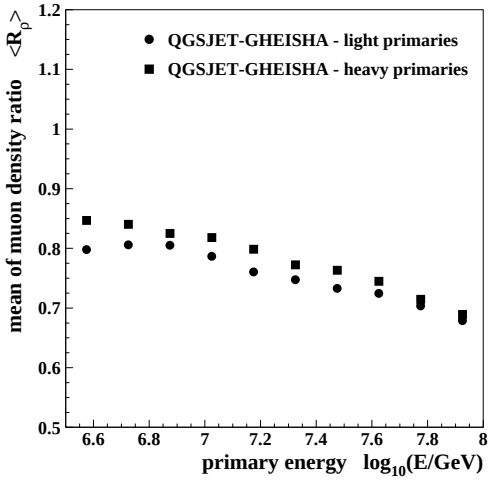

Fig. 4. Expectations of R_ρ for the case of KASCADE-Grande measurements in dependence of the primary energy.

detector, called trigger plane. Here the muon density $\rho_\mu^{\rm tp}$ is estimated for muons with a threshold of 490 MeV for vertical incidence. Global shower parameters like core position, arrival direction, shower size and truncated muon number are reconstructed with help of the KASCADE detector array. The truncated muon number describes the muon content (> 300 MeV) of the shower between 40 m and 200 m core distance and was found to be a valuable coarse primary energy estimator in case of the experimental conditions of KASCADE. The total sample of measured EAS is further divided in "electron-rich" and "electron-poor" showers performed by a cut along the ratio $lg(N_\mu)/lg(N_e)$, i.e. observables estimated by the array data only. The ratio $R_\rho = \rho_\mu^\star/\rho_\mu^{\rm tp}$ is the relevant parameter for the present analyses. As example Fig. 1 shows measured distributions of R_ρ for a certain core distance and primary energy range. Differences for various primaries (electron-rich EAS as predominantly induced by light ions and electron-poor EAS as predominantly induced by heavy ions) are found to be small compared to the width of the distributions.

3. Comparisons with Simulations

A large set of CORSIKA [8] simulations including a full simulation of the detector have been performed using the interaction models QGSJET (vers. of 1998 [10]), SIBYLL (vers.2.1 [4]), and NEXUS (vers.2 [3]) for the high-energy interactions and GHEISHA [5] and UrQMD [2] for interactions below $E_{\rm lab} = 80$ GeV. Observation level, Earth's magnetic field, and the particle thresholds are chosen in accordance with the experimental situation of KASCADE. The simulations cover the energy range of 10^{14} – $3 \cdot 10^{16}$ eV. The calculations are performed for

the zenith angular range $0° - 42°$ and for three primary particle types: protons, oxygen, and iron nuclei.
Fig. 2 shows the dependence of the mean and fluctuations (width of distributions) of the density ratio on the truncated muon number ($\propto E_0$, $E_0 \approx 1 - 10\,\mathrm{PeV}$) for data and predictions by the model combination QGSJET/GHEISHA analyzed by same procedures. The general behavior of decreasing mean and fluctuation with increasing energy is reproduced by the simulations, but in contrast a clear deviation on the mean values and on the amount of fluctuations is visible. To perform a test of the interaction models by comparing the calculated predictions with air shower data the sensitivity to differences in the simulations should be of significance (see also [7]). Fig. 3 compares the mean values for different model combinations, where differences of up to 10% in R_ρ are revealed. None of the models can reproduce the measurements, but the behavior of the models neXus and UrQMD comply better then QGSJET, SIBYLL, or GHEISHA. Next generation of CORSIKA will include FLUKA and NEXUS 3 as new models, which show in first tests a significant different behavior of the muon component (see [9]).

4. Expectations for KASCADE-Grande

At KASCADE-Grande [6] similar measurements can be performed for EAS of primary energies at least up to 10^{17} eV. The muon detection at the KASCADE central detector will then be possible for core distances of $50 - 550$m with reasonable muon statistics. Fig. 4 shows the expectations of Monte Carlo simulations for KASCADE-Grande measurements on the muon density ratio. The test of the validity of the description of the muon component will be of high relevance for the shower simulation procedures at ultra-high energies.

References

1. Antoni T. et al. - KASCADE Coll. 2002, Astropart.Phys. 16, 373
2. Bleicher M. et al. 1999, J.Phys.G 25, 1859
3. Drescher H.J. et al. 2001, Phys. Rep. 350, 93
4. Engel R. 1999, Proc.26^{th} ICRC, Salt Lake City, 1, 415
5. Fesefeldt H. 1985, PITHA-85/02, RWTH Aachen
6. Haungs A. et al. 2003, Proc.28^{th} ICRC, Tsukuba, these proceedings
7. Haungs A. et al. - KASCADE Coll. 2003, Nucl.Phys.B(Proc.Suppl.), in press
8. Heck D. et al. 1998, FZKA 6019 Forschungszentrum Karlsruhe
9. Heck D. et al. 2003, Proc.28^{th} ICRC, Tsukuba, these proceedings
10. Kalmykov N.N. and Ostapchenko S.S. 1993, Yad. Fiz. 56, 105
11. NEEDS-workshop 2002: http://www-ik.fzk.de/~needs/

The Role of Measurements of Muon Arrival Time Distributions for the Mass Discrimination of High Energy EAS

I.M. Brancus[4], T. Antoni[1], W.D. Apel[2], F. Badea[1,a], K. Bekk[2], A. Bercuci[2,a], M. Bertaina[3], H. Blümer[1,2], H. Bozdog[2], M. Brüggemann[5], P. Buchholz[5], C. Büttner[1], A. Chiavassa[3], P. Doll[2], R. Engel[2], J. Engler[2], F. Feßler[2], P.L. Ghia[6], H.J. Gils[2], R. Glasstetter[7], A. Haungs[2], D. Heck[2], J.R. Hörandel[1], A. Iwan[8], K-H. Kampert[7], H.O. Klages[2], Y. Kolotaev[5], G. Maier[2], H.J. Mathes[2], H.J. Mayer[2], J. Milke[2], C. Morello[6], M. Müller[2], G. Navarra[3], R. Obenland[2], J. Oehlschläger[2], S. Ostapchenko[1,c], M. Petcu[4], S. Plewnia[2], H. Rebel[2], M. Roth[1], H. Schieler[2], J. Scholz[2], T. Thouw[2], G.C. Trinchero[6], H. Ulrich[2], S. Valchierotti[3], J. van Buren[2], W. Walkowiak[5], A. Weindl[2], J. Wochele[2], J. Zabierowski[8], S. Zagromski[2]

(1) Institut für Exp. Kernphysik, Universität Karlsruhe, 76021 Karlsruhe, Germany
(2) Institut für Kernphysik, Forschungszentrum Karlsruhe, 76021 Karlsruhe, Germany
(3) Dipartimento di Fisica Generale dell'Università, 10125 Torino, Italy
(4) National Institute of Physics and Nuclear Engineering, 7690 Bucharest, Romania
(5) Fachbereich Physik, Universität Siegen, 57068 Siegen, Germany
(6) Instituto di Fisica dello Spazio Interplanetario, CNR, 10133 Torino, Italy
(7) Fachbereich Physik, Universität Wuppertal, 42097 Wuppertal, Germany
(8) Soltan Institute for Nuclear Studies, 90950 Lodz, Poland
[a] *on leave of absence from (4)*
[b] *on leave of absence from Moscow State University, 119899 Moscow, Russia*

1. Introduction

The temporal structure of the shower disc, especially of the muon component at higher muon energies, arises from geometrical (path length) effects, at least at sufficiently large distances from the shower axis. Thus the arrival time distributions of muons, measured on ground relative to the arrival time either of the shower center (global delays) or of the first locally registered muon (local delays) can be rather directly related to the height of production of the parent pions and kaons and do map the longitudinal EAS development. They are correlated with angle-of-incidence distributions of the muons. Advanced Monte Carlo (MC) simulations of the EAS development provide a good basis for the understanding of the observed distributions in terms of the longitudinal EAS development and mass composition of primary cosmic rays, respectively, or for testing the ingredients (particle propagation, hadronic interaction models) of the MC simulations.

This report compiles the main features of muon arrival time distributions measured with the Central Detector of the KASCADE experiment or studied on basis of corresponding MC simulations using the Monte Carlo EAS simulation program CORSIKA. The experiences with the KASCADE detector setup, restricted to arrival time observations at distances $R_\mu \lesssim 100\,\mathrm{m}$ from the EAS axis

pp. 1–4

are summarized. An outlook to the role of studies of the temporal EAS structure with KASCADE-Grande [3] is given. There muon arrival time distributions gain considerable importance with respect to the mass discrimination power [2].

2. Summary of KASCADE results

The timing facility of the KASCADE Central Detector, an "eye" of 456 pixels of scintillator elements, distributed over 16×20 m^2 with a coverage of 68% of the area, registers the timely sequence of the arriving muons, additionally identified with position sensitive MWPC installed in the souterrain of the Central Detector with an energy threshold of 2.4 GeV and with a minimum multiplicity, spanning the single-event arrival time distribution. From the single distribution various quartiles $\Delta\tau_q$ e.g. the median $\Delta\tau_{0.50}(R_\mu)$, are deduced. The distributions of these quartiles is considered to be representative for the temporal EAS structure and the fluctuations. For details see ref. [1,2].

At shower sizes observed with KASCADE the muon multiplicity registered for single shower events is relatively low which causes some difficulties to define the shower front by the foremost muon. Thus the quartile values additionally fluctuate with the multiplicity i.e. the number of muons (or the muon density $\rho^*_\mu(R_\mu)$) registered by the MWPC at $E_{thr} = 2.4$ GeV. It turns out that reduced quantities $\Delta\tau_q/\rho^*_\mu$ widely cancel such type of fluctuations. The main results of experimental studies and analyses of muon arrival times from KASCADE investigations are [1,2]:

- As simulations show the mass discrimination effects at primary energies around the knee and $R_\mu < 100$ m in terms of arrival time differences are in the order of few nanoseconds. The effects, increasing with the primary energy and the distance R_μ are considerably obscured by the finite time resolution of the apparatus.
- Nevertheless the experimentally observed results, expressed in distributions of various quartiles $\Delta\tau_q$ and by EAS time profiles (i.e. variation of $\langle\Delta\tau_q/\rho^*_\mu\rangle$ and of the dispersions) are in very good agreement with the results of extensive MC simulations adopting a reasonable mass composition.
- Nonparametric analyses of multivariate distributions correlating the EAS time observables with other observables (shower size N_e, the approximate energy estimator N^{tr}_μ, ...) display the minor role for mass discrimination under the conditions of KASCADE, though the good agreement of the phenomenological features considerably enhances the consistency of KASCADE analyses.

3. Expected features of muon arrival time distributions of high-energy EAS observed with KASCADE-Grande

The situation concerning the sensitivity to the primary mass is expected to get improved considerably with KASCADE-Grande observations [3].

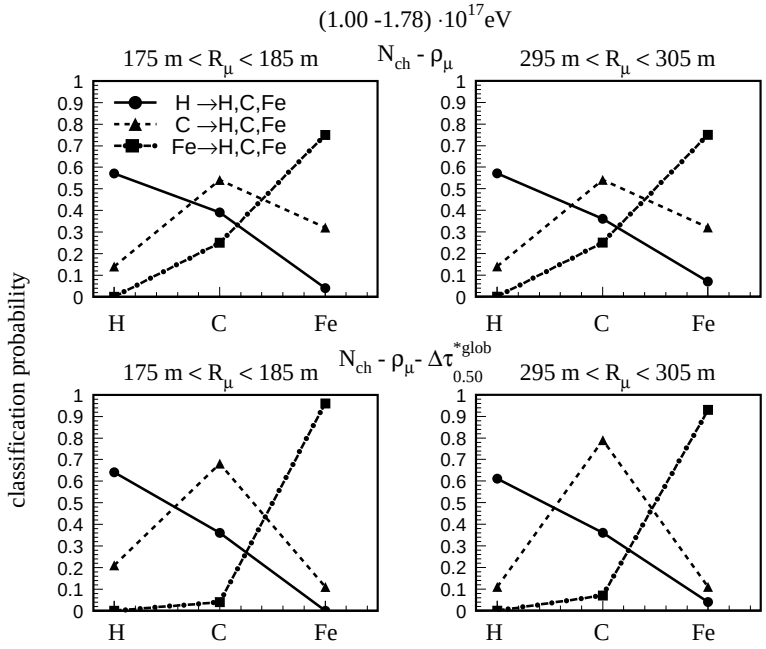

Fig. 1. The effect of the global time parameter $\Delta\tau^{glob}_{0.50}(R_\mu)$ on the true and false classification by the N_{ch} - $\rho_\mu(R_\mu)$ correlation shown for two distances R_μ and the primary energy range (1.0-1.78) $\cdot 10^{17}$ eV.

This expectation is based on extensive MC analyses, inspecting correlations and applying nonparametric statistical analysis techniques to multivariate distributions for the KASCADE-Grande case specifying the improvement of the Bayes risk values of classification. Since KASCADE-Grande will measure only a partial muon number N^{part}_μ (registered with the muon detectors of the embedded KASCADE array), for sake of simplicity the muon density $\rho_\mu(R_\mu)$ (with the observation threshold E_{thr}= 240 MeV) is used to represent N^{part}_μ. Fig.1 displays the true- and misclassification probabilities resulting from the application to a sample of proton, C and Fe induced EAS, classified by use of the correlation of the total number of charged particles N_{ch} with $\rho_\mu(R_\mu)(\propto N^{part}_\mu)$ and compared to the result from the N_{ch} - $\rho_\mu(R_\mu)$ - $\Delta\tau_{0.50}$ correlation. There are improvements of the classification probabilities of the heavy ion induced EAS, which are of considerable significance for reconstruction of the mass composition.

4. Observations of muon arrival time distributions as consistency test

The experimental procedure measuring the muon arrival times imply various conditions about the energy threshold of the muons observed in a certain

distance R_μ and a certain multiplicity threshold for being accepted for the reconstruction. Hence specific subsamples of all registered EAS events are selected. The distortions of the mass composition vary with the distance from the EAS center due to different lateral (and energy) distributions of the EAS particles. In order to reconstruct the original mass composition efficiency (acceptance) corrections have to be introduced, dependent on the observation distance R_μ, on the primary energy, on the multiplicity of the muons etc.. Such corrections invoke necessarily MC calculations with the requirement: The reconstruction of the primary mass composition from each sample observed with the variation of R_μ (and of the multiplicity threshold) must lead to identical composition results within the uncertainties.

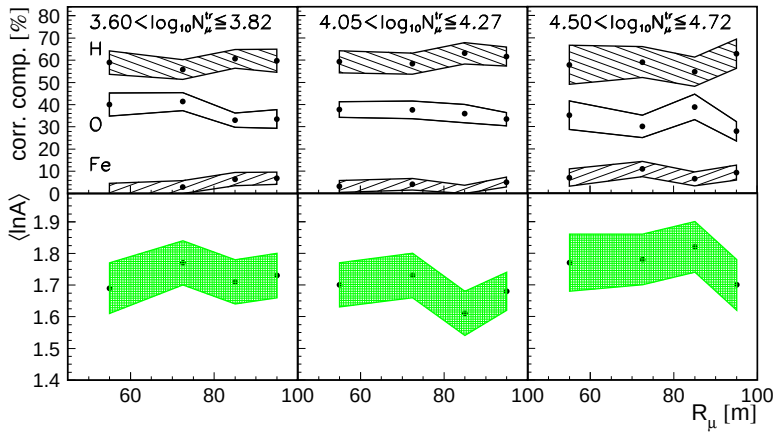

Fig. 2. Variation of the efficiency corrected mass composition and $\langle \ln A \rangle$ deduced from experimental observations at different R_μ.

The procedure has been applied to KASCADE data [2] using the QGSJet model as generator of the CORSIKA MC simulations (Fig.2). The deduced mass composition is in fair agreement with the other results of KASCADE and corroborates the increase of $\langle \ln A \rangle$ beyond the knee.

5. Concluding remarks

The results considering the KASCADE-Grande case tentatively demonstrate that muon arrival time measurements will play a significant role approaching a detailed understanding of the high-energy EAS. The procedure of the consistency test, first applied to KASCADE data can be further refined [4]. Global arrival time distributions turn out to be not significantly improving the sensitivity to the primary mass as compared to local distributions.

1. Antoni T. et al. 2002, KASCADE Collaboration, Astropart. Phys. 16 245
2. Antoni T. et al. 2003, KASCADE Collaboration, Astropart. Phys. 18 319
3. Bertaina M. et al. 2001, Proc. 27th ICRC Hamburg, Germany, vol. 2, p. 792
4. Brancus I.M. et al. 2003, J. Phys. G: Nucl. Part. Phys. 29 453

Energy Spectrum and Elemental Composition in the PeV Region

M. Roth[1], H. Ulrich[2], T. Antoni[1], W.D. Apel[2], F. Badea[1,a], K. Bekk[2], A. Bercuci[2,a], H. Blümer[1,2], H. Bozdog[2], I.M. Brancus[3], C. Büttner[1], A. Chilingarian[4], K. Daumiller[1], P. Doll[2], R. Engel[2], J. Engler[2], F. Feßler[2], H.J. Gils[2], R. Glasstetter[1,b] A. Haungs[2], D. Heck[2], J.R. Hörandel[1], A. Iwan[5], K-H. Kampert[1,2,b], H.O. Klages[2], G. Maier[2], H.J. Mathes[2], H.J. Mayer[2], J. Milke[2], M. Müller[2], R. Obenland[2], J. Oehlschläger[2], S. Ostapchenko[1,c], M. Petcu[3], H. Rebel[2], M. Risse[2], G. Schatz[2], H. Schieler[2], J. Scholz[2], T. Thouw[2], J. van Buren[2], A. Vardanyan[4], A. Weindl[2], J. Wochele[2], J. Zabierowski[5]

(1) Institut für Exp. Kernphysik, Universität Karlsruhe, 76021 Karlsruhe, Germany
(2) Institut für Kernphysik, Forschungszentrum Karlsruhe, 76021 Karlsruhe, Germany
(3) National Institute of Physics and Nuclear Engineering, 7690 Bucharest, Romania
(4) Cosmic Ray Division, Yerevan Physics Institute, Yerevan 36, Armenia
(5) Soltan Institute for Nuclear Studies, 90950 Lodz, Poland
[a] *on leave of absence from (3)*
[b] *now at: Universität Wuppertal, 42097 Wuppertal, Germany*
[c] *on leave of absence from Moscow State University, 119899 Moscow, Russia*

Abstract

One of the main aims of KASCADE is the determination of flux spectra for different primary cosmic ray mass groups to disentangle the knee feature. The field detector array of the KASCADE experiment measures the electron and muon component of extensive air showers in the knee region with high precision. On the basis of these measured data corresponding two-dimensional shower size spectra are investigated. On the arbitrary assumption that the chemical composition consists of five primary mass groups the size distributions are deconvoluted to reconstruct the energy spectra of the groups in the energy range between 10^{15} eV and 10^{17} eV. The energy spectrum results in a knee-like bending and a steepening above the knee. The topology of the individual knee positions suggests a rigidity dependence.

1. Introduction

The knowledge of the energy spectra of different components of primary cosmic rays in the knee region is of vital importance for testing alternative hypotheses of the cosmic ray (CR) origin and acceleration. The analysis of EAS presented benefits from the simultaneous measurement of different observables for each individual event by the KASCADE experiment [6]. Appropriate unfolding procedures, also taking correlations into account, make it possible to deconvo-

pp. 1–**??**

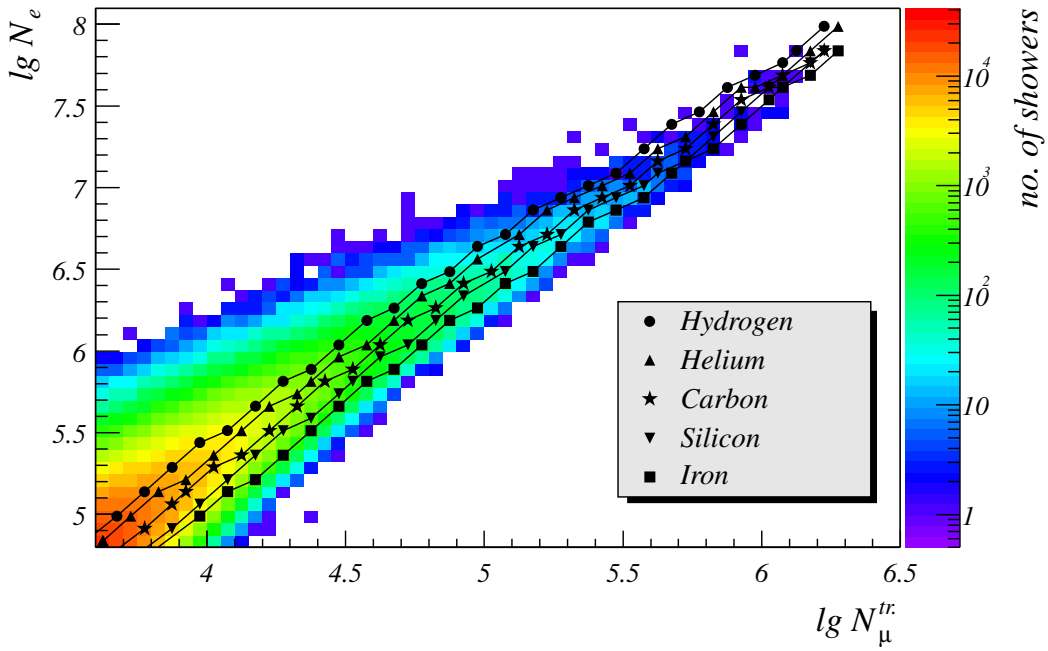

Fig. 1. The two-dimensional shower size spectrum of $\lg N_e$ and $\lg N_\mu^{tr}$. The zenith angle range of the showers is $[0°, 18°]$.

lute such multidimensional size distributions and result in energy spectra for five assumed primary mass groups represented by H, He, C, Si, and Fe.

2. Unfolding

In general the process of measuring distributions of physical observables $g(\lg N_e, \lg N_\mu^{tr})$ (see Fig. 1) is often disturbed by inherent limitations which lead to the nontrivial problem of inferring true distributions from measured ones. Confining conditions like limited acceptance or efficiency of the detector arrangement, finite resolution, strong intrinsic fluctuations and parameter transformations have to be taken into account. Suitable methods to solve the inverse problem are unfolding algorithms based on *Fredholm integral equations of* 1^{st} *kind*

$$g_i(\lg N_e, \lg N_\mu^{tr}) = \int_0^\infty t_i(\lg N_e, \lg N_\mu^{tr}|E) p_i(E) dE \qquad (1)$$

where the transfer function $t_i(\lg N_e, \lg N_\mu^{tr}|E)$ $(i \in \{\text{H, He, C, Si, Fe}\})$ has to cover all the above mentioned limiting effects and is realized by means of detailed Monte Carlo (MC) calculations using the simulation code CORSIKA [4] and the hadronic interaction model QGSJet [5]. In the presented analysis t_i is dominated by the intrinsic shower fluctuations. Various variants of unfolding procedures exist to determine the energy distribution $p_i(E)$ for different masses i. To crosscheck systematic uncertainties due to the method applied, KASCADE data are analysed

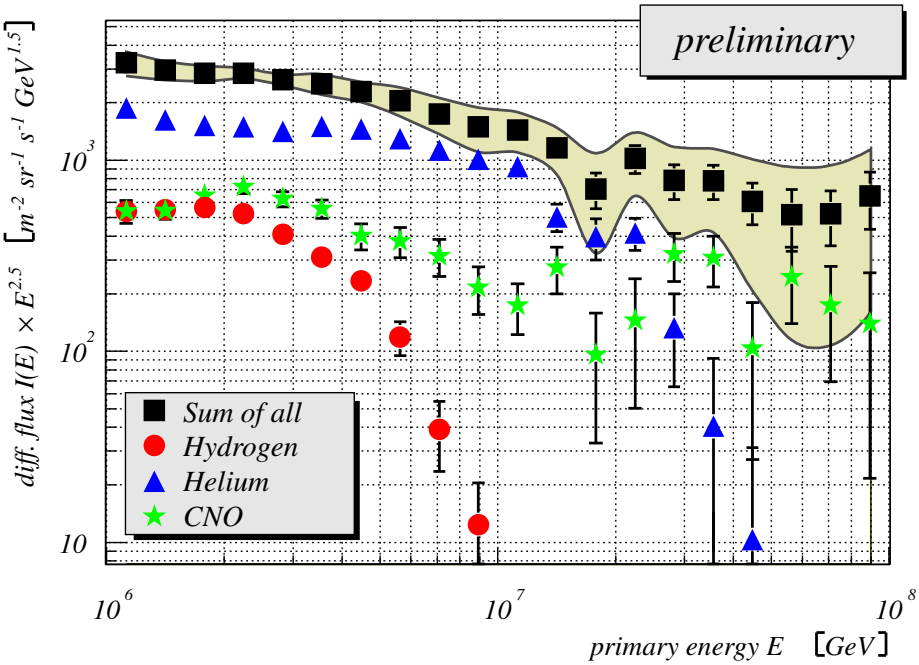

Fig. 2. Result of the Gold unfolding procedure. The given error bars reflect the statistical errors due to the measurement and simulation. The all-particle spectrum as well as the spectra for light elements are displayed. Systematic errors for the all-particle spectrum due to the applied method are indicated by the shaded area.

with conceptually different algorithms: in this paper the Bayesian approach [2,7] and Gold's unfolding method [3,8].

3. Results and Conclusion

The resulting energy spectra applying Gold's algorithm are shown in Fig. 2. Displayed error bars include statistical errors due to the measured and simulated number of events. In case of the all-particle spectrum the shaded area indicates the systematic uncertainty due to the method applied. The knee in the total energy spectrum at about 4 PeV is caused mostly by the steepening of spectra of light elements. The outcome of Gold's unfolding algorithm is corroborated by the aforementioned Bayes unfolding as displayed in Fig. 3. The all particle spectrum agrees with previous KASCADE findings e.g. of a neural network analysis [1] as well. The position of the steepening of the spectrum is shifted to higher energies for heavier components. To investigate the energy dependence the spectra of H and He are shown as a function of rigidity $R \propto E/Z$ in Fig. 4. As a preliminary result a rigidity dependent knee energy seems to be favoured by comparing the shape and the knee energy of the individual spectra. The study of limited MC sample size, $(\lg N_e, \lg N_\mu)$ parameterisations, choice of representatives of different groups of elements etc. as major source of systematic uncertainties is in progress

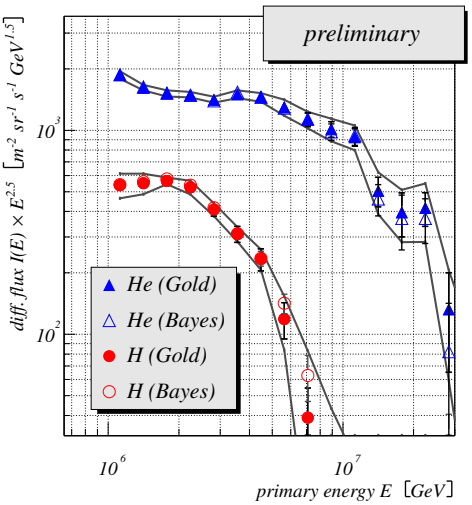

Fig. 3. Comparison of the deconvoluted H and He spectra using Bayesian [2] and Gold [3] unfolding. The solid lines mark the systematic uncertainty of the Gold algorithm.

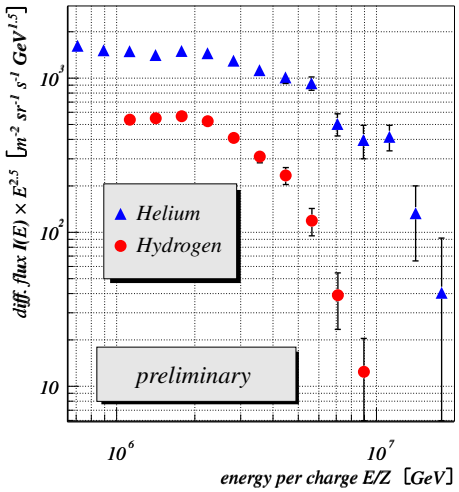

Fig. 4. Individual spectra as a function of the rigidity $R \propto E/Z$. The knee positions of the H and He spectra are nearly at the same position.

and is grossly estimated to be at least not less than 15%. In addition systematic studies with different other interaction models are necessary to exclude distortions from a specific model assumption. By using for example the QGSJet model the contribution of heavy elements is strongly suppressed as can be already estimated by the maximum position of t_i for different elements and energies indicated by the symbols in Fig. 1.

Acknowledgement: One of the authors (M. R.) gratefully acknowledges the support by a grant of the Alexander von Humboldt foundation.

1. Antoni T. et al., KASCADE Collaboration 2002, Astropart. Phys. 16, 245
2. D'Agostini G. 1995, Nucl. Instr. and Meth. in Phys. Res. A 362, 487
3. Gold R. 1964, ANL-6984, Argonne National Laboratory Report
4. Heck D. et al. 1998, FZKA 6019, Forschungszentrum Karlsruhe
5. Kalmykov N.N. and Ostapchenko S.S. 1993, Yad. Fiz. 56 105
6. Klages H.O. et al. 1997, Nucl. Phys. B, Proc. Suppl., 52B 92
7. Roth M. et al. - KASCADE Collaboration 2002, Proc. 12^{th} ISVHECRI, CERN, Nucl. Phys. B (Proc. Suppl.), in press
8. Ulrich H. et al. 2001, KASCADE Collaboration, Proc. 27^{th} ICRC, Hamburg, 97

Analysis of Air Showers at the Trigger Threshold of KASCADE

J. Scholz[2], T. Antoni[1], W.D. Apel[2], F. Badea[1,a], K. Bekk[2], A. Bercuci[2,a], H. Blümer[1,2], H. Bozdog[2], I.M. Brancus[3], C. Büttner[1], A. Chilingarian[4], K. Daumiller[1], P. Doll[2], R. Engel[2], J. Engler[2], F. Feßler[2], H.J. Gils[2], R. Glasstetter[1,b] A. Haungs[2], D. Heck[2], J.R. Hörandel[1], A. Iwan[5], K-H. Kampert[1,2,b], H.O. Klages[2], G. Maier[2], H.J. Mathes[2], H.J. Mayer[2], J. Milke[2], M. Müller[2], R. Obenland[2], J. Oehlschläger[2], S. Ostapchenko[1,c], M. Petcu[3], H. Rebel[2], M. Risse[2], M. Roth[1], G. Schatz[2], H. Schieler[2], T. Thouw[2], H. Ulrich[2], J. van Buren[2], A. Vardanyan[4], A. Weindl[2], J. Wochele[2], J. Zabierowski[5]

(1) Institut für Exp. Kernphysik, Universität Karlsruhe, 76021 Karlsruhe, Germany
(2) Institut für Kernphysik, Forschungszentrum Karlsruhe, 76021 Karlsruhe, Germany
(3) National Institute of Physics and Nuclear Engineering, 7690 Bucharest, Romania
(4) Cosmic Ray Division, Yerevan Physics Institute, Yerevan 36, Armenia
(5) Soltan Institute for Nuclear Studies, 90950 Lodz, Poland
[a] *on leave of absence from (3)*
[b] *now at: Universität Wuppertal, 42097 Wuppertal, Germany*
[c] *on leave of absence from Moscow State University, 119899 Moscow, Russia*

Abstract

The KASCADE experiment measures extensive air showers. It is 100% efficient for showers which are induced by primary particles with energies above 10^{15} eV to pursue its main goal, the examination of the knee in the flux spectrum at $\approx 5 \cdot 10^{15}$ eV. A specially adapted method to calculate two observables (N_{ch}, the number of charged particles and N_μ, the number of muons) by means of a maximum likelihood estimate will be presented. The estimate combines different detector systems and works already at energies around the trigger threshold of KASCADE at $\approx 10^{14}$ eV. These observables are used to reconstruct a preliminary energy flux spectrum which is compared with direct measurements and previous measurements of KASCADE at energies above 10^{15} eV. The reconstruction of energy spectrum and elemental composition around the trigger threshold of KASCADE is important for two reasons. First the estimated spectrum at higher energies has to be congruent with the results of direct measurements. Second it is a cross-check of the interaction models underlying the analysis of extended air showers.

1. Methods

KASCADE[1] is designed to measure extended air showers induced by cosmic rays around the energy region of the so-called knee at ca. $5 \cdot 10^{15}$ eV.

pp. 1–4

Hence the standard reconstruction procedure is optimized for energies starting from $1 \cdot 10^{15}$ eV. This standard reconstruction determines two of the most important observables, the number of electrons N_e and the number of muons N_μ by fitting appropriate lateral distribution functions (NKG-functions) to the particle densities measured in each detector of the KASCADE field array. The separate handling of muons and electrons is possible due to the setup of the array stations at KASCADE, where shielded and unshielded detectors are placed one upon the other. The lateral distribution functions have two parameters, the number of particles (electrons/muons) and the slope of the function. For low particle numbers this two parameter fit does not work. However, simulations show that the slope of the distributions does not vary very much for showers near the trigger threshold at KASCADE observation level. Thus we can assume the slope parameter as being constant and determine efficiently the number of particles with a maximum likelihood estimate[5]. A sacrifice we have to make is that we can no longer differentiate between electrons and muons in the unshielded detectors. So we use as a new observable the number of charged particles N_{ch}^{est} which is the sum of the number of electrons N_e and the number of muons N_μ. The other new observable is the estimated number of muons N_μ^{est}.

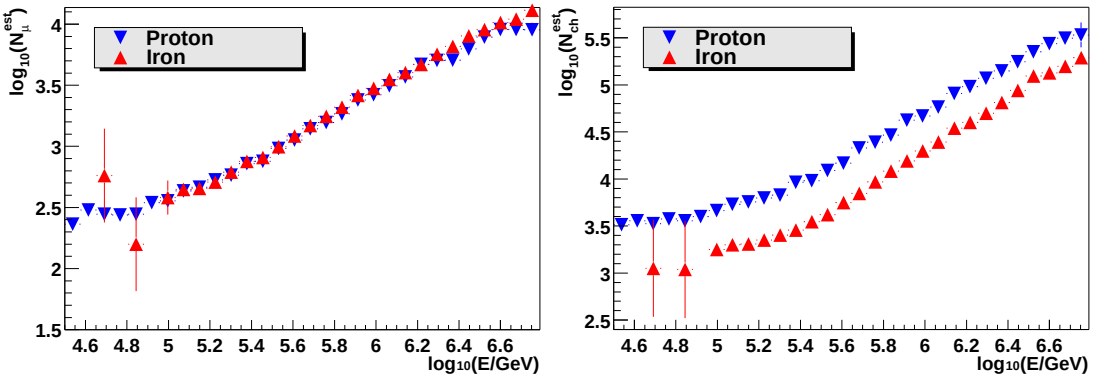

Fig. 1. Dependence of N_μ^{est} and N_{ch}^{est} on the primary energy for simulated proton and iron induced events.

The maximum likelihood estimate allows easily the combination of different detector systems. In our case, the number of charged particles is measured by the unshielded e/γ-detectors of the field array and the so called top cluster of the KASCADE Central Detector ($490\,\mathrm{m}^2$+$25\,\mathrm{m}^2$ sensitive area). The number of muons is measured by combining the shielded μ-detectors of the field array and the trigger plane of the Central Detector ($622\,\mathrm{m}^2$+$208\,\mathrm{m}^2$). As only showers are selected which have their core within a radius of 40 m around the Central Detector, the high coverage of top cluster and trigger plane can be used. This extends the energy range where full trigger and reconstruction efficiency is given down by

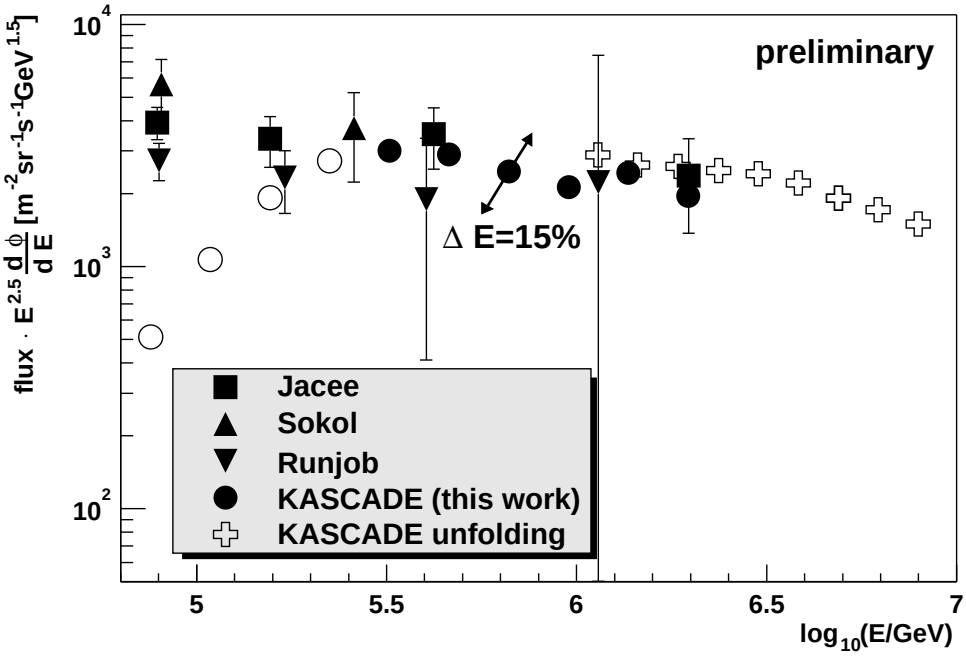

Fig. 2. The energy flux spectrum from KASCADE data. The trigger threshold is at $\log_{10}(\mathrm{E[GeV]}) = 5.5$. Data points below this threshold are marked with open circles. Results from three experiments with direct cosmic ray measurements[3] are shown. The KASCADE unfolding data are taken from [4].

more than half a decade.

With the help of detailed CORSIKA[2] simulations (QGSJET/GHEISHA including full detector simulations), the dependence of these observables on primary mass and energy is examined. As Fig. 1 shows, the relation between primary energy and estimated number of muons is a power law and independent of the primary particle. In a first step, using this dependency, we reconstruct an energy flux spectrum from measured data by taking the number of muons N_μ^{est} for each event and calculating the corresponding primary energy which is then histogrammed. If the simulations are correct, one should get a correct energy calibration at KASCADE for the higher energies and the flux should be compatible with that of direct measurements at lower primary energies.

In a second step, the new observables will be used together with additional hadronic and muonic observables measured by the Central Detector as input to a neural net analysis with which the energy spectrum and the elemental distribution of the measured data will be calculated.

2. Results

Simulations show that the uncertainties of the observables N_{ch}^{est} and N_{μ}^{est} are below 10% in the energy range $5 \cdot 10^{14}\,\mathrm{eV} - 8 \cdot 10^{15}\,\mathrm{eV}$. The flux spectra for both observables follow a power law.

The dependence on mass and energy of the new observables is shown in Fig. 1: Whereas N_{μ}^{est} is a good estimator of the primary energy independent of the primary mass, N_{ch}^{est} is also dependent on the mass of the primary particle, which will be used for mass reconstruction.

Fig. 2 shows a first preliminary flux spectrum calculated by applying the described method to a small set of KASCADE data (75 hours measuring time). The flux is compatible with the direct measurements at low energies (above the threshold of $3 \cdot 10^{14}\,\mathrm{eV}$) and with KASCADE results for high energies. The statistical errors are smaller than the symbol size. Systematical errors have not been fully calculated yet. The effect of an energy uncertainty of 15% due to uncertainties of the underlying interaction model or a different chemical composition is shown for one data point as an arrow in Fig. 2.

3. Conclusions

The energy determination of KASCADE is based on simulations of extended air showers. To check this method, one has to compare the absolut flux at certain reconstructed energies with the flux of direct measurements. As these fluxes match, this is a further hint that the energy calibration at KASCADE is correct.

Together with further observables from the central detector, the new observables can also be used to determine the mass of the primary particle via a neural net at the trigger threshold of KASCADE. The result of the individual particle fluxes will then be compared to the direct measurements, too.

References

1. Antoni T. et al. 2003, Nucl. Instr. Meth. A, submitted
2. Heck D. et al. 1998, FZKA-Report 6019, Forschungszentrum Karlsruhe
3. Hörandel J. 2003, Astropart. Phys. 19, 193
4. Roth M., Ulrich H. et al. 2003, Proc. 28th ICRC, these proceedings
5. Schatz G., Feßler F. et al. 2003, Proc. 28th ICRC, these proceedings

Cosmic Ray Anisotropy with KASCADE

G. Maier[2], T. Antoni[1], W.D. Apel[2], F. Badea[1,a], K. Bekk[2], A. Bercuci[2,a], H. Blümer[1,2], H. Bozdog[2], I.M. Brancus[3], C. Büttner[1], A. Chilingarian[4], K. Daumiller[1], P. Doll[2], R. Engel[2], J. Engler[2], F. Feßler[2], H.J. Gils[2], R. Glasstetter[1,b] A. Haungs[2], D. Heck[2], J.R. Hörandel[1], A. Iwan[5], K-H. Kampert[1,2,b] H.O. Klages[2], H.J. Mathes[2], H.J. Mayer[2], J. Milke[2], M. Müller[2], R. Obenland[2], J. Oehlschläger[2], S. Ostapchenko[1,c], M. Petcu[3], H. Rebel[2], M. Risse[2], M. Roth[1], G. Schatz[2], H. Schieler[2], J. Scholz[2], T. Thouw[2], H. Ulrich[2], J. van Buren[2], A. Vardanyan[4], A. Weindl[2], J. Wochele[2], J. Zabierowski[5]

(1) Institut für Exp. Kernphysik, Universität Karlsruhe, 76021 Karlsruhe, Germany
(2) Institut für Kernphysik, Forschungszentrum Karlsruhe, 76021 Karlsruhe, Germany
(3) National Institute of Physics and Nuclear Engineering, 7690 Bucharest, Romania
(4) Cosmic Ray Division, Yerevan Physics Institute, Yerevan 36, Armenia
(5) Soltan Institute for Nuclear Studies, 90950 Lodz, Poland
[a] *on leave of absence from (3)*
[b] *now at: Universität Wuppertal, 42097 Wuppertal, Germany*
[c] *on leave of absence from Moscow State University, 119899 Moscow, Russia*

Abstract

The anisotropy of cosmic rays with energies in the region of the knee in the energy spectrum is investigated in three different perspectives based on the arrival directions of about 150 Mio. extensive air showers measured by KASCADE. The different analyses are a harmonic analysis of the right ascension distribution and a point source search of showers above 0.5 PeV as well as an autocorrelation analysis of showers above 100 PeV. All three analyses agree inside the statistical limits with an isotropic distribution of the arrival directions of cosmic rays.

1. Introduction

The origin of the knee in the cosmic ray (CR) energy spectrum at about 4 PeV is still under discussion, various theories can be found in literature. Restrictions to these theories can be given by measurements of the anisotropy of the primary CR. While well below 0.5 PeV many experiments reported amplitudes of the first harmonic of the right ascension distribution of CRs of about 10^{-3} or lower [3], the measurements in the interesting knee region suffer from the low flux of CRs. Some theories also predict a mass dependent change of the amplitude and phase at the knee. Results of an analysis with KASCADE concerning this questions can be found in Chapter 3.

Since charged CR are deflected by the galactic magnetic field and photons are absorbed by the CMBR no point sources are expected to be seen in the

pp. 1–4 Correspondence to: G.Maier (gernot.maier@ik.fzk.de)

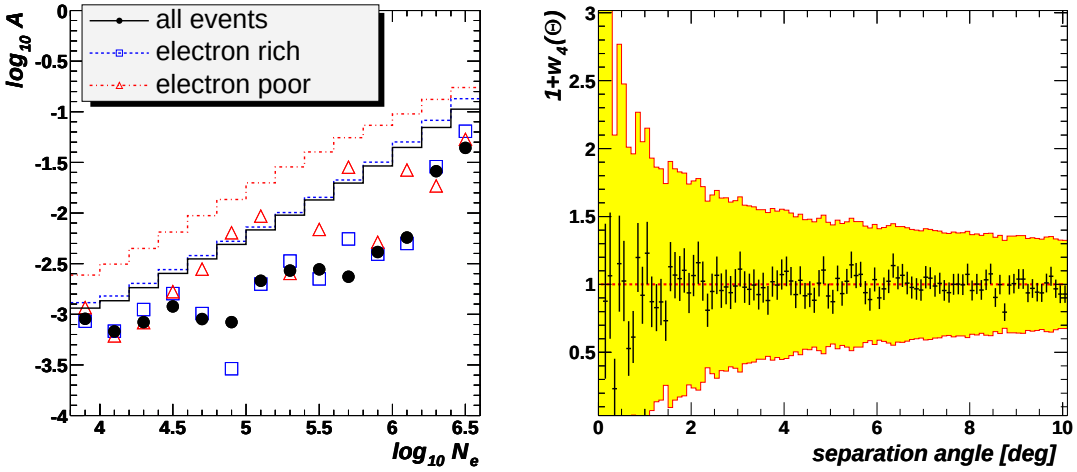

Fig. 1. Left: Rayleigh amplitudes. Right: autocorrelation of the 1000 largest showers.

considered energy region. At large energies the deflection in the magnetic field decreases substantially, point sources could there effect a clustering in the arrival directions. This will be investigated in Chapter 4 and 5.

2. KASCADE: Experiment and Reconstruction

The KASCADE experiment [1], located at the Forschungszentrum Karlsruhe, Germany (110 m a.s.l., 49.1° N, 8.4° E), is designed to measure extensive air showers (EAS) in the energy range of about 0.5 to 100 PeV. In the present analysis data from the 200x200 m^2 field array of KASCADE are used. Electron and muon numbers, shower core and shower direction of EAS are reconstructed from the energy deposits and arrival time measurements of the scintillator counters in the 252 detector stations. Shower directions, which are of particular interest in this anisotropy analyses, are determined by evaluating the arrival times of the first particle in each detector station and the total particle number per station. The reconstruction accuracy of the shower direction is steadily increasing with the number of electrons N_e per shower, from 0.5° at $\log_{10} N_e = 4$ to 0.1° at $\log_{10} N_e = 6$. A comparison with independent measurements from other detectors of KASCADE and Monte Carlo studies shows no systematic error in the reconstruction of the the shower direction. The data set of about 150 Mio. showers was recorded on 1400 days of operation between May 1998 and December 2002

3. Large Scale Anisotropy - Harmonic Analysis

The large scale anisotropy is investigated by the Rayleigh formalism [6], which delivers beside the amplitude A and phase Φ of the first harmonic of the arrival direction distribution in right ascension α also an estimate of the probability $P_{fluc}(n, A)$ of measuring a random fluctuation from a uniform dis-

tribution in α with n events. The amplitude A and phase Φ are influenced by changes in the event rate, e.g. by interruptions in the data taking, or atmospheric influences. To minimize these effects, only data taken over full sidereal days with all detector stations of the field array running are considered. This reduces the number of events in this analysis by about a factor of five corresponding then to 300 sideral days of operational time. To check for a correlation of the amplitude A with the primary mass, the data is divided into electron rich (preferentially light primaries) and electron poor (preferentially heavy primaries) events by a simple linear cut in the muon to electron size ratio at a value of $\log_{10} N_{\mu,tr}/\log_{10} N_e = 0.78$. Fig. 1 (left) shows the amplitude A of the first harmonic for the whole data set (filled points), electron rich showers (open squares) and electron poor showers (open triangles) as a function of electron size N_e (covering an energy range of $E_0 \approx 5 \cdot 10^{14} - 5 \cdot 10^{16}$ eV, the knee position is in the region of $\log_{10} N_e \approx 5.2 - 5.8$). The lines show the 90% confidence limit of $1 - P_{fluc}$. From these lines, the level of sensitivity to large scale anisotropy can be seen. All amplitudes in the three data samples are well consistent with fluctuations from a uniform distribution, no significant large scale anisotropy can be seen.

4. Autocorrelation of EAS above 100 PeV

The 1000 largest EAS by muon size ($\log_{10} N_{\mu,tr} > 5.4$) measured by the KASCADE experiment correspond to primary CR energies around 100 PeV. A possible clustering of these EAS is analyzed using an estimator of the autocorrelation function according to [4]. It describes essentially the ratio of the probabilities of finding a pair of showers separated by a certain angular distance Θ in the measured data set and the one derived from an isotropic distribution: $1 + w_4(\Theta) = (DD - 2DR - RR)/RR$. DD, DR, RR denote the angular distance distributions of data-data, data-random and random-random events. To reproduce an isotropic background, random directions R are generated from the measured directions D using the shuffling technique [2], averaging over 1000 new artificial data samples. Fig. 1 (right) shows the $1 + w_4(\Theta)$ distribution. No significant deviation from the isotropic expectation which is exactly one can be seen. All points are well inside the estimation of the five sigma confidence area indicated by the shaded region.

5. Small Scale Anisotropy - Point Source Search

Small scale anisotropy is studied by comparing the measured arrival direction distributions in equatorial coordinates with an estimation of an isotropic background distribution. This background distribution is generated using again the shuffling technique averaging over 50 new artificial data samples. Significance maps with a bin size of 0.5^o are generated from the deviations between these distributions using the formalism of Li and Ma [5] for different data cuts. Fig. 2 shows the distributions of significance from these maps for the visible sky

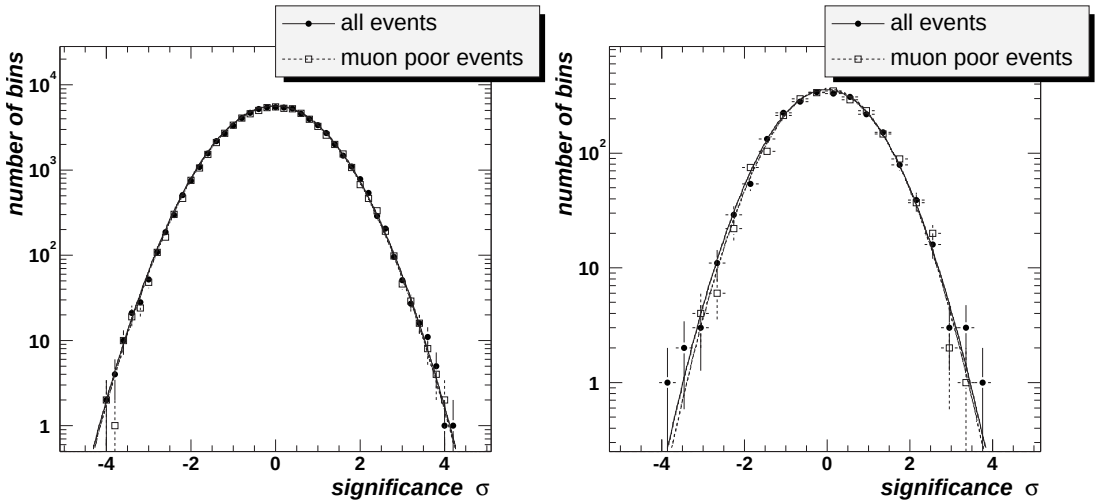

Fig. 2. Significance distribution of the visible sky of KASCADE (left) and of the sky inside a band of 6° around the galactic plane (right).

of KASCADE (left) and a band of 3° width around the galactic plane (right) for all events (filled squares) and a data sample of muon poor EAS ($N_\mu/N_e < 0.01$, open squares). This cut enhances the number of gamma ray shower candidates in the sample. Any deviation from isotropy would result in a distorted Gaussian distribution $N(0,1)$. Fits to the data points, indicated by the lines in Fig. 2, show a very good agreement of all four distributions with $N(0,1)$. Calculation of 90% upper flux limits for point source events yield values between $7 \cdot 10^{-11}$ and $1.5 \cdot 10^{-10}$ m^{-2} s^{-1} depending on declination and the applied data cut.

6. Conclusion

We present KASCADE results on anisotropy measurements of CRs with primary energies in the PeV region. An 90% upper limit of $A \approx 10^{-3} - 10^{-2}$ depending on the size and the primary mass of the EAS for the first harmonic amplitude of the right ascension distribution is given. The autocorrelation function of EAS with energies around 100 PeV is consistent with an isotropic distribution. No hints for point sources in the visible sky of KASCADE or an enhancement of the flux of CRs from the galactic plane is visible in the analyzed data sample, upper flux limits are determined to be below 10^{-10} m^{-2} s^{-1}.

1. Antoni T. et al. 2003, Nucl. Instr. & Meth., submitted
2. Cassiday, G.L. et al. 1990, Nucl. Phys. B (Proc.Suppl.) 14, 291
3. Clay R.W. et al. 1997, Proc. 25$^{\text{th}}$ ICRC Durban, 4, 185
4. Landy S.D., Szalay, A.S. 1983, ApJ 412, 64
5. Li T.-P., Ma Y.-Q. 1983, ApJ 272, 317
6. Mardia K.V., Jupp, P.E. 1999, Directional Statistics (John Wiley & Sons)

Search for Extremely High Energy Gamma Rays with the KASCADE Eperiment

G. Schatz[2,a], F. Feßler[2], T. Antoni[1], W.D. Apel[2], F. Badea[1,b], K. Bekk[2], A. Bercuci[2,b], H. Blümer[1,2], H. Bozdog[2], I.M. Brancus[3], C. Büttner[1], A. Chilingarian[4], K. Daumiller[1], P. Doll[2], R. Engel[2], J. Engler[2], H.J. Gils[2], R. Glasstetter[1,c] A. Haungs[2], D. Heck[2], J.R. Hörandel[1], A. Iwan[5], K-H. Kampert[1,2,c] H.O. Klages[2], G. Maier[2], H.J. Mathes[2], H.J. Mayer[2], J. Milke[2], M. Müller[2], R. Obenland[2], J. Oehlschläger[2], S. Ostapchenko[1,d], M. Petcu[3], H. Rebel[2], M. Risse[2], M. Roth[1], H. Schieler[2], J. Scholz[2], T. Thouw[2], H. Ulrich[2], J. van Buren[2], A. Vardanyan[4], A. Weindl[2], J. Wochele[2], J. Zabierowski[5]

(1) Institut für Exp. Kernphysik, Universität Karlsruhe, 76021 Karlsruhe, Germany

(2) Institut für Kernphysik, Forschungszentrum Karlsruhe, 76021 Karlsruhe, Germany

(3) National Institute of Physics and Nuclear Engineering, 7690 Bucharest, Romania

(4) Cosmic Ray Division, Yerevan Physics Institute, Yerevan 36, Armenia

(5) Soltan Institute for Nuclear Studies, 90950 Lodz, Poland

[a] *present address: Habichtweg 4, D-76646 Bruchsal, Germany; e-mail bgschatz@t-online.de*

[b] *on leave of absence from (3)*

[c] *now at: Universität Wuppertal, 42097 Wuppertal, Germany*

[d] *on leave of absence from Moscow State University, 119899 Moscow, Russia*

Abstract

Data observed with the KASCADE extensive air shower experiment have been analyzed with respect to a possible contribution by primary gamma rays in the energy range of 0.3 to 10 PeV. Possible gamma induced events are identified by their low muon to electron ratios and by the steepness and smoothness of their electron lateral distributions. Our results confirm and to some extent improve upper limits of a possible gamma contribution established by previous experiments.

1. Introduction

Gamma rays represent a small but important fraction of primary cosmic rays. Their importance among primary cosmic rays derives from the fact that they are electrically neutral and hence not deflected by interstellar or intergalactic magnetic fields. Therefore their directions of incidence points back to their points of production. The highest gamma ray energies identified up to now by the imaging atmospheric Cherenkov technique [7] are close to 50 TeV [13]. But the gamma ray spectrum is expected to extend to much higher energies due to the production of neutral pions by charged particles interacting with interstellar matter. It therefore appeared worthwhile to search the data registered by the KASCADE experiment for events which might be attributed to primary gamma rays. This contribution updates a previous one [8]. More details can be

pp. 1–4

found in Ref. [9].

Previous experiments [1,6] have set upper limits of the order of 10^{-5} to 10^{-4} for the gamma ray fraction among primary cosmic rays in the energy range above a few hundred TeV. Identifying such a small fraction is obviously not trivial, especially in view of the large fluctuations inherent in extensive air showers (EASs) which are the only means at present to register high energy cosmic rays. The main feature which can be exploited for discriminating primary gamma rays from charged cosmic ray particles is the ratio of electrons to muons on observation level. Gamma rays interact in the atmosphere predominantly by producing electron-positron pairs. It is only via the photoproduction of hadrons that muons occur to an appreciable extent in EASs induced by gamma rays.

2. Measurements and data analysis

The KASCADE experiment is described in detail elsewhere [5]. The main features relevant for the present analysis are the array with its $490\ \mathrm{m}^2$ of scintillation detectors for registering electrons and $620\ \mathrm{m}^2$ for the measurement of muons. Of the central detector, only the $205\ \mathrm{m}^2$ scintillation detectors of the trigger plane were used to register muons. The signals from the detectors were analysed to yield core position, electron number N_e, steepness of the lateral electron distribution ('age'), muon number N_μ and, from timing, the direction of incidence of the shower. For more details of this analysis cf. Ref. [4].

3. Gamma hadron discrimination

Fig. 1 shows the distribution of the reconstructed events in the $lg(N_e) - lg(N_\mu)$ plane as the light data points. Superimposed are simulated gamma events of fixed energy and zenith angle which concentrate along the lower edge of the observed showers, as expected. These simulations include a complete detector Monte Carlo [4]. For further analysis we concentrate on the events below the straight line in Fig. 1. They amount to 97097 out of a total of 29.5 millions. In the region above this line the density of observed events is so large that identification of the few possible gamma induced events appears hopeless. The events near to and overlapping the simulated gamma events are expected to be mainly due to primary protons because EASs induced by heavy nuclei exhibit a larger muon to electron ratio. A further reduction of this hadron background is obtained by an age cut and by selecting EASs with a smoother lateral distribution. The latter feature is exploited very advantageously for gamma/hadron separation by the imaging atmospheric Cherenkov technique (cf. Fegan [7]). For details of our procedure cf. Ref. [9]. These two cuts reduce the number of events remaining

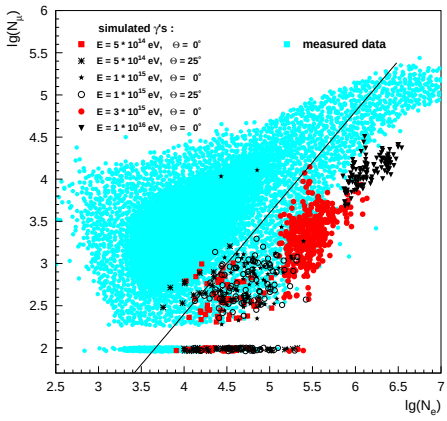

Fig. 1. Distribution of the observed events in the $lg(N_e) - lg(N_\mu)$ plane (light blue) with simulated gamma showers superimposed. The horizontal band at $lg(N_\mu) = 2$ represents EAS with no registered muon (and hence an estimated muon number 0).

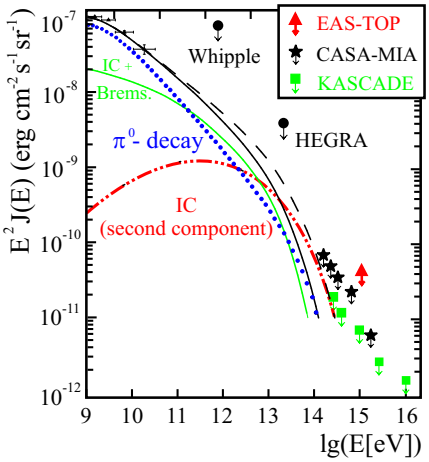

Fig. 2. Comparison of our derived upper limits with previous results by the CASA-MIA [6] and EAS-TOP [1] experiments and with theoretical spectra from Ref. [3].

to 43538 and 38531, respectively.

The usual method applied by previous experiments [1,6,11] to set an upper limit to the number of gammas among the observations is to choose a separating line (in our case in the $lg(N_e) - lg(N_\mu)$ plane) and assume that all events on one side of the line represent gamma rays. In our opinion this procedure is unnecessarily conservative because the distribution of observed events in the region of simulated gamma ray showers does not bear any resemblance with the one expected for gamma rays. Therefore another statistical procedure was developed which exploits the shape difference between the two types of distributions. Detailed descriptions of this procedure and of the algorithm employed are beyond the scope of this paper but can be found in Refs. [9,12].

4. Results

Fig. 2 compares our results with other experiments and with theoretical values by Aharonian and Atoyan [3]. The results of the CASA-MIA [6] and EAS-TOP [1] experiments displayed in this figure have been calculated by multiplying their quoted maximum gamma ray fractions with their observed spectra (Refs. [10] and [2], respectively). Experiments and theory are obviously well compatible with each other. Our lowest points are intriguingly close to the uppermost (dashed) theoretical curve. Since this assumes a hypothetical population of high energy electrons, required to explain the

x-ray spectrum, an improvement of the limit might confirm or otherwise this population and would hence be of considerable astrophysical relevance.

No local enhancement indicative of a point source was observed. The diffuse flux results mainly from interactions of charged cosmic rays with interstellar matter which is concentrated in the Galactic plane. Hence an excess along this plane may be expected. We have therefore investigated the distribution on the sky of the 143 events which appear most 'gamma-like' (i.e. whose distance to the straight line in fig. 1 is the largest). A Kolmogorov-Smirnov test comparing their distribution in Galactic latitude to those of all events after the first and third cuts yields chance probabilities of order 0.05. Hence no observation of gamma rays from the Galactic plane can be claimed. Gamma rays from extragalactic sources are not expected to show up in our data because absorption of gammas rays by the cosmic microwave background radiation attains its maximum in the energy range of this investigation.

Acknowledgements The KASCADE experiment is supported by collaborative WTZ projects in the frame of scientific-technical cooperation between Germany and Romania (RUM 97/014), Poland (POL 99/005) and Armenia (ARM 98/002). The Polish group (Soltan Institute and University of Lodz) acknowledges the support by the Polish State Committee for Scientific Research (grant no. 5 P03B 133 20).

5. References

1. Aglietta, M. et al. 1996, Astropart. Phys., 6, 71
2. Aglietta, M. et al. 1999, Astropart. Phys., 10, 1
3. Aharonian, F. A., A. M. Atoyan 2000, Astron. Astrophys. 362, 937
4. Antoni, T. et al. (KASCADE collaboration) 2001, Astropart. Phys. 14, 245
5. Antoni, T. et al. (KASCADE collaboration) 2003, submitted to NIMA
6. Chantell, M. C. et al. 1997, Phys. Rev. Lett. 79, 1805
7. Fegan, D. J. 1997, J. Phys. G: Nucl. Part. Phys. 23, 1013
8. Feßler, F. et al. (KASCADE collaboration) 2001, Proc. 27^{th} ICRC, contrib. OG 2.1, p. 2370
9. Feßler, F. 2002, PhD thesis, Heidelberg University; Report FZKA 6747, Forschungszentrum Karlsruhe (in German).
10. Glasmacher, M. A. K. et al. 1999, Astropart. Phys. 10, 291
11. Karle, A. et al. 1995, Phys. Lett. B 347, 161
12. Schatz, G. 2001, *Some Statistical Methods Employed for the Gamma Ray Search with KASCADE*, unpublished report, May 2001; a ps-file of the report is available upon request to bgschatz@t-online.de.
13. Tanimori, T. et al. 1998, Astrophys. J. 492, L33

A Measurement of the Energy Spectrum of Unaccompanied Hadrons

M. Müller[2], T. Antoni[1], W.D. Apel[2], F. Badea[1,a], K. Bekk[2], A. Bercuci[2,a], H. Blümer[1,2], H. Bozdog[2], I.M. Brancus[3], C. Büttner[1], A. Chilingarian[4], K. Daumiller[1], P. Doll[2], R. Engel[2], J. Engler[2], F. Feßler[2], H.J. Gils[2], R. Glasstetter[1,b], A. Haungs[2], D. Heck[2], J.R. Hörandel[1], A. Iwan[5], K-H. Kampert[1,2,b], H.O. Klages[2], G. Maier[2], H.J. Mathes[2], H.J. Mayer[2], J. Milke[2], R. Obenland[2], J. Oehlschläger[2], S. Ostapchenko[1,c], M. Petcu[3], H. Rebel[2], M. Risse[2], M. Roth[1], G. Schatz[2], H. Schieler[2], J. Scholz[2], T. Thouw[2], H. Ulrich[2], J. van Buren[2], A. Vardanyan[4], A. Weindl[2], J. Wochele[2], J. Zabierowski[5],

(1) Institut für Exp. Kernphysik, Universität Karlsruhe, 76021 Karlsruhe, Germany
(2) Institut für Kernphysik, Forschungszentrum Karlsruhe, 76021 Karlsruhe, Germany
(3) National Institute of Physics and Nuclear Engineering, 7690 Bucharest, Romania
(4) Cosmic Ray Division, Yerevan Physics Institute, Yerevan 36, Armenia
(5) Soltan Institute for Nuclear Studies, 90950 Lodz, Poland
[a] *on leave of absence from (3)*
[b] *now at: Universität Wuppertal, 42097 Wuppertal, Germany*
[c] *on leave of absence from Moscow State University, 119899 Moscow, Russia*

Abstract

The energy spectrum of unaccompanied hadrons is measured with the large hadron calorimeter of the KASCADE experiment. From the measured flux at detector level the primary proton spectrum at the top of the atmosphere has been derived. The flux obtained is well compatible with results of direct measurements.

1. Introduction

Unaccompanied hadrons are cosmic-ray induced events for which only one hadron has been registered at ground level. They offer a possibility to study details of hadronic interactions in the atmosphere and the primary proton spectrum in the energy range from 100 GeV up to 5 PeV.

Different definitions of an unaccompanied hadron are used in the literature. For the present investigations an unaccompanied hadron is defined as follows: Only one hadron with an energy of at least 50 GeV is reconstructed and the zenith angle is smaller than 30°.

2. Experimental Set-up and Simulations

The measurements have been carried out with the KASCADE air shower experiment [1]. It consists of a 200×200 m^2 scintillator array, equipped with 252

pp. 1–4

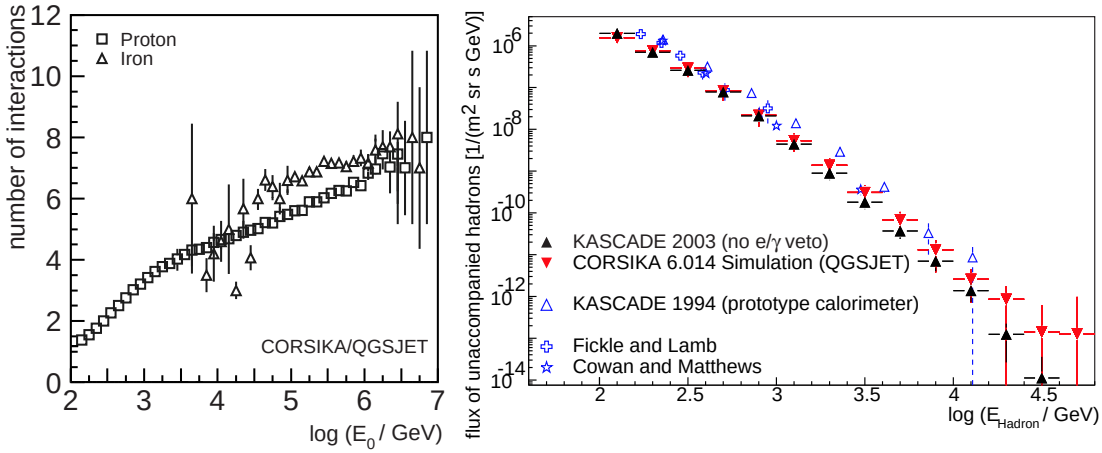

Fig. 1. Left: Number of interactions versus hadron energy at ground level. Right: Flux of unaccompanied hadrons at ground level.

stations to measure the electromagnetic and muonic shower components and a 16×20 m^2 hadron calorimeter [3]. With the calorimeter the energy, as well as the point and angle of incidence of individual hadrons are measured. Between October 1996 and October 2001 more than $3 \cdot 10^8$ events have been recorded with at least one reconstructed hadron in the calorimeter.

Accompanying simulations have been carried out using CORSIKA 6.014 with the GHEISHA and QGSJET01 hadronic interaction codes. In total about $2 \cdot 10^{10}$ events have been simulated in the energy range from 10^2 to $3 \cdot 10^6$ GeV for proton, helium, oxygen and iron induced air showers, using flux values of direct measurements according to a recent compilation [6]. All secondary particles reaching ground level have been treated with a GEANT-based detector simulation program.

3. Results

The average number of interactions in the atmosphere for unaccompanied hadrons registered in the calorimeter is plotted in Fig. 1. (left) versus their energy at ground level according to the CORSIKA simulations. As expected, the unaccompanied hadrons interact only a few times in the 11 interaction length thick atmosphere before they reach the detection level. Integrated over all relevant energies, the average number of interactions is 3.6 ± 1.9 for proton and 6.6 ± 2.3 for iron induced showers. Both values are smaller than the corresponding numbers for all air showers, i.e. 6.4 ± 1.8 for primary protons and 7.6 ± 2.2 for iron induced showers.

The measured flux of unaccompanied hadrons is presented in Fig. 1. (right) as function of energy. It is compared to simulations taking into account the flux values of direct measurements, as mentioned above. The measured and simulated flux values agree reasonable well. An interesting result, since the unaccompanied

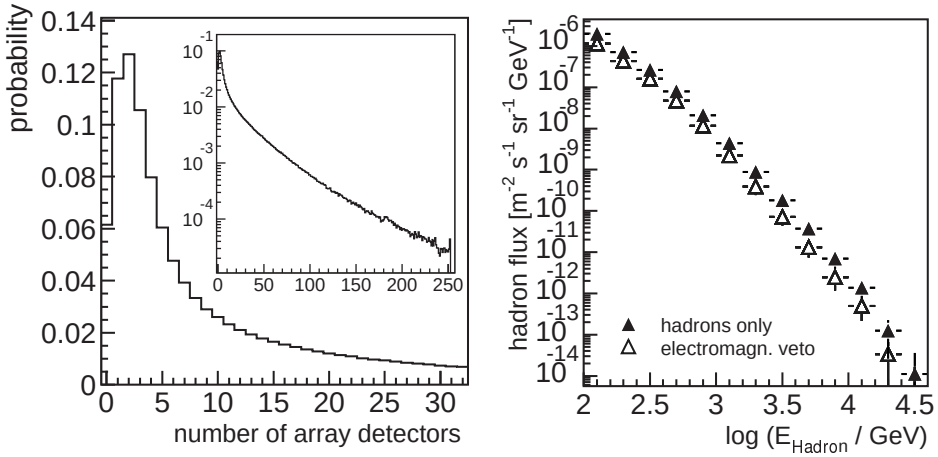

Fig. 2. Left: Number of electromagnetic detectors with $E_{dep} > 5$ MeV for unaccompanied hadrons. Right: Unaccompanied hadron spectrum including electromagnetic veto with $N_{e/\gamma}(E_{dep} > 5 \text{ MeV}) \leq 8$.

hadrons are a very special and untypical class of air shower events, sensitive to inelastic proton-air and pion-air cross-sections. The compatibility indicates that the interactions seem to be described correctly in the model QGSJET up to energies of 10^5 GeV. The flux obtained with the KASCADE prototype calorimeter [7] is somewhat larger as the present result due to the smaller surface of 6 m^2. The KASCADE calorimeter with 320 m^2 surface acts as efficient veto counter. Results from Fickle and Lamb [5] as well as Cowan and Matthews [2] exhibit a similar behavior, their flux values are slightly larger due to a smaller active area.

So far, unaccompanied hadrons were defined using the hadron calorimeter as veto counter against accompanying particles only. Additionally, the number $N_{e/\gamma}$ of electromagnetic detectors in the scintillator array with an energy deposit $E_{dep} > 5$ MeV can be used to identify accompanying particles. The measured probability distribution for $N_{e/\gamma}$ for events with one reconstructed hadron is depicted in Fig. 2. (left). In only 6% of the events no e/γ detector has a reasonable signal. For most of the "unaccompanied" hadrons, electrons are detected in the scintillator array, indicating that the definition of unaccompanied hadrons as one hadron only, as frequently used in the literature, is somehow arbitrary. The influence of the additional electromagnetic veto on the unaccompanied hadron spectrum is illustrated in Fig. 2. (right) for $N_{e/\gamma} \leq 8$. As expected, the absolute flux is reduced. The suppression is stronger for large hadron energies, originating from larger primary energies.

It is interesting to derive a primary energy spectrum form the measured flux of unaccompanied hadrons. The simulated number of events which initiate an unaccompanied hadron is shown in Fig. 3. (left) as function of primary energy for individual elemental groups. Up to 10^5 GeV unaccompanied hadrons originate mostly from primary protons. At larger energies the contamination with heavier

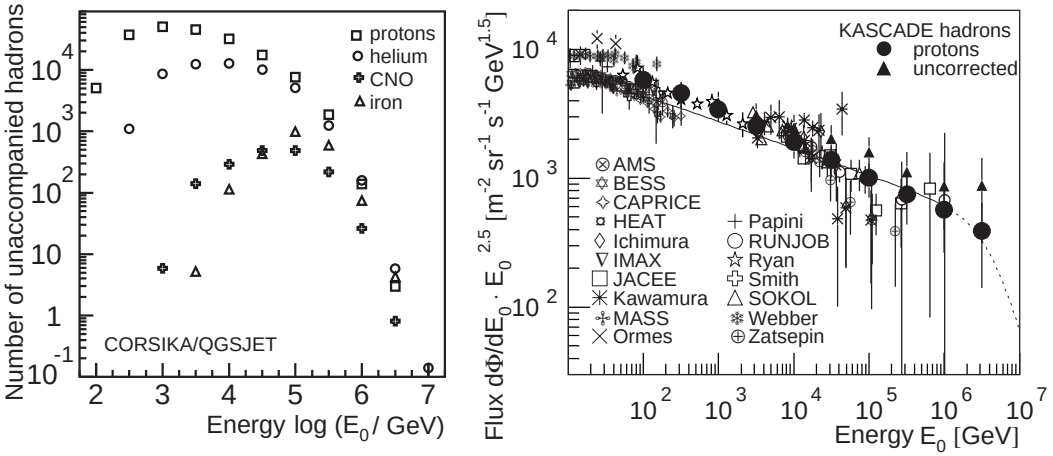

Fig. 3. Left: Number of unaccompanied hadrons versus primary energy for different elemental groups. Right: Primary proton flux reconstructed from unaccompanied hadrons compared to results of direct measurements, for references see [6]. The line represents a fit to the measurements [6].

elements is not negligible.

Based on the simulations the flux of unaccompanied hadrons has been converted to a primary flux at the top of the atmosphere. The result is shown in Fig. 3. (right) as filled triangles. The flux obtained should essentially coincide with direct measurements of the primary proton energy spectrum, shown in the figure as well. Subtracting the contribution of heavy elements, taking into account their abundances according to direct measurements, results in the filled circles, representing the flux of primary protons derived from unaccompanied hadrons. The correction amounts to less than 30%. No indication for a steepening in the proton spectrum between 10^4 and 10^5 GeV, as reported in the literature, can be seen from the derived flux. The derived proton spectrum agrees well with a parametrization of direct and indirect measurements [6], represented as solid and dotted lines. The agreement between the derived proton spectrum and the direct measurements seems to indicate that the underlying physics processes are reasonable well described in the simulation codes up to energies of 10^6 GeV.

References

[1] Antoni T. et al., The cosmic-ray experiment KASCADE, subm. to Nucl. Instr. and Meth.

[2] Cowan E.W. and Matthews K., Phys. Rev. D 4 (1971) 37.

[3] Engler J. et al., Nucl. Instr. and Meth. A 427 (1999) 528.

[4] Heck D. et al., Report FZKA 6019, Forschungszentrum Karlsruhe, 1998

[5] Fickle R.K. and Lamb R.C., Lett. al Nuovo Cimento 25 (1979) 289.

[6] Hörandel J.R., Astropart. Phys. 19 (2003) 193.

[7] Mielke H.-H. et al., J. Phys. G 20 (1994) 637.

Investigation of Geometrical Structures in the Hadronic Shower Core

A. Iwan[5], T. Antoni[1], W.D. Apel[2], F. Badea[1,a], K. Bekk[2], A. Bercuci[2,a], H. Blümer[1,2], H. Bozdog[2], I.M. Brancus[3], C. Büttner[1], A. Chilingarian[4], K. Daumiller[1], P. Doll[2], R. Engel[2], J. Engler[2], F. Feßler[2], H.J. Gils[2], R. Glasstetter[1,b] A. Haungs[2], D. Heck[2], J.R. Hörandel[1], K-H. Kampert[1,2,b] H.O. Klages[2], G. Maier[2], H.J. Mathes[2], H.J. Mayer[2], J. Milke[2], M. Müller[2], R. Obenland[2], J. Oehlschläger[2], S. Ostapchenko[1,c], M. Petcu[3], H. Rebel[2], M. Risse[2], M. Roth[1], G. Schatz[2], H. Schieler[2], J. Scholz[2], T. Thouw[2], H. Ulrich[2], J. van Buren[2], A. Vardanyan[4], A. Weindl[2], J. Wochele[2], J. Zabierowski[5]

(1) Institut für Exp. Kernphysik, Universität Karlsruhe, 76021 Karlsruhe, Germany
(2) Institut für Kernphysik, Forschungszentrum Karlsruhe, 76021 Karlsruhe, Germany
(3) National Institute of Physics and Nuclear Engineering, 7690 Bucharest, Romania
(4) Cosmic Ray Division, Yerevan Physics Institute, Yerevan 36, Armenia
(5) Soltan Institute for Nuclear Studies, 90950 Lodz, Poland
[a] *on leave of absence from (3)*
[b] *now at: Universität Wuppertal, 42097 Wuppertal, Germany*
[c] *on leave of absence from Moscow State University, 119899 Moscow, Russia*

Abstract

The geometrical structure of high-energy hadrons in shower cores measured with the KASCADE calorimeter is analyzed. The angular correlation, especially the degree of alignment, is quantified by means of the commonly used parameter λ_4. The λ_4 distribution obtained by KASCADE is comparable to that derived by other experiments. The analysis shows that the observed λ_4 distribution is not linked to angular correlations due to jet production at high energies. The dependence on the transverse momentum p_t in the simulation of hadronic interactions is marginal. In contrast to λ_4, the maximum distance d_4^{max} between the most-energetic hadrons reveals a sensitivity both on p_t and the primary mass.

1. Introduction

High-energy hadrons in the cores of extensive air showers offer a unique possibility to study interaction features well beyond the kinematic and energy region of earthbound colliders. At primary energies around and above the *knee*, the observation of aligned structures in air showers has motivated many experimental and theoretical investigations, including discussions about sensitivity to specific interaction features as jet formation or hints to new physics (see e.g. [2,4] and references therein). The degree of alignment is commonly described by the parameter λ_4 quantifying the angular correlation between the four most-energetic

pp. 1–4

particles (or particle families)

$$\lambda_4 = \frac{1}{24} \cdot \sum_{i \neq j \neq k}^{4} \cos 2\varphi_{ij}^{k} \tag{1}$$

where φ_{ij}^{k} denotes the angle between the connecting lines of hadron k to i and j. Possible values range between $\lambda_4 = -\frac{1}{3}$ (isotropic distribution) and $\lambda_4 = 1$ (perfect alignment). Events are usually termed "elongated" for $\lambda_4 \geq 0.8$. Another observable is the distance d_4^{max}, which is defined as the maximum distance between one of the four considered hadrons to the geometric center of the other three. As this quantity is correlated to the hadron lateral distribution, some sensitivity to hadronic interaction features can be expected. In the following, both observables will be analyzed using KASCADE [1] data and CORSIKA [5] simulations.

2. Data Preparation

The shower size, direction, and core position are determined by the KASCADE array. Only events with the core well contained in the hadron calorimeter [3] are accepted; additionally, at least four hadrons with energies $\geq$100 GeV have to be reconstructed. Using data from May 1998 to April 2001, 4489 events survived the cuts. After transformation to the shower plane, λ_4 is evaluated for each event. Simulations have been performed with CORSIKA using the QGSJET01 [7] hadronic interaction model for proton and iron induced showers for a primary energy slope of -2.7, followed by a detailed detector simulation.

3. Results

In Fig. 1a, good agreement of simulations and measurement can be seen, especially for elongated events. Despite the much smaller energy per nucleon in case of iron showers, no significant difference between proton and iron induced showers is observed. To investigate the correlation between λ_4 and jet production in high-energy interactions, the azimuth angles of the four hadron positions in each event were sampled randomly. The KASCADE data could be reproduced if the lateral distribution of these hadrons follows the measured one (see Fig. 1b, label "RANDOM"). More detailed studies revealed that even unphysical changes in p_t assumed in shower simulations for the secondary particle production only marginally influence the λ_4 distribution [6].

The λ_4 distributions measured by KASCADE and the emulsion chamber experiment PAMIR [2] agree to each other (Fig. 1c), although PAMIR is located at high altitude and the data refer to so-called "gamma families" with a higher energy threshold. Finally, within the statistical uncertainties no energy dependence of the rate of elongated events could be found (Fig. 1d).

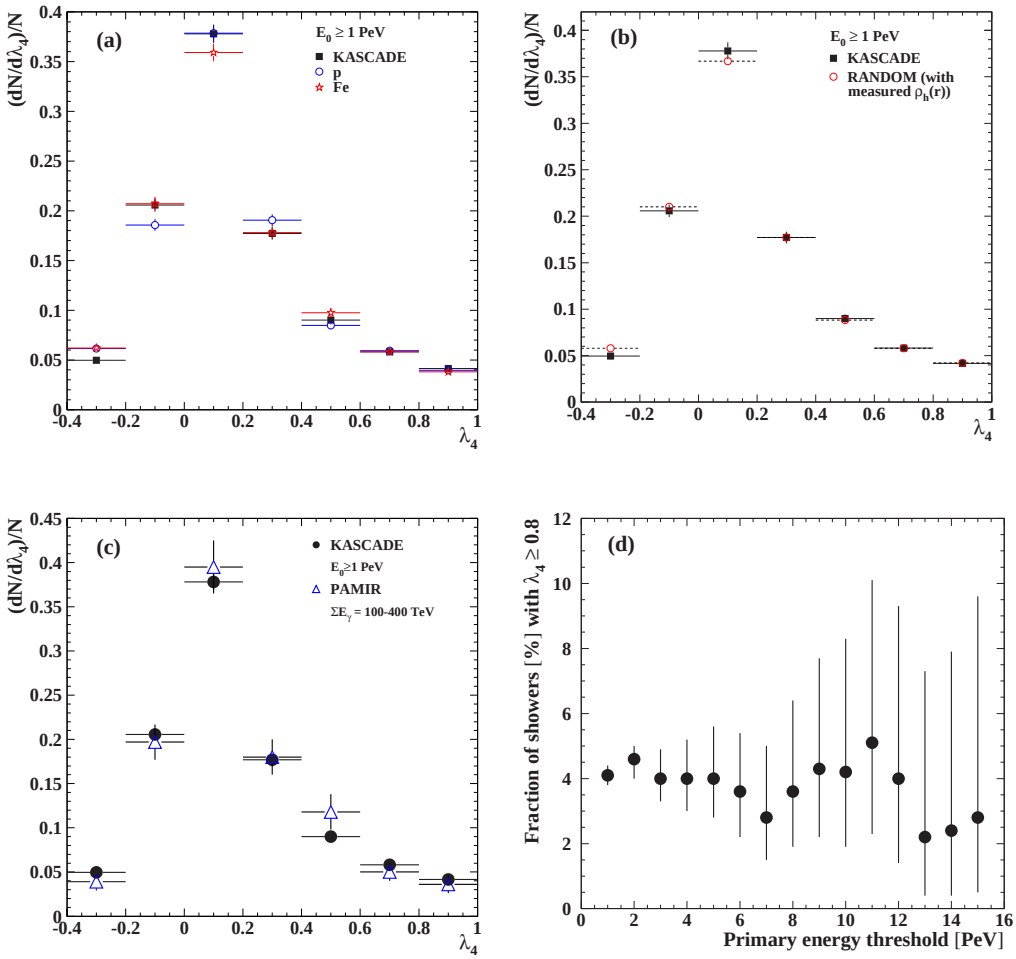

Fig. 1. λ_4 distributions: KASCADE data and (a) CORSIKA/QGSJET01 simulations for primary proton and iron showers, (b) random distribution based on the measured hadron lateral distribution, (c) PAMIR data [2]. In (d), the fraction of elongated events measured at KASCADE is plotted versus the primary energy.

The same KASCADE and CORSIKA data sets have been used to evaluate d_4^{max}. In Fig. 2a, the d_4^{max} distribution is given for the measurement and for simulations. The decrease towards larger d_4^{max} is enhanced by the limited detector size. A clear separation between proton and iron induced events is visible with the KASCADE data in between. The sensitivity of d_4^{max} to the primary mass can be used as cross-check of composition assumptions obtained for a given hadronic interaction model [6]. Moreover, d_4^{max} turned out to be quite sensitive to the p_t values employed in the hadron production. Simulation results are shown in Fig. 2b for a fixed primary energy of 5 PeV. Increasing (arbitrarily) p_t in secondary hadron production by a factor 2 clearly shifts the distributions towards larger d_4^{max} values. The average d_4^{max} values move for proton induced events from 3.4 m to 5.2 m and for iron induced showers from 4.8 m to 6.7 m.

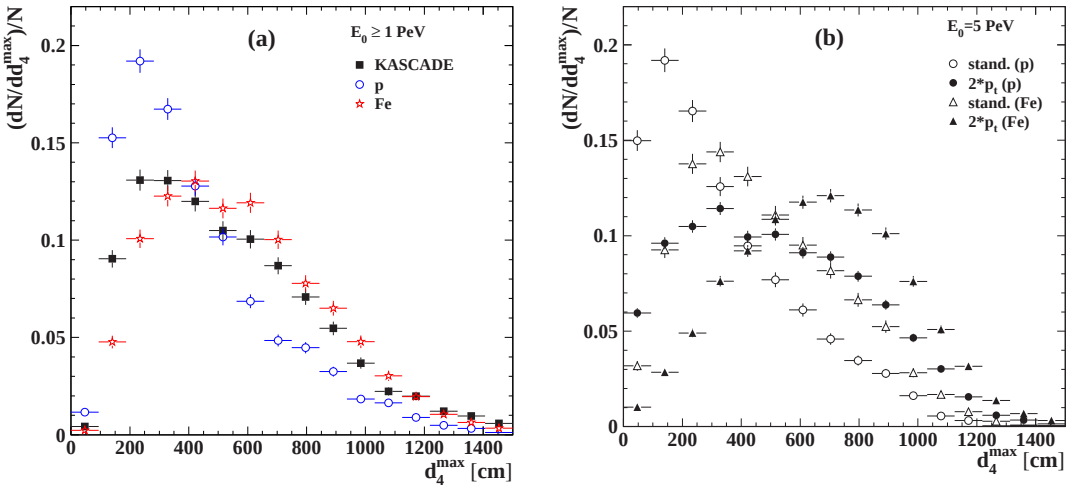

Fig. 2. d_4^{max} distributions: (a) KASCADE data compared with CORSIKA/QGSJET simulations for proton and iron showers, (b) CORSIKA simulations with standard and modified p_t (see text) for proton and iron showers of fixed primary energy.

4. Conclusion

The λ_4 distribution and the rate of elongated events of high-energy hadrons measured with KASCADE are well reproduced by simulations. They follow the expectations from a random azimuth distribution satisfying the measured hadron lateral distribution. No significant dependence on hadronic interaction features, in particular jet production at high energy, was found. No primary energy effect has been observed. In contrast, the d_4^{max} distribution is sensitive to the primary particle mass and the mean transverse momentum of secondaries in hadronic interactions. It can be used for consistency checks in composition analyses.

Acknowledgments. The work was partly supported by KBN grant 5P03B 13320.

References

1. Antoni T. et al., KASCADE Collaboration 2003, Nucl. Instr. Meth., submitted
2. Borisov A.S. et al. 1997, Nucl. Phys. B (Proc. Suppl.) 52B, 218; Capdevielle J.N., Slavatinsky S.A. 1999, Nucl. Phys. B (Proc. Suppl.) 75A, 12
3. Engler J. et al. 1999, Nucl. Instr. Meth. A 427, 528
4. Halzen F., Morris D.A. 1990, Phys. Rev. D 42, 1435
5. Heck D. et al. 1998, Report FZKA 6019, Forschungszentrum Karlsruhe
6. Iwan A. 2003, PhD thesis, University of Lodz (in Polish)
7. Kalmykov N.N. et al. 1997, Nucl. Phys. B (Proc. Suppl.) 52B, 17

Muon Production Height from the Muon Tracking Detector in KASCADE

C. Büttner[1], T. Antoni[1], W.D. Apel[2], F. Badea[1,a], K. Bekk[2], A. Bercuci[2,a], H. Blümer[1,2], H. Bozdog[2], I.M. Brancus[3], A. Chilingarian[4], K. Daumiller[1], P. Doll[2], R. Engel[2], J. Engler[2], F. Feßler[2], H.J. Gils[2], R. Glasstetter[1,b] A. Haungs[2], D. Heck[2], J.R. Hörandel[1], A. Iwan[5], K-H. Kampert[1,2,b] H.O. Klages[2], G. Maier[2], H.J. Mathes[2], H.J. Mayer[2], J. Milke[2], M. Müller[2], R. Obenland[2], J. Oehlschläger[2], S. Ostapchenko[1,c], M. Petcu[3], H. Rebel[2], M. Risse[2], M. Roth[1], G. Schatz[2], H. Schieler[2], J. Scholz[2], T. Thouw[2], H. Ulrich[2], J. van Buren[2], A. Vardanyan[4], A. Weindl[2], J. Wochele[2], J. Zabierowski[5]

(1) Institut für Exp. Kernphysik, Universität Karlsruhe, 76021 Karlsruhe, Germany
(2) Institut für Kernphysik, Forschungszentrum Karlsruhe, 76021 Karlsruhe, Germany
(3) National Institute of Physics and Nuclear Engineering, 7690 Bucharest, Romania
(4) Cosmic Ray Division, Yerevan Physics Institute, Yerevan 36, Armenia
(5) Soltan Institute for Nuclear Studies, 90950 Lodz, Poland
[a] *on leave of absence from (3)*
[b] *now at: Universität Wuppertal, 42097 Wuppertal, Germany*
[c] *on leave of absence from Moscow State University, 119899 Moscow, Russia*

Abstract

The Muon Tracking Detector (MTD; E_μ^{th}=0.8 GeV) [5] of the KASCADE-Grande experiment enables the analysis of the longitudinal shower development by means of the Muon Production Height (MPH). The analysis employes radial and tangential angles of the muon track with respect to the shower direction, and the distance of the muon hit to the shower core. Comparing analysed MPH distributions with Monte Carlo simulations (CORSIKA) [6] an increase of $\langle ln\ A \rangle$ of the primary cosmic rays with $\lg(N_\mu^{tr})$ is observed.

1. Radial and Tangential Angles

Due to transverse momentum of pions in EAS, causing a displacement of the origin of muons from the shower axis, and due to multiple scattering in the atmosphere, muons form an angle in space with the shower axis. To describe the orientation of muon tracks with respect to the shower axis, radial and tangential angles are employed [3]. Zabierowski et al. [8] investigate a transformation of those angles into a pseudorapidity type quantity for shower muons. Both angles are studied with respect to $\lg(N_\mu^{tr})$ which corresponds to the total number of muons that are within 40-200m of the KASCADE array and which represents [7] an approximate energy estimator of the primary cosmic ray.

pp. 1–4

The tangential angle provides a measure of the transverse displacement of the muon direction with respect to the shower axis. The tangential angle distribution is symmetric around zero and exhibits a narrow Gaussian distribution sitting on a broad distribution. The narrow component is attributed to the combined effect of the MTD-Array angle resolution. CORSIKA simulations allow to derive the contribution from multiple scattering in the atmosphere for muons which amounts to 0.5-0.2° for muon energies between 1-10GeV. For large values of $\lg(N_\mu^{tr})$ of about 5, the width of the narrow Gaussian approaches 0.3°. To reduce the influence of low energy particles the tangential angle was limited to ±0.7° for the analysis.

The distributions of radial angles are asymmetric as shown in Fig. 1 (left) because the radial angle is directly correlated with the MPH. With larger muon number $\lg(N_\mu^{tr})$, i.e. larger energy [7], the mean radial angle Fig.1 (right) moves to higher values as the shower maximum develops deeper into the atmosphere.

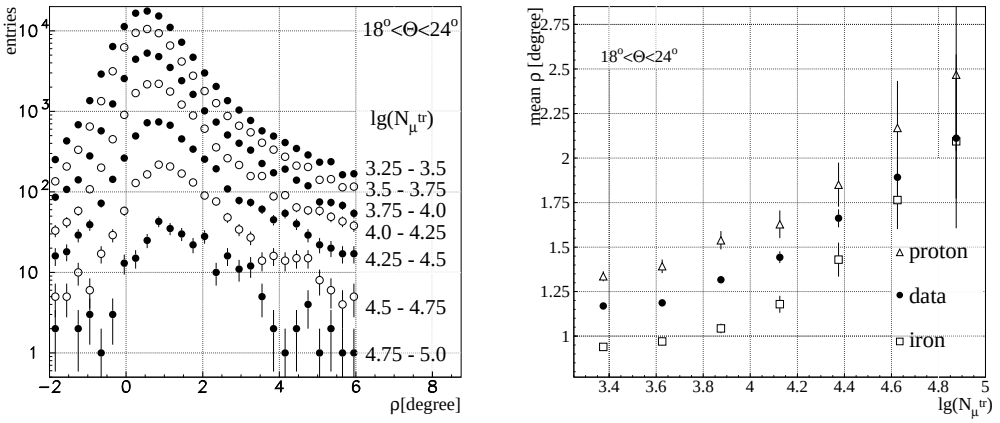

Fig. 1. Radial angle distributions and their mean value dependence on $lg(N_\mu^{tr})$

1.1. Analysis

Shower simulations are based on the CORSIKA program (version 5.644 with QGSJet(1998) and version 5.948 with NEXUS2) and are followed by simulations of the detector elements of the Array and the MTD. In the energy range of 10^{14}eV to 10^{17}eV with zenith angles up to 42° about 560000 showers each for proton, and iron have been simulated in the case of QGSJet and about 360000 showers each in the case of NEXUS. All simulations were done with an $E^{-2.0}$ differential flux spectrum [4] and appropriate event weights (e.g. $\propto E^{-0.7}$) were applied to match the spectrum in the energy region below the knee.

As QGSJet and NEXUS exhibit only few percent differences in the observables presented here, Figs. 1 and 2 (right) show only comparisons with NEXUS

calculations. The Monte Carlo simulations show that, in average, proton induced EAS penetrate deeper in the atmosphere than iron induced EAS at same primary energy. The distributions of radial angles that are plotted in Fig. 1 exhibit a tail to negative values but for calculation of MPH (h_μ in Fig. 2) only positive values of radial angles are used. Further analyses should investigate the influence of negative radial angles on MPH distributions, also with respect to the finite angle resolution of the MTD-Array system.

2. Production Height

The MPH is calculated by triangulation, and taking into account the displacement (tangential angle) of the muons from the shower axis. In Fig. 2 MPH distributions and their mean value dependence on $lg(N_\mu^{tr})$ are shown. The measured distributions (left) are described by weighted distributions of proton and iron simulations. The measured mean values Fig. 2 (right) exhibit a trend from the the proton to the iron simulations with increasing $lg(N_\mu^{tr})$.

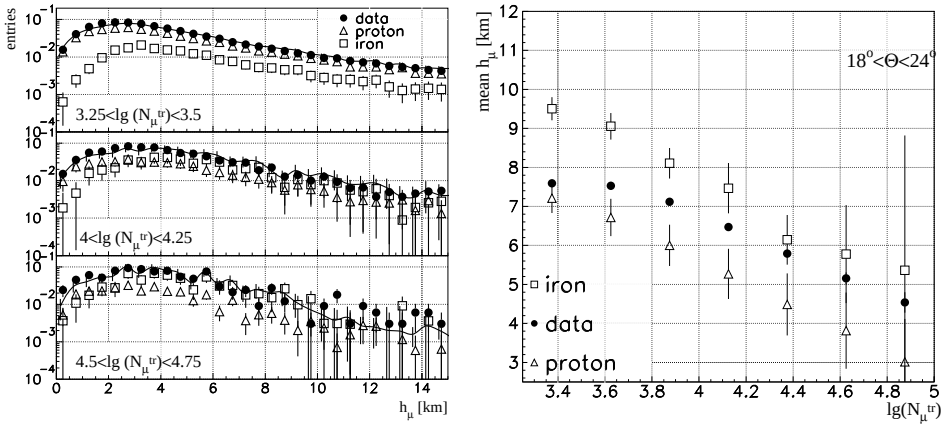

Fig. 2. Production height distributions and their mean value dependence on $lg(N_\mu^{tr})$

3. Production Depth

Comparing the mean radial angles in Fig. 1 (right) and the mean h_μ (MPH) in Fig. 2 (right) with CORSIKA simulations, an increase of $\langle ln\ A \rangle$ of the primary cosmic rays with $lg(N_\mu^{tr})$ is derived as presented in Fig. 3 (left). Badea et al. [2] investigate the influence of the muon track observables on the cosmic ray composition in a Bayesian approach.

In Fig. 3 (right) an atmospheric depth – calculated by using the MPH and the values of the US-standard-atmosphere – in dependence on primary energy [7] is shown. The mean muon production depth (MPD) can be compared with the

mean atmospheric depth deduced from Čerenkov light [1], which is assumed to represent the depth of the maximum shower development. Those experiments seem to reveal a deeper maximum shower development than the findings with the MTD. The muon tracking analysis may be more sensitive to higher energy interactions in the earlier steps of the shower development. The experiments lie between the boundaries of the simulations, each.

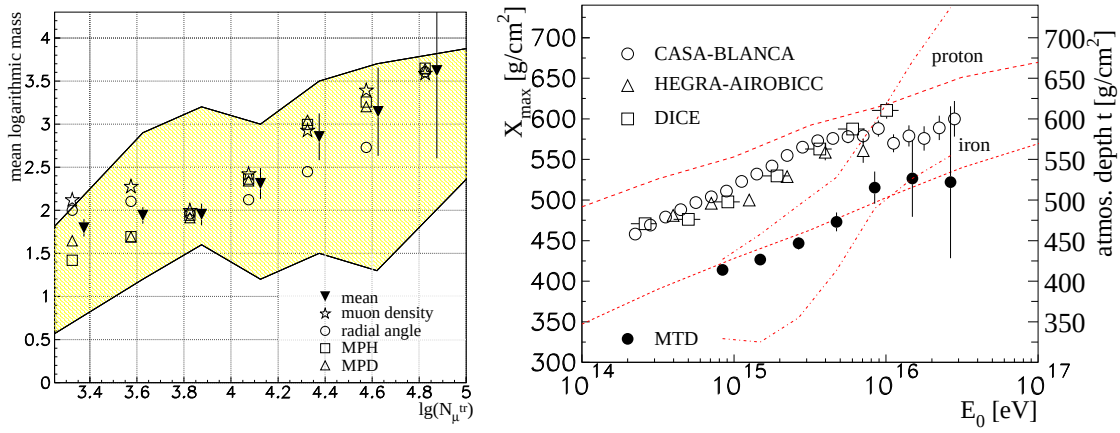

Fig. 3. Mean mass (preliminary) within the range of previous analyses and X_{max} and muon production depth within model (QGSJet) predictions, each.

4. Conclusion

The MTD of the KASCADE-Grande experiment enables the analysis of the longitudinal shower development by means of the MPH. In the meantime the MTD has been upgraded for improved track resolution valuable for high energy muons which are selected by narrow tangential angle cuts.

1. Arqueros F. et al., Astron. and Astrophys. **359**(2000)682, Swordy S.P. et al., Astropart. Phys. **13**(2000)137
2. Badea F. et al., Proc. 28^{th} ICRC, Tsukuba, these proceedings
3. Bernlöhr K., Astropart. Phys. **5**(1996)139
4. Burnett T.H. et al., Astrophys. J. **349**(1990)L25
5. Doll P. et al., Nucl. Instr. Meth. **A**488(2002)517
6. Heck D. et al., FZKA 6019, Forschungszentrum Karlsruhe (1998)
7. Weber J.H. et al., Proc. 25^{th} ICRC, Durban, Vol. 6, p. 153, 1997
8. Zabierowski J., et al. Proc. 28^{th} ICRC, Tsukuba, these proceedings

Test of a Hadronic Interaction Model by a Multidimensional Analysis of Lateral and Longitudinal Air-Shower Observables at KASCADE

F. Badea[1,a], T. Antoni[1], W.D. Apel[2], K. Bekk[2], A. Bercuci[2,a], H. Blümer[1,2], H. Bozdog[2], I.M. Brancus[3], C. Büttner[1], A. Chilingarian[4], K. Daumiller[1], P. Doll[2], R. Engel[2], J. Engler[2], F. Feßler[2], H.J. Gils[2], R. Glasstetter[1,b] A. Haungs[2], D. Heck[2], J.R. Hörandel[1], A. Iwan[5], K-H. Kampert[1,2,b], H.O. Klages[2], G. Maier[2], H.J. Mathes[2], H.J. Mayer[2], J. Milke[2], M. Müller[2], R. Obenland[2], J. Oehlschläger[2], S. Ostapchenko[1,c], M. Petcu[3], H. Rebel[2], M. Risse[2], M. Roth[1], G. Schatz[2], H. Schieler[2], J. Scholz[2], T. Thouw[2], H. Ulrich[2], J. van Buren[2], A. Vardanyan[4], A. Weindl[2], J. Wochele[2], J. Zabierowski[5]

(1) Institut für Exp. Kernphysik, Universität Karlsruhe, 76021 Karlsruhe, Germany
(2) Institut für Kernphysik, Forschungszentrum Karlsruhe, 76021 Karlsruhe, Germany
(3) National Institute of Physics and Nuclear Engineering, 7690 Bucharest, Romania
(4) Cosmic Ray Division, Yerevan Physics Institute, Yerevan 36, Armenia
(5) Soltan Institute for Nuclear Studies, 90950 Lodz, Poland
[a] *on leave of absence from (3)*
[b] *now at: Universität Wuppertal, 42097 Wuppertal, Germany*
[c] *on leave of absence from Moscow State University, 119899 Moscow, Russia*

Abstract

The multi-detector experiment KASCADE enables simultaneous observations of parameters describing the lateral and longitudinal development of Extensive Air Showers. The present analysis is focused on Field Array and Muon Tracking detectors of KASCADE. The Field Array (FA) provides the numbers of electrons and muons in the shower and the Muon Tracking Detector (MTD) measures angles-of-incidence of muons which are related to the longitudinal development of EAS. An identical two step deconvolution method (on primary mass using a Bayesian approach and on primary energy) is performed to calculate the primary mass and energy of cosmic rays using the correlation of FA observables only and by adding MTD observables. The consistency of the CORSIKA/QGSJET simulation code in describing the correlation between lateral and longitudinal developments of the shower is studied by comparing the results obtained from the two sets of observables.

1. FA and MTD Observables

The KASCADE experiment [2] allows extensive air-shower measurements in the primary energy range around the *knee*. The FA consists of shielded and

pp. 1–??

unshielded scintillation detectors measuring the electromagnetic and muonic components with 5 MeV and 230 MeV energy thresholds, respectively. FA provides the basic information about the arrival direction (θ, ϕ) and core position as well as the numbers of muons (N_μ) and electrons (i.e. *shower size* N_e) of the observed EAS. Additionally, the so-called *truncated number of muons* (N_μ^{tr}) is derived, i.e. number of muons between 40 and 200 m distance from the shower core. At KASCADE N_μ^{tr} is used as an approximate primary energy estimator. The Muon Tracking Detector [6] detects muons with 0.8 GeV energy threshold. The MTD consists of 16 towers of 3 horizontal modules (limited streamer tubes) each. There is a strong correlation between the longitudinal development of the muonic component and the radial angles [4] of the muon incidence with respect to the shower axis. For a multiplicity $n \geq 1$ of muons reconstructed from 3-hit-tracks at the 128 m^2 sensitive area of the MTD, two observables of interest are calculated on an event-by-event basis: *mean distance* $(r_{\mu mean})$ of the MTD muons to the shower axis and the *median radial angle* $(\rho_{0.50})$, i.e. the median value [1] of the radial angle distribution.

2. Experimental and Simulated Data

An amount of 40 million EAS events observed with KASCADE has been analysed. The experimental sample shrunk to 600 000 showers after applying the following cuts: $\theta < 40°$, distance between shower core and FA center below 90 m, $3.4 < log_{10} N_\mu^{tr} < 5.4$ and at least one muon track in the MTD. Simulations have been performed with the code CORSIKA (version 5.62) [8] with a full and detailed simulation of the detector response. QGSJET (version 1998) model [9] has been used as generator for high-energy hadronic interactions and GHEISHA [7] for interactions below $E_{lab} = 80$ GeV. The electromagnetic part is treated by the EGS4 program [10]. Around 500 000 showers have been simulated for each of the 4 primaries (proton H, Helium He, Oxygen O and Iron Fe) in the primary energy range from 10^{14} up to 10^{18} eV with a spectral index $\gamma = -2.0$.

3. Primary Mass Discrimination

A non-parametric multivariate analysis has been used for separating different primary masses [5]. The *true-classification* P_{ii} and *misclassification* P_{ij} $(i \neq j)$ probabilities have been calculated for a classification procedure based on Bayes decision rule $(i, j \in \{H, (He), C, Fe\})$. Fig. 1 shows the variation with $log_{10} N_\mu^{tr}$ of the geometrical mean values of the true-classification probabilities for 3 zenith angle ranges and for the cases of classification in 3 and 4 primary masses. A systematic improvement for the primary mass discrimination has been obtained by adding the MTD observables $\{r_{\mu mean}, \rho_{0.50}\}$ to the basic correlation $\{N_\mu^{tr}, N_e\}$ provided by the FA.

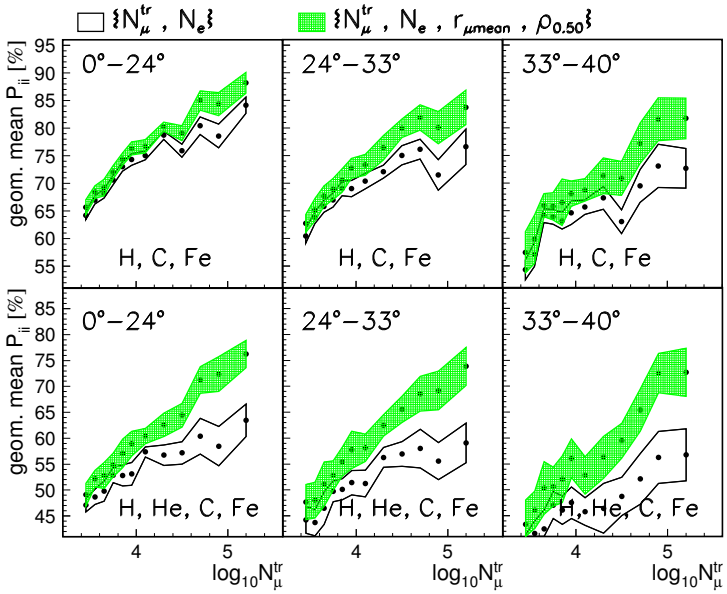

Fig. 1. The dependence of the geometrical mean values of P_{ii} on $log_{10}N_\mu^{tr}$.

4. Test of the Monte Carlo Simulation Procedures

The reconstruction of the primary mass composition depends on the high-energy hadronic interaction model generating the Monte Carlo simulations. An opportunity to test the internal consistency of a model is to derive the primary mass composition(s) by the analysis of different sets of observables. The test is based on primary mass compositions reconstructed by FA observables only and by taking into account the correlation of FA&MTD observables which have to be identical after applying all correction factors. The true-classification and misclassification probabilities, deduced for the 3 zenith angle ranges and for 12 (non-equal) bins of $log_{10}N_\mu^{tr}$, have been used for the reconstruction of the *experimental* sample compositions. Fig. 2A shows the results for 2 zenith angle ranges and 3 primary masses, for FA observables only (upper panel) and for FA&MTD correlation (lower panel). The *statistical* errors shown in all figures have been calculated using a bootstrap method [5]. A good agreement between the sample mass compositions reconstructed for the two sets of observables was found. But differences of the results are revealed by comparing various zenith angle ranges, which can be explained by different acceptance efficiencies for the different primaries [3]. Using simulations, the acceptance matrices have been calculated for each zenith angle range and primary type. These matrices contain for each primary energy bin the fraction of the primaries contributing to different N_μ^{tr} bins. A second deconvolution, on primary energy, has been done by combining the experimental sample compositions (Fig. 2A) with these acceptance matrices. The results of the deconvolution are displayed in Fig. 2B as primary mass compositions (up to a normalisation constant) unified over all 3 zenith angle ranges. The primary mass

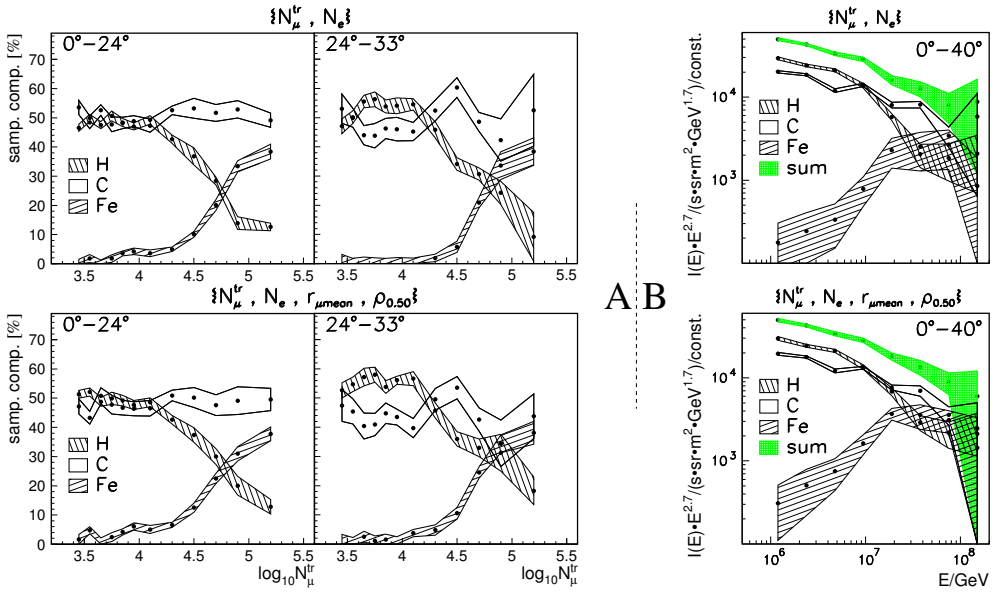

Fig. 2. Experimental sample compositions (A) and primary mass composition (B).

compositions based on the two sets of observables look very similar within the limits of the statistical uncertainties.

5. Conclusions

An improvement of the primary mass discrimination has been found by adding the muon angles-of-incidence to the Field Array information of shower size and number of muons. The behaviours of the total primary spectrum and primary mass composition seen by the present analysis confirm earlier published KASCADE results. The invariance of the primary mass composition with respect to the two sets of observables (FA only and FA&MTD) proves the consistency of the CORSIKA/QGSJET simulation code in describing the threefold correlation shower size - number of muons - longitudinal muon development, but is not a proof on the description of the absolute numbers of muons and electrons in the model.

1. Antoni T. et al. - KASCADE Collaboration 2001, Astropart. Phys. 15, 149
2. Antoni T. et al. - KASCADE Collaboration, submitted to Nucl. Instr. Meth. A
3. Antoni T. et al. - KASCADE Collaboration 2003, Astropart. Phys. 18, 319
4. Büttner C. et al. - KASCADE Collaboration 2003, these Proceedings
5. Chilingarian A.A. 1989, Comp. Phys. Comm. 54, 381
6. Doll P. et al. 2002, Nucl. Instr. Meth. A 488, 517
7. Fesefeldt H. 1985, Report PITHA - 85/02, RWTH Aachen
8. Heck D. et al. 1998, Report FZKA 6019, Forschungszentrum Karlsruhe
9. Kalmykov N.N. et al. 1997, Nucl. Phys. B (Proc. Suppl.) 52B, 17
10. Nelson W.R. et al. 1985, Report SLAC-265, Stanford Lin. Acc. Center

Investigation of the Muon Pseudorapidities in EAS with the Muon Tracking Detector of the KASCADE Experiment

J. Zabierowski[5], T. Antoni[1], W.D. Apel[2], F. Badea[1,a], K. Bekk[2], A. Bercuci[2,a], H. Blümer[1,2], H. Bozdog[2], I.M. Brancus[3], C. Büttner[1], A. Chilingarian[4], K. Daumiller[1], P. Doll[2], R. Engel[2], J. Engler[2], F. Feßler[2], H.J. Gils[2], R. Glasstetter[1,b] A. Haungs[2], D. Heck[2], J.R. Hörandel[1], A. Iwan[5], K-H. Kampert[1,2,b] H.O. Klages[2], G. Maier[2], H.J. Mathes[2], H.J. Mayer[2], J. Milke[2], M. Müller[2], R. Obenland[2], J. Oehlschläger[2], S. Ostapchenko[1,c], M. Petcu[3], H. Rebel[2], M. Risse[2], M. Roth[1], G. Schatz[2], H. Schieler[2], J. Scholz[2], T. Thouw[2], H. Ulrich[2], J. van Buren[2], A. Vardanyan[4], A. Weindl[2], J. Wochele[2]

(1) Institut für Exp. Kernphysik, Universität Karlsruhe, 76021 Karlsruhe, Germany
(2) Institut für Kernphysik, Forschungszentrum Karlsruhe, 76021 Karlsruhe, Germany
(3) National Institute of Physics and Nuclear Engineering, 7690 Bucharest, Romania
(4) Cosmic Ray Division, Yerevan Physics Institute, Yerevan 36, Armenia
(5) Soltan Institute for Nuclear Studies, 90950 Lodz, Poland
[a] *on leave of absence from (3)*
[b] *now at: Universität Wuppertal, 42097 Wuppertal, Germany*
[c] *on leave of absence from Moscow State University, 119899 Moscow, Russia*

Abstract

High angular accuracy of muon track measurements in KASCADE Muon Tracking Detector (MTD), together with the high precision in determination of the shower direction and shower core position, allow to investigate the pseudorapidity of muons in EAS using the concept of radial and tangential angles. Preliminary results of the pseudorapidity distribution of muons registered by the KASCADE experiment are presented. Mean muon pseudorapidity values at different stages of the longitudinal development of the EAS cascade are calculated using additionally the reconstructed muon production height provided by the MTD data. Experimental results are compared with Monte Carlo simulations.

1. Introduction

The KASCADE experiment [1] with its large Muon Tracking Detector (MTD) [4] allows to measure directions of muons in air showers using the concept of tangential (τ) and radial (ρ) angles [2,3]. This directional information, as shown in [9], gives also possibility to investigate momentum components of shower muons and, in particular, their pseudorapidities. The parameter ζ, a certain combination of τ and ρ introduced in [9], is equal to the ratio of transversal to longitudinal momentum components of the muon with respect to the shower direction (for

pp. 1–4

$|\tau| \leq 0.4$ rad and $|\rho| \leq 0.4$ rad):

$$\zeta \equiv \sqrt{\tau^2 + \rho^2} = \frac{p_t}{p_\parallel} \tag{1}$$

Hence, the pseudorapidity η of muons with energy > 0.8 GeV (MTD threshold) can be expressed as follows:

$$\eta = \ln \frac{2 \times p_\parallel}{p_t} \approx -\ln \frac{\zeta}{2} \tag{2}$$

2. Results and discussion

For the analysis KASCADE data registered in the period between November 2000 and October 2002 have been used. In addition, showers simulated with CORSIKA [7] (v.5.644 using QGSJet98 [8] and v.5.946 using neXus2 [5] - with GHEISHA [6] for low energy hadronic interactions in both cases) and full detector Monte Carlo (CRES 1.15/08) were used for testing model predictions. All simulations were done with differential energy spectrum index -2.0 and events were weighted to match the experimental spectrum index -2.7 in the energy region below the knee. No knee structure was assumed here. Muon tracks were measured in the range 20 - 160 m from the shower axis. Only showers with zenith angle $\theta \leq 22^\circ$ were considered.

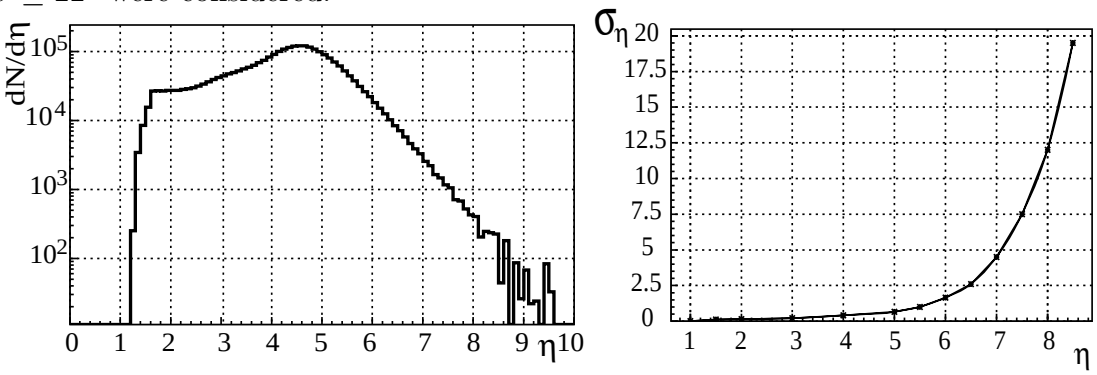

Fig. 1. Pseudorapidity distribution of EAS muons registered in MTD (left) and error in determination of η as a function of η value (right).

In Fig. 1. pseudorapidity (η) distribution of muons (in shower coordinates) registered by KASCADE for all N_μ^{tr} values is plotted. With respect to the pure CORSIKA results [9] the 20 m distance limit reduces the number of entries in the range of high rapidities and cuts away values above 9.5. In the lower end of the distribution the limits on τ and ρ values, as well as 160 m muon-shower core distance limit, show their influence. Even with very good KASCADE resolution of shower direction ($\approx 0.2^\circ$) and muon track ($\approx 0.35^\circ$) the errors in determination of $\eta \geq 6$ (see Fig. 1) become prohibitively large. However, due to large statistics,

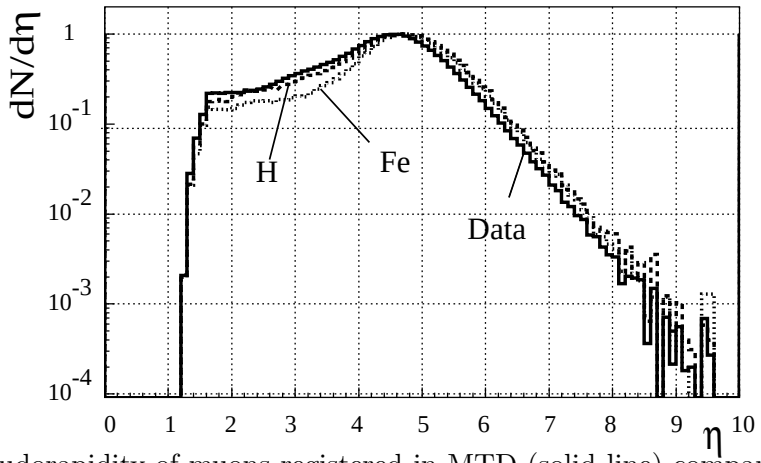

Fig. 2. Pseudorapidity of muons registered in MTD (solid line) compared with simulations using QGSJet model for two primary types: protons (dashed) and iron nuclei (dotted).

errors of mean values are still very small and up to $\eta \approx 8.5$ mean pseudorapidity can be investigated. As an example, in Fig. 2., the pseudorapidity distributions of EAS muons for all N_μ^{tr} values (normalized to the maximum) were compared with the simulations. No differences between results of the two models used were found, so only QGSJet distributions are shown. One observes a shift of the experimental distribution towards lower values with respect to the simulated ones. It may indicate, either underestimation of the mean muon transverse momentum in the parent meson decay reaction or/and overestimation of the longitudinal momentum component of created muons. In the large psedorapidity region (above the maximum) one finds no sensitivity of this variable to the primary mass. On the contrary, below $\eta \leq 4.5$ simulations predict different behaviour of the distribution for protons and iron nuclei.

The pseudorapidity distribution of muons registered on ground is only slightly shifted towards lower values with respect to the distribution at creation. Therefore, it may be a useful probe of high energy hadronic interactions in which pions and kaons are produced, decaying next in a weak process into muons.

For this reason it may be of interest to investigate the pseudorapidity profile of muons in the longitudinal development of showers. The muon production height (MPH) can also be calculated using ζ parameter, which is a measure of the muon angle to the shower axis, and the event geometry. Mean values of MPH, as shown in ref.[9], are very well reproduced by this method. In Fig. 3. experimental longitudinal profiles of mean muon pseudorapidity in EAS for two N_μ^{tr} ranges are shown. Up to the ≈10 km where, due to the large statistics of muons, accuracy in determination of MPH is better than 100 m, the logarithmic dependence of η on MPH is observed with a change in slope at altitude ≈ 2 - 3 km. Above ≈10 km the errors become much larger and it is hard to make any quantitative conclusions.

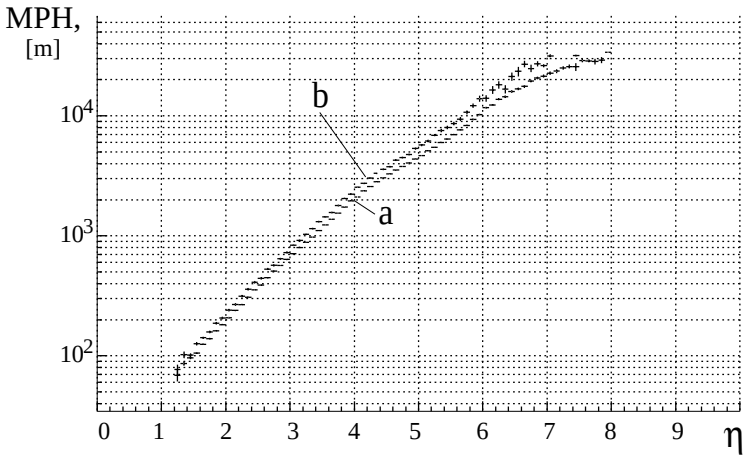

Fig. 3. Relation between mean muon pseudorapidity and their mean production height for experimental data with N_μ^{tr}=3.8-4.0 (a) and N_μ^{tr}=4.4-4.6 (b)

3. Conclusions

Precise measurements of muon directions with respect to the shower axis allow to investigate muon pseudorapidities in EAS and to test hadronic interaction models (high and low energy). Muon pseudorapidity profiles in the longitudinal development of EAS may give another point of view on the extended air shower physics. Presented distributions are just a few examples out of large variety of possible investigations of muon pseudorapidity in EAS (dependence on the zenith angle, shower size, primary type and energy etc.). Tests of other models like newer versions of QGSJet and neXus are of particular interest also. The investigation of high η values requires muons registered close to the shower core, which is very difficult. In the KASCADE-Grande setup, due to the larger muon-shower core distances available, there will be much more statistics in the region of low η values and higher muon production altitudes can be accessed for investigation of longitudinal shower development with reasonable errors.

Polish authors acknowledge support by KBN grant No. 5 P03B 133 20.

1. Antoni T. et al., KASCADE Collaboration, 2003, NIM A, submitted
2. Bernlöhr K. 1996, Astropart. Phys. 5, 139
3. Büttner C. et al., 2003, Proc.28th ICRC, these proceedings
4. Doll P. et al., 2002, NIM A 488, 517
5. Drescher H.J. et al., 2001, Phys. Rep. 350, 93
6. Fesefeldt H. Report PITHA-85/02, RWTH Aachen, 1985
7. Heck D. et al., 1998, FZKA 6019, Forschungszentrum Karlsruhe
8. Kalmykov N.N. and Ostapchenko S.S. 1993,Yad. Fiz. 56, 105
9. Zabierowski J., Daumiller K. and Doll P., astro-ph/0211568, to appear in Nucl. Phys.B (Proc.Suppl), 2003

Status, Performance and Perspectives of the Pierre Auger Observatory

Johannes Bluemer[1] for the Auger Collaboration[2,3]
(1) University of Karlsruhe and Forschungszentrum Karlsruhe, Postfach 3640, D-76021 Karlsruhe, Germany
(2) Observatorio Pierre Auger, Av. San Martin Norte 304, 5613 Malargue, Argentina
(3) Auger Collaboration author list: http://www.auger.org/auger-authors.pdf

Abstract

The Pierre Auger Observatory will be the largest cosmic ray detector ever built, covering 3000 square kilometres in both hemispheres in its full configuration. The first runs have demonstrated a very good performance of the apparatus.

1. Introduction

Cosmic ray research is at the energy forefront of astroparticle physics. Of particular interest are cosmic ray particles with energy $> 10^{20}$ eV. At these energies the protons, nuclei, or photons interact with various background radiation fields and should be strongly attenuated except if the sources are in our cosmological neighborhood (< 100 Mpc). Also protons of these energies may point back to the source and open a new kind of astronomy with charged particles.

2. The Pierre Auger Observatory

The Auger Observatory is designed for full-sky coverage with an aperture of 7350 km^{2}sr in each hemisphere above 10^{19} eV for zenith angles up to 60°. In the final configuration 1600 water tanks will be placed on a triangular grid with 1.5 km spacing to cover 3000 km^2. Twenty-four fluorescence detectors in total will be grouped in four locations at the perimeter of the ground array to oversee the entire surface detector. This hybrid detection technique combines the statistical power of a ground array with calorimetric energy measurement and detailed longitudinal reconstruction for a 10% subset of showers recorded during clear, dark nights. Detailed information may be obtained from the Pierre Auger Project internet portal [http://www.auger.org].

Construction of the Southern site started in 1999 in the Province of Mendoza, Argentina. The observatory campus is located in the city Malargue at the South-east border of the detector field, see Figure 1.

pp. 1–4

2 ——

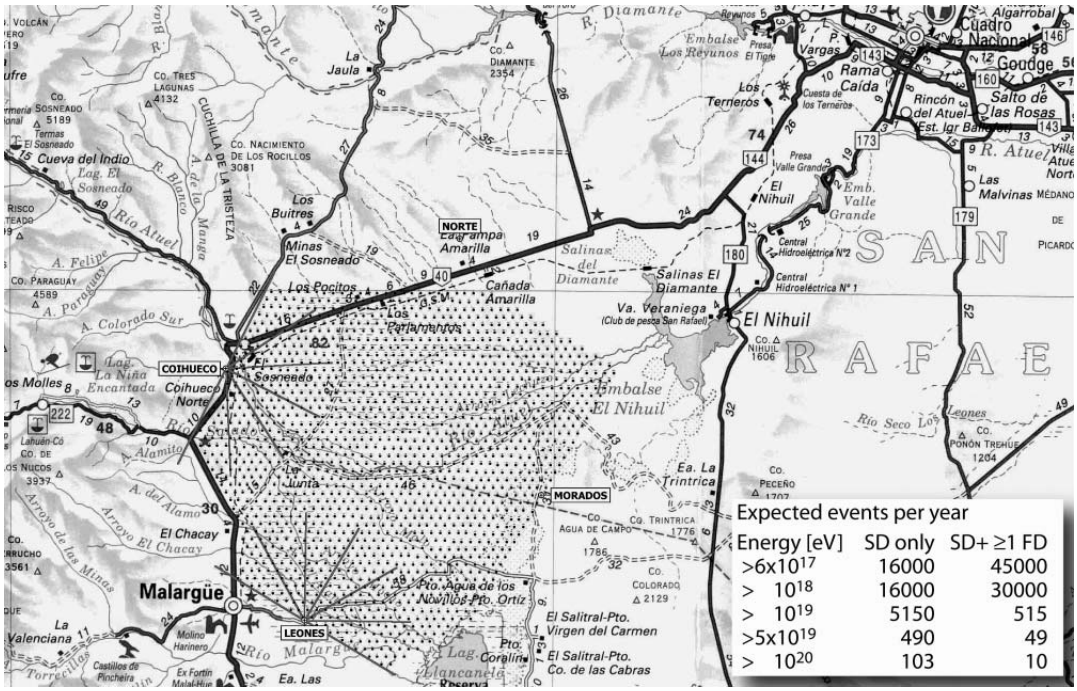

Fig. 1. Location and layout of the Southern Pierre Auger Observatory in Mendoza, Argentina. Each dot represents one water Cherenkov detector. The four telescope stations are placed on small elevations called LEONES, COIHUECO, MORADOS and NORTE. The fields of view for some telescopes are indicated. The inset gives the expected number of events per year for the full configuration assuming the AGASA energy spectrum.

The Surface Detector (SD) is made of water Cherenkov tanks. The tanks have 3.6 m diameter and 1.2 m height to contain 12 m^3 of clean water viewed by three 9" photomultiplier tubes (PMT). A solar panel and a buffer battery provide electric power for the local intelligent electronics, GPS synchronization system and wireless LAN communication. The abundant cosmic ray muons produce an essential calibration signal of about 80 photoelectrons in one PMT. The signals are continuously digitised with 16 bit dynamic range at 40 MHz sampling rate and temporarily stored in local memory. The time structure of PMT pulses carries rich information related to the mass of the primary particle. The trigger conditions will require four or five stations with a significant energy deposit. Detection efficiency will begin around 10^{18} eV and reach 100% at 10^{19} eV.

The Fluorescence Detector (FD) consists of 24 wide-angle Schmidt telescopes grouped in four stations, see Figure 1. Each telescope has a 30° field of view in azimuth and vertical angle. The four stations at the perimeter of the surface array consist of six telescopes each for a 180° field of view inward over the array. Each telescope is formed by segments to obtain a total surface of 12 m^2 on a radius of curvature of 3.40 m. The aperture has a diameter of 2.2 m and is equipped with optical filters and a corrector lens. In the focal surface a photomul-

tiplier camera detects the light on 20×22 pixels. Each pixel covers $1.5° \times 1.5°$ and the total number of photomultipliers in the FD system is 13,200. PMT signals are continuously digitised at 10 MHz sampling rate with 15 bit dynamic range. The FPGA-based trigger system is designed to filter out shower traces from the random background of 200 Hz per PMT.

Attention is given to atmospheric monitoring, making use of laser beams, LIDAR, calibrated light sources and continuous recording of weather conditions. Special efforts are being made to determine the air fluorescence efficiency and its dependence on relevant conditions.

The track reconstruction in a stereo configuration or in a hybrid configuration together with a ground array is greatly improved compared to a monocular reconstruction. The detector is sensitive to the primary particle type exploiting the atmospheric depth in which the shower maximum occurs, the ratio of muons to electrons in the shower, and the time structure of the shower disk. Neutrinos may be identified as nearly horizontal electromagnetic showers just above the surface array. The background for neutrinos is produced by baryonic primaries, and the showers will mainly consist of energetic muons.

3. Results from the Engineering Array

An Engineering Array (EA) consisting of 40 water tanks and 2 prototype telescopes was built to demonstrate the hybrid concept and to validate the techni-

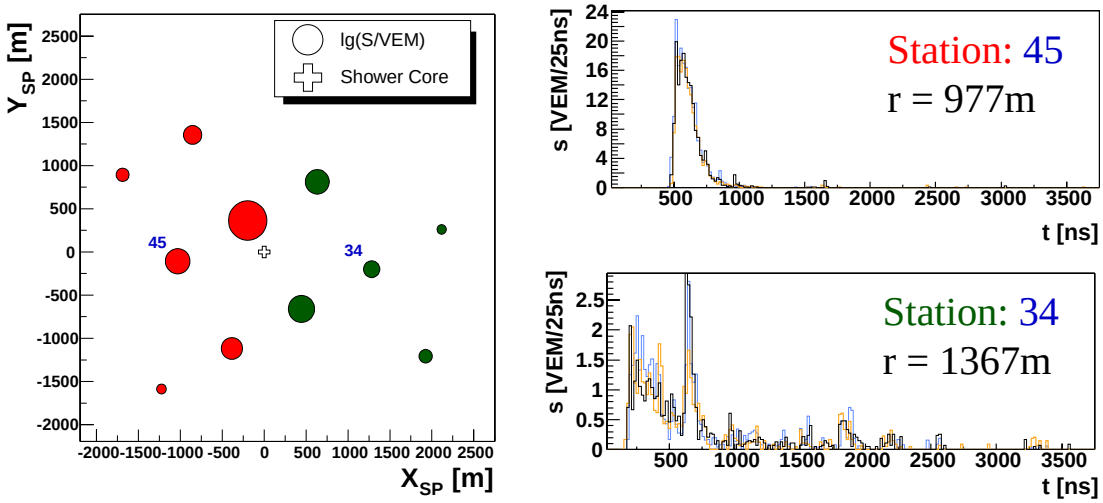

Fig. 2. Examples of events detected with the engineering array. Left panel: Particle densities projected into the plane perpendicular to the shower axis. The energy of this 11-tank shower is $(2-3) \cdot 10^{19}$ eV, the zenith angle is about 54°. Right panels: Close to the core substantial pulseheights are recorded; farther out, individual pulses from electrons (lower, wide-spread signals) and muons (sharp peaks) can be seen.

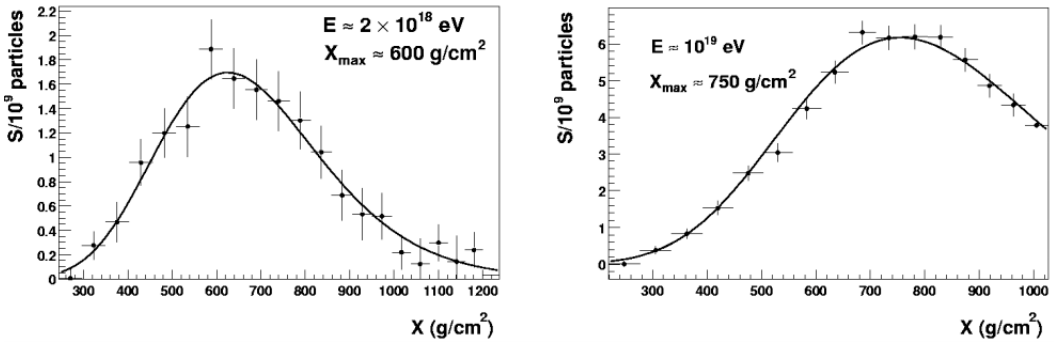

Fig. 3. Two events seen by the fluorescence detector. The reconstructed number of particles is shown as a function of atmospheric depth together with a Gaisser-Hillas curve fit.

cal designs before mass production. The ground array and fluorescence detectors were commissioned with the distributed, asynchronous data acquisition system from December 2001 onwards. During four months, the EA was operated continuously. It recorded several thousand events in either subsystem and about 70 hybrid events. In Figures 2 and 3 we show examples for some events. The SD time synchronization using GPS works well within 50 ns and the angular resolution is the order of 1° or better. The fluorescence detectors were preliminary calibrated and atmospheric corrections were evaluated based on laser beams, LIDAR and calibrated light sources at various distances from the telescope. The sensitivity was estimated to be 10 EeV at 26 km distance. The two telescopes were operated during dark periods at 11% duty cycle as expected and recorded about one event every 20 minutes.

The prototype apparatus has met or exceeded all our specifications; numerous detailed reports are given in these proceedings. We are thus confident to proceed with the construction of the full-scale observatory.

4. Perspectives and Conclusion

At the time of writing about 130 tanks in total have been positioned. Two buildings for fluorescence telescopes at Leones and Coihueco, indicated in Figure 1, are ready for installation of the final telescopes. We expect to operate the surface array together with stereoscopic optical detection starting late 2003. The full configuration of the Southern site will be reached by 2005. Thereafter, it is planned to commence construction of the Northern Auger Observatory. The selected site is in the USA in Millard County, Utah, located at 39° N, 113° W.

The Pierre Auger Observatory, starting up in a few years, will improve significantly our understanding of ultra-high energy cosmic rays.

The Lateral Distribution Function of Shower Signals in the Surface Detector of the Pierre Auger Observatory

Markus Roth[1] for the Auger Collaboration[2]
(1) IEKP, Universität Karlsruhe, POB 3640, D-76021 Karlsruhe, Germany
(2) Observatorio Pierre Auger, Malargüe, 5613 Mendoza, Argentina

Abstract

The surface detector (SD) array of the southern Pierre Auger Observatory will consist of a triangular grid of 1600 water Cherenkov tanks with 1.5 km spacing. For zenith angles $\theta < 60^\circ$ the primary energy can be estimated from the signal S(1000) at a distance of about 1000 m from the shower axis, solely on basis of SD data. A suitable lateral distribution function (LDF) S(r) is fitted to the signals recorded by the water tanks and used to quantify S(1000). Therefore, knowledge of the LDF is a fundamental requirement for determining the energy of the primary particle. The Engineering Array (EA), a prototype facility consisting of 32 tanks, has taken data continuously since late 2001. On the basis of selected experimental data and Monte Carlo simulations various preliminary LDFs are examined.

1. Introduction

High energy cosmic rays (CRs) are detected via the extensive air showers (EAS) they produce in the Earth atmosphere. Direction (θ,ϕ), energy (E) and mass of the primary CR are reconstructed from the secondary particles in the shower. The arrival times of shower particles at various detector locations give information on the arrival direction. The overall number of secondaries at observation level scales roughly with primary energy, and the form of the shower depends to some extent on the primary mass. In the Auger experiment the longitudinal shower development is measured by the Fluorescence Detectors (FD) while the lateral distribution at ground level is recorded by the SD, providing two independent measurements of the shower geometry and primary energy. The event reconstruction is hampered by the coarse sampling of the shower particles and by the statistical fluctuations of the shower development. High-developing showers are expected to have a flat lateral distribution, low-developing showers produce steeper lateral distributions. Fortunately, at about 1 km core distance the signal is virtually independent of primary mass and shower fluctuations, and is a good measure for the primary energy. Thus, the energy reconstruction requires, as a first and crucial step, to estimate S(1000) from few measured signals

pp. 1–**??**

at various distances from an *a priori* unknown core position. A second step is then to determine E from S(1000), which relies to a large extent on shower simulations and is therefore model dependent [1]. We do not discuss the energy calibration of the SD here. Since most of the Auger events have rather few SD stations hit, the reconstruction of the shower is not trivial. The functional form of an LDF, S(r), and its parameters, varies with θ, energy and mass, and its determination requires a good estimate of the core position, which in turn requires a reliable reconstruction of the shower direction, which relies on a precise time measurement and stable trigger performance. The estimation of S(1000) (and thus E) can be greatly improved if the shape of the LDF is known. Here we present various approaches to determine the LDF from experimental data and MC simulations.

2. Probing various LDFs

In contrast to S(1000) the shape of the lateral distribution does not change much with energy. Therefore, it makes sense to decouple the normalisation constant from the shape parameters of an LDF and to combine showers of different energies. Simulations of EAS with AIRES/QGSJET01 in the range E = 1-100 EeV and for θ = 0-60° have been performed for the Auger experiment and their output was processed through a response simulation of detectors at core distances 200-2500 m [2]. The LDF, in units of vertical equivalent muons (VEM), was parametrised with an empirical function of the form $S(r) = \mathrm{E}^{0.95} \cdot 10^{A+Bx+Cx^2}$ with $x = \lg(r/1000\ \mathrm{m})$ and the parameters A, B and C were determined as function of θ (see fig. **??**). Independent from simulations, the LDF was also deduced from experimental data. The EA was operating in very stable conditions during the period May to November 2002. Therefore data from this period have been used for the following analysis. High-quality events have been selected, which had a successful directional reconstruction with $\theta < 60°$, signals above 3 VEM in at least 6 stations and a core position inside the EA. High-multiplicity events are very rare: only 3×10^{-3} of the events have 6 or more stations above threshold. Each event was examined and events or stations with obvious problems were removed from the sample. A few well defined events are better to determine the LDF than many events of lower quality. The following LDFs have been investigated: (i) a simple

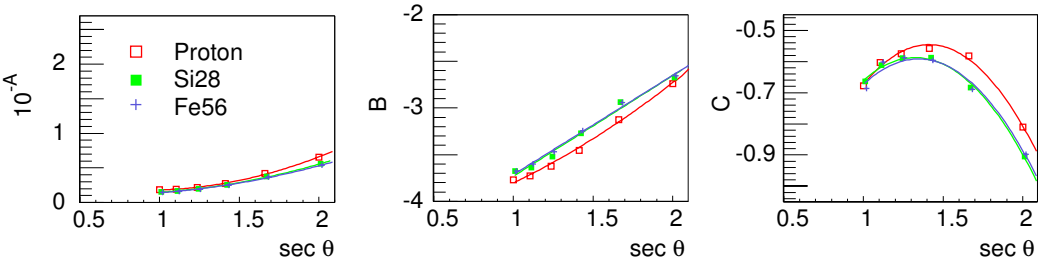

Fig. 1. Shape parameters of LDF as function of $\sec\theta$ as predicted by MC simulations [2].

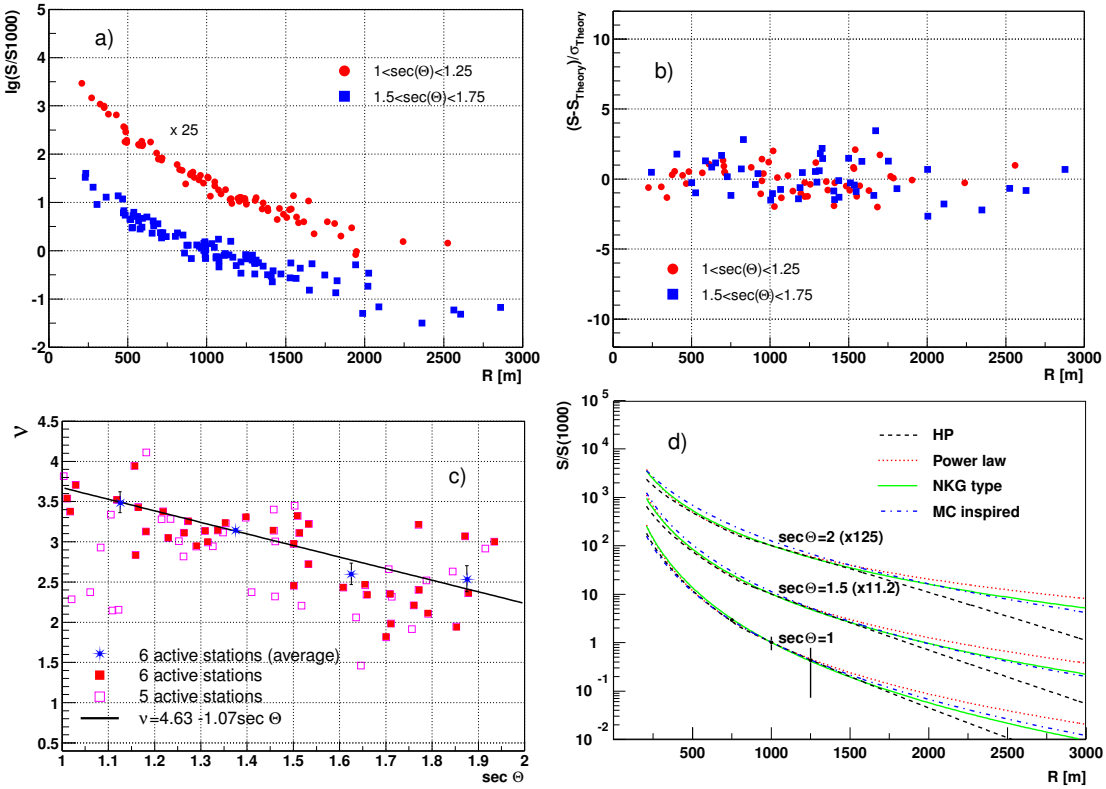

Fig. 2. a) Measured LDF for two zenith angles (for power law fit). Full symbols: stations with signal, open symbols: silent stations. The data for $1 < \sec\theta < 1.25$ have been shifted upwards for clarity. b) Residuals $(S - S_{\rm th})/\sigma_{\rm th}$ as function of r for two values of θ (for power law fit). Open symbols are silent stations. c) Fitted value of ν as function of $\sec\theta$ for individual events (squares) and averaged (stars). Solid line: fit to stars. d) Different LDFs for three zenith angles. For $\sec\theta = 1$ a few error bars are plotted.

power law $S(r) = S(1000)\cdot(r/1000\ \mathrm{m})^{-\nu}$ with a θ dependent index $\nu = a + b\sec\theta$, (ii) an NKG-type function: $S(r) = \text{const.}\ (r/r_s)^{-\beta-0.2}\cdot(1+r/r_s)^{-\beta} = S(1000)\cdot(r/1000\ \mathrm{m})^{-\beta-0.2}\cdot((r+r_s)/(1000\ \mathrm{m}+r_s))^{-\beta}$ with $\beta = a + b\sec\theta$ and $r_s = 700$ m*, and (iii) the MC inspired LDF $S(r) = 10^{A+Bx+Cx^2}$. These forms were fitted to individual events using a maximum likelihood fit of core location and LDF at the same time. Silent (i.e. alive but no signal above threshold) and saturated stations are properly included in the fit. The error $\sigma(S)/S = \sqrt{0.08^2 + 0.6/S}$ of a signal S (in VEM) is taken from an analysis [4] of data from a closely positioned detector pair. For the power law and the NKG-type LDFs two analyses were performed. First, in a two-parameter fit, the slope parameters ν and β, resp., have been varied together with the scale factor S(1000). Then a parameterisation of ν and β as function of θ was determined, which was then used in a second analysis with only fitting S(1000). Fig. **??**a) shows the measured LDF (divided by S(1000))

*Since β and r_s are strongly correlated, we have fixed $r_s = 700$ m and left β to vary.

$\sec\theta$ range	N_{evt} with # stations		power law				NKG				MC	
			ν free		ν fixed		β free		β fixed			
	≥ 5	≥ 6	m	σ	m	σ	m	σ	m	σ	m	σ
[1.00, 1.25]	21	11	-0.05	0.50	-0.11	0.65	-0.03	0.49	-0.05	0.57	-0.14	0.66
[1.25, 1.50]	18	9	-0.07	0.61	-0.07	0.62	-0.02	0.53	-0.05	0.57	0.06	0.93
[1.50, 1.75]	18	12	-0.05	0.65	-0.04	0.73	-0.03	0.63	-0.02	0.71	0.02	0.80
[1.75, 2.00]	12	8	-0.08	0.83	-0.15	1.15	-0.11	1.13	-0.10	1.17	-0.15	1.29

Table 1. Moments (mean, σ) of residual distribution of exp. data with various LDFs. Only events with ≥ 6 stations were used in the present analysis.

for two zenith angles when the power law assumption is used for the core finding. To quantify the quality of the fit, residuals $(S - S_{\rm th})/\sigma_{\rm th}$ as a function of r are formed (see fig. **??**b)). For a good LDF the residuals should scatter for all r symmetrically around 0 with a variance of 1. Means and standard deviations of the distribution of the residuals are used to compare different LDFs. For the power law fit the fitted values on ν are shown as function of θ in fig. **??**c). It is evident that higher-multiplicity events have a smaller scatter. A line is fitted to the averages (stars) of the full symbols that yields $\nu = 5.1(\pm 0.4) - 1.4(\pm 0.2)\sec\theta$. With the θ dependence of ν fixed, the only fit parameter left for the LDF fit is S(1000), leading to more stable fit results for low multiplicity events. In the same way for the NKG function the variation of β was found: $\beta = 3.3(\pm 0.2) - 0.9(\pm 0.2)\sec\theta$. Fig. **??**d) shows that the three chosen LDFs, with suitably adapted parameters, agree well within the experimental errors. For completeness also the Haverah Park LDF [3] is shown, that predicts smaller densities at large core distances.

3. Results

The moments of the residual distributions from experimental data including silent stations obtained with different LDFs are listed in table **??** There is no major bias apparent and all the distributions have about the same widths, which indicates that all three LDFs describe well the data presently available. Previous experiments have shown that a pure power law cannot describe the shower signals at large core distances [3]. The results presented here are still preliminary as the statistics of events from the Auger EA, especially for energies $> 10^{19}$ eV, are small and since preliminary algorithms for directional and core reconstruction are used. In future each improvement on the statistics, angular and core resolution, and specifically hybrid events with their superior geometric reconstruction, will also improve the knowledge on the LDF and permit finer details to be analysed.

1. Billoir P., Auger Collaboration internal note, GAP 2002-075
2. Billoir P., Da Silva P., Auger Collaboration internal note, GAP 2002-073
3. Coy R.N. et al., Astrop. Phys. 6 (1997) 263
4. Yamamoto T. for the Auger Collaboration, these proceedings

Atmospheric Effects on the Development and the Fluorescence Detection of Extensive Air Showers

Bianca Keilhauer[1], Johannes Blümer[1,2], Hans Klages[1], Markus Risse[1]
(1) Forschungszentrum Karlsruhe, Institut für Kernphysik, Karlsruhe, Germany
(2) Universität Karlsruhe, Institut für Experimentelle Kernphysik, Karlsruhe, Germany

Abstract

Radiosonde measurements of atmospheric profiles above the Pampa Amarilla in Argentina, the location of the southern Pierre Auger Observatory, have been carried out. A detailed knowledge of the atmospheric conditions and its variations is mandatory especially for the fluorescence technique of air shower observations. The atmosphere influences the shower development and the detection in several ways: Firstly, the shower development is mainly determined by the amount of traversed matter. However, fluorescence telescopes observe the geometrical development. For the transformation from depth to geometrical height, the air density profile is required, otherwise misinterpretations of the shower maximum depth of order 30-50 g/cm^2 are possible. Secondly, the fluorescence efficiency of air depends on the local pressure and temperature. And thirdly, the propagation of light is affected by attenuation and scattering, again depending on the air density profile. The measured air pressure and temperature profiles, taken in all 4 seasons up to altitudes of 25 km, and the resulting variables are presented. The importance of in-situ measurements for the interpretation of fluorescence observations is discussed.

1. Introduction

Using the fluorescence technique for detecting Extensive Air Showers (EAS), informations on the longitudinal shower development are obtained. However for interpreting the measurements, assumptions about environmental conditions are necessary. Usually the US Standard Atmosphere from 1976 (US-StdA) forms the basis. For estimating the influence of realistic atmospheres, we measured temperature (T) and pressure (p) profiles up to 25 km with meteorological radiosondes launched on Helium filled balloons [1]. First of all, the effect of seasonal air density profiles on the shower development is discussed. Afterwards, the fluorescence emission of that showers is calculated. Finally, the transmission of the fluorescence light towards the telescope is outlined.

pp. 1–4

2. Longitudinal Shower Development

The EAS development is mainly determined by the amount of traversed air. Thus, the path integral of the air density, called atmospheric depth X, indicates the stage of the EAS. Since the fluorescence telescopes observe the light at given geometrical height h, we have to know the relation between atmospheric depth and geometrical height.

The measured data sets are obtained in sufficiently small height intervals, on average every 20 m. The atmospheric depth profile is calculated by

$$X(h) = X_b + \sum_{h=h_b}^{h_{start}} \Delta X(h), \tag{1}$$

where X_b is the atmospheric depth at the height of balloon burst h_b using the simple proportionality between X and p, and $\Delta X(h)$ is the local additional atmospheric depth $= 1/2 \cdot (\rho(h_1) + \rho(h_2)) \cdot (h_2 - h_1)$ within each measured interval [3]. For using the measured atmospheric profiles in the shower simulation program CORSIKA [2], the atmospheric depth profiles are fitted according to

$$X_i(h) = a_i + b_i \cdot exp(-h/c_i), \tag{2}$$

subdivided into $i = 1 - 4$ ranges up to 100 km. The differences between the measured profiles and the US-StdA can be seen in Fig. 1. The solid lines are fits

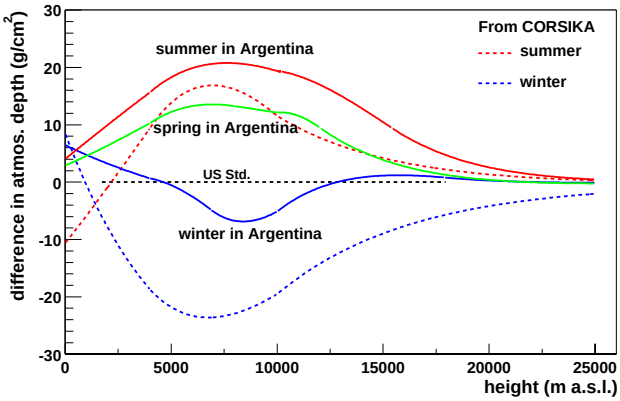

Fig. 1. Difference of measured atmospheric depth profiles to the US-StdA.

to several measured data obtained in different seasons, and the dashed curves are extreme atmospheres for Europe available in CORSIKA. The largest differences of $\Delta X \approx 27$ g/cm^2 between summer and winter in Argentina occur at 7 - 10 km a.s.l. At that height, 40° - 65° inclined EAS of 10^{19} - 10^{20}eV reach their maximum. The maximum position of an EAS with zenith angle Θ is shifted by $\Delta X/cos\Theta$. The data were recorded in August and November 2002, as well as in February 2003. Representative curves were found out neglecting daily variations. In total 33 launches were carried out. 2002 was an *El Niño* year perhaps being untypical.

The particles of the EAS lose energy during their passage through the atmosphere, exciting the nitrogen molecules in air. Part of the de-excitation happens via isotropic fluorescence emission. The Fluorescence Yield is proportional to the local energy deposit. Thus, we simulate the longitudinal development of the energy deposit [4] for different seasons in Argentina (see Fig. 2). The position of the shower maximum depends on the type of the primary particle. However, it also depends on the atmospheric depth profile. The example in Fig. 2 shows averages of 100 simulated iron induced EAS. The shift in the shower maximum position amounts to 580 m in vertical height between summer and winter conditions.

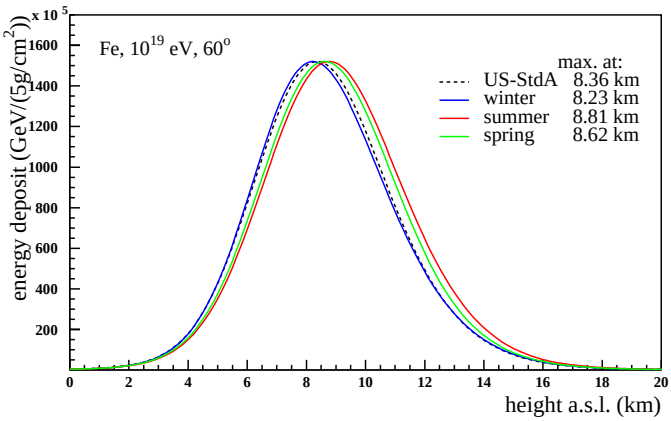

Fig. 2. Longitudinal energy deposit profiles for EAS in measured atmospheres in Argentina.

3. Fluorescence Light Emission and Transmission

The fluorescence light production is one part of the de-excitation of the nitrogen molecules in air. It competes with collisional quenching which depends on the rate of impacts by further molecules. This process is determined by the collisional cross sections and also by the temperature and density ρ of the gas affecting the speed of molecules. Thus the Fluorescence Efficiency depends on the atmospheric profiles and also the resulting Fluorescence Yield defined as

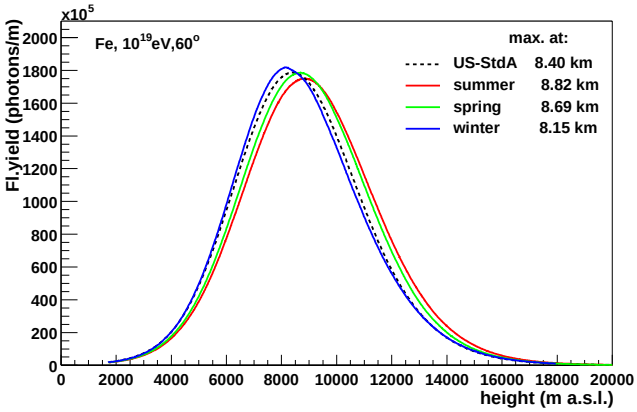

Fig. 3. Longitudinal Fluorescence Yield profiles for EAS in measured atmospheres in Argentina.

$$Fl.Yield\ [\text{photons/m}] = Fl.Eff.\ [\text{photons/GeV}] \cdot \frac{dE}{dx} \cdot \rho_{air}. \qquad (3)$$

The emitted light curves for the EAS shown above are plotted in Fig. 3. The Fl. Yield curve is additionally shifted and distorted as against the energy deposit.

The position of the fluorescence maximum is separated by 670 m between summer and winter conditions. The pure Fl. Yield difference amounts to 5%.

The difference in the maximum position between iron and proton induced EAS is nearly 80 g/cm^2 or 770 m for 60° inclined EAS of 10^{19}eV in the US-StdA (Fig. 4). Combining the effects of deeper penetrating proton EAS and

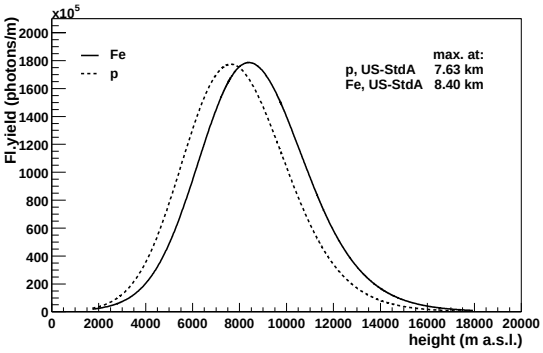

Fig. 4. Fluorscence Yield profiles for iron and proton induced EAS in the US-StdA, 10^{19}eV, 60° inclination.

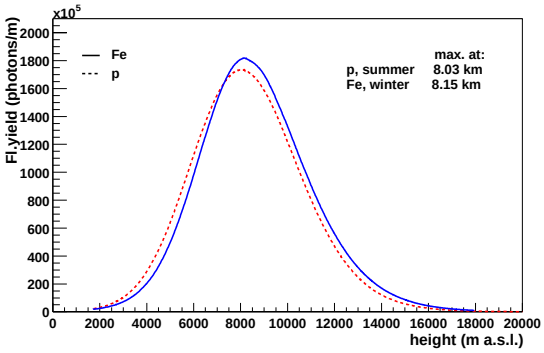

Fig. 5. Fluorescence Yield profiles for iron EAS in winter and proton EAS in summer,10^{19}eV, 60° inclination.

earlier developing EAS in summer, the possible misinterpretations concerning the primary particle mass become obvious (Fig. 5). The clear detectable seperation of 770 m between proton and iron EAS has shrunk to 120 m for the measured atmospheres.

During the propagation towards the telescope, the light suffers absorption and scattering. Since Rayleigh scattering is T and p dependent, seasonal effects show up. For a distance between EAS and telescope of 15 km, the difference in the transmission between summer and winter in Argentina yields $\approx 5\%$ depending on the wavelength.

4. Conclusions

The atmosphere influences the longitudinal EAS development as well as their detection in terms of different light production and transmission. Measurements of atmospheric profiles and comparisons with the US-StdA show significant effects on the interpretation of EAS data especially concerning the type of the primary particle by shower maximum determinations.

References

1. Dr. Graw Messgeräte GmbH & Co, Nürnberg, Germany, http://www.graw.de
2. Heck D. et al. 1998, Report FZKA 6019, Forschungszentrum Karlsruhe
3. Keilhauer B. et al. 2003, Auger technical note GAP-2003-009
4. Risse M., Heck D. 2002, Auger technical note GAP-2002-043

Importance of Atmospheric Model in Shower Reconstruction

B. Wilczyńska[1], D. Góra[1], P. Homola[1], B. Keilhauer[2], H. Klages[2], J. Pękala[1] and H. Wilczyński[1]
(1) H. Niewodniczański Institute of Nuclear Physics, ul. Radzikowskiego 152, 31-342 Kraków, Poland
(2) Forschungszentrum Karlsruhe, Institut für Kernphysik, 76021 Karlsruhe, Germany

Abstract

The influence of an atmospheric model on shower reconstruction is studied. In the fluorescence detection technique, one of the key measurements is the depth of shower maximum in the atmosphere, X_{max}. The altitude corresponding to X_{max} depends considerably on distributions of atmospheric pressure and temperature, used in the shower reconstruction. In this paper, measured atmospheric profiles at different geographic locations are compared to the US Standard Atmosphere model. A study of the atmospheric effect in shower reconstruction as a function of shower inclination and energy is done. Seasonal variations of atmosphere are shown to affect considerably the X_{max} determination.

1. Introduction

The atmosphere serves both as a target and a part of an extensive air shower detection system. The main parameter governing the shower development is the amount of traversed air. Therefore, the local distribution of air density along the shower path is of primary importance. In the fluorescence detection technique, the longitudinal profile of shower development is reconstructed as a function of altitude above ground. An accurate conversion of the altitude into grammage of air traversed is necessary in order to extract such important quantities like depth of shower maximum, X_{max}. In addition, light attenuation in the atmosphere depends on the air density distribution, making the detailed knowledge of the atmosphere even more important.

The US Standard Atmosphere model [5] is widely used in air shower simulation codes and in analysis of shower measurements. It has been shown [4] that the time variation of the atmosphere can be significant, so that the actual distribution of the atmospheric density can differ considerably from the model one. In this paper, we study profiles of the atmosphere density in northern and southern hemispheres and compare them to the US Standard Atmosphere.

pp. 1–4

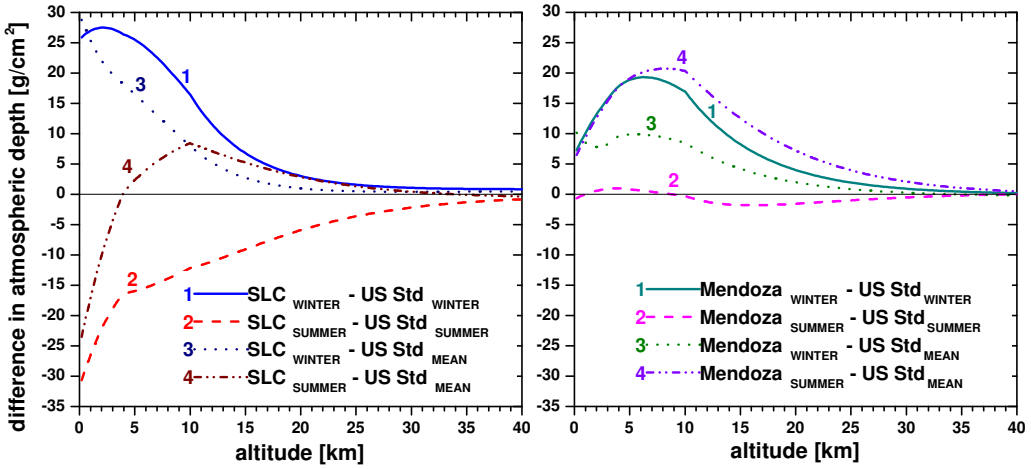

Fig. 1. Comparison of measured atmospheric depth to the US Standard Atmosphere at Salt Lake City (SLC) and Mendoza.

2. Measurements of atmospheric profiles

The atmospheric depth at an altitude h is the integral of density of overlying air: $X(h) = \int_h^\infty \rho(h)dh$. Since the air density is not measured directly, it must be inferred from the ideal gas law based on measurements of pressure p and temperature T: $\rho(p,T) = pM_{mol}/(RT)$, where M_{mol} is the molar mass of air and R is the universal gas constant. The pressure and temperature profiles are measured by radiosondes suspended to small balloons. The balloons typically reach altitudes between 20 and 30 km and provide temperature and pressure readings at predefined standard pressure levels.

The US Standard Atmosphere model (with the 1966 Supplement) provides the temperature and pressure profiles at the northern hemisphere, for mid-latitude winter and summer, as well as average atmosphere. At the southern hemisphere, e.g. at the southern Auger Observatory in Argentina, the US Standard Atmosphere model may not be appropriate. The COSPAR International Reference Atmosphere (CIRA86) [2] provides temperature and pressure profiles at altitudes above 20 km at many latitudes at both hemispheres. However, most of air shower development takes place at altitudes smaller than 20 km, so the CIRA86 model is not sufficient for air shower studies.

We use the UK Met Office data [1] which contain the temperature and pressure profiles measured by radiosondes at a number of locations worldwide, including Salt Lake City (USA) and Mendoza (Argentina), which are near the northern and southern Pierre Auger Observatory sites. Averages over several years of measurements in winter (January at Salt Lake City, July at Mendoza) and summer (July and January, respectively) were used for comparison with winter,

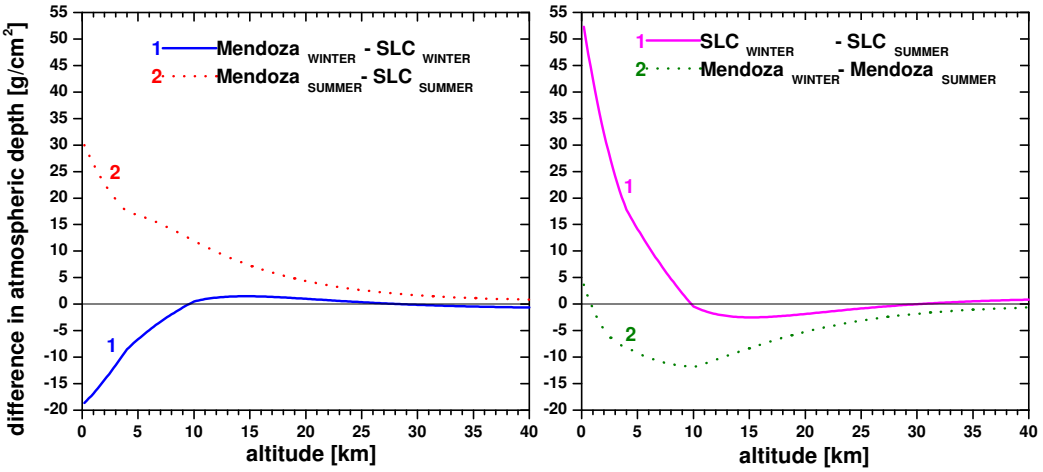

Fig. 2. Comparison of measured winter and summer atmospheric depth at Salt Lake City (SLC) and Mendoza, and seasonal variation at both sites.

summer and annual average US Standard Atmosphere model.

3. Comparison of atmospheric models

The BADC data were used to derive a parameterization of the atmosphere analogous to that used in the CORSIKA shower simulation package [3], i.e. separate fits to atmospheric depth in altitude ranges 0-4, 4-10, 10-40, 40-100 and above 100 km. Since the BADC radiosonde data cover altitudes below about 30 km, at higher altitudes the CIRA86 data were used. Differences in atmospheric depth versus altitude between actual measurements (BADC data) and US Standard model are shown in Figure 1 for Salt Lake City (SLC) and Mendoza. Seasonal variations of the atmosphere in Salt Lake City do not quite follow the US Standard Atmosphere model: the difference between measured and model atmospheric depth reaches ± 30 g/cm^2 at low altitudes. It is interesting to note that the US Standard Atmosphere model happens to describe the actual atmosphere in Mendoza much better than in Salt Lake City.

Figure 2 shows a comparison of the SLC and Mendoza measured atmospheres as well as their seasonal variations. The profiles of the atmosphere at these sites are clearly very different, both in winter and in summer.

Since the seasonal variations of the atmospheric profiles seem to be rather large, it is important to check their influence on shower reconstruction. A set of shower simulations were performed using CORSIKA for proton- and iron-induced showers at various energies and zenith angles. Differences in altitudes of shower maximum, using winter and summer atmospheres, were found. These differences were rescaled by the average difference in shower maximum altitude between proton and iron showers in order to see how important they are. The results are

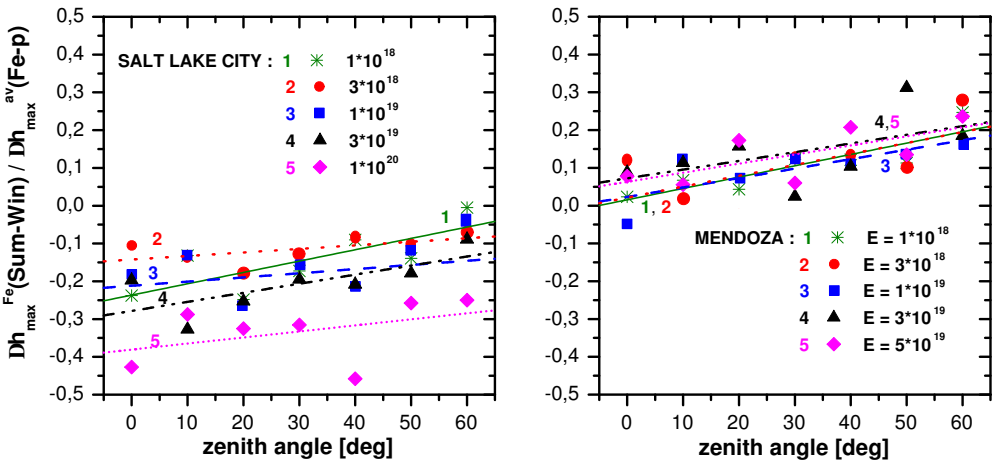

Fig. 3. Seasonal differences in shower maximum altitude of iron-initiated showers relative to average iron-proton difference in altitude of shower maximum.

shown in Figure 3. It is seen that the effects due to seasonal variations can be as large as 40% of the iron-proton difference, and are different in Salt Lake City and in Mendoza.

4. Conclusion

Atmospheric profiles actually measured in Salt Lake City and in Mendoza were compared to the US Standard Atmosphere model. Large differences between the data and the model are observed. The seasonal variation of the data differs significantly from that assumed in the model. A clear conclusion emerges: a *global* atmospheric model is not satisfactory for use in extensive air shower studies. Instead, atmospheric profiles *measured* as locally as possible should be used. Since local measurements are available for each month, they should be used to follow the seasonal variations of the atmosphere as closely as possible. Even daily variations of the atmospheric properties should be accounted for.

Acknowledgements. The access to the UK Meteorological Office data, granted to us by the British Atmospheric Data Centre, is gratefully acknowledged. This work was partially supported in Poland by the KBN grants No. PBZ KBN 054/P03/2001 and 2P03B 11024 and in Germany by the BMBF grant No. POL 99/013.

1. http://badc.nerc.ac.uk/data/radiosglobe/radhelp.html
2. http://nssdc.gsfc.nasa.gov/space/model/atmos/cospar1.html
3. Heck D. et al. 1998, Report FZKA 6019, Forschungszentrum Karlsruhe
4. Keilhauer B. et al.,Auger Notes GAP2002-022,GAP2003-009; these proceedings
5. http://nssdc.gsfc.nasa.gov/space/model/atmos/us_standard.html

A Top-Down Technique as an Analysis Tool for Auger Fluorescence Data

C. K. Guérard[1], Martina Bohacova[2], and Lorenzo Perrone[3]
(1) IEKP, Universität Karlsruhe, Postfach 3640, D-76021 Karlsruhe, Germany
(2) Institute of Physics FZU, Na Slovance 2 Prague, Czech Republic
(3) Fachbereich Physik, Universität Wuppertal, D-42097 Wuppertal, Germany

Abstract

The Auger Observatory aims at the detection of Ultra-High-Energy Cosmic-Rays by employing an array of ground-particle counters overviewed by atmospheric fluorescence telescopes -a mini prototype of which has been operative since 12/2001 near the town of Malargue in the province of Mendoza, Argentina. Conventional bottom-up fluorescence data analyses techniques convert photons entering the telescope's diaphragm to shower size; energy and primary composition are then estimated by fitting a Gaisser-Hillas distribution. In this paper we discuss the potential capabilities of a top-down technique based on a robust primary energy estimator. Such technique uses hundreds of very fast-simulated shower longitudinal profiles and calculates their corresponding photon profiles seen by the telescopes. Primary energy and composition follow from maximum likelihood or chi-squared analyses.

1. Introduction

Bottom-up methods currently used in Fluorescence Detector (FD) analysis convert ADC-raw data as function of time to shower size as function of traversed atmospheric depth. This is done in two steps: 1) Conversion of ADC(t) to photons(t) entering the diaphragm, and 2) conversion of diaphragm photons(t) to shower size(depth). Primary energy and composition follow from a fit to a Gaisser-Hillas function.

In this paper we present an alternative stand-alone method for analysis of FD data, and demonstrate that FD data in individual showers can be reproduced (up to inevitable fluctuations in the detection) by thorough simulations of air showers with atmospheric propagation and detector response.

2. The Method

A flow-chart diagram of the method is shown on Fig. 1, and can be summarized as follows:

- Raw ADC-data are extracted for all relevant pixels. Pulse finding and

pp. 1–4

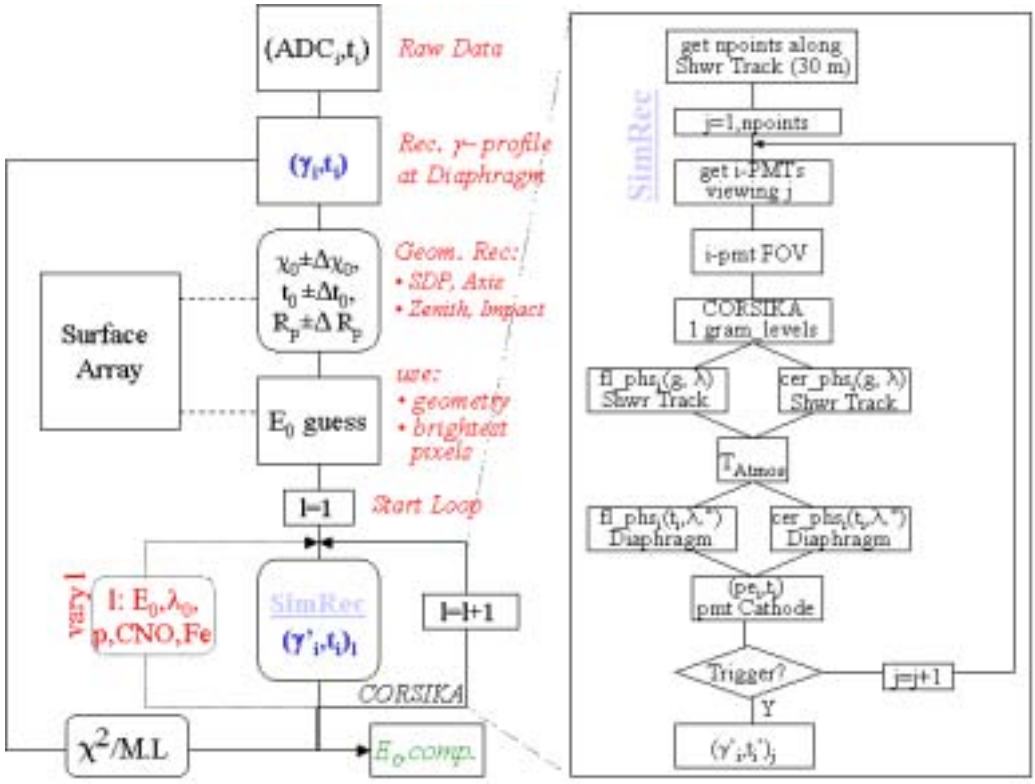

Fig. 1. Flow-chart diagram of the Top-Down FD-analysis technique.

pedestal subtraction algorithms are applied. A gaussian is fit to each pulse to get a better pulse centroid (for asymmetric pulses). Pulse-shape- and time-Vs.-elevation cuts are applied to discriminate random pulses.

- Calibration files are applied to convert ADC(t) to photons(t) entering the diaphragm.
- Shower Detector Plane, axis, zenith, azimuth, and core are calculated.
- A fast energy guess is made by taking into account the signal at the brightest camera row and the reconstructed shower geometry.
- Taking the energy guess and reconstructed shower geometry as reference, hundreds of simulated shower longitudinal profiles are fastly generated [1], each corresponding to a unique combination of primary energy, composition, and first interaction length.
- For each simulated shower profile, the atmospheric fluorescence yield is calculated and transmitted through the atmosphere down to the FD telescopes, producing both simulated photon(t) and ADC(t) profiles. (See next section on photon(t) profile simulation).
- Maximum likelihood techniques are used to compare both raw and simulated profiles in order to extract primary energy and composition.

2.1. Photon(t) Profile Simulation

Photon(t) profile simulation follows directly from the flow-chart diagram shown on the right-hand side of Fig. 1. In very general terms it can be described as follows:

- A shower-axis vector of vertical length 90 km is constructed and divided into 30 m steps (100 ns time-intervals along shower-axis).
- For each point along the axis, one identifies the pixel(s) viewing the point.
- Fluorescence yield and Cherenkov light are calculated for all points within the PMT's FOV by using the fastly simulated longitudinal shower profiles.
- All fluorescence and Cherenkov photons are transmitted through the atmosphere using realistic atmospheric models for the site, and followed down to the detector which is also modeled. A photon(t) (and ADC(t)) profile is saved for all triggered pixels.

3. Example of Event Reconstruction

We have analyzed 25 Auger Engineering Phase (EP) hybrid events. During the EP a $\sim 80 km^2$ mini surface array (MSA) overviewed by two fluorescence telescopes ∼12 km away, was operative between 12/2001 and 3/2002. In Fig. 2, we plot the deviation of our energy guesses with respect to those calculated using a full bottom-up reconstruction method for the 25 hybrid events. The deviation is quite small, proving the goodness of the energy guess algorithm. In order to visualize the capabilities of the method we show, in Fig. 3, an example of a simulated Auger hybrid event.

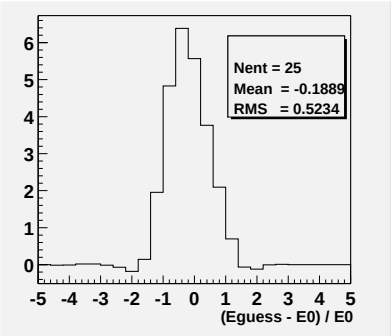

Fig. 2. Primary energy-guess deviation.

We throw a nearly vertical 1.5 EeV iron primary in the the middle of the MSA (see figure captions). From the photomultiplier trigger times we reconstruct the shower axis. Knowing this, we use the Bartol code [1] to generate 100 iron and 100 proton shower longitudinal profiles with energies distributed around the energy guess of 1.7 EeV. From these we follow all steps previously described in order to simulate their corresponding photon profiles entering the telescope's diaphragm. The fact that the profiles start and end precisely with the raw signal is indicative of the goodness of the geometrical reconstruction. The best fitted profile corresponds to a 1.5 EeV iron primary with $X_{max} = 693\ g \cdot cm^{-2}$, in accordance with simulated primary parameters. Inevitable fluctuations in the detection in real events may make such reconstruction not so accurate, yet the observed shift on simulated signal maxima between proton and iron primaries can be used to extract statistically more significant information on primary energy and composition than that obtained with bottom-up methods. The entire reconstruction process takes just under 4 hours on a 1GHz Linux machine.

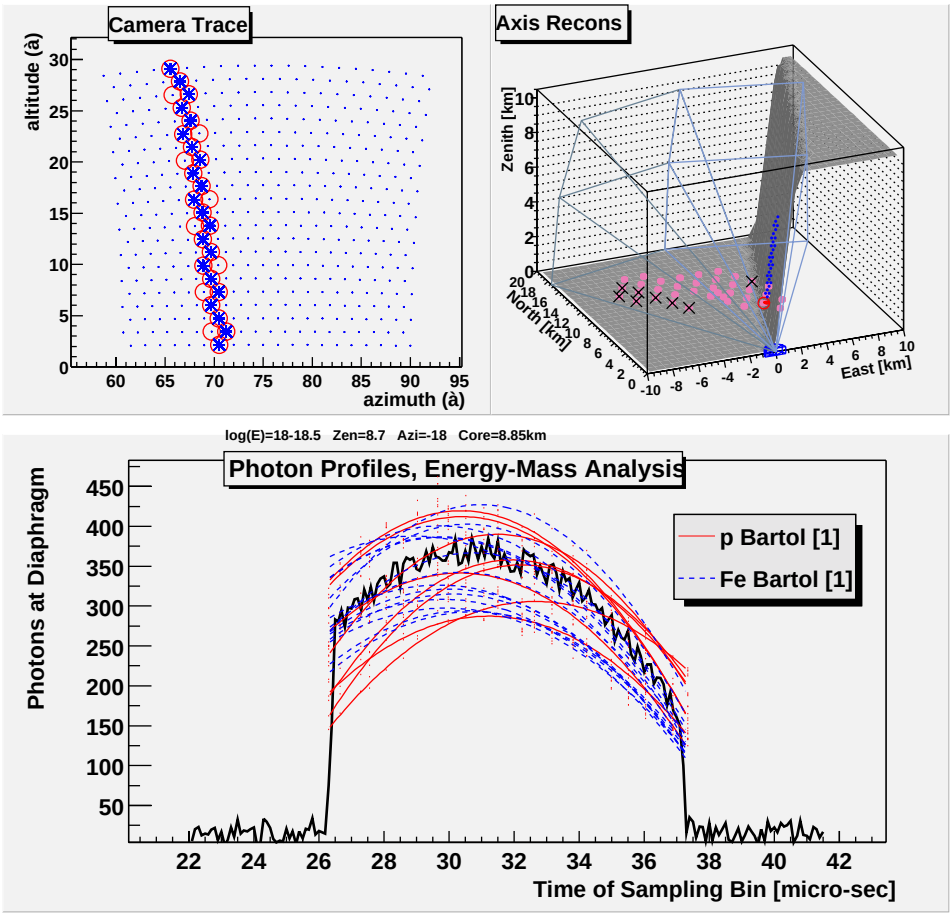

Fig. 3. Example of reconstruction of a simulated Auger Engineering-Array Hybrid Event landing 8.85 km from the telescope, with 8.7° zenith angle, for which the energy guess was 1.7 EeV. Upper left: Circles (stars): simulated triggered camera pixels (reconstructed shower-axis projected on camera's FOV). Upper right: 3D graph showing position of fluorescence telescope (origin), of operative water Cherenkov tanks (those not crossed out), of simulated triggered tank (encircled one), of reconstructed shower-axis (string of dots), and of reconstructed impact point (single dot). Lower: A sample of simulated proton (continuous lines) and iron (dashed) photon profiles entering the telescope's aperture superimposed on the simulated raw photon profile (continuous thick line). These (sample) profiles were generated according to the method described in the text, and corresponding to primaries with energies distributed between $(1-3)$ EeV. The best fitted profile corresponds to a 1.5 EeV iron primary with $X_{max} = 693\ g \cdot cm^{-2}$ in accordance with simulated primary parameters.

4. References

1. Alvarez-Muniz, J. et al. 2002, Phys. Rev. D 66, 033011.

Analytical versus Monte Carlo Description of Cherenkov Contribution in Air Showers

F. Nerling[1], R. Engel[1], C. Guerard[2], L. Perrone[3], and M. Risse[1]
(1) Forschungszentrum Karlsruhe, Institut für Kernphysik, 76021 Karlsruhe, Germany
(2) Universität Karlsruhe, Institut für Experimentelle Kernphysik, 76021 Karlsruhe, Germany
(3) Universität Wuppertal, Fachbereich Physik, 42097 Wuppertal, Germany

Abstract

The CORSIKA simulation code is used to calculate the longitudinal profile of Cherenkov photons for showers at the highest energies. The results are compared to analytical calculations based on the longitudinal shower size profile and electron energy distribution. A new, universal parametrization of the electron energy distribution in high-energy showers is presented. This parametrization allows us to derive the longitudinal Cherenkov profile both in a purely analytical way and *a posteriori* using the longitudinal particle number provided by CORSIKA. Necessary corrections in the normalization due to the specific energy threshold used in the simulation are discussed. The parametrization can be used in calculations e.g. for fluorescence telescope observations and shower reconstruction.

1. Introduction

For the determination of the primary energy using the fluorescence observation technique, a good knowledge of the Cherenkov background in the measured signal is mandatory. The CORSIKA code [3] has been adapted to calculate the longitudinal Cherenkov profile while generating the shower. Alternatively, the number of Cherenkov photons dN_γ produced per slant depth dX in a shower at depth X can be calculated analytically by

$$\frac{dN_\gamma}{dX}(X) = \int_{\ln E_t}^{\infty} N(X)\ y_\gamma(h, E)\ f(X, E)\ d\ln E \qquad (1)$$

$N(X)$ is the charged particle number as function of depth X, which will be taken from CORSIKA. $y_\gamma(h, E)$ denotes the Cherenkov yield of a single particle with energy E at altitude h in the atmosphere and E_t the local Cherenkov energy threshold, which depends on the refractive index $\eta = \eta(h)$ of air. For a given shower geometry, $h = h(X)$ follows from the atmospheric model assumed (US standard atmosphere in the following). y_γ shows the well-known sharp threshold

pp. 1–4

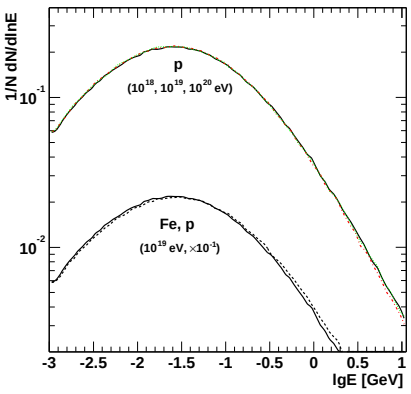

Fig. 1. Electron energy spectra at $s = 1$. Simulations with CORSIKA for different primary energies and primary particles.

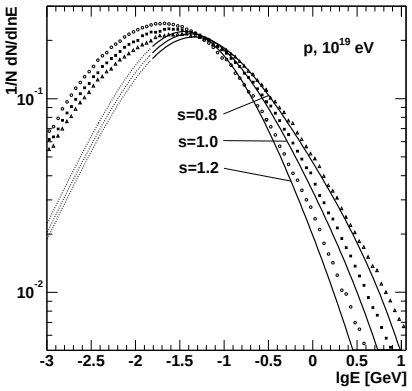

Fig. 2. Electron energy spectra from CORSIKA (symbols) for $s = 0.8$, 1.0, and 1.2 compared to parametrizations according to Hillas [4] (lines).

dependence. $f(X, E) = dN/(N\ d\ln E)$ is the (normalized) differential energy spectrum at shower stage X, which can be obtained e.g. by shower calculations [5]. A parametrization of the electron energy spectrum, depending only on the shower age $s = 3X/(X+2X_{max})$, was provided by Hillas based on 100 GeV photon shower simulations using a low-energy particle cutoff of 50 keV [4]. Traditionally this approximation is used to calculate the Cherenkov contamination of fluorescence light signals from high-energy showers, see for example [1].

The plan of the paper is as follows. At first, energy spectra obtained from CORSIKA are studied and compared to those given in [4]. A new parametrization, better reproducing the CORSIKA spectra, is introduced. The resulting predictions of the longitudinal Cherenkov profile using the different spectrum parametrizations are then compared to a full CORSIKA simulation.

2. Electron Energy Spectra

In Fig. 1, electron energy spectra at shower maximum obtained by CORSIKA are shown for different combinations of primary energy and mass. The normalization of the energy spectra, being important for the final calculation of the Cherenkov profile, is discussed below. The spectral shape does not depend in the considered energy range on primary parameters, which allows a parametrization valid for a large range of primary energies and masses. A dependence of the spectra on the shower age has already been considered in the parametrizations given by Hillas [4]. In Fig. 2, these spectra are compared to the CORSIKA results for different shower ages. Given the fact that the parametrizations were obtained for low-energy primary photons, a larger disagreement to CORSIKA above ener-

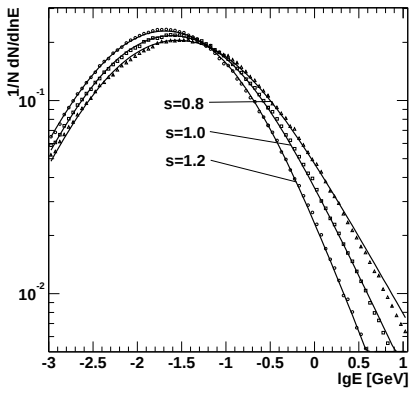

Fig. 3. CORSIKA energy spectra (see also Fig. 2) compared to the new parametrization.

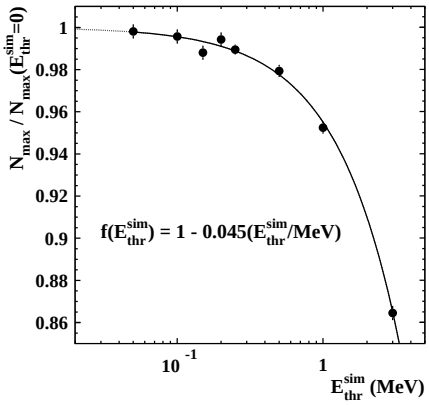

Fig. 4. Shower particle content as function of simulation energy threshold (see text) and its parametrization.

gies of 15 MeV (the lower validity limit given in [4]) might have been expected. A better description of the CORSIKA energy spectra, taking the age dependence into account and being also applicable to lower energies, has been achieved using the functional form

$$f_{para}(s, E) = a_0 \cdot \frac{E}{(E + a_1)(E + a_2)^s} \tag{2}$$

As can be seen in Fig. 3, the CORSIKA spectra can be reproduced well using $a_1 = 6.879 - 2.092 \cdot s$ and $a_2 = 122.0$ (for E in MeV). Another independently developed functional form is discussed in [2].

The energy spectra shown in Fig. 3 have been normalized according to

$$f_{para}(s, E) = \frac{1}{N}\frac{dN}{d\ln E} \quad , \quad \text{with} \quad \int_{\ln E_{thr}^{sim}}^{\infty} f_{para}(s, E) d\ln E = 1, \tag{3}$$

where E_{thr}^{sim} is the energy threshold adopted in the simulation (1 MeV in the examples shown). This normalization is necessary to be consistent with the shower size profile, as N provided by the simulation refers only to the particles above this energy threshold. As an example, the reduction of the maximum particle number with increasing energy threshold is illustrated in Fig. 4. Hillas' parametrization does not give an adequate description of the particle spectrum at energies below 20 MeV. Therefore it is not suited for calculations based on Eq. (1) if a threshold different from 50 keV was used for calculating the longitudinal shower profile.

3. Longitudinal Cherenkov Profile

The longitudinal Cherenkov profile generated by CORSIKA for an exemplary primary proton of 10^{19} eV is shown in Fig. 5 together with the results based

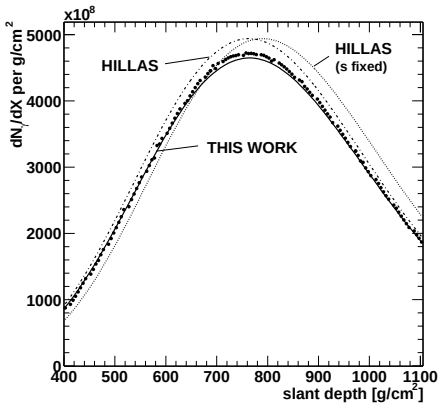

Fig. 5. Longitudinal Cherenkov profile obtained by CORSIKA, different parametrizations (see text).

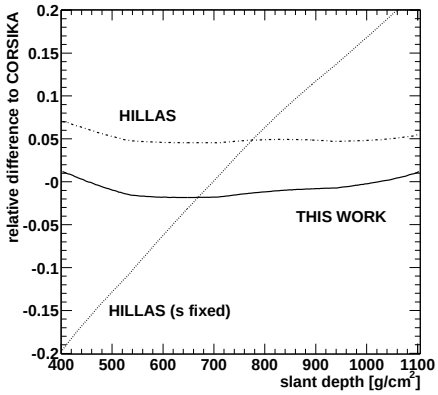

Fig. 6. Relative difference of the profiles shown in Fig. 5 to the CORSIKA profile.

on the different parametrizations. The relative difference of the profiles to the CORSIKA one is displayed in Fig. 6. The calculation labeled "Hillas (s fixed)" employs Hillas' parametrization for $s = 1$ only, as often used (see e.g. [1]). This approximation leads to a shift of the Cherenkov profile by about 30−40 g/cm^2 towards larger depths, due mainly to the neglected reduction of high-energy electrons with growing age. It could be cured to a large extend by taking the s-dependence of [4] into account. However, the predicted Cherenkov production exceeds the CORSIKA one by $\simeq$ 5%. The best agreement is obtained using the new parametrization. Around the Cherenkov profile maximum, the deficit is less than 1−2%. The angular dispersion of particles, effectively increasing the Cherenkov yield per traversed depth dX along the axis, has not yet been taken into account in the analytical approaches. This might result in a modest increase of the predicted curves.

4. Conclusions

CORSIKA can be used to directly calculate the Cherenkov longitudinal profile. For analytical applications, an improved parametrization of the electron energy spectra is proposed based on CORSIKA simulations. It can also be used to infer the Cherenkov profile from a given charged particle output.

1. Baltrusaitis R.M. et al. 1985, Nucl. Instr. Meth. A240, 410
2. Giller M. et al. 2003, these proceedings
3. Heck D. et al. 1998, Report FZKA 6019 (Forschungszentrum Karlsruhe)
4. Hillas A.M. 1982, J. Phys. G 8, 1461
5. Risse M. et al. 2001, Proc. 27th ICRC (Hamburg) 2, 522

Simulation of Cherenkov Contamination for Cosmic-Ray Showers Observed with the Auger Fluorescence Telescopes

L. Perrone[1], C.K. Guerard[2], F. Nerling[3] and M. Risse[3]
(1) Universität Wuppertal, Fachbereich Physik, D-42097 Wuppertal, Germany
(2) Universität Karlsruhe, IEKP D-76021 Karlsruhe, Germany
(3) Forschungszentrum Karlsruhe, Institut für Kernphysik, 76021 Karlsruhe, Germany

Abstract

Any measurement of cosmic ray shower features relying on the fluorescence light technique requires a good knowledge of Cherenkov light contribution along shower development. The results of a simulation study concerning properties of Cherenkov light emission are shown using GEANT and CORSIKA. An evaluation of the Cherenkov contribution to the photon profile detected by fluorescence telescopes has been carried out by performing shower simulations with CORSIKA. For a given primary energy and geometry, an analytical function is then built, providing the number of Cherenkov photons at any depth and for any angle to shower axis. This method has been applied to a few hybrid events collected during the engineering prototype phase of the Auger Fluoresence Detector (12/2001-3/2002).

1. Introduction

For the primary energy determination by means of fluorescence telescopes, a reliable estimate of the Cherenkov contamination is required. The basic Cherenkov emission properties are studied using the GEANT [1] simulation tool and compared to the predictions given by the CORSIKA [2] code. Then, a simulation study of the (direct) Cherenkov contribution to the signal expected at the diaphragm of the Auger Fluorescence Telescopes [3] has been carried out using CORSIKA shower simulations.

2. Comparison of Basic Emission Properties

The GEANT and the CORSIKA predictions concerning Cherenkov light emission properties, i.e. number and angle of emitted photons, are compared for different air densities. Single electrons are simulated and the Cherenkov wavelength range has been chosen between $300-400$ nm. Since in GEANT the Poissonian fluctuations are taken into account, an average of 1000 events is calculated

pp. 1–4

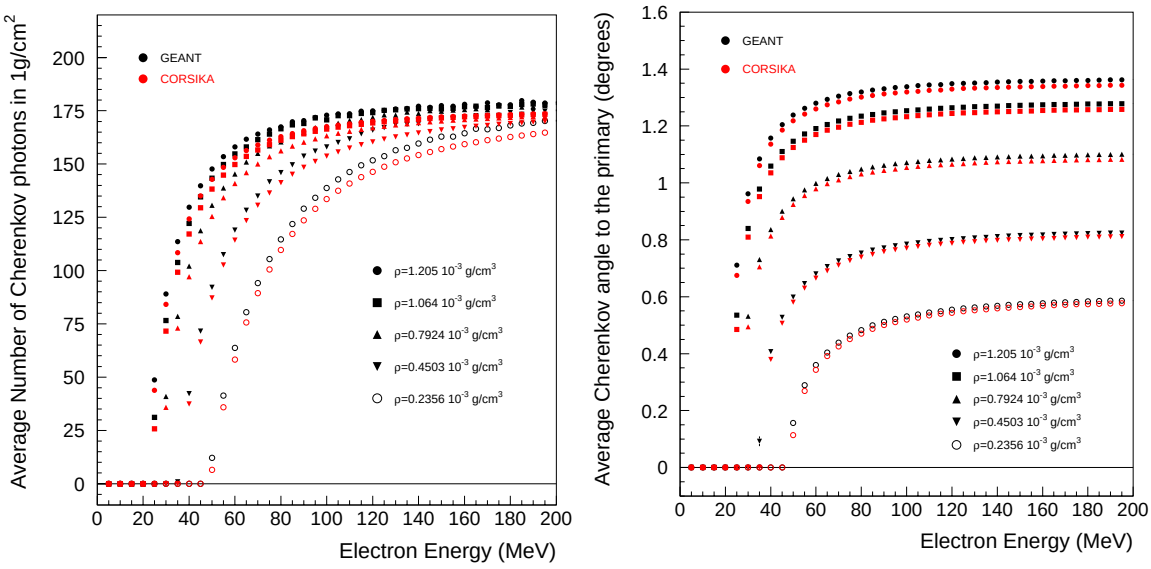

Fig. 1. Average number of Cherenkov photons produced by individual electrons in the next 1 g/cm^2 (left) and corresponding average emission angle (right) vs. electron energy. GEANT and CORSIKA values are compared for different air densities.

for each combination of electron energy and air density. In Fig. 1 (left), the average number of Cherenkov photons produced in the next 1 g/cm^2 is shown as a function of electron energy. The energy threshold for the production of Cherenkov photons ($v > c/n$ with v the velocity of the emitting particle and n the refractive index), as well as the "saturation region" for large electron energies can be clearly seen in figure. The agreement is fairly good, failing at most at the level of a few percent. The main reason of the slight difference is given by the different treatment of the refractive index. Indeed, CORSIKA is currently neglecting the wavelength dependence of this quantity. The calculation of the average number of Cherenkov photons has been repeated taking in GEANT the same index of refraction as used in CORSIKA. In this case, the relative disagreement is reduced at the level of 1.5% or better. A GEANT based study shows that the fluctuations of the average number of Cherenkov photons produced in the next 1 g/cm^2, stay, far from the energy threshold, at the level of 8%. In Fig. 1 (right), the average Cherenkov emission angles are shown as a function of electron energy and compared for different air densities. In this case the agreement between the two calculations is at the level of 1.5% and the fluctuations are always well below 1%.

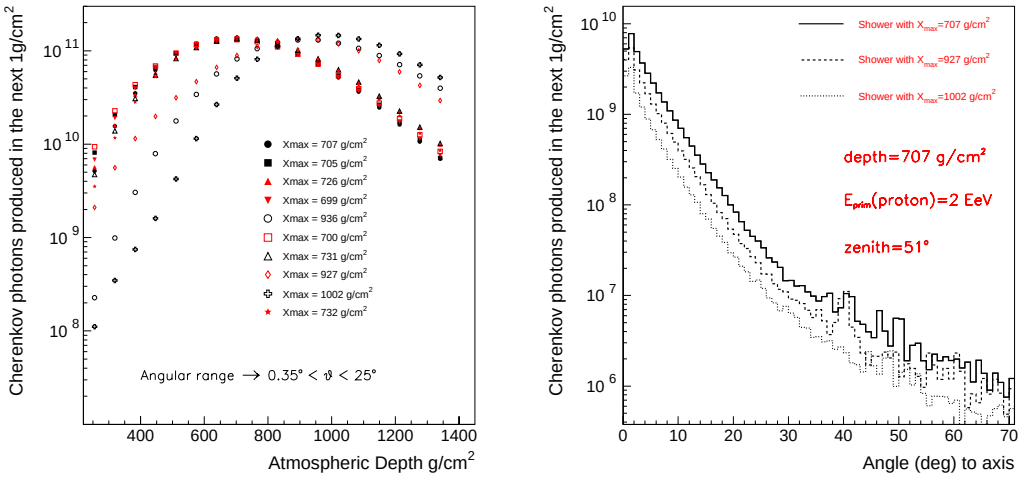

Fig. 2. *Left*: Number of Cherenkov photons produced in the next 1g/cm^2 and up to 25° to shower axis as a function of atmospheric depth, for ten proton-initiated showers. (E$_{prim}$= 2 EeV, zenith=51°). Corresponding depths at shower maximum are also given. *Right*: Angular distribution of Cherenkov photons at slant depth of 707 g/cm^2 for three of the ten showers shown on the left.

3. Simulation of the Cherenkov Contribution

CORSIKA shower simulations have been performed in order to evaluate the Cherenkov light contribution along the shower development. Ten inclined proton-initiated showers with primary energy of 2 EeV and with zenith angle of 51° have been simulated for this study. The angular distribution of Cherenkov photons is extracted in bins of 0.250° and in vertical layers of 40 g/cm^2. In Fig. 2 (left), the number of Cherenkov photons produced in the next 1 g/cm^2 and up to 25° to shower axis is shown as a function of atmospheric depth. The shift in the profiles are due to different points of first interaction. The corresponding shower maxima (X_{max}) are also given with different keys. In Fig. 2 (right), the Cherenkov photon angular distribution at slant depth of 707 g/cm^2 is shown for three of the ten showers shown on the left. Geometry and primary energy have been chosen following the method described in [4], based on a preliminary reconstruction of a hybrid event collected during the engineering prototype phase of the Auger Fluorescence Detector. Using these simulations and a Spline algorithm for interpolation, a two dimensional function giving the number of Cherenkov photons produced at any depth and any angle to shower axis is then calculated. The photons falling in the field of view of any particular photomultiplier are transmitted through the atmosphere down to the detector. Since the shower track is pointing roughly towards the observer we expect a large direct Cherenkov con-

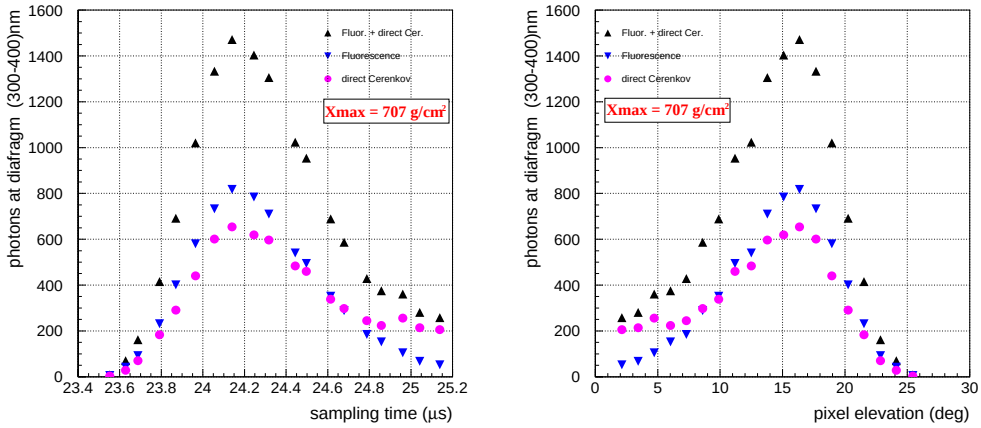

Fig. 3. Simulated photon profiles at the detector diaphragm as a function of time (left) and mirror pixel elevation (right). A proton-initiated shower with primary energy of 2 EeV and with zenith angle of 51° has been used for this study. The contribution of direct Cherenkov and fluorescence photons, as well as the total light signal, are shown with different keys.

tribution. (More details on the photon profile simulation adopted here are given in [4]). In Fig. 3, the number of photons received at the detector diaphragm is shown as a function of time (left) and mirror pixel elevation (right). The shower with $X_{max} = 707$ g/cm^2 has been used for this plot. The contribution of direct Cherenkov and fluorescence photons, as well as the total light signal, are shown in Fig. 3 with different keys.

4. Conclusion

The agreement between GEANT and CORSIKA predictions for the basic Cherenkov emission features (number of emitted photons and emission angle) is at the level 2–3%. A simulation study concerning the direct Cherenkov photon contamination in the light signal received at the fluorescence detectors has been presented. This is mainly intended as a tool for contributing to the current and upcoming analyses of Auger Fluorescence Detector data.

Acknowledgments. The support by D. Heck is gratefully acknowledged.

5. References

1. GEANT 3.21, 1994 CERN Program Library Long Writeups W5013
2. Heck D. et al. 1998 Report **FZKA 6019**, Forschungszentrum Karlsruhe
3. Argiro S. for the Auger Collaboration, these Proceedings
4. Guerard C.K. et al., these Proceedings

The Slow Control System of the Auger Fluorescence Detectors

N. Barenthien[1], C. Bethge[1], K. Daumiller[1], H. Gemmeke[2], K.-H. Kampert[3] and C. Wiebusch[3]
(1) Universität Karlsruhe, Institut für Experimentelle Kernphysik, PF 6980, 76128 Karlsruhe, Germany
(2) Forschungszentrum Karlsruhe, Institut für Prozessdatenverarbeitung und Elektronik, PF 3640, 76021 Karlsruhe, Germany
(3) Universität Wuppertal, FB8 Physik, Gaußstr. 20, 42097 Wuppertal, Germany

Abstract

The fluorescence detector (FD) of the Pierre Auger experiment [1] comprises 24 telescopes that will be situated in 4 remote buildings in the Pampa Amarilla. It is planned to run the fluorescence detectors in absence of operators on site. Therefore, the main task of the Slow Control System (SCS) is to ensure a secure remote operation of the FD system. Thus, the Slow Control System works autonomously and continuously monitors those parameters which may disturb a secure operation. Commands from the data-acquisition system or by the remote operator are accepted only if they do not violate safety rules that depend on the actual experiment conditions (e.g. high-voltage, wind-speed, light, etc.). In case of malfunctions (power failure, communication breakdown, ...) the SCS performs an orderly shutdown and subsequent startup of the fluorescence detector system. The concept and the implementation of the Slow Control System are presented.

1. Introduction

The Auger experiment intends to measure Extended Air Showers (EAS) produced by highest-energy cosmic rays ($> 10^{19}$ eV). At these energies, the particles of the EAS stimulate N_2 molecules in the atmosphere to emit fluorescence light which can be used to examine the longitudinal development of the shower. The fluorescence light will be measured by the fluorescence telescopes, while additionally 1600 water Čerenkov particle detectors will be used to examine the lateral distribution of the particles in the EAS.

To ensure a secure operation, the SCS permanently has to monitor the current experimental conditions in each of the 4 FD buildings, especially those who endanger the telescopes (e.g. sunlight and wind). In addition, the SCS must be able to activate actuators (e.g. electric motors for shutters, failsafe curtains etc.) to protect the telescopes if necessary. A summary of control functions is

pp. 1–4 empty

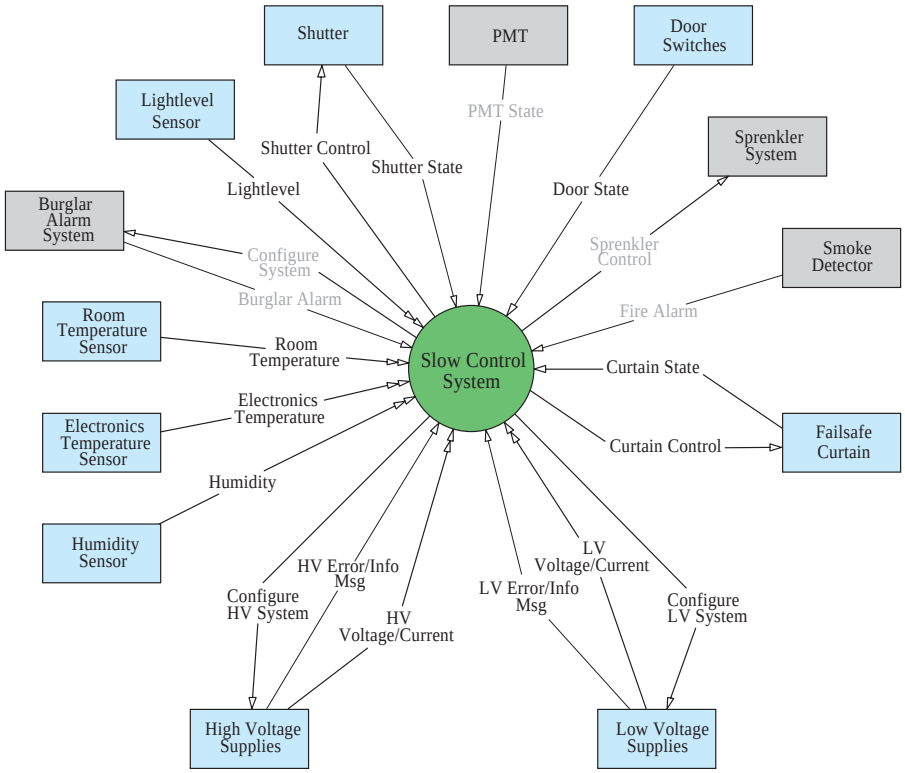

Fig. 1. Overview of the components that are monitored and controlled by the SCS

sketched in figure 1.

This necessity for reliable supervision and the desire for high flexibility and stability of the SCS led to a system based on industrial components. The hard- and software implemented for the Auger FD telescopes will be presented in the following.

2. Hardware

2.1. The PROFIBUS-*system*

PROFIBUS-systems (PROcessing FIeld BUS) are usually used in industrial environments where production processes are automated (e.g. car production). Major advantages are its simplicity, stability and high flexibility.
The used system is composed of several bus-terminals with specific functions (e.g. analog input, digital output, relay etc.). The connected terminals build up a modular bus-system which allows to address and control each terminal via PC. Through this concept, we were able to design a system that is exactly adapted to

the requirements but can also be easily modified, if requirements change.

2.2. The Field-PC

The so called *Field-PC* is the central instance of the SCS and runs the main control software under a *Windows-NT* operating system. It is a commercial product designed for heavy duty applications [2]: it has no peripheral devices attached, is dust protected, needs no fans and is controlled by hardware watchdogs. Within our experience, gained in 2 year operation, we observed no system failure.

3. Software

The main control software is implemented using a commercial product *4CONTROL* [3]. This software provides an integrated development environment for for multi-target control and automation systems. It provides the access to the *PROFIBUS* and an *OPC* (OLE for Process Control) server and client to communicate of other parts of the experiment. The OPC-server as well as an integrated *HTTP*-server allow remote operation via graphical user interfaces. The system supports programming in several languages: the Pascal like *ST* (Structured Text), the graphical language *SFC* (Sequential Function Chart), as well as *JAVA*.

4. Implementation

The implemented system for one of the fluorescence detector buildings is shown in figure 2. Each building hosts six telescopes in so-called *bays*. In each bay the system operates the shutter doors. Protection of the telescope is achieved by monitoring the entrance doors and the light-level. In case of too much light a failsafe curtain is dropped in front of the telescope. too much light. The power supply for each bay, data acquisition (DAQ) and the *Field-PC* are monitored. In case of a power cut, uninterrupted power supplies allow that the SCS puts the telescopes, front-end electronics and DAQ computers into a safe state. Additional sensors watch the outside environment, such as wind, rain, temperature and light. In case of extreme conditions the SCS can take appropriate actions, e.g. closing of shutters in case of strong wind. The high and low voltages for the PMTs of the telescopes are monitored using the *4Control* OPC client and a *Caen* OPC server [4]. Other systems of the experiments, the DAQ and the graphical user interface in the main control room, interact with the SCS using the *4Control* OPC server. They collect data and can request changes of the operation mode, unless in contradiction to SCS safety rules.

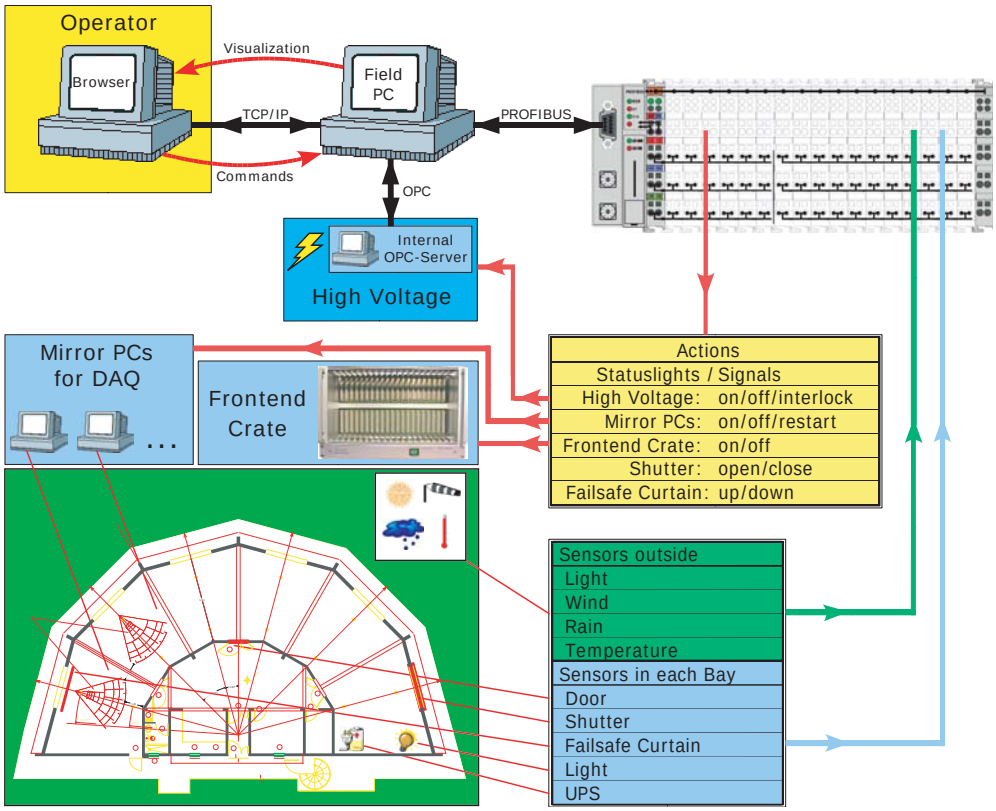

Fig. 2. Scheme of the SCS at the Auger experiment

5. Status and Outlook

All different hardware components have been integrated and tested at experimental site. Presently, two buildings are equipped with SCS systems. Installation of remaining components is taking place. A first version of the operation software has been released and is continously running. It is planned to allow the operation of 6 telescopes with full slow control by the end of summer 2003.

6. References

1. Some Auger citation
2. Softing, 4CONTROL Field PC, data-sheet, `www.softing.de`.
3. `Softing, 4CONTROL, www.softing.de.`
4. `Caen, OPC server for Caen power supplies, www.caen.it.`

Statistical Calibration and Background Measurements of the Auger Fluorescence Detector

Hartmut Gemmeke, Matthias Kleifges, and Alexander Menshikov
Forschungszentrum Karlsruhe, IPE, 76021 Karlsruhe, POB 3640, Germany

Abstract

In the framework of the hybrid cosmic ray experiment Auger a precise calibration of the fluorescence detector (FD) is necessary to ensure the energy scale of the measurement. Aging of the photomultiplier tubes (PMT) induce long-term variations of their response; whereas varying light intensities, and power-on and off cycles result in short term changes of gain. Therefore, a simple and fast statistical method was developed to calibrate the gain of all channels simultaneously. Test measurements with the prototype showed that our method is insensitive to drifts of the light intensity and could also be applied to evaluate PMT after-pulses. A simplified version of the method measures continuously the sky background and single stars down to 7^{th} magnitude.

1. Introduction

The prototype detectors of the Auger experiment [1] have been successfully tested and operated. Currently the final design version of the detectors and electronics are under installation. The electronics of the FD [2] continuously records the input of each pixel in a ring buffer of $100\mu s$ length with a $10 MHz$ clock rate. Each PMT is powered by a positive high voltage at the anode; therefore its signal is AC-coupled to the front-end amplifier containing a 4^{th} order Bessel filter for anti-aliasing. The quantum and photoelectron collection efficiency of the system, gain of the PMTs and associated electronics, time constants of the filter, and their changes with time have to be included in event reconstruction and detector Monte-Carlo.

An absolute light calibration [5] will be performed several times a year. However, a prompt calibration after interesting events is necessary several times during a night of observation. The choice of a rectangular light pulse of a blue LED with a length of about $70\mu s$ allows us to collect in a very short time sufficient statistic for the evaluation of variance and mean value of ADC values. The gain is then deduced from the ratio of variance and mean [3]. Furthermore the measurement of the LED brightness by a Si-Pin-diode will calibrate the relative light sensitivity at the same time.

pp. 1–4

Although the entire electronic system was designed for best sensitivity to short PMT pulses we need also to determine the average DC light level or a current monitor at each PMT for 3 reasons: 1. Protection of the PMTs against excess light to avoid destruction or fast aging, 2. knowledge of the sky brightness on a pixel-to-pixel basis to determine atmospheric conditions, and 3. tracking of stars across the camera verify the absolute pointing of the telescopes. The AC coupling prevent a direct measurement of the PMT current. Thus, a statistical analysis of the ADC values [4] was installed to determine the sky brightness.

In the following sections we describe some results gained with the prototype applying the new methods of calibration.

2. Statistical Method

Illumination of a PMT may be considered as bombarding the PMT photocathode with a sequence of photons described by a Poisson process. That holds for the light produced by a LED and also by stars in the sky background.

In our model of the electronic system [3] the impulse response function is determined by the anti-aliasing filter and the AC-coupling network with its time constant τ_{AC} of $0.8ms$. The anti-aliasing filter with a time constant of about $150ns$ determines completely the high-frequency behavior of the system. The noise of the PMTs and electronics including digitization noise are small compared to the fluctuations of the photoelectron signal, simplifying the method.

From the theory of random functions generated by a Poisson process it follows that the mean of the response of the amplifier $M(t)$ to a step-like light impulse is well approximated by

$$M(t) \approx \overline{i_{phel}}\, G\, \exp\left(-t/\tau_{ac}\right) = M_0\, \exp\left(-t/\tau_{ac}\right)\ (ADC\text{-}counts) \tag{1}$$

and the variance of the response D and the gain G are given by

$$D \approx \overline{i_{phel}}\, G^2\, (1+\nu_g)\ F/5\ (ADC\text{-}counts^2) \tag{2}$$

$$G \approx 5\, D/(M_0\ (1+\nu_g)\ F)\ (ADC\text{-}counts/(phel/100ns)) \tag{3}$$

with the average photoelectron current $\overline{i_{phel}}$ and the noise equivalent bandwidth $F(MHz)$. The approximations (1) and (2) are exact for times t considerably larger than the time constant of the anti-aliasing filter. Equ. (2) is valid for noise-free amplification systems. For a realistic case the variance of the electronic noise has to be subtracted.

For the current monitor we have to calculate the variance D of successive ADC values. Using Equ. (2) we derive the cathode DC current from the variance D for constant G, ν_g and F over the measuring period:

$$\overline{i_{phel}} \approx 5\, D/(G^2\ (1+\nu_g)\ F)\ (phel/100ns) \tag{4}$$

The value of ν_g varies from PMT to PMT within a batch in the 10% range, which induces an error of 2.8% in the number of photoelectrons.

The calculation of variance D is done continuously in the FPGAs on the frontend-boards described in more detail in [4]. The statistical accuracy of the method with 2^{16} samples was about 0.5% for the variance.

3. Measurement Results

3.1. Gain measurements, Drifts and noise equivalent bandwidth F

A series of 50 to 100 LED pulses ($70\mu s$ long) provides the necessary amount of samples for evaluation of the variance D and the parameter M_0 of the mean value. The illumination level was kept low enough to avoid short-term gain drifts of the PMTs. We confirmed the quality of the short-term stability of LED and PMTs gain, by comparison of the amplitude at both edges of the pulse. The total error of the gain measurements depends on the uncertainty of ν_g and the errors of variance and mean and is smaller than 5.5%.

The ratio D/M obtained with and without digital integration yields the noise equivalent bandwidth F of each channel. These values have to be evaluated only once and then with high statistics.

3.2. Distortions induced by afterpulses

We investigated afterpulses using our $50\mu s$ long LED pulses with a sharp falling edge. We found only very small distortions at the end of each pulse of the PMTs. The response of each channel was averaged over 100 LED pulses and normalized to the amplitude of the light pulse. After that an averaged response of all channels of the camera was calculated. We found an afterpulse ratio of 1.3%. We measured two well-separated peaks in the afterpulse distribution at 0.9 and $2.2\mu s$ after the falling edge.

3.3. Results and comparison with other measurements

Using 100 light flashes of $70\mu s$ we got 60 000 samples. We obtained an averaged gain of 1.84 ($ADC\text{-}counts/photoelectrons/100ns$) for the complete camera with a statistical error of 0.2%. We assume that all PMTs have the same single photoelectron resolution of 0.4. The fluctuation analysis applied to the absolute calibration data obtained with 150 LED flashes ($35\mu s$ long) produces an average gain of about 1.76 ($ADC\text{-}counts/photoelectrons/100ns$) [3], and both measurements are consistent within the errors.

3.4. Equalizing the gain of the detector

At first the amplification of the electronics was set to the same nominal value and the gain of the camera was measured with the described method.

From the measurements we got a $\Delta G/G$ of 30% in the gain and calculated the amplification correction factors for each channel to obtain a uniform gain over the detector. Then the amplification of the electronics was adjusted accordingly and the absolute gain of the camera was re-measured. Uniformity of the camera gain was drastically improved. The remaining channel-to-channel deviation of the gain was on average 3%. In a few channels the regulation range of the gain was exceeded and the absolute gain could not be set to the desired value.

3.5. Statistical current monitor

Every 30 s the ADC variance and pedestal for each pixel was recorded. At the beginning we measured the variance with the shutter in front of the telescope closed and used this data to subtract the background caused by electronic noise. This contribution was stable over time and amounts to less than 10% of the variance due to sky background. The statistical current monitor was also applied to track stars in the field of view of one prototype camera. It was possible to find light peaks from stars if they cause at least a 5% increase in light intensity corresponding to a star of 7^{th} magnitude.

4. Conclusion and Outlook

The complete calibration procedure for each pixel of the detector including the analysis and adjustment of the amplifiers takes a few minutes, which is about an order of magnitude faster compared to previous methods [4]. Furthermore the described method evaluates the mean value for each macro pulse of 70μs and thus avoids problems due to drifts and AC-coupling.

Our measurements with the prototype detector proved that the statistical current monitor gives a very good approximation of the night sky light level and provides a precise instrument to measure the alignment of the FD telescopes.

The experiment started data acquisition with the final FD telescope design in May 2003. From this time on the statistical current monitor and gain calibration system willbe in routinely operation during cosmic ray measurements.

5. References

1. Blümer J. for Auger Collaboration 2003, 28th ICRC, Tsukuba
2. Gemmeke H. for Auger Collaboration 2001, 27th ICRC, Hamburg.
3. Menshikov A. et al 2003, to be published in IEEE Trans. Nucl. Sci.
4. Kleifges M. et al 2003, to be published in IEEE Trans. Nucl. Sci.
5. Roberts M.D. for Auger Collaboration 2003, 28th ICRC, Tsukuba

Auger-South Hybrid Sensitivity to Highly Inclined Hadron-Induced Air-Showers: Mass Composition at High Energy

M. Ave [1], C. K. Guérard[2], L. Perrone[3], R.A. Vazquez[4] and E.Zas[4]
(1) Center for Cosmological Physics, University of Chicago, 933 S. Ellis Av, Chicago 60637, USA
(2) IEKP, Universität Karlsruhe, Postfach 3640,D-76021 Karlsruhe, Germany
(3) Fachbereich Physik, Universität Wuppertal, 42097 Wuppertal, Germany
(4) Departamento de Fisica de Particulas, Campus Sur s/n, Universidad de Santiago de Compostela, E-15706 Santiago de Compostela, Spain

Abstract

The Auger Observatory aims at the detection of Ultra-High-Energy Cosmic-Rays using atmospheric fluorescence telescopes over-viewing a 3000 km^2 array of water Cherenkov tanks, a mini prototype of which has been successfully taking data since 12/2001 in the province of Mendoza, Argentina. In this paper we present a Monte Carlo calculation of the hybrid sensitivity of the Auger-South Observatory to highly inclined hadron-induced air-showers, and show that such showers can play an important role to extract the mass composition of the highest energy cosmic rays.

1. Introduction and Outline of the Method

Efforts to understand the origin of cosmic rays at energies above 100 TeV are greatly hampered by our lack of knowledge of the mass distribution in the incoming cosmic ray beam. While there is a common assumption that protons dominate at energies above 10^{18} eV, hard experimental evidence is lacking.

The number of muons at ground level can be used to determine the mass distribution of the cosmic ray beam, as heavier primaries are more effective producing muons. However, we have to face the experimental challenge of counting muons using water Cherenkov detectors. Two approaches can be used: (1) We can use the FADC traces of the recorded events and try to separate the muonic from the electromagnetic component. (2) The approach proposed in this work: To use inclined showers (with zenith angles larger than 60°). Inclined showers would not be very different from vertical showers except for the fact that they develop in the upper part of the atmosphere. As a result the electromagnetic part of the shower, produced mainly from π° decay, is mostly absorbed well before the shower front reaches ground level. However, the muon front propagates through the atmosphere mixed with an electromagnetic halo coming from muon

pp. 1–4

Bremsstrahlung, pair production and muon decays. This halo is continuously generated and represents less than 15% of the signal in a Cherenkov tank as long as one is sufficiently far away from the core (a few tens of meters).

The spatial distribution of muons at ground is related to the distance travelled by the muons from their production points to ground. These distances vary slightly for different primaries. As an example, for 70° zenith angle showers it is 30 (33) km for proton (iron) primaries. It is explicitly shown in [1] that the muon distributions at ground level are hardly different in shape for iron and proton primaries.

From the previous discussion, it becomes clear that the signal recorded by water Cherenkov tanks at any given position relative to shower core is approximately proportional to the number of muons in the shower. Unfortunately, in order to reconstruct the energy of an inclined event we have to make an assumption on primary composition. Here is where the hybrid capability of the Auger Observatory takes a key role. The energy can be obtained using the fluorescence technique with only a small systematic uncertainty due to the unknown mass. Moreover, knowledge of the position of the shower maximum (X_m), sensitive to primary composition as well, can also be used.

Fig. 1 shows the correlation between X_m and the number of muons (N_μ) obtained with simulations for a zenith angle of 66° and a primary energy of 10^{19} eV. We have used a library of showers generated by S. Sciutto using the computing facilities in Fermilab. The Monte Carlo code used is AIRES [2]. The separation between proton and iron primaries is clear. The correlation between X_m and N_μ is small, as expected, since the fluctuation in N_μ is related to the fluctuations in the number of charged pions produced in the first interactions which have little effect on the position of the shower maximum.

In the next section, a calculation of the predicted number of hybrid inclined hadron initiated showers is presented.

2. Calculation of the Hybrid Rate

It is shown in [3] that inclined showers with cores inside the array, energies above 10 EeV and zenith angles larger than 60° have a trigger efficiency close to 100 %. The number of hybrid inclined showers is then determined by the fluorescence detection efficiency.

Fluorescence telescopes detect the optical fluorescence from the ionization of N_2 molecules when cosmic rays shoot through the atmosphere. The fluorescence yield has proven to be proportional to charged-particle energy deposit [4]. It is isotropic and, depending on air density and temperature, can vary from 3 to 5.6 photons/m/charged-particle with wavelengths ranging from $\sim$ 280 to 450 nm. The fluorescence technique has the great advantage that fluorescence light can be detected very far away from its point of emission. The question then

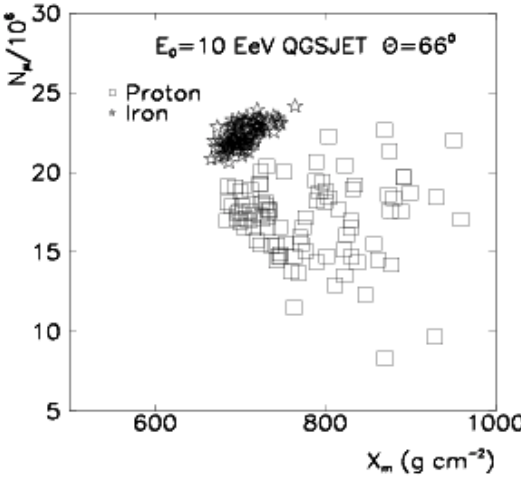

Fig. 1. Correlation between X_m and N_μ obtained with simulations for a zenith angle of 66° and a primary energy of 10^{19} eV.

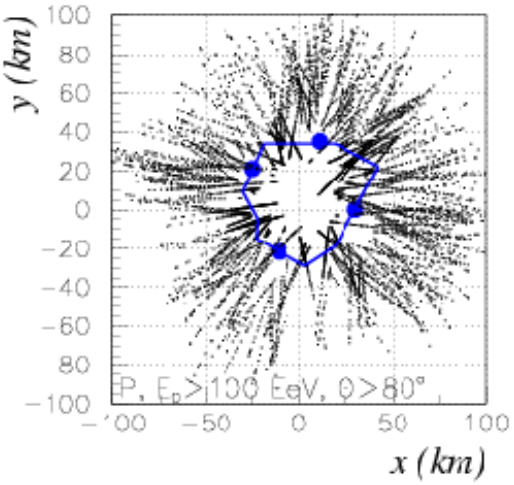

Fig. 2. Simulated ground projected trajectories of hybrid stereo detected EAS for Proton primaries with energies greater than 100 EeV and zenith angles greater than 80°.

arises whether (highly) inclined hadron-initiated showers can be detected by the Auger Fluorescence Telescopes, since for depths exceeding 70° the $N_{e^-e^+}$ size has already diminished by almost three orders of magnitude with respect to the size at shower maximum. In principle, depending on combinations of primary energy, zenith angles and heights above ground, shower detection may become possible. In order to answer this question, we have made a Monte Carlo calculation in which all EAS have been constrained to land (randomly) within the boundaries of the Auger Surface Array. The incoming direction of each primary has been uniformly distributed in azimuth between 0 and 2π, and in zenith angle as $\sin\theta\ \cos\theta$. Depending on zenith, a vector of length ranging from (90-1,000) km has been built and segmented into 30 m intervals (100 ns intervals along shower axis). At each point the slant depth has been calculated taking into account Earth's curvature. Next, a Gaisser-Hillas function has been used with the functional dependence of shower maximum and shower size at maximum obtained from simulations for proton and iron primaries. Fluorescence yield is calculated from shower size. A mirror trigger condition is met when 4 aligned pixels (out of 5) trigger.

3. Results

We have calculated the Auger hybrid sensitivity based on the detection of 400 iron and 400 proton primaries having energy thresholds of 10 EeV, 50 EeV and 100 EeV (distributed according to a power-law spectrum with differential energy spectral-index of 2.7), and zenith angles above 60°, 70°, and 80°. In Fig. 2 we plot the ground projected trajectories of the part of the track of each shower

Table 1. Montecarlo Auger hybrid Mono and Stereo efficiencies for iron and proton primaries. The numbers in parenthesis are the expected yearly event rate assuming a normalization of the cosmic ray flux at 10 EeV taken from [6].

EeV	Zenith	Fe-Mono	Fe-Stereo	P-Mono	P-Stereo
10	60	0.85 (102)	0.78 (93)	0.84 (100)	0.77 (92)
	70	0.69 (40)	0.54 (31)	0.68 (40)	0.56 (32)
	80	0.08 (1.2)	0.03 (0.45)	0.10 (1.5)	0.04 (0.6)
50	60	0.89 (6.2)	0.85 (6.0)	0.93 (6.5)	0.90 (6.2)
	70	0.81 (2.6)	0.75 (2.4)	0.84 (2.7)	0.76 (2.4)
	80	0.30 (0.24)	0.16 (0.13)	0.34 (0.3)	0.20 (0.16)
100	60	0.94 (1.9)	0.91 (1.82)	0.95 (2)	0.92 (1.84)
	70	0.86 (0.8)	0.81 (0.76)	0.88 (0.82)	0.82 (0.77)
	80	0.43 (0.1)	0.25 (0.05)	0.50 (0.1)	0.30 (0.07)

detected at least by two eyes. The fact that no EAS are detected beyond 82° zenith angle opens the possibility for interpreting any such event as a neutrino-like induced shower [5]. In Fig.2 we can observe the 4 eyes (circles) positioned on the perimeter of the surface array (SA) (each viewing $30° \cdot 30°$ of sky above the SA which is composed by 1600 water Cherenkov tanks -not shown on the graph for clarity- spaced 1.5 km from each other in a triangular pattern). In Table 1 we summarize our results for each combination of primary composition, energy and zenith angle. The hybrid efficiencies are given both for the mono (showers only detected by one eye) and stereo mode (at least two eyes). The numbers in parenthesis are the expected yearly event rate assuming a normalization of the cosmic ray flux at 10 EeV taken from [6].

The aim of this work is to show that hybrid inclined events will be detected by the Auger Observatory. A calculation of the predicted number of events is presented. Further work is in progress to establish the power of these events to estimate mass composition of high energy cosmic rays.

1. Ave, M M., Hinton, J. A., Vázquez, R. A., Watson, A. A., and Zas, E., 2002, Phys. Rev. D65 063007.

2. Sciutto, S.J., 1999, Proc. XXVI Int. Cosmic Ray Conf., vol. 1, p. 411; astro-ph/9911331.

3. Ave, M. et al. 2003, Phys.Rev. D67 043005.

4. Kakimoto, F., Loh, E. C., Nagano, M., Okuno, H., Teshima, M., and Ueno, S., 1996, Nucl. Inst. Meth. Phys. Res. A372, p.244

5. Guerard, C.Kj., 2001, Proc. XXVII Int. Cosmic Ray Conf., vol. 2, HE, pp.760-63.

6. Abu-Zayyad, T. et al., submitted to Astroparticle Physics, astro-ph/0208301

Identification of Photons in Ultra-High Energy Cosmic Rays

P. Homola[1], D. Góra[1], D. Heck[2], H. Klages[2], J. Pękala[1], M. Risse[2], B. Wilczyńska[1], and H. Wilczyński[1]
(1) H. Niewodniczański Institute of Nuclear Physics, ul. Radzikowskiego 152, 31-342 Kraków, Poland
(2) Forschungszentrum Karlsruhe, Institut für Kernphysik, 76021 Karlsruhe, Germany

Abstract

The possibility of discerning extensive air showers initiated by ultra-high energy (UHE) photons from those induced by hadrons is studied. Two effects characteristic only for UHE photons are taken into account: LPM effect and photon conversion/cascading in the geomagnetic field. First conclusions about the possibility of identification of photons in the UHE cosmic-ray spectrum are presented and the "primary photon hypothesis" for the Fly's Eye $3.2{\cdot}10^{20}$eV event is shortly discussed.

1. Introduction

The existence of cosmic rays with energies above 10^{20}eV is experimentally proven but their nature and origin are still unknown. Theoretical models encounter large difficulties in explaining how protons or nuclei can be accelerated to such extremely high energies. There are, however, many so-called exotic scenarios considering photons as cosmic rays. Such photons could subsequently induce extensive air showers (EAS) in the Earth's atmosphere. Photon-induced showers can be distinguished from hadron-induced ones thanks to the two physical effects that are characteristic only for photons at energies above 10^{19}eV: gamma conversion with subsequent cascading in the geomagnetic field and the Landau-Pomeranchuk-Migdal (LPM) effect [5]. At energies above 10 EeV, in the presence of the geomagnetic field, a photon can convert into an e^+e^- pair before entering the atmosphere. The resultant electrons will subsequently lose their energy by magnetic bremsstrahlung. The emitted photons can convert again if their energy is high enough. In this way, instead of one high energy photon at the top of atmosphere, a number of less energetic particles, mainly photons and a few electrons, will enter the atmosphere. We will call this cascade a "preshower" since it originates and develops above the upper atmosphere, i.e. before the "ordinary" shower development in the air. A superposition of subshowers induced by the

pp. 1–4

preshower particles should be seen by fluorescence detectors as one EAS which usually reaches its maximum much earlier than an EAS induced by a single photon of equal energy, starting at the top of atmosphere and later than a shower initiated by a hadron. Thus, the atmospheric depth of shower maximum (X_{max}) can be used as a signature of primary photon. In this paper we concentrate on the X_{max} as the most promising primary photon signature in the shower longitudinal profile. We combine CORSIKA [3] (which includes the LPM effect) with the Krakow preshower code which treats the propagation of UHE photons in magnetosphere before they enter the Earth's atmosphere.

2. Methods

Both photon conversion and magnetic bremsstrahlung depend strongly on the transverse component of the magnetic field – small variations of the field vector can cause dramatic changes of the preshower properties, and, consequently, the changes of the longitudinal development profile of the resultant EAS [4]. In our simulations we use the IGRF model [6] of the geomagnetic field and the numerical procedures [9] allowing for calculation of the field components at any given position. The photon propagation simulations are started about 5 Earth's radii above sea level. Initially, the photon trajectory is followed in steps of $dr =$ 10 km. In each step the transverse magnetic field is computed, and then the probability of conversion is found using Eq. (1):

$$p_{conv}(r) = 1 - \exp[-\alpha(\chi(r))dr] \simeq \alpha(\chi(r))dr \tag{1}$$

where $\alpha(\chi) = 0.5(\alpha_{fs} m_e c/\hbar)(B_\perp/B_{cr})T(\chi)$, $\chi \equiv 0.5(h\nu/m_e c^2)(B_\perp/B_{cr})$, α_{fs} is the fine structure constant, $B_\perp$ is the magnetic field component transverse to the direction of photon motion, $B_{cr} \equiv m_e^2 c^3/e\hbar = 4.414 \cdot 10^{13}$ G, and $T(\chi)$ is the magnetic pair production function which is negligible if $\chi \ll 1$, has a maximum around $\chi = 5$ and then decreases slowly to zero [2, 4].

If conversion takes place, the photon creates an e^+e^- pair; the e^{+-} particles begin to emit bremsstrahlung. The probability of emitting a photon by a single electron over a small distance dr is calculated in every 1 km with use of Eq. (2):

$$p_{brem}(B_\perp, E, h\nu, dr) = dr \int_0^E I(B_\perp, E, h\nu) \frac{d(h\nu)}{h\nu} \tag{2}$$

where $I(B_\perp, E, h\nu)$ is the spectral distribution of radiated energy, E is the electron initial energy and $h\nu$ is the energy of the emitted bremsstrahlung photon [8, 4]. Once a photon is emitted, its energy is assigned according to the probability distribution given by Eq. (2), and the energy of the radiating electron is diminished respectively. Bremsstrahlung photons of energies lower than 10^{12}eV have a very small influence on the air shower evolution and hence they can be

E_0[eV]	direction	fraction of converted	$\langle X_{max} \rangle$ [g/cm^2]
10^{20}	weak $B_\perp$	1/50	1125 ± 105
	strong $B_\perp$	48/50	920 ± 55
10^{21}	weak $B_\perp$	50/50	1025 ± 45
	strong $B_\perp$	50/50	945 ± 15

Table 1. X_{max} and RMS values for photon-induced showers of two different primary energies and arrival directions.

neglected. The preshower simulations are finished when the top of atmosphere is reached. Then all preshower particles are passed to CORSIKA. The resultant EAS is simulated by CORSIKA as a superposition of subshowers initiated by the preshower particles.

3. First Results for the Pierre Auger Southern Site

In Table 1 we compare X_{max} and RMS of X_{max} for simulated photon-induced showers for two different primary energies and arrival directions. The results presented here were obtained for the Southern Pierre Auger Observatory (PAO) in Malargüe, Argentina (35.2°S, 69.2°W) [7], but other geographical positions can be easily adopted. Here the strong $B_\perp$ direction is defined as $\theta = 53°$, $\phi = 177°$ and weak $B_\perp$ as $\theta = 53°$, $\phi = 357°$ in the local frame at Malargüe with the azimuth increasing in the counter-clockwise direction beginning from the geographical North. In all cases the shower maxima are well inside the atmosphere at the Southern PAO with a slant depth of 1450 g/cm^2 for a zenith angle $\theta = 53°$. For proton-induced EAS a X_{max} value of 820 ± 60 g/cm^2 for 10^{20}eV and 870 ± 50 g/cm^2 for 10^{21}eV is expected.

For $E_0 = 10^{20}$eV and weak $B_\perp$, almost all photons remain unconverted when entering atmosphere, which results in large $\langle X_{max} \rangle$ and large fluctuations due to the LPM effect. A comparison with hadronic primaries allows for the conclusion that unconverted primary photons should be well distinguishable from p and Fe on an event-by-event basis. At the primary energy of 10^{21}eV all photons convert, whatever the arrival direction. We still see the directional dependence of $\langle X_{max} \rangle$, but it is not as strong as previously. The fluctuations of X_{max} in this case are significantly lower (by about a factor of 3) than for 10^{20}eV primaries. Table 1 shows that at 10^{21}eV it is more difficult to distinguish a single photon primary from a proton one on the basis of X_{max} value. Since in the Auger Experiment we don't expect large statistics of such events, it might be a challenge to notice the azimuthal asymmetry of X_{max} or the decrease of RMS fluctuations. Studies of the elongation rates for different arrival directions seem to be promising. From Table 1 we find out that at Malargüe, for the strong $B_\perp$ direction, the elongation rate of photon-induced showers between 10^{20}eV and 10^{21}eV is much

less than 50-60 g/cm^2 expected for proton or iron showers. For the weak $B_\perp$ we even have a *negative* elongation rate. This is because the preshowering effect for photons at 10^{21}eV splits the initial energy into energies less than 10^{20}eV and at this energy level, for the weak $B_\perp$ direction, almost all the primary photons remain unconverted and they induce air showers with deeper X_{max}. Lower than expected or negative elongation rates should be an additional good signature of photon showers, provided a sufficient statistics is available.

4. Fly's Eye Highest Energy Event

The methods and tools described above were applied to real data of the highest-energy shower ever detected – a cosmic ray event recorded by the Fly's Eye Experiment in 1991 [1]. To estimate the probability that the recorded EAS was induced by a photon, we used our preshower+CORSIKA program to simulate 250 shower profiles with the parameters of the event: primary photon with initial energy $E_0 = 3.2 \cdot 10^{20}$eV, zenith angle $\theta = 43.9°$, azimuth $\phi = 32.0°$ (counter-clockwise from East) and for the geographical location of the detector (40°N, 113°W). The experimental value of the shower maximum is $X_{max} = 815^{+60}_{-53}$ g/cm^2 [1], while from the simulations we get an average value of $X_{max}(sim) = 925 \pm 25$ g/cm^2. For each simulated profile a χ^2 value and the probability that the profile fits the data were computed. The average probability that the record EAS detected by Fly's Eye was initiated by a photon is about 1-2% whilst the probability for the profile closest to the data is about 40%. These preliminary results do not allow to exclude a photon as primary particle.

Acknowledgements. This work was partially supported in Poland by the KBN grants No. PBZ KBN 054/P03/2001 and 2P03B 11024 and in Germany by the BMBF grant No. POL 99/013.

1. Bird D.J. et al. 1995, ApJ 441, 144
2. Erber T. 1966, Rev. Mod. Phys. 38, 626
3. Heck D. et al. 1998, Report FZKA 6019, Forschungszentrum Karlsruhe
4. Homola P. et al. 2002, Pierre Auger Note GAP-2002-077; www.auger.org
5. Landau L.D. and Pomeranchuk I.J. 1953, Dokl. Akad. Nauk SSSR 92, 535 and 735; Migdal A.B. 1956, Phys. Rev. 103, 1811
6. National Geophysical Data Center, USA, www.ngdc.noaa.gov
7. Pierre Auger Project Design Report 1997; www.auger.org
8. Sokolov A.A. and Ternov I.M. 1986, Radiation from Relativistic Electrons; Springer, Berlin
9. Tsyganenko N.A., National Space Science Data Center, NASA GSFC, Greenbelt, MD 20771, USA, http://nssdc.gsfc.nasa.gov/space/model/magnetos/data-based/geopack.html

Shower Simulation Input for Fluorescence Yield Measurements

Markus Risse and Dieter Heck
Forschungszentrum Karlsruhe, Institut für Kernphysik, 76021 Karlsruhe, Germany (correspondence to: markus.risse@ik.fzk.de)

Abstract

The CORSIKA simulation code has been adapted for an extensive study of the energy release of shower particles during the cascade development. The contributions to the energy deposit from different particle species and energies as well as the typical particle densities are investigated. The dominant contribution stems from electrons and positrons from sub-MeV up to a few hundred MeV, with typical distances between particles exceeding 1 mm for 10 EeV showers. Special care is taken of particles falling below the simulation energy threshold which contribute around 10% to the total deposition.

1. Introduction

For the primary energy determination of extensive air showers observed by fluorescence telescopes, it is generally assumed that the yield of fluorescence photons is locally proportional to the energy release in air. This has been justified to some extent by fluorescence yield measurements [5]. Different approaches, some of them at accelerator facilities, are underway to further check the validity of this assumption and to improve our knowledge about this quantity [4]. To give a guideline for the preparation of such experiments, it is investigated which particle types and energies contribute to the energy release in air showers and which are the typical particle separations in the region of main fluorescence production.

2. Calculation of the Energy Release

Shower simulations for proton, iron and photon primaries at energies of 10^{18}-10^{20} eV have been performed with the CORSIKA code [2]. The electromagnetic interactions are treated in CORSIKA within the EGS4 code [7] which has been upgraded to allow simulations at the highest energies [3]. More details about CORSIKA features at the highest energies are given in [6,8].

The energy release is determined following the concept of "restricted stopping power" [1]: The energy loss to particles below the simulation energy threshold is treated as continuous process whereas production of particles above the

pp. 1–4

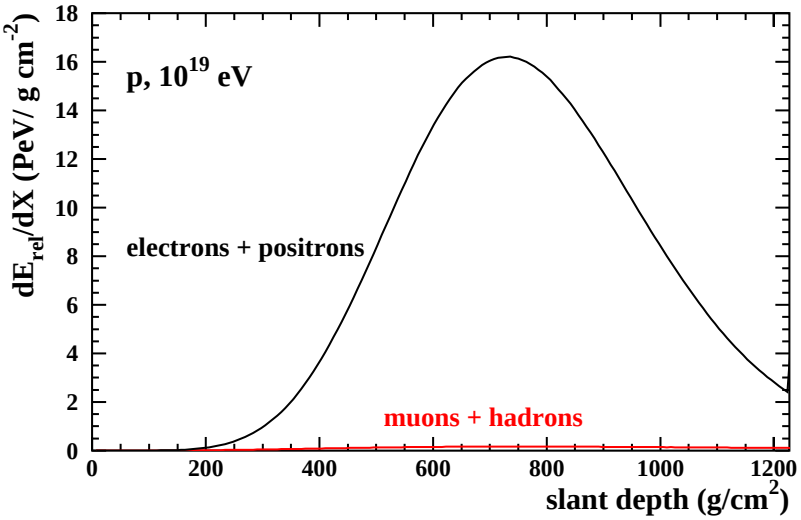

Fig. 1. Longitudinal energy release of different shower components.

threshold is simulated explicitely. In case of a particle directly produced below or reaching the threshold, a *releasable energy* is defined and written to an output table which consists at least of the kinetic energy plus some species-dependent part. The latter effectively takes processes such as future annihilation or decay into account. In case of positrons, annihilation quanta are produced for further tracking. A detailed description is given in [9].

3. Results

In Fig. 1, the longitudinal development of individual contributions to the energy release is shown. As the main shower features relevant for this analysis turn out to dependent only modestly on the considered primary particle and energy, only results for proton showers of 10^{19} eV are plotted (for others see [9]). As expected, the main energy release is provided by electrons and positrons, the most numerous particles (photons contribute indirectly via production of charged particles). Around shower maximum, less than 2-3% are provided by muons and hadrons. Thus, electromagnetic particles should be the main target for the study of energy release.

In Fig. 2, the energy spectrum of electrons and positrons at shower maximum (which is of most interest for fluorescence observations) is given. Particles with energies below 1 GeV dominate the energy release. A large portion stems from energies slightly below the critical energy of electrons in air ($\simeq$84 MeV), with a tail towards small energies. While at higher kinetic energies ($E_{\rm kin} > 300$ MeV) electrons and positrons contribute about equally to the energy release, at lower energies only electrons survive due to the positron annihilation. The annihilation

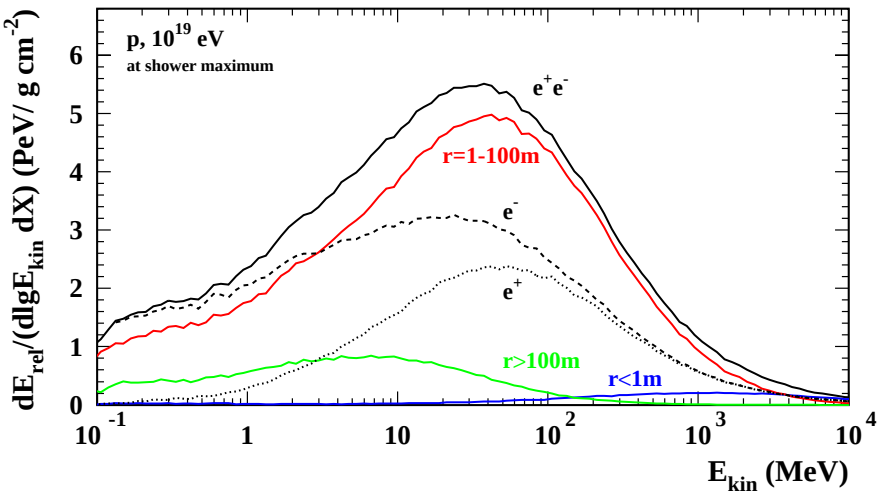

Fig. 2. Contribution to the energy release per matter traversed in shower direction as a function of the kinetic particle energy. Simulation for primary proton, 10^{19} eV, at shower maximum. The sum of $e^{\pm}$ and their individual distributions are shown. Additionally, the total contribution has been divided in three different distance ranges from the shower axis as indicated.

Table 1. Estimates for the contribution of different ranges in $e^{\pm}$ kinetic energies to the electromagnetic energy deposit. Uncertainty of the values is about ±2 (in %).

Energy in MeV	< 0.1	0.1-1	1-10	10-100	100-1000	>1000
Contribution in %	10	12	23	35	17	3

photons will eventually transfer the energy by Compton scattering to electrons. As a guideline, in Table 1 the contribution to the electromagnetic energy deposit for different energy ranges is estimated. The value for $E_{\rm kin} < 0.1$ MeV is given by the releasable energy of the particles below threshold.

The spectral shape mainly reflects the particle energy spectrum [8]. Especially the contributions of the lower energies are more pronounced, however. This is due firstly to the increased specific energy loss (Bethe-Bloch formula), and secondly to a larger average path length through the considered layer, since at lower energies the dispersion of particle angles is increasing.

The range of mainly contributing energies is to a good approximation quite independent of the primary particle type (including primary photons), primary energy, and shower age. For instance, at earlier development stages the spectrum is only slightly shifted to higher electron energies. This result may be understood, since the particle energy spectrum is known to show a small, but in this context only minor dependence on primary type and shower age [8].

Also indicated in Fig. 2 are contributions from different lateral distance ranges. Most of the energy is released in the distance range of 1−100 m. The fraction provided by particles with less than 1 m distance to the shower axis is quite small: Though the densities are largest here, the absolute particle number is comparatively small. A correlation of the average particle energy with distance to the shower axis reveals that the contributions are shifted towards higher $E_{\rm kin}$ values for the smaller distances. More detailed analyses [9] show that the main energy release occurs at core distances of $\simeq$30 m, implying typical particle separations exceeding 1 mm for 10 EeV showers (scaling with the inverse primary energy). With respect to the ionization region around the particles, this is a large separation resulting in a relatively "undisturbed" de-excitation of the air molecules. Thus, high-density particle bunches should be avoided in fluorescence yield measurements as the fluorescence yield might be obtained in conditions not typical for air showers.

4. Conclusion

The energy release in air showers has been studied with respect to currently planned fluorescence yield measurements. Most relevant is the determination of the yield for electrons and positrons with energies in the range from sub-MeV up to a few hundred MeV. The typical particle separation is relatively large with 1 mm or more for 10 EeV showers at shower distances which mainly contribute to the energy release and thus, presumably, to the fluorescence light. For shower calculations, the energy release provided by CORSIKA can be transformed to fluorescence light based on existing and upcoming fluorescence yield measurements.

Acknowledgments. The discussions with R. Engel, H. Klages, J. Knapp, and T. Waldenmaier are gratefully acknowledged.

1. Berger M.J., Seltzer S.M. 1964, Report NASA-SP-3012; Kase K.R., Nelson W.R. 1979, Concepts of Radiation Dosimetry (Pergamon Press, New York)
2. Heck D. et al. 1998, Report FZKA 6019 (Forschungszentrum Karlsruhe)
3. Heck D., Knapp J. 1998, Report FZKA 6097 (Forschungszentrum Karlsruhe)
4. International workshops in Utah (USA) 2002, and Bad Liebenzell (Germany) 2003; see www.physics.utah.edu/~fiwaf/done and www.auger.de/events
5. Kakimoto F. et al. 1996, Nucl. Instr. Meth. A 372, 527; Nagano M. et al. 2003, subm. to Astropart. Phys., astro-ph/0303193
6. Knapp J. et al. 2003, Astropart. Phys. 19, 77
7. Nelson W.R. et al. 1985, Report SLAC 265 (Stanford Linear Acceler. Center)
8. Risse M. et al. 2001, Proc. 27^{th} ICRC (Hamburg) 2, 522
9. Risse M., Heck D. 2003, in preparation; also Auger Note GAP-2002-043 2002

Study of Shower Optical Image Based on Energy Deposits Derived from CORSIKA

D. Góra[1], D. Heck[2], P. Homola[1], H. Klages[2], J. Pękala[1], M. Risse[2], B. Wilczyńska[1] and H. Wilczyński[1]
(1) H. Niewodniczański Institute of Nuclear Physics, ul. Radzikowskiego 152, 31-342 Kraków, Poland
(2) Forschungszentrum Karlsruhe, Institut für Kernphysik, 76021 Karlsruhe, Germany

Abstract

Using the CORSIKA shower simulation package, the spatial distribution of energy deposited by the shower in the atmosphere through ionization is obtained and the distribution of light arriving to the detector is calculated. The resulting shower image is compared with that obtained using the NKG distribution of particles in the shower and a constant fluorescence yield. Taking into account the distribution of energy deposited by the shower leads to a small dependence of the size of shower image on the primary particle.

1. Introduction

The fluorescence method of extensive air shower (EAS) detection is based on recording light emitted by air molecules, excited by charged particles of the shower. The amount of fluorescence light is closely correlated to the particle content of a shower and provides therefore a calorimetric measure of the primary energy. It has been commonly assumed that the fluorescence yield, i.e. the number of fluorescence photons emitted per unit length of a charged particle track, is approximately constant, the same for all particles in the shower. However, since the fluorescence light is induced by exciting the molecules of the ambient medium (the air), the fluorescence yield is expected to depend on the ionization density along a charged particle track [5]. Most particles in the shower have energies below 1 GeV, i.e. in the energy range of considerable dependence of ionization density on particle energy. Therefore, one should expect that the total fluorescence signal induced by the shower should depend not just on the number of particles in the shower, but rather on the total energy deposited in the air through ionization.

2. Simulations

In this paper we analyze the image of the shower using two different approaches. First: we keep the constant value of fluorescence yield $N_\gamma = 4.02$

pp. 1–4

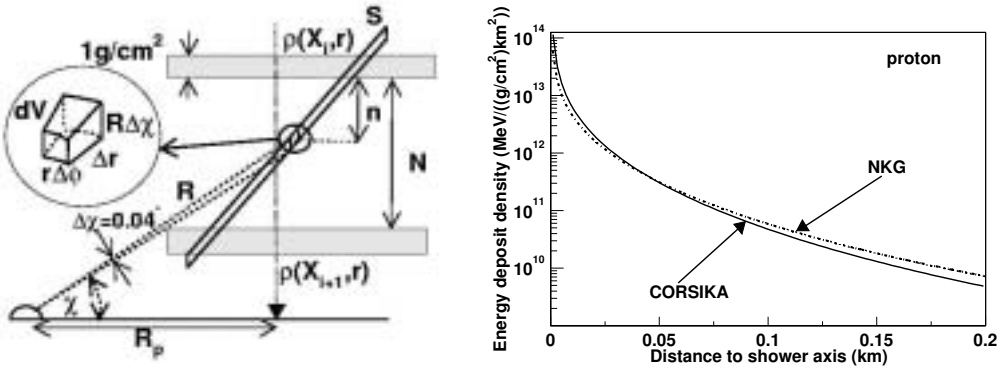

Fig. 1. (A-left) Geometry of an EAS as seen by the fluorescence detector. Photons which arrive simultaneously to the eye originate from surface S. (B-right) The lateral distribution of energy deposit density in CORSIKA and NKG approximations, calculated for an average vertical proton shower, with energy $E_0 = 10^{19}$ eV.

photons per meter, as used by the Fly's Eye group, and assume the NKG distribution of particles in the shower (NKG approximation). The lateral distribution of particles in the shower can be written as $\rho_N(X, r) = N(X)f(r)$, where $f(r)$ is the lateral shape function. The width of the shape function $f(r)$ is proportional to the width of the shower image. The size of the shower image $\Delta\theta$ is defined as the diameter of the shower image spot at an elevation angle χ, i.e. the apparent angular size of the surface S (see Fig.1), as seen from the detector. In the second approach using the CORSIKA shower simulation package [4,6], the lateral energy deposit distribution $\rho(X_i, r)$ is calculated at 20 horizontal layers of thickness $\Delta X = 1$ g/cm^2.

The photons which constitute an instantaneous image of the shower originate from a range of shower development stages, namely from surface S shown in Fig. 1. The small element of surface S in polar coordinates corresponds to a small volume ΔV. The value of energy deposit $\rho(X_n, r)$ in the volume ΔV at distance r can easily be constructed by linear interpolation, see Ref. [3] for more details. Using this interpolation, the number of photons N_γ from each volume element ΔV emitted towards the detector can be calculated.

In this way, the spatial distribution of points of origin of the simultaneous photons around the shower axis is obtained. These photons are propagated towards the fluorescence telescope, using the `Hybrid_fadc` simulation software [1]. The software incorporates the atmospheric light scattering mechanism: the Rayleigh scattering on molecules of air and Mie scattering on aerosols. The atmospheric attenuation is also accounted for, so that a total photon flux (including scattered Cherenkov photons) arriving at the detector is obtained. Finally, the angular distribution of these simultaneously arriving photons is constructed to form the image of the shower.

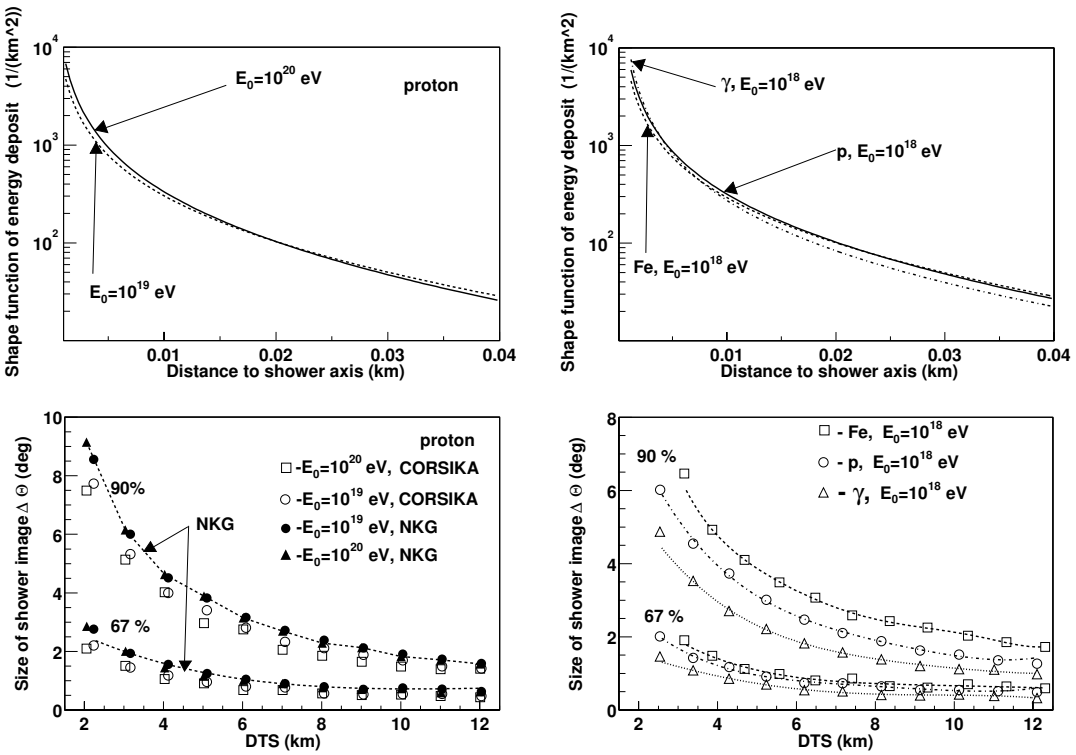

Fig. 2. (A-upper left) Shape function of average CORSIKA lateral distribution $f(r)$ vs distance to shower axis for vertical proton showers with different energies. (B-lower left) Size of the shower image containing 90% and 67% of light versus the detector to shower (DTS) distance, using CORSIKA and NKG distribution of energy deposit. (C-upper right) Shape function of average CORSIKA lateral distribution vs distance to shower axis r, for vertical proton, iron and γ shower. (D-lower right) Size of the shower image containing 90% and 67% of light versus detector to shower distance using CORSIKA distributions of energy deposit for iron, proton and γ primaries (at shower maximum).

3. Results and discussion

Simulation runs were done for primary proton, iron and γ showers with different energies of primary particle E_0. Vertical showers landing at variable core distance $R_p = 2, 3, ..., 11$ and 12 km were studied at their maxima.

Fig. 1B shows the calculated lateral distribution of the energy deposit versus distance to shower axis at any point of surface S. In case of the CORSIKA approach, the energy deposit density (solid line in Fig. 1B) was obtained using the two-dimensional histogram of energy deposited. It is seen that the energy deposit obtained using CORSIKA histograms becomes smaller than NKG for distances to shower axis greater than 45 m. This implies that locally one should expect

values of energy loss and also lateral distribution of particles in the shower which differ from those used in the NKG approximation. Since close to shower axis the value of energy deposit obtained by CORSIKA is greater than that from NKG, it means that there are more energetic particles close to the shower axis.

In Fig. 2A (upper left) the shape functions of CORSIKA lateral distributions for proton showers with primary energies $E_0 = 10^{20}$ and 10^{19} eV are shown. Fig. 2B (lower left) shows the size of the shower image $\Delta\theta$ containing 90% or 67% of light as a function of distance from the detector to the shower (DTS), for showers with different core distance R_p. It is seen that the spot size in the shower maximum is independent of energy in the NKG approximation and that the NKG approximation leads to larger sizes of shower image than those derived from CORSIKA. Moreover, for a shower with higher energy, the image size from CORSIKA is noticeably smaller than that from NKG. These differences can be understood taking into account differences of the shape function. Finally, we discuss the differences of the shower image between showers induced by different primary particles of the same energy. In Fig. 2C (upper right) the shape functions are presented for γ-, proton- and Fe-induced showers. One can see clear differences in the shape functions. The γ profile dominates over the other profiles at small distances ($r < 5$ m) from shower axis. On the other hand, Fe profile dominates at distances far from shower axis ($r > 23$ m). On the basis of Fig. 2C, one expects differences in the size of shower image. Thus, the image spot size of an Fe shower will be larger than the proton one, which in turn exceeds the spot size of a γ shower. This agrees with results presented in Fig. 2D (lower right). It can be seen that differences are quite considerable. We note that when just the *number of particles* is used (thus assuming implicitly the same ionization for all particles), there are no differences visible in the image spot size between proton and iron showers [2]. However, using the *distribution of deposited energy* leads to the difference in image size shown in Fig. 2D. Therefore, the study of shower image may be helpful in identification of primary particles.

Acknowledgements. This work was partially supported in Poland by the State Committee for Scientific Research under grants No. PBZ KBN 054/P03/2001 and 2P03B 11024 and in Germany by the International Bureau of the BMBF under grant No. POL 99/013.

1. Dawson B., private communication
2. Góra D. et al. 2001, Proc. 27^{th} ICRC, Hamburg, **2** 543
3. Góra D. et al. 2002, Pierre Auger Project Note GAP-2003-057
4. Heck D. et al. 1998, Report FZKA 6019, Forschungszentrum Karlsruhe
5. Kakimoto F. et al. 1996, Nucl. Instr. Meth. **A 372** 527
6. Risse M. and Heck D. 2002, Pierre Auger Project Note GAP-2002-043

Shower Fluorescence Light Profile Derived from CORSIKA

D. Góra[1], D. Heck[2], P. Homola[1], H. Klages[2], J. Pękala[1], M. Risse[2], B. Wilczyńska[1] and H. Wilczyński[1]
(1) H. Niewodniczański Institute of Nuclear Physics, ul. Radzikowskiego 152, 31-342 Kraków, Poland
(2) Forschungszentrum Karlsruhe, Institut für Kernphysik, 76021 Karlsruhe, Germany

Abstract

Simulations of optical image of a shower are implemented into a procedure of shower energy determination. This "top-down" approach starts with shower development and fluorescence light production in the air, to obtain the expected detector response. In this paper, distributions of energy deposited by a shower in the air through ionization, as obtained from CORSIKA, are used to derive the flux of fluorescence light arriving at a detector. The longitudinal profile of the light flux is constructed and compared to real events recorded by fluorescence telescopes of the Engineering Array of the Pierre Auger Observatory.

1. Introduction

A reconstruction of an extensive air shower from the fluorescence detector (FD) raw data involves two main tasks: the geometrical reconstruction, i.e. determining the position of the shower axis, and evaluation of the energy of the shower, after the geometry fit is done. In the latter task, a longitudinal shower profile, i.e. the number of shower particles $N_{ch}(X)$ as a function of atmospheric depth, is determined based on the amount of light received at the FD and hence – the energy of the primary particle is inferred.

Traditionally, the "bottom-up" reconstruction scheme is used, in which one converts the raw FADC data to the photon flux at the diaphragm $F(t)$. Taking into account the light propagation in the atmosphere, the longitudinal shower profile is determined. Finally, using a fit of the Gaisser-Hillas function to this $N_{ch}(X)$ profile, the total energy of the shower is determined on the basis of an integral of energy deposited by the shower particles, with the assumption that all particles have the same average ionization density. In an alternative "top-down" approach, one starts with a simulation of the shower development in the atmosphere, getting a longitudinal profile of the light induced by the shower along its path. The light is then propagated through a realistic atmosphere towards the

pp. 1–4

FD so that the profile of the light flux $F(t)$ arriving at the detector is obtained. The fluorescence yield per particle in a shower is not constant, but depends on the particle ionization density [6]. The total fluorescence signal of the shower is thus assumed to be proportional to the energy deposited by the shower in the air through ionization. Distributions of the energy deposited are now available from the CORSIKA shower simulation software [5,7]. Therefore, a possible reconstruction scheme would be to make an initial estimate of shower energy; perform multiple shower simulations with slightly varied primary parameters and for different primary particles; and finally pick the shower parameters which give the best agreement of simulation with measured data. The feasibility of such a procedure is shown here. A similar approach has also been started elsewhere [4].

2. Simulations

The distribution of energy deposited by a shower in the air is a convolution of the distribution of particles in the shower and the distribution of ionization density of particles. These distributions can now be simulated with the CORSIKA program. On the other hand, photons which arrive simultaneously at the detector, i.e. those which constitute an instantaneous image of the shower, originate from a range of shower development stages. The CORSIKA program provides particle distributions at a set of altitudes in the atmosphere. By using an appropriate interpolation procedure, presented in detail in Ref. [3], one can derive the required 3-dimensional particle distribution.

In this way, the spatial distribution of points of origin of the simultaneous photons around the shower axis is obtained as well as distribution of the photon intensities. These photons are propagated towards the FD, so the attenuation of light through Rayleigh scattering (on air molecules), Mie scattering (on aerosols) as well as scattered Cherenkov photons are taken into account in the simulation software (Hybrid_fadc [2]). In this paper, we show the calculated photon flux in which fluorescence dominates the received signal, so possible inaccuracies in the Cherenkov photon distribution are not expected to strongly influence the results.

3. Preliminary results

Simulation runs were done for proton and iron showers with geometries and energies as reconstructed using the traditional bottom-up procedure in two real events recorded by the FD telescopes of the Engineering Array of the Pierre Auger Observatory [1].

The Event1 will be discussed first. Ten proton showers and five iron ones were simulated with different depth of first interaction X_0 and depth of shower maximum X_{max}, of which several are shown in Fig. 1A. This Figure shows simulated photon flux profiles $F_s(t)$ for these proton and iron primaries versus time.

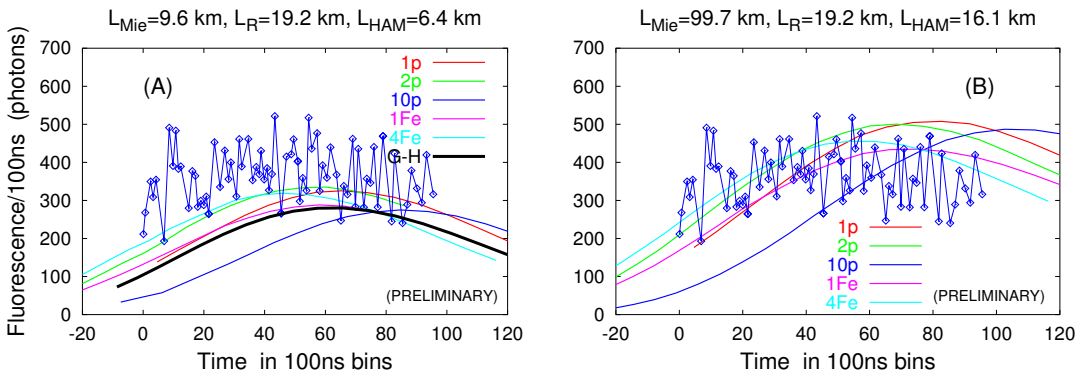

Fig. 1. The calculated fluorescence flux at telescope aperture using energy deposited from CORSIKA. (A) Display of Event1 using Hybrid_fadc default values of Mie and Rayleigh scattering lengths and (B) with a measured value of L_{HAM} from the horizontal attenuation monitor.

The recorded light profile is shown as data points, the color curves represent the simulated showers and the black thick line is the photon flux calculated using a constant value of fluorescence yield $N_\gamma = 4.07$ photons/meter and the Gaisser-Hillas function. In this plot the default value of the total (Rayleigh and Mie) horizontal attenuation length* ($L_{HAM} = 6.4$ km at 365 nm) was used in the simulation code. The simulations are about 15-20 % lower than the measured values. Fortunately, for this event there is a measured value of $L_{HAM} = 16.1$ km [1], so one can easily calculate $L_{Mie} = 99.7$ km at 365 nm. We note that measured value of L_{HAM} is about 2 times larger than the default value in the Hybrid_fadc program, so the total received signal should increase when we use the measured values of L_{HAM} in the simulations, especially for larger atmospheric depth, where light scattering is most important. Indeed, in the plot shown in Fig. 1B the calculated photon fluxes are always higher than the fluxes obtained using the default value of L_{HAM}, shown in Fig. 1A. The difference between new and old fluxes increases with increasing time from the beginning of FD trace, i.e. with atmospheric depth in this case. This demonstrates the importance of atmospheric monitoring.

Next we discuss the Event2. Unfortunately, L_{HAM} was not measured for this event, so we used the average value of $L_{HAM} = 12.7$ km at 365 nm measured at the Auger Observatory. Fig. 2A and 2B show the simulated photon flux at the diaphragm $F_s(t)$ for four iron and ten proton showers with different depth of first interaction and position of shower maximum. An agreement within about 10% is seen of the simulation profiles (color curves) with measured data (diamonds). Despite the fluctuations in the raw data itself, one can see a better agreement

*$1/L_{HAM} = 1/L_R + 1/L_{Mie}$; L_{Mie} and L_R are the Mie and Rayleigh scattering lengths, respectively.

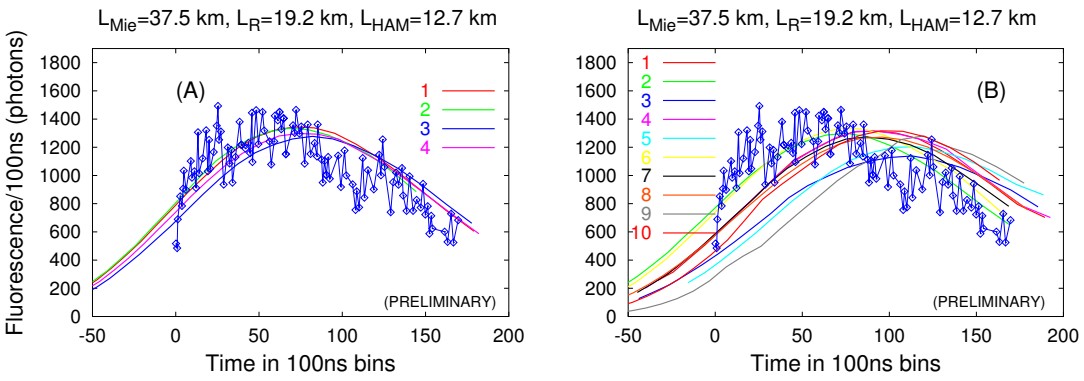

Fig. 2. The calculated fluorescence flux at telescope aperture using energy deposited from CORSIKA. Display of Event2: (A) the fluorescence signal using energy deposited for iron showers and (B) for proton showers.

with the iron simulated profiles than with the proton ones. However, two proton profiles (numbers 2 and 6), corresponding to showers with X_{max} about 700 g/cm^2 fit the data just as well. We note that differences between the simulated $F_s(t)$ and the data could be due to inaccurate assignment of primary energy and/or to an inaccurate L_{HAM}. Measurement of atmospheric attenuation is essential. Then, by varying the energy, one can find its value for which best agreement with data is obtained.

In summary, a first implementation of the "top-down" approach to analyzing the fluorescence detector data based on CORSIKA energy deposits has been presented. The simulated distributions of energy deposited by the shower in the air incorporate the variations of particle energies in the shower, and thus account for varying fluorescence yield of the shower particles. In addition, these simulations enable the study of shower profiles for various primary particles, therefore they will provide an additional constraint useful for identification of the primary.

Acknowledgements. This work was partially supported in Poland by the KBN grants No. PBZ KBN 054/P03/2001 and 2P03B 11024 and in Germany by the BMBF grant No. POL 99/013.

1. Auger Collaboration, 2003, Nucl. Instr. Meth A, to be published
2. Dawson B., private communication
3. Góra D. et al. 2003, Pierre Auger Project Note GAP-2003-006
4. Guérard C., private communication 2002
5. Heck D. et al. 1998, Report FZKA 6019, Forschungszentrum Karlsruhe
6. Kakimoto F. et al. 1996, Nucl. Instr. Meth. **A 372** 527; Nagano M. et al. astro-ph/0303193
7. Risse M. and Heck D., 2002, Pierre Auger Project Note GAP-2002-043

Influence of Low-Energy Hadronic Interaction Programs on Air Shower Simulations with *CORSIKA*

D. Heck[1,†], R. Engel[1],
G. Battistoni[2], A. Fassò[3,*], A. Ferrari[2,*], J. Ranft[4], P.R. Sala[2,+]
(1) Forschungszentrum Karlsruhe, Institut für Kernphysik, D-76021 Karlsruhe, Germany
(2) Instituto Nazionale di Fisica Nucleare, I-20133 Milano, Italy
(3) Gesellschaft für Schwerionenforschung, D-64291 Darmstadt, Germany
(4) Universität Gesamthochschule Siegen, D-57068 Siegen, Germany
(†) corresponding author; e-mail: dieter.heck@ik.fzk.de
(*) *on leave at CERN, CH-1211 Geneva 23, Switzerland*
(+) *on leave at ETH, CH-8093 Zurich, Switzerland*

Abstract

In hadron-induced extensive air showers (EAS) low-energy collisions of secondary hadrons with nuclei of the atmosphere form the final branches of the hadronic shower skeleton. In the EAS Monte Carlo simulation program CORSIKA these interactions were treated up to now by the GHEISHA code. Recently correction patches became available for GHEISHA, overcoming a number of obvious deficiencies in the simulated kinematics of low-energy interactions. Additionally the hadronic part of the FLUKA code has been coupled for the description of low-energy hadronic interactions as an alternative to GHEISHA. The predictions of the implemented low-energy models are compared to data and their influence on the simulated EAS development is investigated.

1. Introduction

The simulation of EAS is inherently linked to modeling hadronic multiparticle production over a wide energy range. The dependence of EAS simulations on high-energy hadronic interaction models has been discussed in [14, 15]. The present contribution focuses on the influence of low-energy ($E_{\rm lab} \lesssim 100$ GeV) hadronic interactions in EAS simulations with CORSIKA [13]. In the past mostly GHEISHA routines [11] have been used for this purpose, but it is known [10] that GEANT-GHEISHA suffers from deficiencies in handling the reaction kinematics properly. For example, in EAS simulations using GHEISHA the sum of the energy of the secondary particles and the deposited energy is often larger than the primary energy by several %, depending on the primary energy and the low-energy threshold (typically 300 MeV) above which hadronic particles are followed. As

pp. 1–4

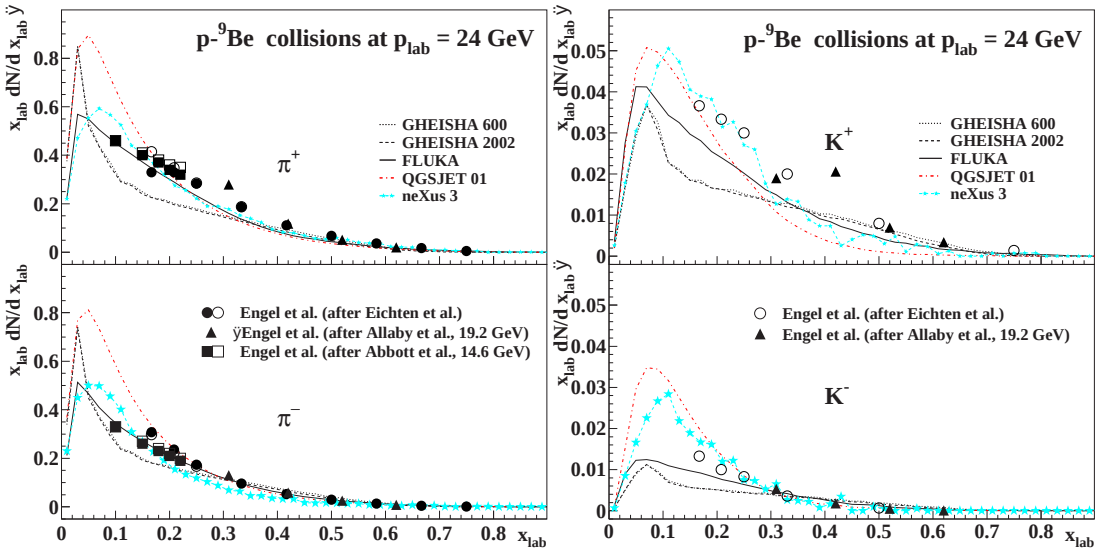

Fig. 1. Distribution of secondary particle momenta $x_{\rm lab} = p_{\rm tot}/p_{\rm beam}$ in p-^{9}Be collisions at $p_{\rm lab} = 24$ GeV. *Left*: Pions. *Right:* Kaons. The experimental data points were derived [8] from the measurements of [6, 2, 1].

an alternative to GHEISHA, the hadronic event generator of the FLUKA 2002 code [9] has been coupled with CORSIKA. Independently, correction patches [4] for GHEISHA became available which improve energy and momentum conservation, but do not change basic properties like particle multiplicities or differential cross sections. In the following we compare these models to fixed-target data and calculate air shower predictions using various combinations of low- and high-energy interaction models. We also study the importance of the threshold energy (currently $E_{\rm lab} = 80$ GeV) for switching from low- to high-energy models.

2. Comparison with Experimental Data

As in EAS ^{14}N is by far the most frequent target nucleus, a check of low-energy interaction models should be performed with target materials with similar nucleon number. For p-^{9}Be interactions several experimental data sets are available [6, 2, 1] at $E_{\rm lab} \approx 20$ GeV. In Fig. 1 the distributions of secondary mesons in $x_{\rm lab} = p_{\rm tot}/p_{\rm beam}$ are shown. The data points are obtained by integrating the published double differential cross sections [8]. For completeness the high-energy hadronic interaction programs QGSJET 01 [16] and NEXUS 3 [5], which technically handle these low energies, have been included in the comparison.

The good agreement of FLUKA predictions on pseudorapidity distributions has already been demonstrated in [3]. Generally the experimental data are well described by FLUKA, while GHEISHA (600 = uncorrected; 2002 = corrected) produces significantly less mesons at $x_{\rm lab} \approx 0.15$ and slightly more in the

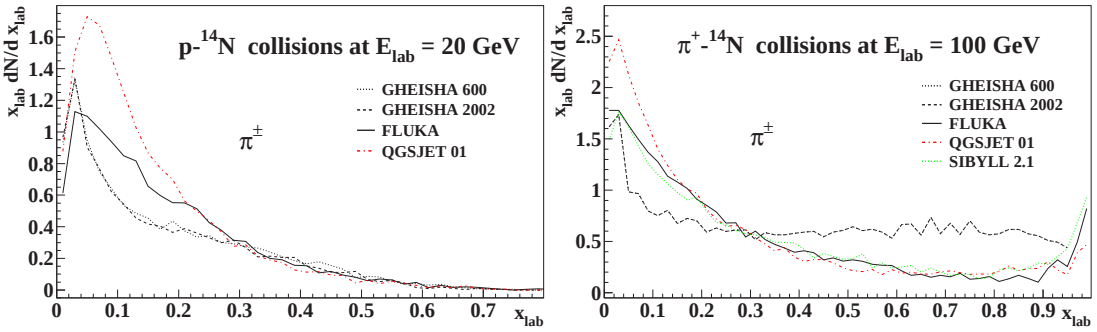

Fig. 2. Distributions of charged pion momenta $x_{\rm lab} = p_{\rm tot}/p_{\rm beam}$. *Left:* p-^{14}N collisions at $E_{\rm lab} = 20$ GeV. *Right:* π^+-^{14}N collisions at $E_{\rm lab} = 100$ GeV.

region of $x_{\rm lab} \approx 0.45$. This feature holds also for other types of hadronic collisions with ^{14}N targets, as is demonstrated in Fig. 2. In EAS simulations the understanding of π-^{14}N collisions is very important since charged pions are by far the most frequent secondary hadrons.

3. Influence on Shower Parameters

GHEISHA and FLUKA predict different momentum distributions of secondary $\pi^{\pm}$-mesons. Therefore spectra of muons with $E_{\rm lab} \lesssim 30$ GeV, which result mainly from the decay of pions produced in low-energy interactions, depend on the used low-energy model. Fig. 3 displays muon energy spectra for several combinations of low- and high-energy interaction models with transition energies of 80 GeV and 1.5 TeV. For all combinations 500 proton induced EAS with vertical incidence were averaged, considering all muons arriving at ground irrespective of their distance from the shower axis.

The largest differences between the energy spectra amount to ≈ 15 % at $E_\mu \approx 0.8$ GeV and they are clearly correlated with the differences in the predicted distributions of π-mesons at $x_{\rm lab} \approx 0.15$. Another difference of ≈ 10 % is observed at $E_\mu \approx 10$ GeV, probably related to the distribution of charged pions in π^+-^{14}N collisions at $x_{\rm lab} \approx 0.6$. The uncorrected GHEISHA 600 shows a flatter muon energy spectrum below 1 GeV than the corrected version. This difference has to be attributed to secondaries of protons emitted with by far too high energy in preceding collisions that do not conserve energy.

4. Conclusions

While the electron densities of simulated EAS show no significant dependence on the used low-energy model, its influence on the hadronic and muonic component is obvious. For CORSIKA applications that are sensitive to low-energy muon numbers and energy spectra the replacement of GHEISHA by FLUKA is

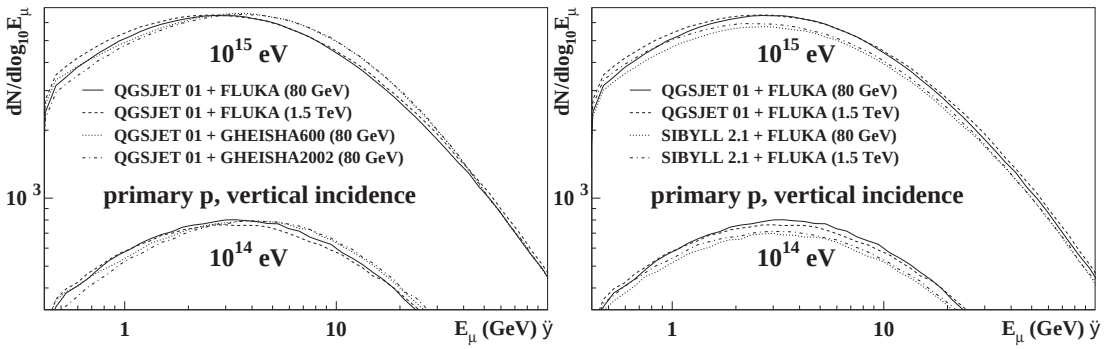

Fig. 3. Energy spectra of muons arriving at detector level (110 m a.s.l.) for primary protons of 10^{14} and 10^{15} eV, vertical incidence. *Left:* QGSJET 01 [16] combined with different low-energy models and transition energies. *Right:* QGSJET 01 and SIBYLL 2.1 [7] combined with FLUKA at transition energies of 80 GeV and 1.5 TeV.

recommended. The KASCADE detector allows the measurement of muons with different energy thresholds (approx. 490 MeV and 2.4 GeV) [12]. The observed ratio of the muon rates in EAS seems to favor FLUKA, but a detailed analysis is needed to specify the significance of the improvement.

Acknowledgements. The CORSIKA authors thank A. Chou (Fermilab) to bring their attention to the GHEISHA correction patches, and R. E. Cassell and G. Bower (SLAC) to make them available.

References

[1] Abbott T. et al. 1992, *Phys. Rev.* **D 45**, 3906
[2] Allaby J.V. et al. 1970, *CERN Yellow Report* **70-12** (CERN, Geneva)
[3] Battistoni G. et al. 2003, *Astropart. Phys.* **19**, 269 & 291
[4] Cassell R.E. and Bower G. (SLAC), private communication
[5] Drescher H.J. et al. 2001, *Phys. Rep.* **350**, 93
[6] Eichten T. et al. 1972, *Nucl. Phys.* **B 44**, 333
[7] Engel R. et al. 1999, Proc. 26^{th} ICRC, Salt Lake City (USA), **1**, 415
[8] Engel R. et. al. 2000, *Physics Lett.* **B 472**, 113
[9] Fassò A. et al. 2001, Proc. 'Monte Carlo 2000' Conf., eds. Kling et al. (Springer, Berlin) 955; http://www.fluka.org/heart/rh.html
[10] Ferrari A., Sala P.R. 1996, ATLAS int. Note **PHYS**-No-086 (CERN, Geneva)
[11] Fesefeldt H. 1985, Report **PITHA-85/02** (RWTH, Aachen)
[12] Haungs A. et al. 2003, Proc. 28^{th} ICRC, Tsukuba (these proceedings)
[13] Heck D. et al. 1998, Report **FZKA 6019** (Forschungszentrum Karlsruhe); http://www-ik.fzk.de/˜heck/corsika/
[14] Heck D. et al. 2001, Proc. 27^{th} ICRC, Hamburg (Germany) 233
[15] Heck D. et al. 2003, *Nucl. Phys. B (Proc. Suppl.)* in print; astro-ph/0210392
[16] Kalmykov N., Ostapchenko S., Pavlov A.I. 1997, *Nucl. Phys. B (Proc. Suppl.)* **52B**, 17

Simulation of Atmospheric Neutrino Fluxes with CORSIKA

J. Wentz[1,2], I. M. Brancus[1], A. Bercuci[2], D. Heck[2], J. Oehlschläger[2], H. Rebel[2], and B. Vulpescu[3]
(1) Horia Hulubei - National Institute of Physics and Nuclear Engineering, P.O.Box MG 6, 76900 Bucharest, Romania
(2) Forschungszentrum Karlsruhe, Institut für Kernphysik, Postfach 3640, 76021 Karlsruhe, Germany
(3) Universität Heidelberg, Physikalisches Institut, Philosophenweg 12, 69120 Heidelberg, Germany

Abstract

The three dimensional Monte Carlo simulation code CORSIKA is used to calculate the fluxes of atmospheric neutrinos with the hadronic interaction models DPMJET, VENUS, and UrQMD. For this purpose the original CORSIKA is extended by a parametrization of the solar modulation and a microscopic calculation of the directional dependence of the geomagnetic cut-off functions. A precise description for the geography of the Earth has been included by a digital elevation model, tables for the local magnetic field in the atmosphere, and various atmospheric models for different geographic latitudes and annual seasons. The neutrino fluxes obtained are compared with other calculations.

1. Introduction

After the experimental results of Super-Kamiokande have established the atmospheric neutrino anomaly with high statistical accuracy [5,6], it is now the turn of theoretical calculations to provide precise neutrino fluxes needed in the analysis of the neutrino oscillation parameters. Neutrino fluxes have been calculated by various groups. A recent overview and comparison of the results can be found in Ref. [10]. This paper presents a full three dimensional simulation for atmospheric muon and neutrino fluxes using the standard air shower simulation code CORSIKA [4]. The actual attempt includes a complete description of the geographical parameters of the Earth.

2. CORSIKA and its extension

The air shower simulation code CORSIKA has been designed for the simulation of extensive air showers with energies around 10^{15} eV. In order to simulate

pp. 1–4

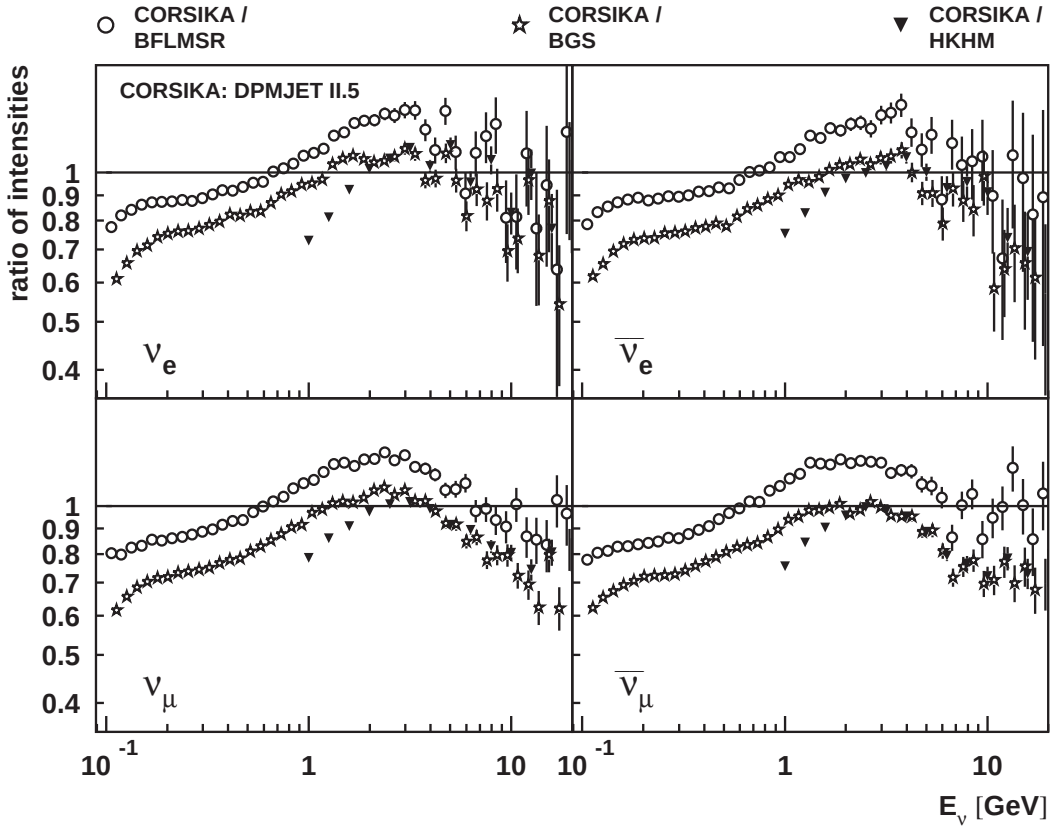

Fig. 1. The vertical differential intensities of the different neutrino flavors in Kamioka, displayed as the ratio between the CORSIKA results using DPMJET as hadronic interaction model and the calculations of BGS, HKHM and BFLMSR.

atmospheric particle fluxes induced by low energy primary particles, the version 6.000 of CORSIKA was extended by a precise calculation of the geomagnetic cut-off and a parametrization of the solar modulation. For the calculation of atmospheric neutrino fluxes a digital elevation model of the Earth, tables for the local magnetic field in the atmosphere, and various atmospheric models for different climatic zones and annual seasons have been added, too. Details about these extensions and results of tests with atmospheric muon fluxes can be found in Ref. [10].

3. Calculation of atmospheric neutrino fluxes for Kamioka

The calculation of atmospheric neutrino fluxes for Kamioka is split in two separate calculations. The downward going neutrinos are simulated locally for Kamioka, while the upward going neutrinos are calculated from primary particles distributed over the entire Earth and only neutrinos passing in a circle of 1000 km distance from Kamioka are used in the further analysis.

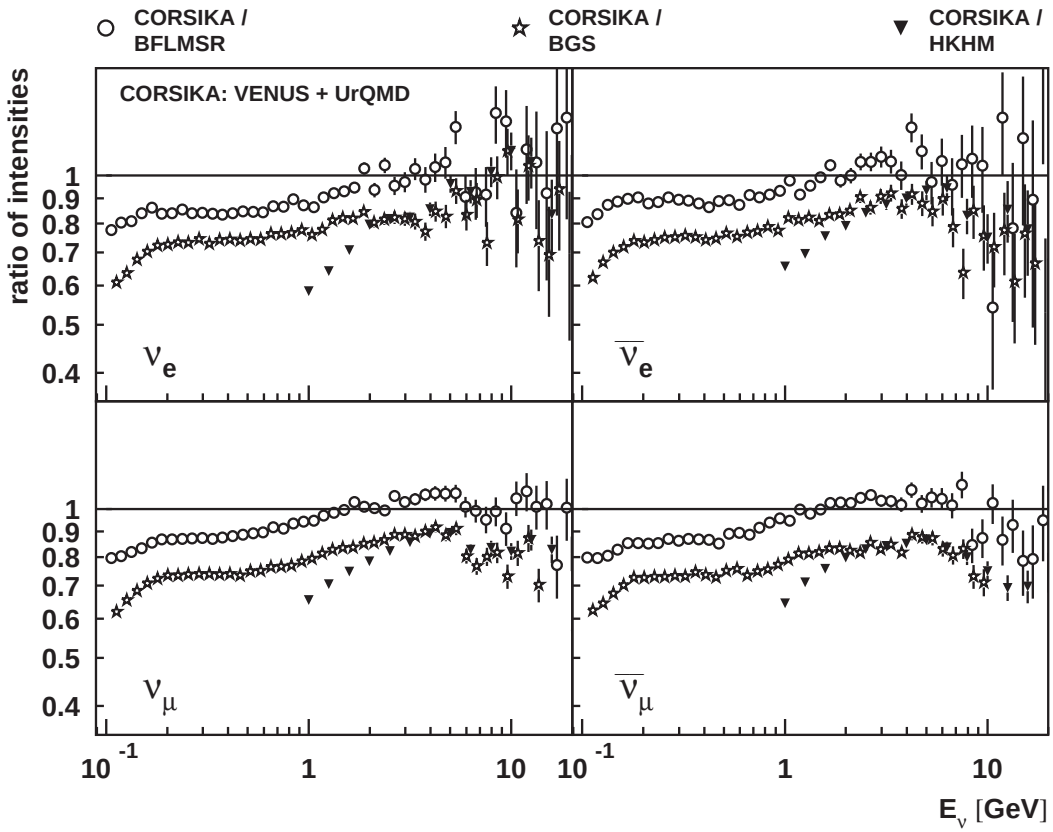

Fig. 2. The vertical differential intensities of the different neutrino flavors in Kamioka. Shown is the ratio between the CORSIKA results using VENUS + UrQMD as hadronic interaction model and the calculations of BGS, HKHM and BFLMSR.

Fig. 1 shows the results of CORSIKA using DPMJET II.5 [9] as hadronic interaction model, and Fig. 2 shows the corresponding results using VENUS 4.125 [11] and UrQMD 1.1 [3]. The energy threshold between VENUS and UrQMD is set to $E_{Lab} = 80\,\mathrm{GeV}$. The results are compared with calculations of Barr, Gaisser and Stanev (BGS) [1]; Honda et al. (HKHM) [8]; and Battistoni et al. (BFLMSR) [2]. Fig. 3 displays the directional dependence of the neutrino fluxes.

4. Conclusion

CORSIKA have been used for a precise calculation of atmospheric neutrino fluxes. The fluxes obtained are lower than the results of one dimensional calculations of BGS and HKHM, but comparable to the results of the three dimensional calculation of BFLMSR. Further results and detailed comparisons can be found in Ref. [10].

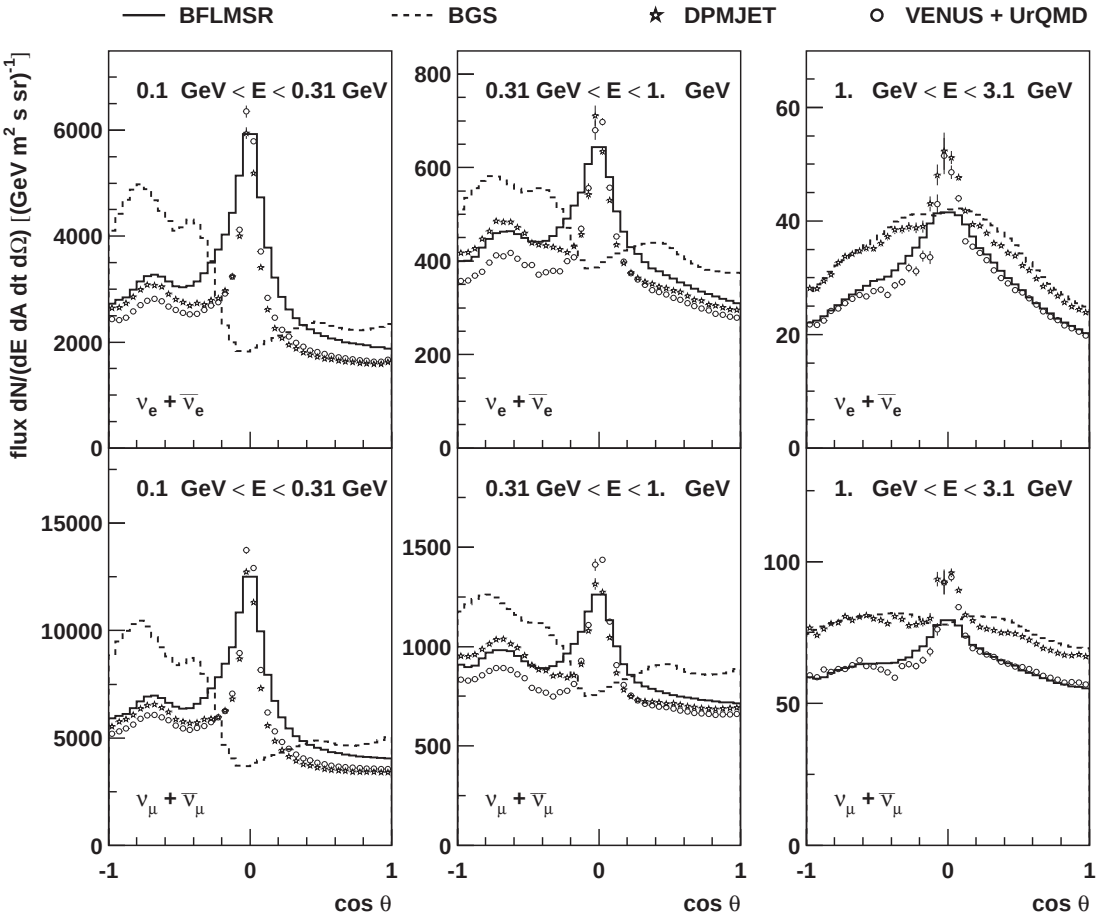

Fig. 3. The zenith angle dependence of the neutrino intensities in Kamioka as calculated by CORSIKA with DPMJET and with VENUS + UrQMD in comparison with the calculations of BFLMSR and BGS.

5. References

1. Agrawal V. et al., 1996, PRD 53, 1314
2. Battistoni G. et al. 2003, ApP 19, 269
3. Bleicher M. et al. 1999, JPG 25, 1859
4. Heck D. et al. 2003, Forschungszentrum Karlsruhe, Report FZKA 6019
5. Fukuda Y. et al. 1998, PLB 433, 9
6. Fukuda Y. et al. 1998, PRL 81, 1562
7. Gaisser T.K, Honda M. 2002, Ann. Rev. Nucl. Part. Sci. 52, 153
8. Honda M. et al. 1995, PRD 52, 4985
9. Ranft J. 1999, hep-ph/9911232
10. Wentz J. et al. 2003, PRD 67, 073020
11. Werner K. 1993, PRep 232, 87

Systematic Uncertainties in High-Energy Hadronic Interaction Models

Min Zha[1], Johannes Knapp[1] and Serguei Ostapchenko[2]
(1) Dept. of Physics and Astronomy, University of Leeds, Leeds LS2 9JT, UK
(2) IEKP, Universität Karlsruhe, D-76021 Karlsruhe, Germany

Abstract

Hadronic interaction models for cosmic ray energies are uncertain since our knowledge of hadronic interactions is extrapolated from accelerator experiments at much lower energies. At present most high-energy models are based on Gribov-Regge theory of multi-Pomeron exchange, which provides a theoretical framework to evaluate cross-sections and particle production. While experimental data constrain some of the model parameters, others are not well determined and are therefore a source of systematic uncertainties. In this paper we evaluate the variation of results obtained with the QGSJET model, when modifying parameters relating to three major sources of uncertainty: the form of the parton structure function, the role of diffractive interactions, and the string hadronisation. Results on inelastic cross sections, on secondary particle production and on the air shower development are discussed.

1. Introduction

Cosmic rays at energies $\gg 10^{14}$ eV cannot be recorded directly but are measured via the extensive air showers (EAS) of secondary particles they produce in the Earth's atmosphere. Direction, energy and mass of the primary particles have to be deduced from the properties of the showers as observed by the experimental setup. Since the relation of the primary properties to those of the air showers is complicated the event reconstruction relies on numerical models which simulate the interaction and particle transport through the air in great detail. A major source of uncertainty in those models is the simulation of the nuclear and hadronic interactions, cross sections and particle production, at very forward emission angles and at energies far beyond what can be examined at man-made accelerators. Specifically, it is not well defined how to combine consistently soft (non-perturbative) interactions, which are most important for EAS, and hard (QCD-type) interactions, which become prevalent with rising energy. The model uncertainty translates into a systematic error of every physics result that is inferred from experimental data, and is, unfortunately, for some cosmic ray analyses already the dominant error. In the past various independent shower programs and hadronic interaction models have been constructed. Usually they

pp. 1–4

are tuned at lower energies to reproduce the existing accelerator data and are then extrapolated in various ways to higher energies, small emission angles and nuclear projectiles and targets. In principle the differences between their predictions allow an estimate of the size of the systematic uncertainties. However, the models are not really independent. Most of them use the same theoretical framework as a basis and the actual differences come from differences in its implementation and in the modelling of extensions to the basic processes, such as the nuclear collisions, diffraction or string fragmentation. Therefore, the differences between existing models are likely just a lower limit of the systematic uncertainties. The theoretical model at the basis of most current air shower programs is the Gribov-Regge theory (GRT) of multi-Pomeron exchange. It has proven very successful in describing many cosmic ray experiments over a wide range of energies [5]. While a number of free parameters of those models are fixed by the overall structure of GRT and by tuning the simulations to reproduce experimental data, there are a few major unknowns at the core of the models that dominate the uncertainties. They are: (i) the parton (quark & gluon) momentum distributions, (ii) treatment of diffraction, and (iii) string hadronisation. In this paper we examine the influence these quantities have on inelastic cross sections and particle production, and, thus, on the EAS development.

2. Model variants

To study the systematics, CORSIKA [2] with QGSJET [3,4] as hadronic interaction model was used. For all three unknowns mentioned above the driving parameters were identified and values were chosen that somehow map out the range from conservative (standard) values to "extreme cases". The form of the parton distribution function (PDF) inside a nucleon for small values of Feynman x determines crucially the rise of total and inelastic cross sections at high energies. In principle a PDF can be inferred from hadron structure functions measured in deep inelastic scattering. However, this leads directly to a contradiction with measured hadronic interaction cross sections. To solve this one is forced to consider non-linear screening corrections to the interaction dynamics, i.e. enhanced Pomeron diagrams [1,6]. On the other hand, the form of the PDF depends on the choice of so-called factorisation scale M_{F}^2 at which the PDF should be evaluated for the production of partons of given $p_\perp$, i.e. $M_{\mathrm{F}}^2 = f \cdot p_\perp^2$ [1]. Also the contribution of semi-hard processes, leading to high-$p_\perp$ parton jets, depends strongly on the choice of the transverse momentum cutoff Q_0^2 which defines the border between non-perturbative "soft" physics ("soft" Pomeron exchange), and perturbative parton evolution (QCD). Choosing a higher Q_0^2 or a smaller f, decreases the semi-hard contribution to the cross sections. Diffraction is difficult to measure at accelerator experiments since its secondary particles emerge at very small angles to the incoming beam. Diffractive events can be simulated in various

option	1	2	3	4	5
Q_0^2 (GeV^2)	2.25	2.25	9	9	9
f	1/4	1/4	1	1	1
K	1.5	1.5	2	2	2
α	-0.5	-0.5	-0.5	-0.7	-0.9
Λ	1.5	1.5	1.6	1.6	2.7
Diffraction	2-comp.	quasi-eik.	2-comp.	2-comp.	2-comp.

Table 1. Parameter settings for the 5 options of QGSJET investigated. (see text)

ways, and since diffractive interactions leave the projectile virtually unchanged, they can transport energy effectively deep into the atmosphere. A modified fraction of diffractive events, therefore, influences the shower development markedly. Finally, there is a basic uncertainty concerning the energy-momentum partition between particle production processes in hadronic (and nuclear) collisions and the treatment of hadronisation for those processes. In practice, one chooses different momentum distributions for parton ends of the strings, which is governed by the effective exponent α of the distribution at low x, and the choice of string tension, governed by Λ, for the string fragmentation procedure [1,6]. Though one can describe available data at low energies choosing either "valence-like" string distributions ($\alpha \approx -0.5$) and low string tension or using "sea-like" distributions ($\alpha \approx -1$) and high string tension. The two settings give quite different results at very high energies: valence-like strings produce flat and long distributions of secondaries in rapidity, while sea-like strings produce particles mostly in the central rapidity region. 5 non-standard options of QGSJET have been constructed with the parameters as listed in Table 1. Each option was tuned to reproduce the experimental data at lower energies. All options are characterised by a steeper (improved) gluon momentum distributions compared to the original model version and lead therefore to a steeper energy increase of both total interaction cross section and of multiplicity of secondary hadrons. Opt. 1 and 2 employ a comparatively low Q_0^2 and f. Correspondingly the factor K, which accounts for higher order QCD corrections, is set to 1.5. The difference between them is the treatment of diffraction: opt. 1 uses the multi-component approach with two active diffraction states [3], whereas opt. 2 is based on the quasi-eikonal approach from the standard version of QGSJET [4]. While giving essentially equivalent diffraction spectra for low energy interactions the two approaches differ at much higher energies and for hadron-nucleus reactions. The amount of diffractive events is reduced in opt. 1, where diffraction production corresponds to just peripheral interactions. Opt. 3 is similar to opt. 1, but employs a higher Q_0^2, f and K. Opt. 4 and 5 are similar to opt. 3 but use different string end distributions than opt. 1-3. Opt. 3-5 have increased string tension. Apart from the parameters mentioned here, a number of auxiliary parameters have been adjusted for each option to improve the agreement with data at low energies.

3. Preliminary results

The cross sections of all options agree at low energies but diverge above about 10^{16} eV (see fig. 1). As expected, opt. 5 with higher Q_0^2 and f produces about 20% higher cross sections than opt. 2, with enhanced diffraction. However, the variation between the QGSJET options is smaller than the variation between other models (e.g. DPMJET and SIBYLL). The spread in the average charged multiplicity $\langle N_{\rm ch}\rangle$ between the options is about 20% at 10^{19} eV and approaching 100% above 10^{20} eV. Also here the variation between opt. 1-5 is much smaller than the differences to other models (see e.g. [5]). The e/γ densities of 10^{19} eV proton showers at ground level at about 1 km core distance vary within 20% (opt. 2 more opt. 5), whereas muon numbers change by about 30% (opt. 5 more opt. 2). As expected opt. 5 reaches the shower maximum highest in the atmosphere and opt. 2 lowest. Proton showers simulated with CORSIKA and the 5 options of QGSJET exhibit differences in $x_{\rm max}$ of the order of 30 g/cm^2. Due to limited statistics these numbers have still large errors. Nevertheless, it seems that even substantial variation of parameters within one specific model cannot produce the systematic differences between different models.

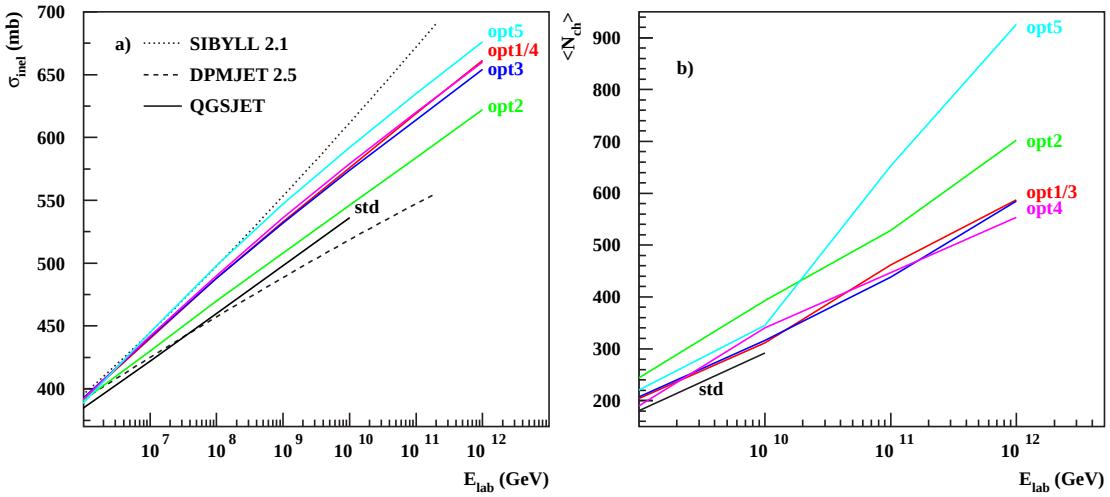

Fig. 1. a) Cross section for inelastic proton-air collisions, $\sigma_{\rm inel}$, for the 5 options and some models used in CORSIKA. b) Average charged multiplicity, $\langle N_{\rm ch}\rangle$, in p-$\bar{\rm p}$ collisions.

Support from British Council and from BMBF (Grant 05 CU1VK1/9) is highly appreciated.

References

1. Drescher H.J. et al., Phys. Rep. 350 (2001) 93
2. Heck D. et al., Forschungszentrum Karlsruhe, FZKA 6019 (1998) and references therein
3. Kalmykov N.N. et al., Phys. Atom. Nucl. 56 (1993) 346
4. Kalmykov N.N. et al., Nucl. Phys. B (Proc. Suppl.) 52B (1997) 17
   Heck D. et al., Proc. 27$^{\rm th}$ ICRC Hamburg (2001) HE1.3 p 233
5. Knapp J. et al., Astropart. Phys. 19 (2003) 77
6. Ostapchenko S., J. Phys. G: Nucl. Part. Phys. 29 (2003) 831

One-dimensional Hybrid Simulation of EAS Using Cascade Equations

N.N. Kalmykov[1], M.K. Alekseeva[1], T. Bergmann[2], V. Chernatkin[4], R. Engel[2], D. Heck[2], J. Moyon[4], S.S. Ostapchenko[3,1], T. Pierog[2], T. Thouw[2], and K. Werner[4]
(1) Skobeltsyn Institute of Nuclear Physics, Moscow State University, Leninskie Gory 1, 119992, Moscow, Russia
(2) Forschungszentrum Karlsruhe, Institut für Kernphysik, Postfach 3640, 76021 Karlsruhe, Germany
(3) Institut für Experimentelle Kernphysik, University of Karlsruhe, 76021 Karlsruhe, Germany
(4) SUBATECH, Universite de Nantes, EMN, IN2P2/CNRS, Nantes, France

Abstract

A hybrid simulation code is developed that is suited for fast one-dimensional simulations of shower profiles, including fluctuations. It combines Monte Carlo simulation of high energy interactions with a fast numerical solution of cascade equations for the resulting distributions of secondary particles. First results obtained with this new code, called CONEX, are presented and compared to CORSIKA predictions, focusing on the treatment of the electromagnetic shower component.

1. Introduction

At high energy, the number of air showers that can be simulated within conventional Monte Carlo approaches is mainly limited by the currently available computing power. The hybrid simulation technique allows a drastic reduction of the simulation time by combining explicit Monte Carlo simulation of high-energy interactions with fast numerical methods to describe sub-showers initiated by low-energy particles. Since shower fluctuations mainly arise from the fluctuations of the first few interactions of the primary particle and its energetic secondaries, the hybrid method allows good description of both mean shower properties as well as their distribution (see, for example, [2]).

In this work we employ a previously developed code for the treatment of the cascade equations for the hadronic shower core [1] and supplement it with a Monte Carlo simulation of high-energy hadronic interactions and a fast numerical solution of the electromagnetic cascade equations. Our approach is characterised by large flexibility. No libraries of previously simulated showers are needed and all shower parameters, including the atmospheric profile can vary from shower to

pp. 1–4

shower.

2. The shower simulation code CONEX

In CONEX explicit Monte Carlo simulation of propagation, decay and interaction is performed for all particles above a given threshold, typically $E_0/100$. Hadronic high-energy interactions are calculated using either neXus 3 [3] or QGSJET 01 [7]. The extension to other models such as SIBYLL [4] and DPMJET [9] is planned. The Monte Carlo simulation of electromagnetic interactions is handled by the EGS4 code [8]. Particles falling below the energy threshold are binned according to their type in energy-depth tables. These tables are used as initial distribution for the cascade equations. The system of coupled differential equations are solved for each shower using the techniques described in [1].

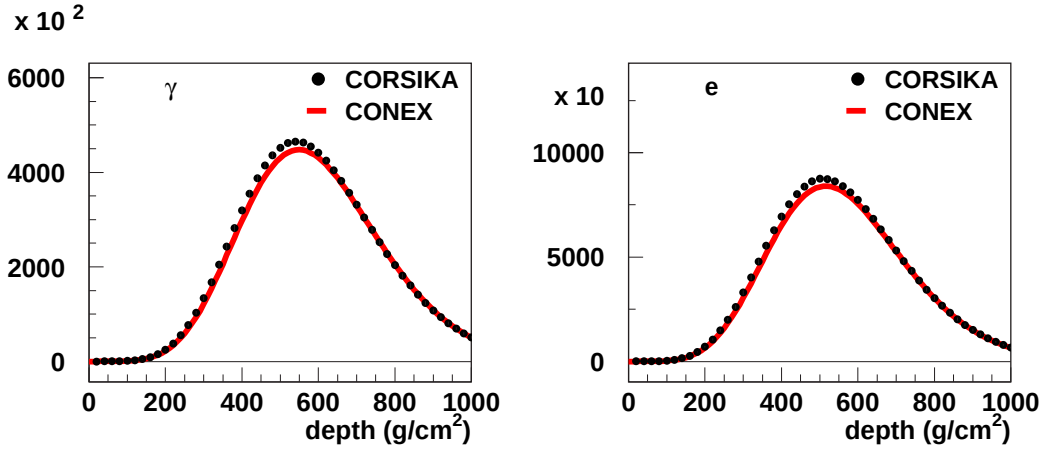

Fig. 1. Number of photons (left) and electrons/positrons (right) as function of slant depth for photon-induced showers of 10^{14} eV. Only particles with kinetic energy greater than 1 MeV are considered.

3. Comparison to CORSIKA results

To test the numerical treatment of the electromagnetic cascade equations we compare our results with CORSIKA simulations. Fig. 1 shows the average longitudinal shower profile of electrons and photons in 10^{14} eV photon-induced showers as predicted by CORSIKA [5] together with our calculation. Examples of electron and photon energy distributions at fixed atmospheric depths are given in Fig. 2. In all cases a good agreement is found, but some differences can be seen at very low energy.

Finally, in Fig. 3 we compare the longitudinal shower profiles of electrons and photons for 10^{18} eV proton-induced showers as obtained with CONEX and

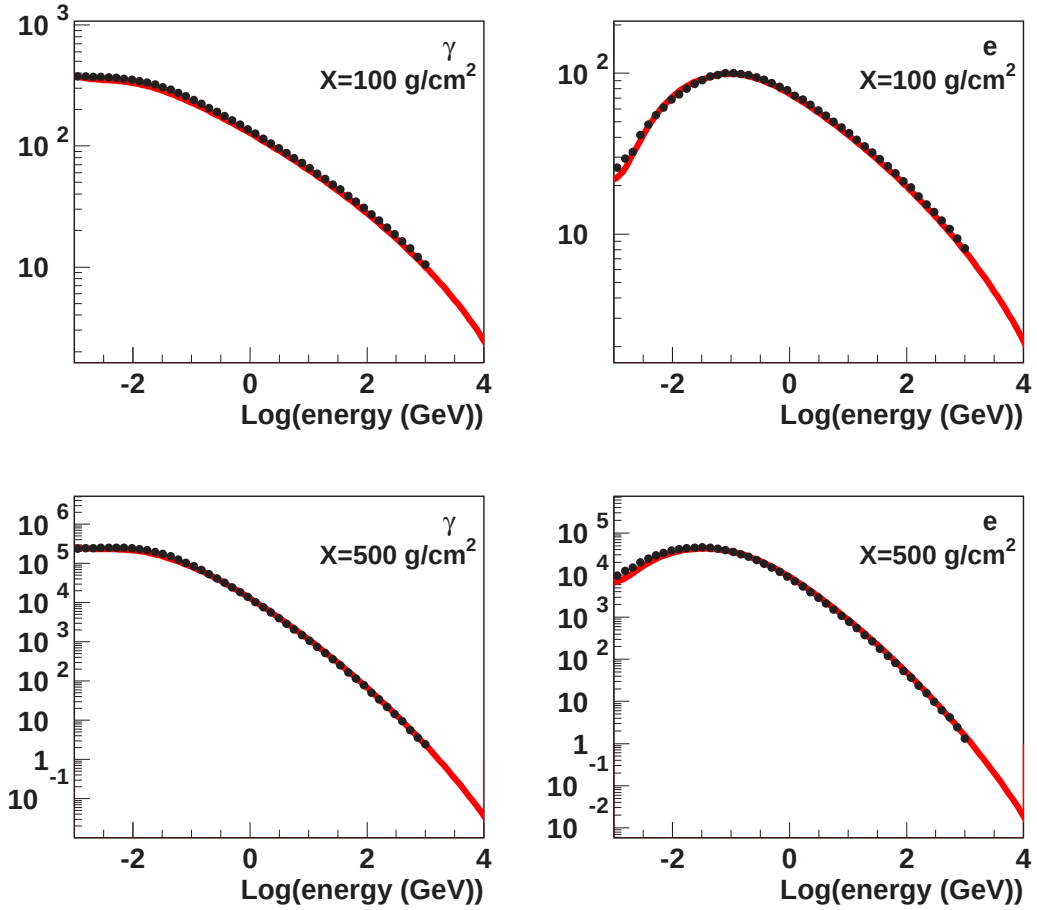

Fig. 2. Energy distributions of photons (left) and electrons (right). The symbols are CORSIKA predictions and the curves represents the results of the numerical solution of the cascade equations.

CORSIKA (100 events each). Again, only particles with $E_{\rm kin} \geq 1\,\mathrm{MeV}$ are shown. The CONEX predictions are lower than that of CORSIKA by about 5%. This agreement is reasonable, given the fact that CONEX uses a completely different, independently developed formalism of the hadronic and electromagnetic shower parts.

We plan to investigate the reasons for the differences between the CONEX and CORSIKA predictions in detail.

4. Conclusions and outlook

CONEX is a newly developed code for fast hybrid simulation of air showers. Its predictions are in good agreement with the results of the well-tested CORSIKA Monte Carlo program. CONEX is ideally suited for realistic shower

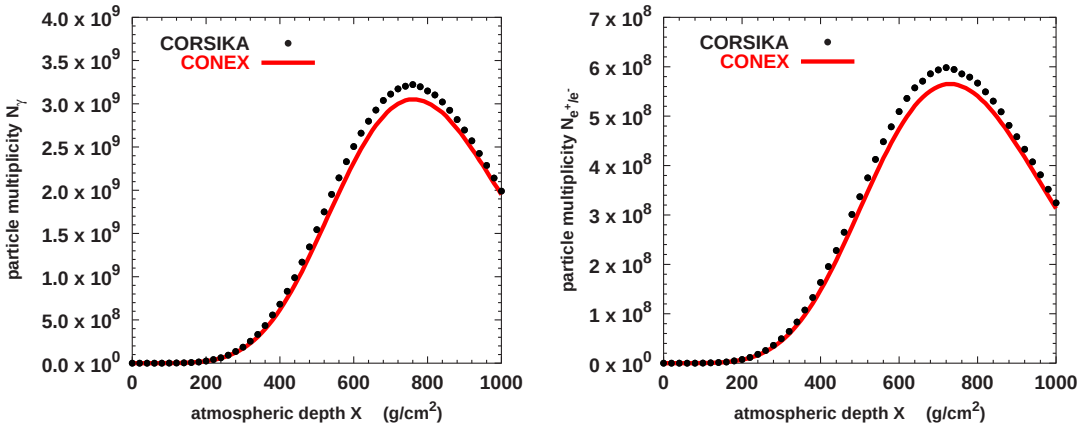

Fig. 3. Mean longitudinal shower profiles of photons (left) and electrons and positrons (right) for vertical proton-induced showers of energy 10^{18} eV. The curves represent CONEX hybrid simulations and the symbols are CORSIKA results.

profile simulations as needed for EAS experiments measuring fluorescence light, e.g. Auger, EUSO, or OWL. The current version of CONEX is restricted to the one-dimensional treatment of showers. It is planned to extend the code to allow a full three-dimensional description of extensive air showers [6].

Acknowledgements: S.O. acknowledges the support by the German Ministry of Education and Research (BMBF, grant 05 CU1VK1/9).

References

[1] Bossard, G. et al. 2001, Phys. Rev. **D63**, 054030.
[2] Dedenko, L.G. 1968, Can. J. Phys. **46**, 178; Lagutin, A.A. et al., 1999, Nucl. Phys. (Proc. Suppl.) **75A**, 290; Gaisser, T.K., Lipari, P. & Stanev, T., 1997, *25th Int. Cosmic Ray Conf.* (Durban) **6**, 281; Alvarez-Muniz, J. et al., 2002, Phys. Rev. **D66**, 033011; Drescher, H. & Farrar, G.R., astro-ph/0212018.
[3] Drescher H.J. et al. 2001, Phys. Rep. **350**, 93
[4] Engel, R. et al. 1999, *26th Int. Cosmic Ray Conf.* (Salt Lake City) **1**, 415.
[5] Heck, D. et al. 1998, Report FZKA 6019 (Forschungszentrum Karlsruhe); http://www-ik.fzk.de/˜heck/corsika/
[6] Kalmykov, N.N., Ostapchenko, S.S., & Werner, K. 2002, proc. of 12th Int. Symposium on Very High Energy Cosmic Ray Interactions, Geneva, Nucl. Phys. B (Proc. Suppl.), in print.
[7] Kalmykov, N., Ostapchenko, S., & Pavlov, A.I. 1997, Nucl. Phys. B (Proc. Suppl.) **52B**, 17.
[8] Nelson, W.R., Hirayama, H., & Rogers, D.W.O. 1985, Report SLAC 265, Stanford Linear Accelerator Center.
[9] Roesler, S., Engel, R., & Ranft, J. 2001 *27th Int. Cosmic Ray Conf.* (Hamburg) **1**, 439.

TARGET 2.2 – a hadronic interaction model for studying inclusive muon and neutrino fluxes

R. Engel[1], G. Barr[2], T.K. Gaisser[3], S. Robbins[2] and T. Stanev[3]
(1) Forschungszentrum Karlsruhe, Institut für Kernphysik, Postfach 3640, 76021 Karlsruhe, Germany
(2) University of Oxford, Keble Road, Oxford, OX1 3RH, England
(3) Bartol Research Institute, University of Delaware, Newark, DE 19716, U.S.A.

Abstract

We present a new version of the hadronic interaction model TARGET which includes a model for baryon pair production, an explicit simulation of target nucleons, and updated leading baryon distributions. As an example for a typical application the inclusive muon flux prediction calculated with TARGET is compared to recent L3 measurements.

1. Introduction

The Monte Carlo event generator TARGET [12],[9] is ideally suited to investigate the role of hadronic particle production in atmospheric neutrino and muon flux calculations. In contrast to more sophisticated models such as DPMJET [16] and FLUKA [10] it is based on parametrizations of accelerator data and a minimum number of additional model assumptions. TARGET is designed to optimally simulate particle production in phase space regions important for inclusive neutrino and muon flux predictions [8]. Due to its intrinsic simplicity TARGET is a very flexible model that can be easily tuned to existing and new data.

In the following we summarize improvements recently implemented in the code (TARGET version 2.2) and compare it with the measurement of the inclusive atmospheric muon flux by the L3 Collaboration [17]. The previous version of the model, TARGET 2.1, is described in [9] and compared to other models in [14].

2. New features in TARGET

TARGET as an event generator primarily intended for calculation of lepton fluxes in the GeV energy range is constructed to simulate all relevant physics processes of nucleon-, pion- and kaon-air interactions in the energy range from 1 to several 100 GeV. In this energy range the production of baryon-antibaryon pairs, such as p-$\bar{p}$, is kinematically suppressed. However, it becomes increasingly

pp. 1–4

important at high energy. To make the high-energy extrapolation more reliable we implemented the simulation of baryon-antibaryon pair production. Fig. 1 shows the TARGET results on the mean antiproton production multiplicity in p-air collisions. The data points are measurements from p-p collisions. The small shift of the threshold energy between the TARGET curve and the p-p data is due to the Fermi motion of the nucleons in the nucleus. In addition the total multiplicity is slightly higher in p-air collisions since, on average, more than one target nucleon participates in the scattering, sharing the total energy available. The momentum distribution of the nucleons is sampled using an updated version of the inclusive differential cross section given in [11].

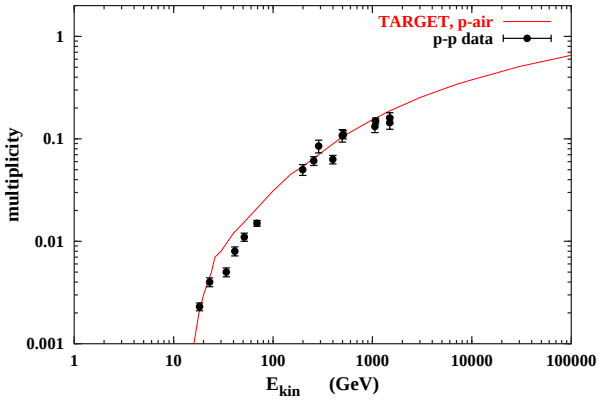

Fig. 1. Antiproton production multiplicity – TARGET results are compared to p-p data [1].

For tuning TARGET to forthcoming data from virtually 4π acceptance experiments such as HARP [2] the simulation of target fragmentation effects is needed. Previously only leading nucleon production was considered in p/n-air collisions, however, accounting for the participating nucleon recoil energy. In the new version of TARGET both the participating target nucleons and the associated slow (diffractive) pion production are simulated, employing the same distributions as used for leading particle production. In addition, improved parametrizations of the leading proton and neutron distributions were implemented. A comparison of the leading nucleon distribution in p-air collisions to NA49 data on 158 GeV p-p collisions [5] is shown in Fig. 2. The NA49 data were slightly rescaled to ensure that the sum of protons and neutrons equals unity. As expected the leading proton distribution is somewhat harder in p-p collisions than p-air interactions. In Fig. 2 the model is compared with p-Be data at 24 GeV [6], finding good agreement.

3. Inclusive atmospheric muon flux at high energy

A comparison of TARGET predictions to the low-energy muon flux measurement of CAPRICE98 [4] can be found in [3]. Here we will compare the new version of TARGET to L3 data [17].

One important input to any such calculation is the primary cosmic ray spectrum. In Ref. [13] different primary flux measurements are compared and a

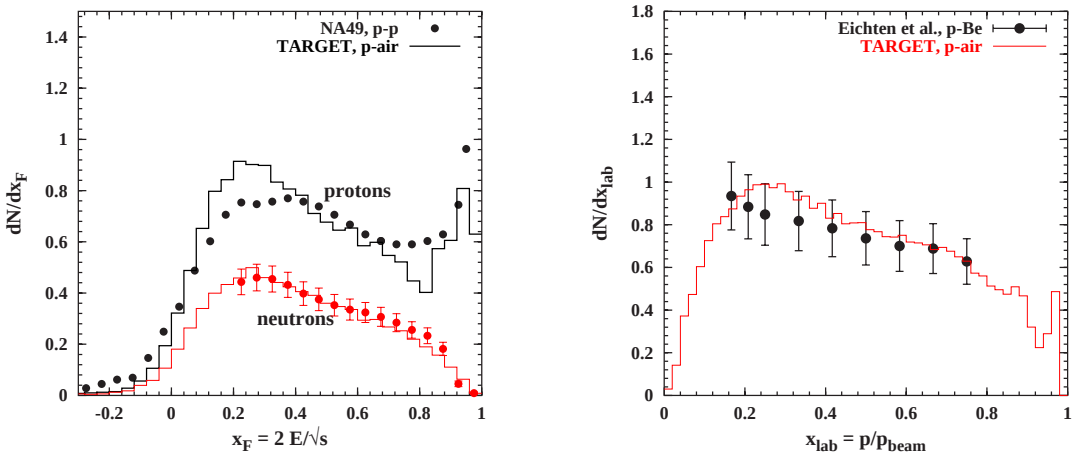

Fig. 2. Comparison of TARGET predictions to different measurements of nucleon distributions (see text).

flux parametrization, covering a wide energy range, is given. The results discussed in the following are based on this parametrization and have to be rescaled if one adopts, for example, the CAPRICE98 flux measurement [4]. Fig. 3. shows

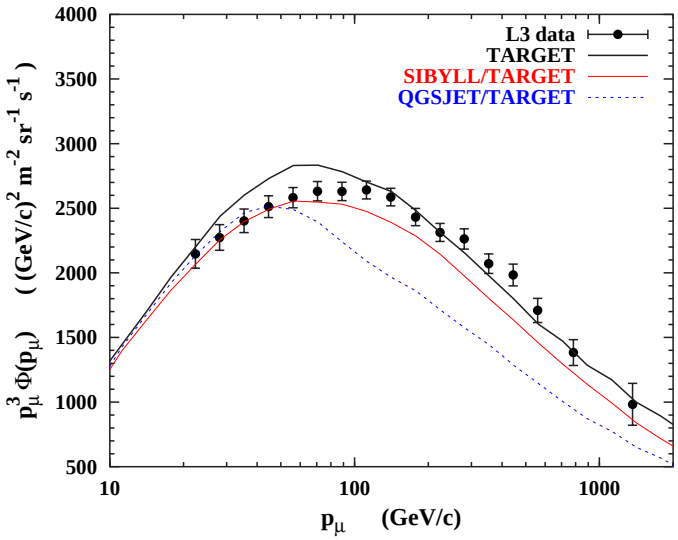

Fig. 3. Comparison of inclusive muon flux predictions to L3 data [17]. Shown are calculations using QGSJET 98 [15], SIBYLL 2.1 [7] and TARGET as high-energy hadronic interaction model.

muon flux predictions obtained with different model combinations together with L3 data. In the simulations all interactions at energies below 200 GeV were simulated with TARGET. The curves labeled SIBYLL and QGSJET refer to simulations in which TARGET was replaced by the respective model for collisions at higher energies. Therefore one expects the differences due to the interaction models to be fully visible only at energies greater than $\sim 100\,\mathrm{GeV}$. It is known that QGSJET gives a good description of the muon production in extensive air showers (EAS) in the primary energy range $10^{14} - 10^{16}\,\mathrm{eV}$. Furthermore, SIBYLL

predicts in general fewer muons in EAS than QGSJET. However, in the case of inclusive muon production different regions of the secondary particle phase space are important and the situation is the opposite.

4. Conclusions

Inclusive muon flux measurements provide important cross checks of the reliability of hadronic interaction models. They are complementary to muon measurements in EAS. The comparison with L3 data shows that the TARGET model gives a good description of the inclusive high-energy muon flux. SIBYLL 2.1 provides a similarly good description of the L3 data.

Acknowledgements The research of TKG and TS is supported in part by the US Department of Energy contract DE-FG02 91ER 40626.

References

[1] Antinucci, M. et al., 1973, Lett. Nuovo Cim. 6, 121.
[2] Barr, G., et al., 2001, *Proc. 27th Int. Cosmic Ray Conf.* (Hamburg) 4, 1585.
[3] Boezio, M. et al., these proceedings.
[4] Boezio, M. et al., CAPRICE Collab., 2003, Phys. Rev. D67, 072003
[5] Cole, B.A., 2001, talk given at Quark Matter 2001, Long Island and Fischer, H.G. et al., NA49 Collab., hep-ex/0209043.
[6] Eichten, T. et al., 1972, Nucl. Phys. B44, 333.
[7] Engel, R. et al., 1999, *26th Int. Cosmic Ray Conf.* (Salt Lake City) 1, 415.
[8] Engel, R., Gaisser, T.K., & Stanev, T., 2000, Phys. Lett. B472, 113.
[9] Engel, R., Gaisser, T.K., Lipari, P. & Stanev, T., 2001, *Proc. 27th Int. Cosmic Ray Conf.* (Hamburg) 4, 1318.
[10] Fassò, A. et al. 2001, Proc. 'Monte Carlo 2000' Conf., eds. Kling et al. (Springer, Berlin) 955; http://www.fluka.org/heart/rh.html
[11] Gaisser, T.K., & Maurer, R.H., 1973, Phys. Rev. Lett. 30, 1264.
[12] Gaisser, T.K., Protheroe, R.J., & Stanev, T., 1983, *Proc. 18th Int. Cosmic Ray Conf.* (Bangalore) 5, 174.
[13] Gaisser, T.K. et al., 2001, *Proc. 27th Int. Cosmic Ray Conf.* (Hamburg) 5, 1643.
[14] Gaisser, T.K. & Honda, M., 2002, Ann. Rev. Nucl. Part. Sci. 52, 153.
[15] Kalmykov, N., Ostapchenko, S., & Pavlov, A.I., 1997, *Nucl. Phys. B (Proc. Suppl.)* **52B**, 17
[16] Roesler, S., Engel, R., & Ranft, J., 2001 *Proc. 27th Int. Cosmic Ray Conf.* (Hamburg) 1, 439.
[17] Unger, M. et al., L3 Collab., these proceedings.

Comparison Between CAPRICE98 Atmospheric Muon Data and Simulations with TARGET

M. Boezio[1], P. Carlson[2], R. Engel[3], T.K. Gaisser[4], P. Hansen[2], E. Mocchiutti[2] & T. Stanev[4]

(1) INFN section and Physic Department, University of Trieste, Trieste, Italy

(2) Department of Physics, The Royal Institute of Technology (KTH), AlbaNova Universitetscentrum, 10691 Stockholm, Sweden

(3) Forschungszentrum Karlsruhe, Institut fuer Kernphysik, 76021 Karlsruhe, Germany

(4) Bartol Research Institute, University of Delaware, Newark DE 19716, U.S.A.

Abstract

On 28 May 1998 the balloon-borne experiment CAPRICE98 was launched from Fort Sumner, New Mexico. During the three hour ascent to float altitude it recorded both positive and negative muon data in a wide momentum range from 0.3 to 20 GeV/c. We simulate the muon fluxes in several altitude bins and at ground level (885 g/cm^2) with the 3D interaction code TARGET. This code accounts for the muon deflection in the geomagnetic field at Fort Sumner. As input for the simulation it employs the primary proton and He spectra measured by the experiment itself, thus reducing the systematic experimental uncertainties related to the absolute flux calculations.

1. Introduction

Calculations of the atmospheric lepton fluxes need two different sets of inputs: the primary cosmic ray flux at the time of the measurement and a hadronic interaction code that describes correctly the interaction properties in the whole phase space. The uncertainties in these two sets of input determine the uncertainty in the calculated fluxes.

We make an attempt to decrease the uncertainties by using primary cosmic ray and secondary muon fluxes measured by the same instrument in the same flight [1,2]. In addition to the H and He fluxes measured by CAPRICE98 in 1998 we use the parametrization of the fluxes of heavy nuclei [3] presented at the Hamburg conference. The all nucleon flux obtained in this way is shown in Fig. 1 in comparison to other fluxes used in calculations of atmospheric leptons.

The inclusion of nucleons from heavy nuclei make the CA98 flux model better than the formerly used [4] CA94 flux model that included only the H and He contribution. It is still, however, significantly lower than the models of

pp. 1–3

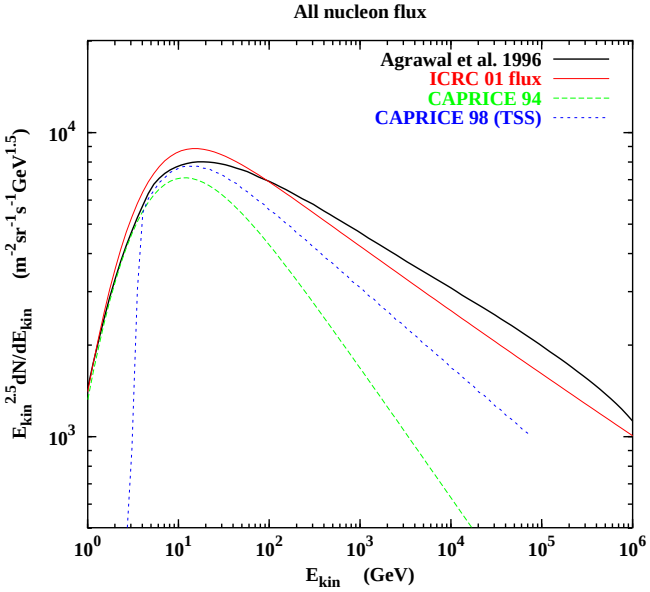

Fig. 1. Comparison of the all nucleon flux used in this calculation with other cosmic ray flux models.

Refs. [3,5] at high energy. This is however relatively unimportant for the flux of muons of momentum below 20 GeV/c measured by CAPRICE98.

2. Some results of the simulation

We were not able to complete the whole set of simulations on time to include it in this paper. For this reason we only compare the experimental results to simulated spectra in three of the higher altitude measurements in Fig. 2.

Muon fluxes at float altitude (5.5 g/cm^2) were not well enough measured and are not shown, although the agreement with the two measured data points is good. At 48.4 g/cm^2 the fluxes of positive muons are predicted well, but the negative muon fluxes are underpredicted. Some of the differences may be due to the rough treatment of the muon momentum spectra in the figure, which assumes that the average muon momentum is the geometric mean for the bin.

Another assumption that may have some influence is that all muons are detected at the average altitude. A better comparison should account for the altitude dependence of the muon flux in different momentum intervals.

The good agreement of the calculation with the measured fluxes is encouraging. The altitude of 165 g/cm^2 is close to the maximum production depth for GeV muons and suggests that the representation of the hadronic interactions in the energy range up to 200 GeV is very reasonable.

The steeper primary energy spectrum does not affect the muon flux predictions at high altitude, but it may show up in the prediction of the muon fluxes at ground level.

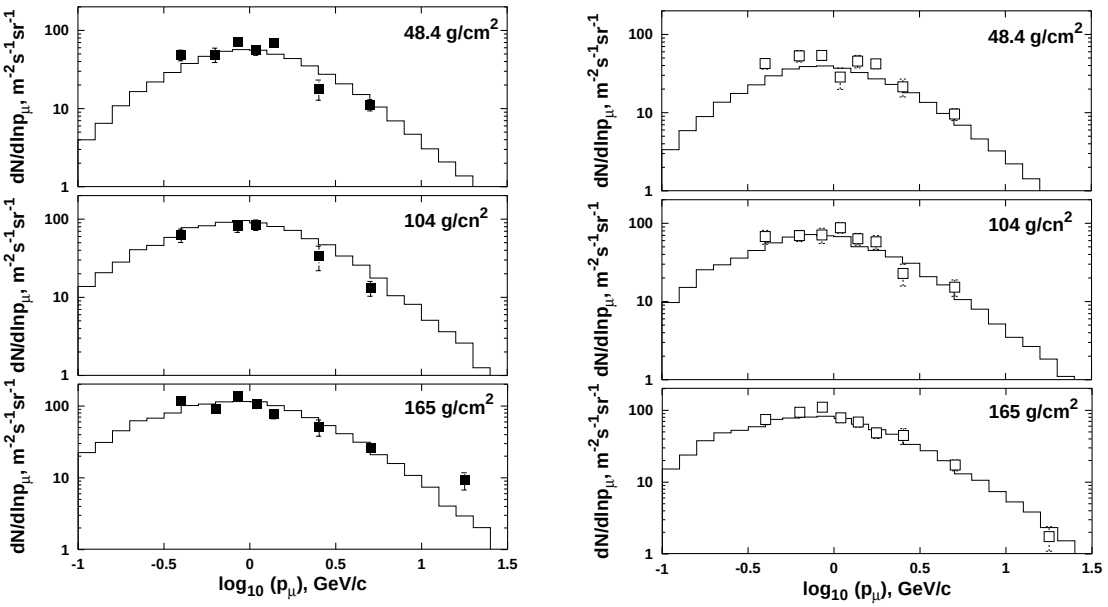

Fig. 2. Comparison of the calculated with detected muon fluxes at three relatively high altitudes. Lefthand panel: positive muons, righthand panel: negative muons.

At the Conference we will compare the full set of predictions with the CAPRICE98 muon data and will discuss the development of the muon flux in the atmosphere and the effects of the magnetic field on it.

Acknowledgments The research of TKG and TS is supported in part by the US Department of Energy contract DE-FG02 91ER 40626.

3. References

1. Boezio, M. et al, Phys. Rev. **D67:072003** (2003)

2. Boezio, M. et al., Astrop. Phys, to appear, astro-ph/0212253 (2003)

3. Gaisser, T.K. et al, Proc. 27th ICRC (Hamburg), **5**, 1643, (2001)

4. Engel, R. et al, Proc. 27th ICRC (Hamburg), **3**, 1029, (2001)

5. Agrawal, V. et al., Phys. Rev. **D53**, 1314 (1996)

Air shower fluctuations and the measurement of the proton-air cross section

J. Alvarez-Muñiz[1], R. Engel[2], T. K. Gaisser[3], J. A. Ortiz[4], and T. Stanev[3]
(1) Departamento de Física de Partículas, Universidade de Santiago de Compostela, 15706 Santiago, A Coruña, Spain
(2) Forschungszentrum Karlsruhe, Institut für Kernphysik, Postfach 3640, 76021 Karlsruhe, Germany
(3)Bartol Research Institute, University of Delaware, Newark, DE 19716, USA
(4)Instituto de Física "Gleb Wataghin", Universidade Estadual de Campinas 13083-970 Campinas-SP, Brazil.

Abstract

We explore the influence of fluctuations in the extensive air shower (EAS) development on the possibility to determine the proton-air cross section at high energy. This contribution concentrates on the two classical methods of obtaining the cross section in EAS experiments, (i) the measurement of the attenuation of the rate of showers with fixed muon and electron sizes with zenith angle, namely the constant intensity cut method, and (ii) the measurement of the distribution of the depth of maximum. We demonstrate that, depending on the selection method, shower fluctuations can strongly influence the characteristics of the selected showers in method (i). Method (ii) is subject to model dependence.

1. Introduction

Measuring extensive air showers is currently the only way to study the cosmic ray spectrum at energies above 10^{14} eV, as well as the properties of hadronic interactions at $\sqrt{s}$ above 1.8 TeV. EAS are detected with air shower arrays which usually measure electron and muon densities and derive the total number of electrons N_e and muons N_μ at the detector level. At energies $E \geq 10^{17}$ eV the shower development can also be directly observed by measuring the fluorescence light from atmospheric nitrogen, induced by the ionization of the charged shower particles. These experiments can determine the depth at which the number of charged particles reaches its maximum value ($X_{\rm max}$) in a shower.

Here we study the influence of fluctuations in shower development on the possibility to determine the proton-air cross section in EAS experiments by two different methods (see (i) and (ii) in the abstract).

pp. 1–4

2. The constant N_e-N_μ method

The determination of the inelastic p-air cross section from ground array data is performed by measuring the attenuation with zenith angle θ of the rate of showers having the same energy. It is assumed that N_μ gives a good estimate of the primary energy. Experimentally the fraction of proton-showers in the sample is enriched by selecting showers with large N_e within the same N_μ bin. Under the assumption of no shower fluctuations, selecting showers of fixed N_μ and N_e at different θ would guarantee that they have the same energy and that they only differ in the depth at which the first primary p-air interaction has occurred. This allows the measurement of the *absorption* length ($\Lambda_{\rm abs}$), which determines how the flux of the selected showers decreases with atmospheric depth, and is related to the inelastic p-air cross section. The absorption length is determined from the ratio of the frequency (f) of showers falling in a given (N_μ, N_e) bin measured at two zenith angles (θ_1 and θ_2):

$$R(\theta_1,\theta_2) = \frac{f(N_\mu, N_e, \theta_1)}{f(N_\mu, N_e, \theta_2)} = \exp\left[-\frac{X_{\rm v}}{\Lambda_{\rm abs}}(\sec\theta_1 - \sec\theta_2)\right] , \qquad (1)$$

where $X_{\rm v}$ is the vertical depth of the detector.

In general, the primary cosmic ray flux consists of nuclei of a variety of mass numbers. Here we simplify the problem with the assumption that all primary particles are protons. We simulated 500,000 proton-induced showers at several zenith angles using the hybrid code described in [1]. Shower energies were drawn from an E^{-3} differential spectrum in the energy range between 10^{16} and 10^{18} eV and both SIBYLL 2.1 [4] and QGSjet98 [6] were used as hadronic interaction models. The detector induced fluctuations in $\log_{10} N_\mu$ ($\log_{10} N_e$) were implemented by Gaussian resolution functions of widths 0.1 (0.05), in order to match the errors reported by the Akeno group [5]. The detector is at Akeno depth $X_{\rm v} = 920$ g/cm^2.

We apply the constant $N_e - N_\mu$ method by first selecting showers which have $\log_{10} N_\mu$ between 5.25 and 5.45 at observation level as done in the Akeno analysis [5]. Only muons above the energy threshold of the Akeno experiment $E_\mu > 1$ GeV $\times \sec\theta$ are considered. We then select showers with constant N_e within that N_μ bin. In Fig. 1a we show the frequency ratios (1) of the showers as a function of the selected N_e. The ratio depends strongly on the N_e bin used for shower selection. According to Eq. (1) it should be constant over a certain range in N_e for all different zenith angle combinations, which is only the case in Fig. 1a for $\log_{10} N_e > 7.4$ in both SIBYLL 2.1 and QGSjet98 models. For large N_e values we do not see a significant model dependence. The bin in N_e chosen by Akeno for the cross section analysis ($\log_{10} N_e$ between 6.8 and 7.0, marked by the vertical lines in Fig. 1a) is located in a region where the intensity ratios depend strongly on N_e. The figure suggests that zenith angle dependent bins in electron

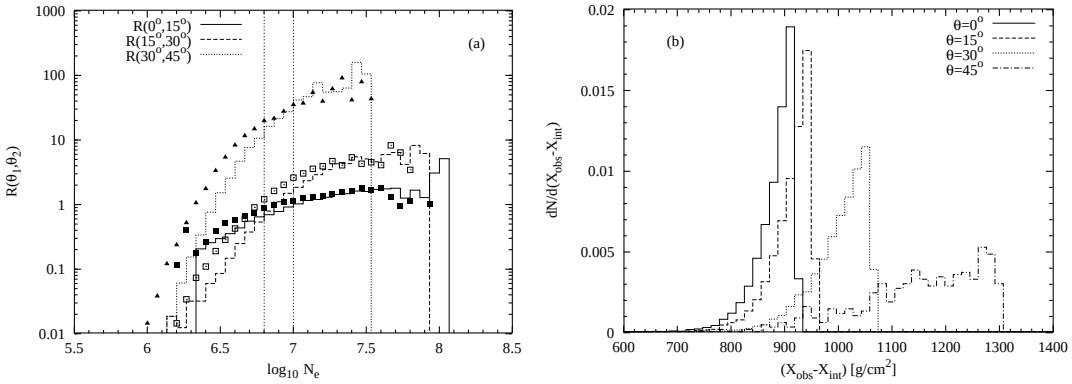

Fig. 1. Left panel: Ratios of number of proton-initiated showers having a muon number between $10^{5.25}$ and $10^{5.45}$ as a function of N_e. Histograms correspond to showers simulated using SIBYLL 2.1 and points show the results obtained with QGSjet98. Right panel: Distribution in $X_{\rm obs} - X_{\rm int}$ of the showers that fall in the $(\log_{10} N_\mu, \log_{10} N_e)$=(5.25-5.45,6.8-7.0) bin.

size should be used in order to get an angular-independent value of $\Lambda_{\rm abs}$.

The ultimate reason why the constant $N_e - N_\mu$ method does not work is that shower selection is dominated by the intrinsic fluctuations in shower development [2]. Our simulations indicate that an angle dependent selection bias is introduced by the constant $N_e - N_\mu$ method, so that instead of selecting showers which have developed through the same amount of matter between the first interaction $X_{\rm int}$ and observation level $X_{\rm obs}$, the selected showers have widely different "shower lengths" (defined as $X_{\rm obs} - X_{\rm int}$). Fig. 1b illustrates the distribution of shower lengths of showers with $(\log_{10} N_\mu, \log_{10} N_e)$=(5.25-5.45,6.8-7.0). The average values (σ) of the $X_{\rm obs} - X_{\rm int}$ distributions of the selected showers at $\theta = 0, 15, 30$ and 45 deg. are $\langle X_{\rm obs} - X_{\rm int} \rangle$ = 881.3 (35.7), 911.1 (37.6), 1002.0 (50.6) and 1152.9 (109.7) g cm^{-2} respectively.

3. The $X_{\rm max}$ method

The technique used to infer the p-air inelastic cross sections from the distribution of $X_{\rm max}$ at fixed shower energy exploits the correlation between the first interaction point and the depth of maximum [3]. In case of a perfect correlation one could use directly the slope (Λ_X) of the exponential tail of the $X_{\rm max}$ distribution of showers with large $X_{\rm max}$, to calculate the proton-air cross section. However, intrinsic shower fluctuations before the maximum is reached modify this correlation. A way to quantify this is to introduce a so-called k factor relating Λ_X and the p-air interaction length $\lambda_{\rm int}$ such that $\Lambda_X = k\lambda_{\rm int}$. The factor k depends on the pace of energy dissipation in the early stages of shower evolution, which in turn depends on the fluctuations of the features of the hadronic interactions, mainly inelasticity and multiplicity. The general rule is that large shower

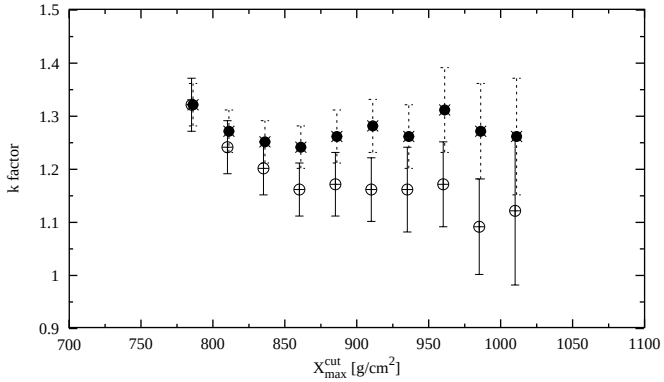

Fig. 2. Numerical values of the k factor as a function of $X_{\rm max}^{\rm cut}$ for proton showers at $E = 10^{19}$ eV. Filled (empty) symbols: Showers simulated with QGSjet (SIBYLL).

fluctuations lead to a larger k factor.

To explore the model dependence of the k factor we simulated proton-induced showers at $E = 10^{19}$ eV using SIBYLL 2.1 and QGSjet98 hadronic interaction models and calculated Λ_X from the predicted distribution of $X_{\rm max}$. Then we determine the k factor using $\lambda_{\rm int}$ provided by the model. In Fig. 2 we show the k factor as a function of $X_{\rm max}^{\rm cut}$, the minimal atmospheric depth above which we performed the fit to the tail of the $X_{\rm max}$ distribution. Firstly it can be seen that the k factor is larger for QGSjet due to the larger fluctuations in the inelasticity and multiplicity distributions predicted by this model as compared to SIBYLL. The dependence of k on $X_{\rm max}^{\rm cut}$ is also apparent, illustrating the fact that in general the $X_{\rm max}$ distribution is not exponential due to fluctuations in shower development. The determination of the dependence of k on $X_{\rm max}^{\rm cut}$ is needed for inferring the p-air cross section from real data. In this case, a cut in $X_{\rm max}$ is applied to avoid contaminating the sample with showers from heavy primaries. We are investigating this issue and the results will be published elsewhere.

Acknowledgments: The authors are supported by NASA Grant NAG5-10919, by the US DoE contract DE-FG02 91ER 40626 and by the Spanish MCYT (FPA 2001-3837 & FPA 2002-01161). The simulations were performed on Beowulf clusters funded by NSF grant ATM-9977692. J.A.O thanks Bartol Research Institute for its hospitality.

1. Alvarez-Muñiz J. *et al.* 2002, Phys. Rev. D 66, 033011
2. Alvarez-Muñiz J. *et al.* 2002, Phys. Rev. D 66, 123004
3. Baltrusaitis R.M. *et al.* 1984, Phys. Rev. Lett. 52, 1380
4. Engel R. *et al.* 1999, *Proc. of the 26th ICRC*, Vol. 1, p. 431; Engel R. *et al.* 2001, *Proc. of the 27th ICRC*, p. 415
5. Honda M. *et al.* 1993, Phys. Rev. Lett. 70, 525
6. Kalmykov N.N. *et al.* 1997, Nucl. Phys. B (Proc. Suppl.) 52B, 17

Distortion of UHECR spectra by regular magnetic fields

Todor Stanev[1], David Seckel[1] & Ralph Engel[2]
(1) Bartol Research Institute, University of Delaware, Newark, DE 19716, USA
(2) Forschungszentrum Karlsruhe, Institut für Kernphysik, Postfach 3640, 76021 Karlsruhe, Germany

Abstract

We propagate ultra high energy protons in the presence of large scale, extragalactic magnetic fields of regular structure and find that the observed proton energy spectrum depends strongly on the position of the observer in respect to both the source and the magnetic field configuration. Effects of the magnetic field exhibit themselves in many different ways.

1. Introduction

Structures of magnetic fields that are coherent over large scales can influence the arrival directions as well as the energy spectrum of ultra high energy cosmic rays (UHECR), see e.g.[1-6]. Here we study the effect of the possible existence of ordered extragalactic magnetic fields correlated with the matter density distribution assuming that the UHECR are protons. We consider an infinite Supergalactic plane (SGP) coinciding with the $y = 0$ plane in Cartesian coordinates as illustrated in Fig. 1. The magnetic field is in $+z$ direction. The non-random magnetic field strength is constant ($B_0 = 10$ nG) within 1.5 Mpc of the plane and decreases exponentially as $B \propto \exp -|y|/3\mathrm{Mpc})$. We also assume a random field component that is $B_0/2$ but never smaller than 1 nG. The random field os implemented as a turbulent magnetic field using a Kolmogorov distribution [7]. We concentrate on two simple source scenarios: a central source that emits UHECR isotropically in the $+z$ hemisphere and an external source that emits a plane wave of protons moving with $\hat{n} = (1,0,0)$. The two sources are shown in the lefthand panel of Fig. 1 labeled by a and b, respectively. The particles are emitted with energy above $10^{18.5}$ eV on a flat $\alpha = 2$ spectrum with an exponential cutoff at $E_c = 10^{21.5}$ eV.

All particles are followed until they intersect a 20 or 40 Mpc "observer" sphere around the origin, where the central source is located. Particles propagating more than $1.3{\times}10^9$ years are abandoned. We account for the proton energy loss due to photoproduction, pair production and redshift. The propagation technique is described in detail in Ref. [7]. The Hubble constant in this calculation is $H_0 = 75$ km/s/Mpc.

pp. 1–4

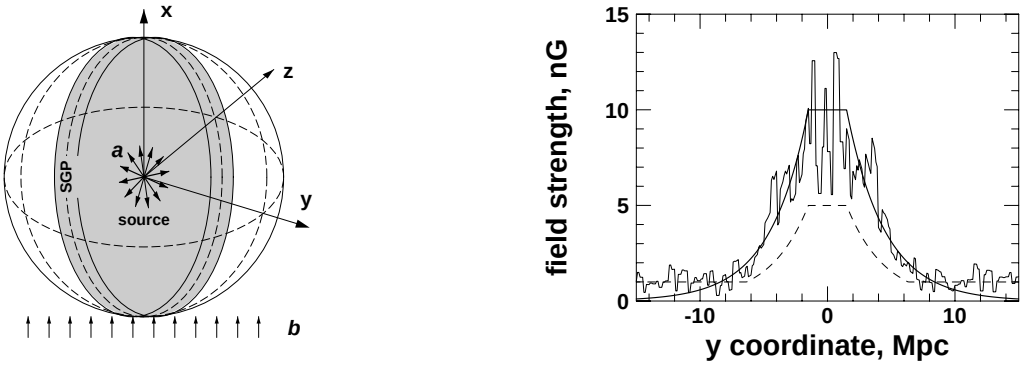

Fig. 1. Lefthand panel - geometry of the SGP and the *observer*'s sphere. The central source scenario is indicated as *a* and the external source scenario is indicated with *b*. Righthand panel - one of the realizations of $B_{||}$ - the magnetic field component parallel to the SGP.

2. Central source

Fig. 2 shows the energy spectra of the protons emitted by the central source that leave the simulation through several 9 Mpc^2 patches on the surface of the sphere. Four of them are centered about one of the axes of the coordinate system: patch *front* is in positive z direction, *side* - in y direction and *top* - in x direction, and *back* is in $-z$ direction toward which no protons were injected. The other two patches are at positive z at angles of 45° in the appropriate planes.

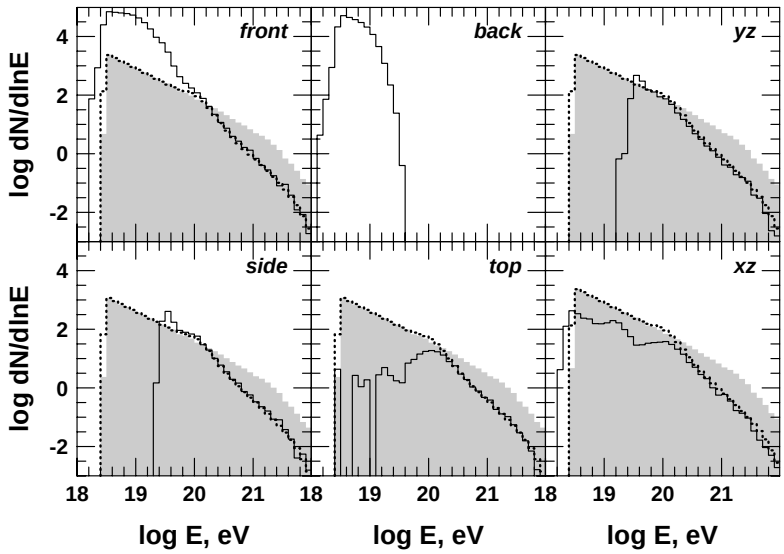

Fig. 2. Energy spectra of the particles leaving a 20 Mpc sphere around a central source in six patches described in the text. The shaded histogram shows the injection spectrum towards these patches. The dotted histogram shows spectra propagated over 20 Mpc without magnetic field.

The particles leaving the 20 Mpc sphere through the *front* patch show an enhance-

ment by almost two orders of magnitude at energy below $10^{19.5}$ eV. The source of the enhancement is the proton diffusion along the field lines, as demonstrated in the spectrum of the *back* patch, towards which no protons were injected. Only back scattered low energy protons reach this patch.

There is a deficit of low energy particles in all other patches. To reach those patches the protons have to propagate across magnetic field lines and only the highest energy protons can do that. The *side* and *yz* patches are underpopulated below $10^{19.5}$ eV because of deflection in the magnetic fields. The deflection in the *top* and *xz* is even stronger, but proton propagation in these directions is assisted by drifts.

To study the dependence of these effects on the radius of the *observer* sphere we enclosed the 20 Mpc one in a 40 Mpc concentric sphere. The effects were qualitatively similar. In addition the 20 Mpc *observers* within the SGP observe a strong flux of back-scattered 10^{19} eV protons similarly to the *back* patch in Fig. 2.

3. External source

The patches defined for a central source were not suitable for studies of a plane wave external UHECR proton flux and we define 6 different patches, all centered in the $z = 0$ plane and azimuth angles $\phi = 0(\hat{x})$, 45, 135, 180$(-\hat{x})$, 225, and 315 degrees. The energy spectra

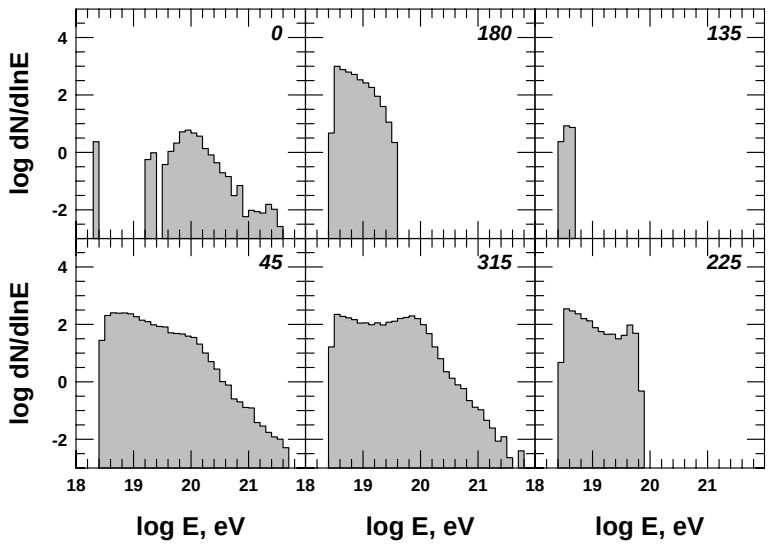

Fig. 3. Energy spectra of the particles leaving a 20 Mpc sphere in different locations around the *z=0* plane after injection as a plane wave in $+x$ direction on the negative x hemisphere. The patches are marked with the values of the ϕ angle on which they are centered.

of the protons leaving the 20 Mpc sphere through these patches are shown in Fig. 3. The spectrum in the $\phi = 0$ patch consists only of UHE protons that

manage to penetrate all the way through the SGP. Patch 180 accepts only lower energy particles that exit mostly after traveling half a gyro-orbit in the field. Patch 135 - (-20/$\sqrt{2}$, 20/$\sqrt{2}$) accepts no particles at all, while the opposite patch 315 has an excess of 10^{20} eV particles, that are swept out of the SGP. Patch 225 - (-20/$\sqrt{2}$-20/$\sqrt{2}$) accepts mainly low energy particles which drift back and the opposite patch 45 has a spectrum similar to the injected one, since both high and low energy particles that drift are accepted.

4. Conclusions

We have intentionally dealt with single sources in a simple geometry to be able to understand the proton propagation in the presence of non-random magnetic fields. These fields affect strongly not only the directions of the protons reaching the observer, but also change their energy spectrum. A separate set of spectral changes is related to the time delay of particles emitted in bursts.

We show that in both the case of an internal or an external source observers located at different positions on the 20 Mpc sphere would observe spectra that have no similarity with each other or with the injection spectrum. At energies below $10^{19.5}$ eV the differences can reach 3-4 orders of magnitude.

It is thus very dangerous to attempt estimates of the luminosity of the UHECR sources from observational data in the energy range of 10^{19} eV.

Only above 10^{20} eV UHECR follow the injection spectrum after accounting for the energy loss due to propagation. It is thus a task left for future giant air shower detectors, such as the Pierre Auger Observatory [8], EUSO and OWL [9] to study the location and luminosity of these sources.

Once the proper statistics of such events is collected, the data can be used for estimates of magnetic fields structure of the cosmologically nearby Universe.

Acknowledgements This work is supported in part by NASA grant NAG5-10919.

5. References

1. M. Lemoine et al., Ap. J., **486**, L115 (1997)
2. G.A. Medina Tanco, Ap. J., **505**, L79 (1998)
3. G. Sigl, M. Lemoine & P.L. Biermann, Astropart. Phys., **10**, 141 (1999)
4. Y. Ide et al., Publ. Astr. Soc. Japan, **53**, 1153 (2001)
5. P.L. Biermann et al., Nucl. Phys. B (Proc. Suppl.), **87**, 417 (2000)
6. T. Stanev, D. Seckel & R. Engel, astro-ph/0108338
7. T. Stanev et al., Phys. Rev. D**62**: 093005 (2000)
8. J. Blümer et al., Pierre Auger Collaboration, J. Phys. G, **29**, 867 (2003)
9. The status of the proposals is available at *http//www.ifcai.pa.cnr.it* and *http//owl.gsfc.nasa.gov*

The last Gamma Ray Burst in our Galaxy? On the observed cosmic ray excess at 10^{18} eV

Peter L. Biermann[1,2], Gustavo Medina Tanco[3], Ralph Engel[4], Giovanna Pugliese[5]
(1) Max-Planck Institute for Radioastronomy, Bonn, Germany
(2) Department for Physics and Astronomy, University of Bonn, Germany
(3) Instituto Astronomico e Geofisico, Universidade de Sao Paulo, Brasil
(4) Forschungszentrum Karlsruhe, Karlsruhe, Germany
(5) European Southern Observatory, Munich, Germany

Abstract

Here we propose that the excess flux of particle events of energy near 10^{18} eV from the direction of the Galactic center region is due to the production of cosmic rays by the last one or two Gamma Ray Bursts in our Galaxy. The basic idea is that protons get accelerated inside Gamma Ray Bursts, then get ejected as neutrons, decay and so turn back into protons. These meander around the inner Galaxy for some time, and then interact again, turning again to neutrons to be observed at our distance from the Galactic center region, where most star formation is happening in our Galaxy. We demonstrate that this suggestion leads to a successful interpretation of the data, within the uncertainties of cosmic ray transport time scales in the inner Galaxy, and in conjunction with many arguments in the literature.

1. Introduction

For some time now, the detection of an excess in 10^{18} eV cosmic rays from the general direction of the Galactic center by the air shower array AGASA [7] has been a special riddle in Galactic cosmic ray research. This excess has been supported at the time by the air fluorescence detector Fly's Eye [3], and is now roughly confirmed in a recent analysis of data from the air shower array SUGAR, [2]. Although the SUGAR results disagree with that of AGASA in details, they confirm the gross features of the excess.

Gamma Ray Bursts have long been argued to produce high energy cosmic rays. Here we will show what the observational signature should be and try to demonstrate that the AGASA excess can be attributed to the last one, or last few Gamma Ray Bursts in our inner Galaxy.

Already the AGASA team concluded, that the energy and the spatial correlation suggested that these particles are neutrons, implying an energy per

pp. 1–4

nucleon of again 10^{18} eV. The flux of the observed excess particles can be turned into a luminosity of particles beyond 10^{18} eV of about 4×10^{30} erg/s. Since AGASA cannot observe the entire region, this inferred luminosity must be a lower limit, with the true luminosity possibly being a factor of 3 - 10 larger.

There are three main mechanisms and respective sites to accelerate particles in the Galaxy: supernova explosions either in the interstellar medium, in young and hot star bubbles, or in massive star winds. In any of the three cases such an energy per nucleon cannot be reached for any reasonable parameter of shock velocity and/or magnetic field. The only way to accelerate particles to such an energy per nucleon in a normal galaxy as ours is relativistic shocks. Such relativistic shocks are, for example, produced in Gamma Ray Bursts (GRBs) [10],[8].

As shown in Rachen & Mészáros, [9], because of adiabatic losses, the highest energy particles that emerge from a GRB are mostly neutrons; protons are captive in the magnetic field and so suffer extensive adiabatic losses on the way out. These neutrons will decay after they travel their corresponding decay distance, turning into protons, which are then caught by the magnetic field in the Galaxy, and rumble around with a rather short residence time scale. There is a small, but finite probability that they will produce a neutron again in interactions with the interstellar medium. These secondary neutrons then could travel undeflected to us to be observed. We will try to follow the neutrons originally ejected from a Gamma Ray Burst.

2. The last GRB event in our Galaxy

We estimate the remaining traces of any activity of cosmic rays ejected and/or produced by Gamma Ray Bursts.

The expected flux today, from the last GRB occurring 10^6 yrs ago is now given by 10^{51} ergs, per 10^6 yrs, down by 300 (from the proton diffusion out from the Galaxy), down by 20 (from the interaction probability to make neutrons again from protons), down by 3 (from the geometry), down by 100 (at 10^{18} eV, for an injection spectrum of $E^{-2.2}$, [1]), and down by 2 (from the direction of pointing), and so 10^{31} erg/s. This is just above what is observed, and so allowing for uncertainties mainly due to the limited sky coverage of AGASA, a very plausible estimate to explain the data.

The observed spectrum would be completely dominated by the two step propagation of the secondary neutrons in such a picture. Therefore the spectrum is the folding of the production spectrum, with the decay probability inside the available space, so a hump from the minimum distance to get any neutrons, to the maximum energy possible from GRB productions, usually estimated to be near to or above 10^{19} eV.

We conclude that the observed distribution is rather likely to be the result of one or two GRB events in the Galactic center region.

3. Predictions and tests

Large numbers of photons, electrons and neutrinos are produced the collisions that give rise to the second generation neutrons in such a picture. It is convenient to express the secondary particle spectra in terms of the primary proton spectrum by multiplying it with appropriate reduction factors. Simulations using the Monte Carlo event generator SIBYLL 2.1 [6],[5] predict the following reduction factors: for secondary protons and antiprotons 0.27, for neutrons and antineutrons 0.09, for photons 0.11, for electron-positron pairs 0.05, and for neutrinos (all flavours) 0.13. All these numbers are normalized to a primary proton spectrum, using a powerlaw of $E^{-2.2}$, and the energy range 10^{17} - 10^{18} eV. These numbers are the ratio of the fluxes far below the upper energy cutoff. Observable is the ratio of the uncharged components, e.g., the ratio of neutrons to gamma-rays, which is here close to 1; however, near to the upper cutoff the photons drop off earlier than the neutrons. Given a reliable spectrum, we could infer the upper energy cutoff from an observed ratio of neutron flux to photon flux. The curves will look the same relative to maximum energy (here 10^{18} eV with a following exponential cutoff).

To see an appreciable flux of neutrons peaking near 10^{18} eV with a visible extension to 2×10^{18} eV requires that the primary proton/neutron flux extends to at least about 6×10^{18} eV. A measurement of the ratio of neutrons to photons, with a simultaneous determination of the injected powerlaw slope, would then allow to estimate the real cutoff energy of the injected proton/neutrons.

It is interesting to consider the time evolution of such a neutron flux: There is a last phase, when we pass the diffusive reservoir time of about 10^5 years, the flux begins to decay with $t^{-5/2}$, as protons leak out from the probable interaction volume.

4. Conclusions

We have shown that it is rather plausible that the observed AGASA excess of events near 10^{18} eV energies coming to us from the Galactic center region is due to the last one or two Gamma Ray Burst events in the Galaxy. We predict a corresponding flux in photons and neutrinos.

In fact, if the predicted details can be confirmed, we will have established i) that GRB cosmic ray signature can be detected, ii) the cosmic ray production of Gamma Ray Bursts to be of order 10^{51} erg, iii) that their particle energy extends to at least 6×10^{18} eV, iv) that the maximum particle energy can be estimated with a measurement of both neutrons and photons, as well as the slope of the injection spectrum, and v) that their contribution to the overall energetics of Galactic cosmic rays is minor. To check this will be a major contribution of the Pierre Auger Observatory whose southern part is ideally located to observe the

Galactic center region and is currently under construction [4]. The combination of fluorescence and surface detectors of this experiment allow measurements in the energy region from several 10^{17} eV to the highest energies.

5. Acknowledgements

Work with PLB is mainly being supported through the AUGER theory and membership grant 05 CU1ERA/3 through DESY/BMBF (Germany); further support for the work with PLB comes from the DFG, the DAAD, the Naumann-Foundation, and the Humboldt Foundation (all Germany), grant 2000/06695-0 from FAPESP (Brasil) through G. Medina-Tanco, KOSEF (Korea) through H. Kang and D. Ryu, ARC (Australia) through R.J. Protheroe, a NATO-grant (with S. Moiseenko, Russia) and European INTAS/ Erasmus/ Sokrates/ Phare grants. GMT is also supported through grants from FAPESP and CNPq (Brasil). GP wishes to thank ESO for the kind hospitality. The authors appreciate comments from Alan Watson. PLB also wishes to acknowledge comments from T. Kellmann.

References

[1] Bednarz, J., Ostrowski, M., PRL 80, 3911 - 3914 (1998).

[2] Bellido, J. A., Clay, R. W., Dawson, B. R , Johnston-Hollit, M., (2000), astro-ph/0009039.

[3] Bird, D.J., et al., ApJ 511, 739 (1999).

[4] Blümer, J., et al., Pierre Auger Collaboration, JPhG 29, 867 (2003).

[5] Engel, R., Gaisser, T. K., Lipari, P. Stanev, T., Proc. of 26th ICRC (Salt Lake City) 1, p. 415 (1999).

[6] Fletcher, R. S., Gaisser, T. K., Lipari, P., Stanev, T., PRD 50, 5710 (1994).

[7] Hayashida, N. et al., ApP 10, 303 (1999), astro-ph/9807045.

[8] Piran, T., Physics Reports 314, 575 (1999).

[9] Rachen, J.P., Mészáros, P., PRD 58, ms. 123005 (1998).

[10] Vietri, M., PRL 80, 3690 - 3693 (1998).

The Knee in the Energy Spectrum of Cosmic Rays in the Framework of the Poly-Gonato and Diffusion Models

J.R. Hörandel[1], N.N. Kalmykov[2], and A.I. Pavlov[3,4]
(1) University of Karlsruhe, PO Box 3640, 76021 Karlsruhe, Germany
(2) Skobeltsyn Institute, Moscow State University, Leninskie Gory 1, 119992, Moscow, Russia
(3) University of Mannheim, D7-27, 68131 Mannheim, Germany
(4) Institute of Astronomy RAS, 48 Pyatnitskaya str., 119017, Moscow, Russia

Abstract

Results of an analysis of the cosmic-ray energy spectrum using the poly-gonato and diffusion models are presented. Both models produce similar energy spectra and one may conclude that the results are quite consistent with each other. This may indicate that the knee in the cosmic-ray energy spectrum is caused by diffusion processes in the Galaxy.

1. Introduction

Although the knee in the energy spectrum of primary cosmic rays (PCR) at $\approx (3-5) \cdot 10^{15}$ eV was firstly reported more than 40 years ago, [6] its nature is still far from being ultimately established. Up to now, the experiments in the energy region of the knee have been performed with ground-based detector systems investigating extensive air showers (EAS). As these studies provide no direct measurements of PCR fluxes, the reconstruction of the primary energy spectrum from experimental data is a considerable challenge. Hence, recent results of the KASCADE array [9] for energy spectra of individual nuclear groups present a major achievement in the field.

In [2] a phenomenological model, named poly-gonato (Greek "many knees") model, was developed to link the results from direct and indirect measurements. Using this model it proved possible to extrapolate energy spectra of individual elements measured directly to super-high energies. After some slight renormalization of the energy spectra obtained with different EAS arrays the poly-gonato model describes successfully the all-particle energy spectrum as a result of subsequent cut-offs for individual elements (a cut-off proportional to their nuclear charge Z is assumed). Moreover, the primary mass composition extrapolated from energies below 10^{14} eV to super-high energies may be considered as compatible with results derived from EAS experiments and the predictions of the poly-gonato model for individual energy spectra present the experimental results of the KASCADE

pp. 1–4

array reasonably well.

So it would be proper to search for some theoretical foundations for the poly-gonato model. The knee may be due to cosmic-ray acceleration and/or propagation. But as there is no accomplished theory of these processes (even for the energy region below the knee) we presently consider only one possibility and try to connect the poly-gonato model with predictions of modern diffusion theory taking into account the drift of cosmic rays in the large scale regular magnetic field (the so-called Hall diffusion) [4][5][7]. If the knee is basically the result of the cosmic-ray propagation in our Galaxy, then the steepening of the PCR energy spectrum stems from the increasing leakage of cosmic rays from the Galaxy when the influence of the Hall diffusion becomes dominant.

2. Basic assumptions

In the region of interest (at energies $E > 10^{15}$ eV) the energy spectrum for cosmic-ray particles with charge Z takes the form [2]

$$\frac{d\Phi_Z}{dE}(E) = \Phi_Z^0 E^{\gamma_Z} \left[1 + \left(\frac{E}{E_Z}\right)^{\epsilon_c}\right]^{\frac{\gamma_c - \gamma_Z}{\epsilon_c}} . \qquad (1)$$

where the absolute flux Φ_Z^0 and the spectral index γ_Z define a power law before the knee; γ_c and ϵ_c characterize the change in the spectrum at the cut-off energy E_Z. γ_c and ϵ_c are assumed to be independent on Z. As was shown in [2] it is also possible to use a constant difference $\Delta\gamma$ between the spectral indices before and after the knee. This ansatz leads to

$$\frac{d\Phi_Z}{dE}(E) = \Phi_Z^0 E^{\gamma_Z} \left[1 + \left(\frac{E}{E_Z}\right)^{\epsilon_c}\right]^{\frac{-\Delta\gamma}{\epsilon_c}} . \qquad (2)$$

We assume also the dependence $E_Z = ZE_p$ where E_p is the cut-off energy for protons. The all-particle spectrum is obtained by summation over all elements. According to the analysis carried out in [2] there are no statistically significant differences between values of parameters restored when one uses (2) instead of (1).

The diffusion and drift of cosmic rays are considered in the framework of the model adopted in [5]. This model combines Rand-Kulkarni's structure of the regular magnetic field in the Galactic plane [8] and an extended halo as in [7]. Cosmic-ray sources are distributed in the disk with a thickness $2h_s = 400$ pc. The regular magnetic field coincides with Rand-Kulkarni's field in the disk and incorporates a large halo with symmetric or antisymmetric configuration of the magnetic field. The sinusoidal boundary provides necessary signs of the field. The cosmic-ray transport is described by the following equation for the particle

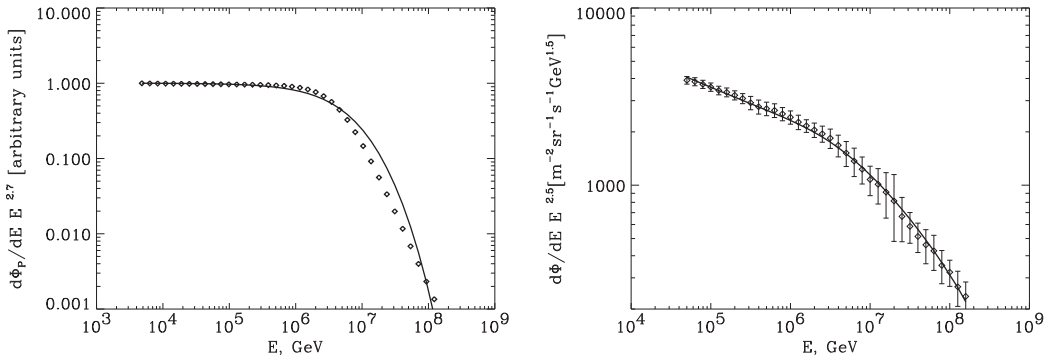

Fig. 1. Left: proton spectrum ($\diamondsuit$ – poly-gonato model, solid curve – diffusion model with the radial distribution of sources following the law $Q(r) \sim \delta(r - 4\ \mathrm{kpc})$). Right: $\diamondsuit$ – average all-particle spectrum [2] and diffusion model for elements from H to U according to [2].

concentration $N(r, z)$ (the dependence on E is omitted):

$$\left[-\frac{1}{r}\frac{\partial}{\partial r}rD_\perp\frac{\partial}{\partial r} - \frac{\partial}{\partial z}D_\perp\frac{\partial}{\partial z} - \frac{\partial}{\partial z}(D_A)\frac{\partial}{\partial r} + \frac{1}{r}\frac{\partial}{\partial r}(rD_A)\frac{\partial}{\partial z}\right] N(r,z) = Q(r,z) \quad (3)$$

where $Q(r, z)$ is the source term, $D_\perp$ and D_A are transverse and Hall diffusion coefficients respectively. Equation (3) is written in a cylindrical frame of reference (r, z), the dependence on ϕ is neglected due to the dominance of the toroidal field component. When solving equation (3) for different Z one must take into account that $D_\perp \propto (E/Z)^m$ and $D_A \propto (E/Z)$. Floating boundary conditions are applied in order to calculate $N(r, z)$ with appropriate accuracy near the Galactic plane. Equation (3) is valid up to energies $\geq 10^{17}$ eV and the detailed solution technique may be found in [3].

3. Results of calculations

We have considered a number of variants differing by regular magnetic field configurations, by values of m in $D_\perp(E)$ dependence and also by an effective halo height h_{eff}. The latter is defined as follows [7]:

$$h_{eff}^{-1} = (\partial N/\partial z)/N \quad (4)$$

where the concentration and its derivative are taken at $z = 0$. Values of m and h_{eff} are chosen (for any adopted field configuration) to optimize the agreement between the calculated spectra and the predictions of the poly-gonato model.

Fig. 1 (left) presents the energy spectrum of protons calculated in the framework of the diffusion theory and the corresponding spectrum obtained with the poly-gonato model. It may be seen that sufficiently good agreement could be achieved and, therefore, both models should produce similar all-particle spectra.

Indeed, taking the intensities of different elements and their spectral indices according to [2] we obtain quite a good fit of the calculated all-particle energy

spectrum to experimental data derived from EAS observations (see Fig. 1 (right)). Extragalactic protons are not taken into account and so the data for energies $\geq 2 \cdot 10^{17}$ eV are not shown. We would like to point out also that the experimental all-particle energy spectrum might be reproduced quite satisfactory even if the predictions of the diffusion and poly-gonato models for individual elements would agree worse.

Equation (3) used to analyze the cosmic-ray transport ignores interactions of nuclei and this assumption, of course, is not exactly valid as these interactions do exist. Some amount of protons and light nuclei should be produced due to nuclear collisions and so the PCR spectrum derived using the diffusion model should display a more complicated behavior after the knee.

4. Conclusion

The energy spectra adopted in the poly-gonato model are almost the same as predicted by modern diffusion theory. So it is quite possible to draw the conclusion that the knee in the PCR energy spectrum may be attributed to diffusion in our Galaxy. But this notion implies that the energy spectra at the sources have to be essentially steeper below the knee as it follows from the standard theory of shock acceleration (see [1]). Indeed, the spectral index at the sources should be about $\gamma_s \approx \gamma_{obs} - m$ and m is close to $0.2 - 0.3$. Though there are no ultimate arguments in favour of the validity of the shock acceleration mechanism some dissatisfaction exists. We would not like to state definitely that the knee in the PCR spectrum is due to the cosmic-ray diffusion only. Probably the adequate reason for the knee should be searched for considering combined influence of acceleration and diffusion processes.

Acknowledgments

N.N. Kalmykov acknowledges the financial support of the RFBR (grant 02-02-16081). A.I. Pavlov acknowledges the financial support of Klaus Tschira Foundation.

References

[1] Gaisser T.K., Cosmic Rays and Particle Physics, Cambridge University Press 1990

[2] Hörandel J.R., Astropart. Phys. 19 (2003) 193

[3] Kalmykov N.N. & Pavlov A.I., Preprint SINP MSU 97-4/455 (1997) 1

[4] Kalmykov N.N. & Pavlov A.I. , Proc. 25th ICRC, Durban 4 (1997) 293

[5] Kalmykov N.N. & Pavlov A.I., Proc. 26th ICRC, Salt Lake City 4 (1999) 263

[6] Kulikov G.V. et al., JETP 35 (1958) 635

[7] Ptuskin V.S. et al, Astron. Astrophys. 268 (1993) 726

[8] Rand R.I. & Kulkarni S.R. , Ap. J. 343 (1989) 760

[9] Ulrich H. et al., Proc. 27th ICRC, Hamburg 1 (2001) 97

LOPES – Detecting Radio Emission from Cosmic Ray Air Showers

A. Horneffer,[1] H. Falcke,[1,2] A. Haungs,[3] K.H. Kampert[4], G.W. Kant[5], H. Schieler[3]
(1) Max-Planck-Institut für Radioastronomie, Bonn, Germany
(2) Dept. of Astronomy, University of Nijmegen, Nijmegen, The Netherlands
(3) Institut für Kernphysik, Forschungszentrum Karlsruhe, Karlsruhe, Germany
(4) Fachbereich 8 Physik, Wuppertal, Germany
(5) ASTRON, Dwingeloo, The Netherlands

Abstract

Radio pulses from air showers were measured during the late 1960ies in the frequency range from 2 MHz to 520 MHz. Mainly due to difficulties with radio interference these measurements ceased in the late 1970ies. LOFAR (**Lo**w **F**requency **Ar**ray) is a new digital radio interferometer under development. Due to its fully digital nature it will be able to filter out interference and form beams even after a transient event like an air shower has been detected. To test this new technology and demonstrate its ability to measure air showers we are building a **LO**FAR **P**rototyp**e** **S**tation (LOPES) for the frequency range of 40 to 80 MHz at the site of KASCADE-Grande in Karlsruhe/Germany. The 10 antennas of the first phase of LOPES are now set up and four are taking air shower data.

1. Introduction

A standard method to observe cosmic rays is to measure the secondary particles of an air shower with an array of particle detectors on the ground. Very useful information for the determination of primary particle energy and type can be obtained by additionally observing the air shower as it evolves. So far this is only done by observing optical emission like Cherenkov or fluorescence light. This requires dark, clear and moonless nights and thus limits the available efficiency to about 10%.

Measuring radio emission from air showers might be an alternative method for such observations, providing a much better efficiency. This becomes particularly relevant since a new generation of digital radio telescopes – designed primarily for astronomical purposes – promises a new way of measuring air showers.

2. Radio Properties of EAS

Radio emission from cosmic ray air showers were discovered for the first time by Jelly [5] at 44 MHz. The results were soon verified and in the late 1960's emission from 2 MHz up to 520 MHz were found. In the following years these

activities ceased due to difficulty with radio interference, uncertainty about the interpretation of the results, and the success of other methods.

The radio properties of extensive air showers are summarized in an excellent review by Allan [1]. The main result of this review can be summarized by an approximate formula for the received voltage:

$$\epsilon_\nu = 20 \left(\frac{\mathrm{E_p}}{10^{17}\mathrm{eV}}\right) \sin\alpha \cos\theta \exp\left(\frac{-\mathrm{R}}{\mathrm{R}_0(\nu,\theta)}\right) \left[\frac{\mu\mathrm{V}}{\mathrm{m\,MHz}}\right] \quad (1)$$

Here $\mathrm{E_p}$ is the primary particle energy, α is the angle to the geomagnetic field, θ is the zenith angle, R is the distance to the shower center, R_0 is around 110 m at 55 MHz, and ν is the observing frequency. The spectral form of the radio emission seems to be valid in the range $2 < \nu < 520$ MHz but in general is fairly uncertain. Recent results suggest that the emission may be geosynchrotron emission (see [2] and [4]).

3. LOFAR and LOPES

LOFAR is a new attempt to revitalize astrophysical research at 10-200 MHz with the means of modern information technology. The basic idea of LOFAR is to build a large array of 100 stations of 100 omnidirectional dipole antennas in which the received waves are digitized and sent to a central super-cluster of computers.

A new feature is the possibility to store the entire data stream for a certain period of time. If one detects a transient phenomenon one can then retrospectively form a beam in the desired direction. LOFAR therefore combines the advantages of a low-gain antenna (large field of view) and a high-gain antenna (high sensitivity and background suppression). This makes it an ideal tool to study radio emission from cosmic ray air showers. With its range of baselines between 10 m and 400 km LOFAR will be capable to detect air showers from $> 2 \cdot 10^{14}$ eV to $\sim 10^{20}$ eV.

To test the technology of LOFAR and demonstrate its capability to measure air showers we are building LOPES at the site of KASCADE-Grande in Karlsruhe/Germany (see [3]). The data from a well tested air shower experiment not only allows us to calibrate the radio data with other air shower parameters, it also provides us with starting points for the air shower reconstruction, simplifying the development process. This will enable us to clarify the nature and properties of radio emission from air showers and provide an energy calibration for future radio air shower experiments. Also, LOPES will provide KASCADE-Grande with valuable additional information about the air shower, as the radio data and the particle data come from different stages in the evolution of a shower.

4. The Hardware of LOPES

The first stage of LOPES consists of 10 antennas. This will be extended to an improved system with 100 antennas in the second stage. LOPES will be sensitive to cosmic rays from 10^{15} to 10^{17}eV. It operates in the frequency range

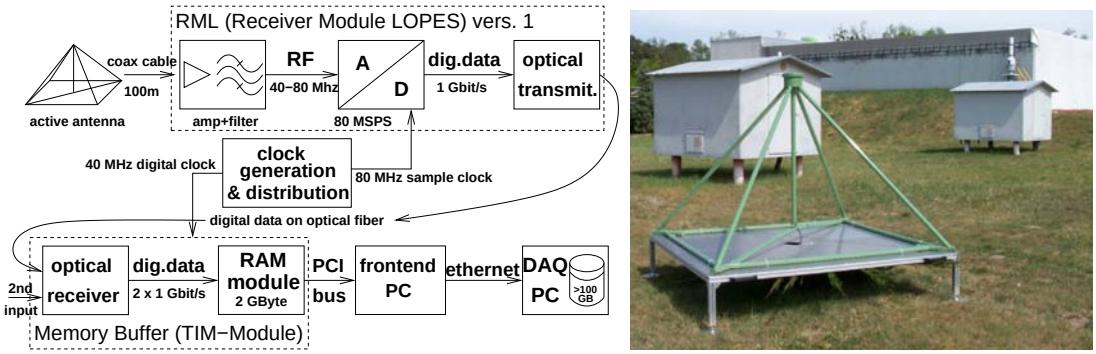

Fig. 1. (left:) Outline of the hardware of the first LOPES stage (right:) One of the LOPES antennas at the KASCADE-Grande site

of 40–80 MHz, because in this range there are only few strong radio transmitters (the FM band is avoided) and the radio emission from air showers are strong compared to the sky noise.

As basic element the short dipole antennas, developed for LOFAR by ASTRON, are used. The radio frequency signal is sampled without the use of a local oscillator inside the receiver module (see Figure 1). The necessary dynamic range to detect weak pulses while not saturating the ADC with radio interference is achieved by using 12-bit ADCs. In the first stage the ADCs work at 80 MHz, allowing 2nd Nyquist sampling of the signal. The sample clock for the ADCs is generated on a central clock module and is then distributed to all A/D-boards. This allows us to combine the data from all antennas as a phased array and thus enhance the sensitivity. The digital data is transferred via fiber optics to a memory module on a front-end PC. The module can store up to six seconds of data for two channels in a digital ring buffer. After a trigger signal is received the data is read out and sent to a central DAQ-PC, where it can be analyzed online or stored on hard disk. The specialized hardware (active antenna, A/D-electronics, memory module and clock distribution) was developed at ASTRON in Dwingeloo.

5. Status and First Results

The first stage of LOPES is nearly complete. The system and ten antennas are set up at the KASCADE-Grande site at the positions shown in Figure 2 (left panel). At the time of writing four of the antennas are taking air shower data.

A preliminary analysis of the first data has already been performed. Some candidates for air shower radio pulses have been identified. In Figure 2 (right panel) one of those candidates is plotted. The origin of the x-axis is the arrival time of the trigger. The three lines are the block-averaged power of the radio signal normalized to give the same noise level. We show the raw data from one antenna, the same data after filtering radio interference in frequency space, and the data of four filtered datasets after combining and beam forming. The jump

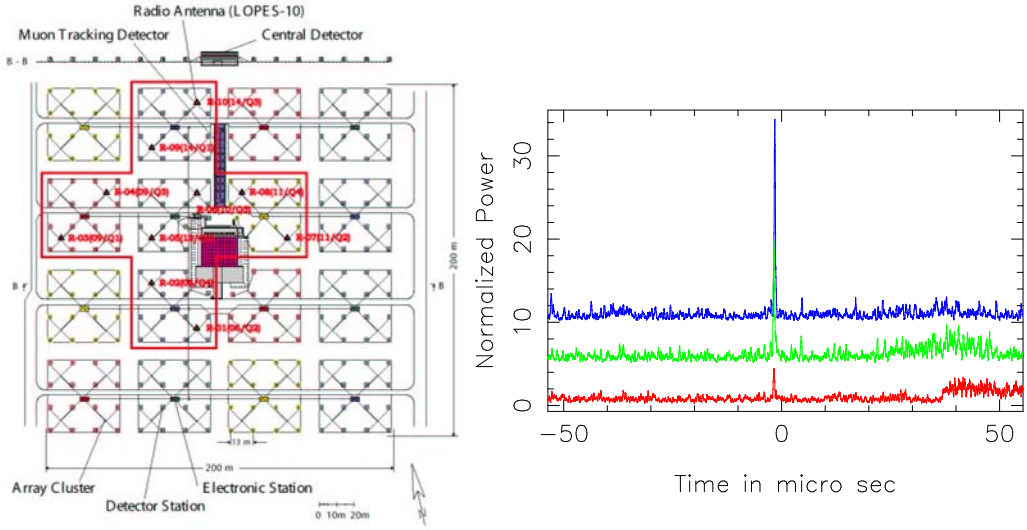

Fig. 2. (left:) Layout of the first 10 LOPES antennas at KASCADE-Grande (right:) Average power of a possible air shower radio pulse normalized to the background noise. Bottom: raw data, middle (offset +5): after filtering of narrow band interference, top (offset +10): after beam forming of four antennas

in noise at $+37\,\mu$sec originates in triggered electronics of KASCADE-Grande.

6. Outlook

Currently we are working on the data analysis and an improved system for the second stage, which is scheduled to be implemented in early 2004. Possible improvements are full Nyquist sampling of the 80 MHz, A/D conversion at the antenna, better noise performance, and lower production costs.

The same technology can be applied to other forthcoming digital radio telescopes like LOFAR and the SKA, providing additional detection area for high energy cosmic rays. In the long run a digital radio telescope could even form the northern part of the Pierre Auger Project.

7. Acknowledgments

LOPES is supported by the German Federal Ministry of Education and Research, under grant No. 05 CS1ERA/1 (Verbundforschung Astroteilchenphysik).

8. References

1. Allan H.R. (1971), Prog. in Elem. part. and Cos. Ray Phys., Vol 10, 171
2. Falcke H. & Gorham P. (2003), Astropart. Phys, Vol 19, 477
3. Haungs A. et al. (2003), Proc. 28th ICRC Tsukuba, these proceedings
4. Huege T. & Falcke H. (2003), A&A submitted
5. Jelly J.V. et al. (1965), Nature 205, 327

Transition Radiation Detectors for Cosmic Rays Near the Knee

S.P. Wakely[1], F.H. Gahbauer[1], J.R. Hörandel[2], D. Müller[1], and S. Plewnia[2]
(1) Enrico Fermi Institute, University of Chicago, Chicago, IL 60637, USA
(2) Institute for Nuclear Physics, University of Karlsruhe, Germany

Abstract

Precise observations of the energy spectra and relative abundances of cosmic-ray nuclei require instruments that exhibit individual charge resolution and a calibrated energy response. If energies up to $\sim 10^{15}$ eV are to be covered, the low intensity of the heavier nuclei ($Z \gtrsim 3$) also mandates detector areas of several square meters. X-ray transition radiation detectors (TRDs) appear to provide the only practical means of fulfilling all of these requirements for balloon or space-borne instruments. However, for measurements up to the cosmic-ray "knee", care must be taken that the energy response of the TRD does not saturate for Lorentz factors less than $\sim 10^5$. We have designed detectors to meet this goal, and have successfully tested prototypes at an accelerator beam at CERN. We shall present and discuss the results of these measurements.

1. Introduction

The determination of the energy spectra and composition of the elements in cosmic rays at very high energies, i.e., approaching the knee region above 10^{15} eV, has been a long-standing goal in cosmic-ray astrophysics. Achieving this goal with direct measurements requires instruments which are not only very large, but which have an extended and well-understood response. Precision TRDs can meet these requirements [4,5]. Because the TR process responds to Lorentz factor ($\gamma = E/mc^2$), rather than energy, calibrations at ground-based facilities may be performed prior to the deployment of the instrument. Furthermore, because TR emission is not a nuclear effect, TRDs do not require large masses of "target" material. This allows for relatively large detector areas for a given mass.

Unlike accelerator-oriented threshold TRDs, precision TRDs are employed to make accurate measurements of Lorentz factors over large ranges of energy. This is possible because the transition radiation yield scales with nuclear charge, as Z^2 [3]. However, if energies as high as the cosmic-ray knee are to be reached, a TRD must be carefully designed to maintain sensitivity up to Lorentz factors of $\gamma \sim 10^5$, *while retaining effectiveness at lower Lorentz factors,* $\gamma \lesssim 10^3$.

pp. 1–4

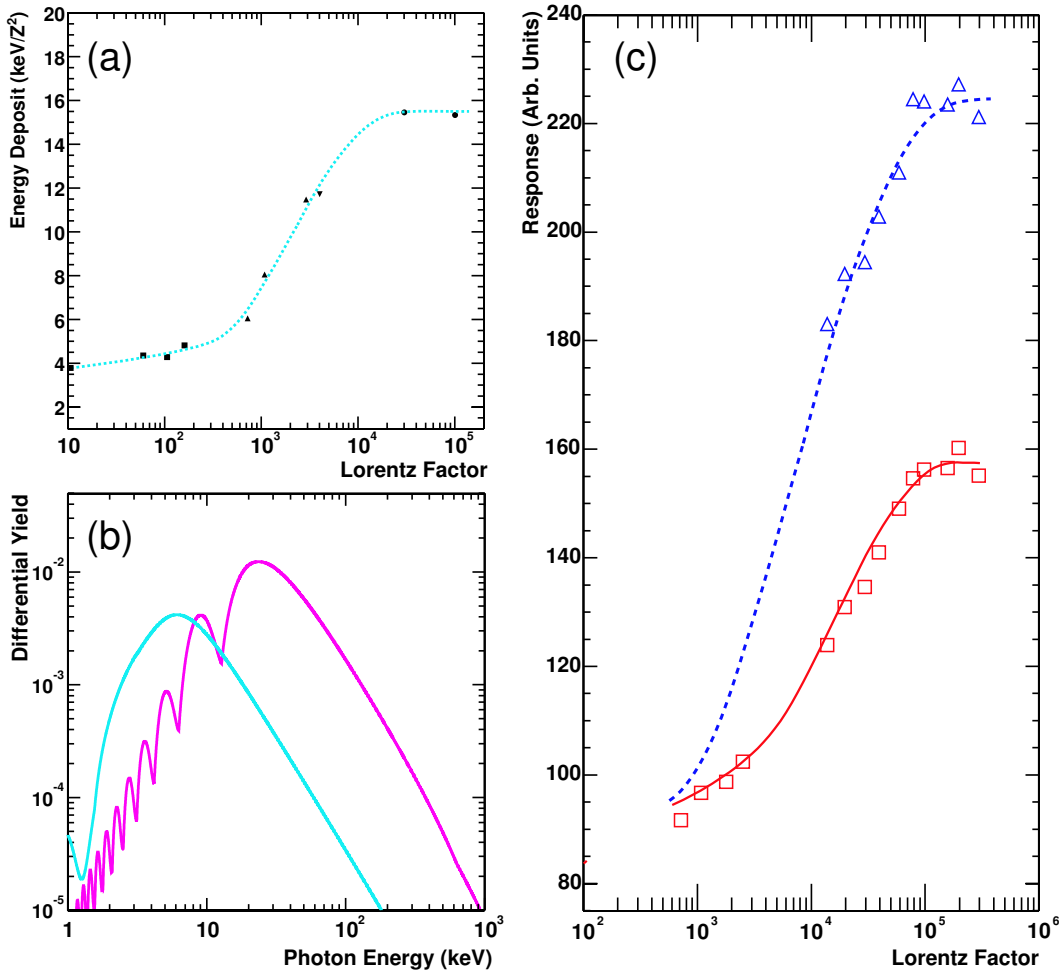

Fig. 1. Panel a: The response curve of the CRN TRD [2]. Panel b: Differential TR spectra. Panel c: The TRD response curve for two detector prototypes. Squares: Configuration A. Triangles: Configuration B. Solid line: Simulation. See text for details.

2. Transition Radiation Properties

Transition radiation is emitted in the x-ray region when a relativistic charged particle traverses a dielectrically inhomogeneous radiator, such as a stack of foils stretched in air, or a volume of plastic foam or fibers. The energy yield of the TR varies with the Lorentz factor of the primary particle, allowing estimates to be made of particle energy. However, the range of Lorentz factors over which such estimates can be made is limited. In practice, for any given radiator, *saturation* effects will set in, reducing its sensitivity at higher energies. This can be seen in Figure 1a, which shows the response curve (detector signal versus Lorentz factor) of the CRN instrument [2]. This instrument was designed to provide ex-

cellent response at lower Lorentz factors. Consequently, the TR signal becomes noticeable around $\gamma \gtrsim 500$, and saturates around $\gamma \gtrsim 2 \times 10^4$.

The properties of the TR emitted from a radiator are affected by the geometric configuration of the radiator, i.e., on the thickness, spacing, and total number of interfaces in the volume, as well as the plasma frequencies of its materials (for a review, see [1]). An example can be seen in Figure 1b, which shows the differential emission spectra of two radiators differing only in their foil thickness. The light line is for ~ 5 μm Mylar foils, and the darker line is for thicker foils, ~ 50 μm. Self-absorption effects have been included, reducing the emission at low energies. As can be seen, the radiation yield peaks at considerably lower x-ray energy for the thin-foil radiator than for the thick-foil configuration. This dependence can be exploited to shift the emission spectrum of a radiator to features in the photoelectric response of the detector gas.

This provides a certain freedom in the "tuning" of a radiator to achieve the performance goals required for any specific purpose. In particular, by varying the thickness and spacing of the radiator's interfaces, it is possible to raise and lower the sensitive region (in Lorentz factor) of a given radiator. By *combining* radiators with different tunings, it is possible to build an instrument with an aggregate response which extends beyond that of any of its component parts. These designs are called composite, or graded radiators.

3. Prototype Design and Measurements

One may try to push the saturation point of a TRD to $\gamma \sim 10^5$ by increasing the distance between the interfaces within a radiator [5]. However, for a fixed detector height, this requires a reduced number of interfaces, and therefore, a diminished TR yield. Alternatively, one may increase the thickness of the foils in the radiator. This, however, also increases the hardness of the radiation, making it more difficult to detect. In practice, achieving a high saturation point requires some compromise between thicker foils (lower detection efficiency) and larger gaps (smaller TR yield).

Just such a compromise is possible by using foils which have been selected specifically to target the highest-energy absorption edge of the detector gas. In the case of a Mylar radiator and xenon detector gas, for instance, this suggests foils of ~ 75 μm thickness. Such foils, when combined with a spacing of several mm, should be able to provide a high saturation energy. This idea is tested in our first prototype TRD, Configuration A. This radiator comprises 51 76 μm (3 mil) Mylar sheets, spaced at 15 mm. The simplicity of this design facilitates easy comparisons with simulations.

A radiator specialized for high Lorentz factors is not expected to perform as well at lower Lorentz factors. Therefore, to achieve a truly extended response, one should combine multiple radiators with different regions of sensitivity. For

example, Configuration B combines the foils of Configuration A with additional pieces of radiator material, including a 5 cm block of DOW Ethafoam 220 and a 7.6 cm blanket of 17 μm-thick Herculon fibers. The addition of this radiator material is meant to increase the total TR yield while improving the response at lower Lorentz factors.

Measurements of these configurations were carried out at CERN in the autumn of 2001. Pions and electrons ranging in Lorentz factor from $\gamma \approx 7 \times 10^2$ to 5×10^5 were used in the tests. The radiator materials were placed in front of a 2 cm thick multiwire proportional chamber (MWPC) filled with a xenon-methane mixture (95%/5% by volume).

4. Results and Discussion

Figure 1c shows the detector signal versus Lorentz factor for the two test TRD configurations. Configuration A (open squares) has data for nearly three orders of magnitude in Lorentz factor. The resulting response curve does not saturate until $\gamma \gtrsim 10^5$, confirming the design principles. Superimposed on the data (solid line) is the output of a full simulation using GEANT 4.3.2. The absolute normalization to the data is arbitrary, but the agreement in shape is quite excellent.

Also shown (open triangles) in Figure 1c are the results obtained for the composite TRD, Configuration B. Once again, saturation appears at $\gamma \gtrsim 10^5$, but now, the overall TR yield has been increased substantially. Though we presently have no measurements at the lower Lorentz factors, a likely response curve (the dashed line) suggests a considerable improvement over the low-end response of Configuration A.

5. Conclusions

X-ray transition radiation detectors currently seem to offer the best option for obtaining direct measurements of the energies of heavy ($Z \gtrsim 3$) cosmic rays up to the knee region, with high statistics and sufficient energy resolution. Our measurements demonstrate that configurations can be found which exhibit excellent energy response over a large energy range, $500 \lesssim \gamma \lesssim 10^5$.

6. References

1. Cherry, M.L. et al., 1974, Phys. Rev. D10, 3594.
2. L'Heureux, J. et al., 1990, NIM A295, 246.
3. Swordy, S.P. et al., 1990, Phys. Rev. D42, 3197.
4. Wakely, S.P. et al., 2001, Proc. 27th ICRC, 6, 2247.
5. Wakely, S.P., 2002, Astroparticle Physics 18, 67.

Precise Identification of Heavy Cosmic-Ray Nuclei: The Role of Delta Rays

F. Gahbauer, G. Hermann[1], J. Hörandel[2], D. Müller, and A. A. Radu [3]
The Enrico Fermi Institute, The University of Chicago, 933 E. 56th Street, Chicago, IL 60637, USA
(1) presently at Max Planck Institut für Kernphysik, Heidelberg
(2) presently at University of Karlsruhe, Germany
(3) presently at Institute for Space Sciences, Bucharest

Abstract

Relativistic δ rays may lead to detector response functions, both in charge and energy, which are different from those expected for unaccompanied particles. These effects are particularly noticable for cosmic ray nuclei with large charge number, Z. We shall demonstrate some of these features with balloon-borne data obtained with the TRACER instrument, and compare the measurement with Monte Carlo calculations. Our results illustrate how δ-ray effects can lead to false charge assignments or acceptance efficiencies if not properly taken into account, but also how they can be helpful in extending the energy response of some of the counter elements.

1. Introduction

When a relativistic particle traverses a detector, such as a plastic scintillator or a Čerenkov counter, the recorded signal may have significant contributions due to δ rays. These either are produced by the particle in the detector material, or may accompany the particle but have been generated before the particle entered the detector. The energy dependence of the signal contributions due to δ rays may be different from that of signals due to particles unaccompanied by δ rays. This feature is difficult to determine for singly charged particles because of the long tails of signal distributions, but it does become apparent for the much narrower distributions at higher Z and must be taken into account in the analysis of the measurement.

We discuss these effects for the TRACER instrument, which is a balloon-borne detector built to measure the intensities of the heavier nuclear species in the cosmic rays up to energies of 10 TeV/nucleon (see Müller et al, this conference). It includes two plastic scintillators to trigger the instrument and to measure the charge of each particle. These are located at the top and at the bottom of the instrument, respectively, and thus permit rejection of nuclei that may have inter-

pp. 1–4

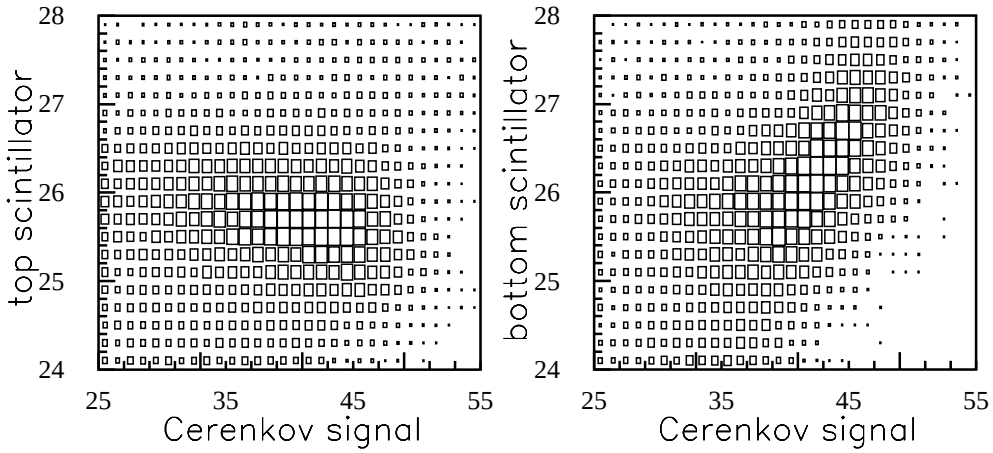

Fig. 1. Scintillator signals versus Čerenkov signals for iron flight data.

acted in the detector. Also at the bottom of the instrument is an acrylic Čerenkov counter to reject low-energy particles. The bulk of the TRACER instrument between the two scintillators consists of arrays of single-wire proportional tubes that either measure the specific ionization in gas or also detect superimposed signals from transition radiation x-rays that are generated in plastic fiber radiators. Each of the detector elements has a characteristic but different energy response, and the correlation of signals for each cosmic-ray particle leads to a measurement of its energy.

2. Observations

The scintillation counter signals serve as an energy-independent means of measuring the particle charge, Z above minimum ionization. Towards lower energies, the scintillator signals increase while the Čerenkov counter signals decrease. Thus, a scatterplot of a scintillator signal versus the Čerenkov signal easily identifies those particles whose energy is below minimum ionization and allows them to be rejected. The flight data, however, reveal a more complex situation. Figure 1 shows scatterplots of the signals from the two scintillators versus the Čerenkov signal for iron nuclei. Two different correlations are apparent. The slight decrease in the top scintillator signal with increasing Čerenkov signal reveals that some of the particles that have been observed are below minimum ionization. Beyond minimum ionization, the top scintillator signal does not vary significantly with energy. The situation is quite different, however, for the bottom scintillator. This signal exhibits an increase with increasing Čerenkov signal. When the Čerenkov

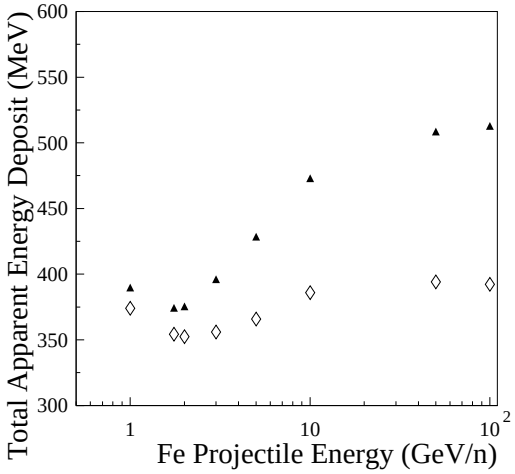

Fig. 2. Scintillator energy deposit. top scintillator (open diamonds); bottom scintillator (filled triangles)

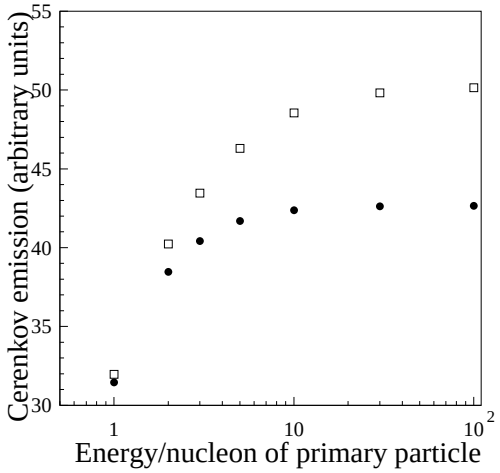

Fig. 3. Čerenkov light yield. Čerenkov counter without δ rays (filled circles); with δ rays (open squares)

signal reaches saturation, the bottom scintillator signal indicates an apparent charge that is greater than that of iron by almost one charge unit.

3. Monte Carlo Studies and Interpretation

These effects can be explained quantitatively by the production of penetrating δ rays. There is relatively little material to produce δ rays upstream of the top scintillator, but the material between the two scintillators generates a number of δ rays with sufficient energy to reach the bottom of the detector. The number of penetrating δ rays increases with primary particle energy up to about 10 GeV/n, but reaches saturation between 10 and 100 GeV/n. The δ rays generate a significant fraction of the total energy deposited in the bottom scintillator. This is qualitatively investigated in a Monte Carlo simulation.

The simulation generates δ rays along the primary particle's trajectory, which are tracked until they either stop or leave the instrument. The energy they deposit in the scintillators and the Čerenkov light they generate are recorded. Figure 2 illustrates the results of this calculation for the two scintillators. Shown is the total *apparent* energy deposit from both δ rays and primary ionization. Note that the δ rays are weighted more heavily in the total *apparent* energy deposit than the *actual* energy deposits would indicate. This is due to the fact that the conversion of deposited energy to light becomes nonlinear along the track of a heavily ionizing primary particle with $Z > \sim 10$. The δ rays, on the other hand,

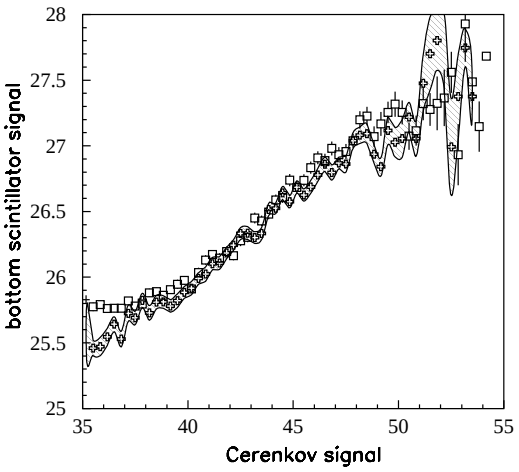

Fig. 4. Average scintillator signal as a function of Čerenkov signal.

simulation (boxes) and flight data (crosses) for iron

are spatially separated from the primary trajectory and singly charged, so their energy deposit is more efficiently converted into light. Figure 3 shows the results of the Monte Carlo calculation for the Čerenkov counter. The figure shows the calculated Čerenkov yield with and without taking δ rays into account.

A surprising but quite desirable feature of the δ-ray contribution is that it extends the region where the response of the acrylic Čerenkov counter increases with energy to beyond 10 GeV/nucleon, well beyond the saturation of a "pure" Čerenkov counter.

The results of the above studies are parametrized and fed into a GEANT 4 Monte Carlo of the entire detector. Random fluctuations consistent with real signal fluctuations are added to the simulated signals. Figure 4 shows the average scintillator signal in the bottom scintillator versus the Čerenkov signal. We notice excellent agreement between the simulation and the measured data in flight.

4. Conclusion

The Z^2 dependence of the electromagnetic energy loss processes allows precise measurements of the specific energy loss of heavy cosmic-ray nuclei. However, these gains in resolution for heavy nuclei uncover subtle energy dependencies that are hidden in the fluctuations for singly charged particles. If these effects are not carefully studied and understood, they can lead to false charge assignments or energy-dependent efficiencies. However, the effect of δ rays has also been found to be advantageous in TRACER as it extends the energy response of the Čerenkov counter and improves its low-energy discrimination ability.

Energy Spectra and Relative Abundances of Heavy Cosmic-ray Nuclei around 1 TeV/nucleon

D. Müller, F. Gahbauer, G. Hermann[1], J. Hörandel[2], and A. A. Radu[3]
The Enrico Fermi Institute, The University of Chicago, Chicago, IL 60637, USA
(1) presently at Max Planck Institut für Kernphysik, Heidelberg
(2) presently at University of Karlsruhe, Germany
(3) presently at Institute for Space Sciences, Bucharest

Abstract

We describe a measurement of the intensities of heavy primary cosmic-ray nuclei with the Transition Radiation Array for Cosmic Energetic Radiation (TRACER) up to energies around a few TeV/nucleon. Absolute cosmic-ray fluxes are presented for O, Ne, Mg, Si, and Fe obtained during a one-day test flight from Ft. Sumner, NM in preparation for a 20-day circum-polar balloon flight. The results of TRACER are largely consistent with previous observations in this energy range.

Introduction

Direct measurements of the elemental composition and energy spectra of cosmic-ray nuclei at high energies, beyond a TeV/nucleon, and approaching the cosmic-ray *knee* above total energies of 10^{15} eV, are expected to provide a sensitive test of the current paradigm that all cosmic rays are generated with the same energy spectrum at the source, up to a maximum rigidity around 10^{14} V for shock acceleration in supernova remnants, and that their propagation pathlength through the galaxy decreases with increasing energy. However, new observational data are slow in coming because the low particle intensity necessitates long exposures of very large-area instruments. With this need in mind, TRACER was constructed for a long-duration balloon flight. A successful 30-hour test flight was conducted from Ft. Sumner, NM, in September 1999. A subsequent long-duration balloon flight along the Northern Polar circle could not be accomplished due to lack of required international agreements. The instrument is currently scheduled for a long-duration flight in Antarctica in 2003/4. This report will present and discuss results obtained with the 1999 test flight.

The Instrument

Figure 1 shows the detector arrangement. The main elements are (a) plas-

pp. 1–4

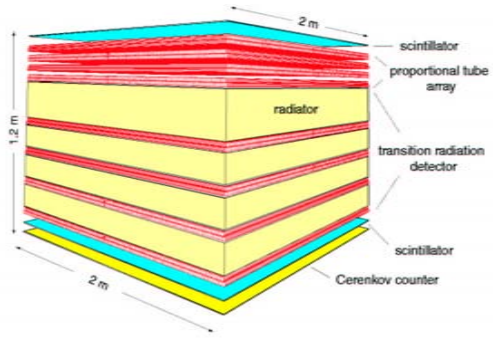

Fig. 1. TRACER schematic

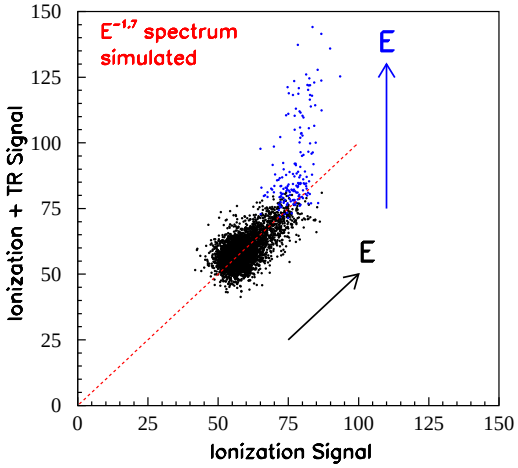

Fig. 2. Identification of TR events

tic scintillators on top and at the bottom of the detector stack, (b) an acrylic Čerenkov counter at the bottom, and (c) eight double layers of single-wire proportional tubes (a total of $\sim$ 1600 tubes, each 2 m long and 1 cm in radius) to measure the specific ionization of traversing cosmic rays, and for the lower four layers, to measure the superimposed transition radiation signals generated in plastic fiber radiators. The scintillators serve as coincidence triggers and measure the nuclear charge, Z. The Čerenkov counter rejects particles with energies below the minimum ionization level and also provides an energy measurement around 10 GeV/nucleon. The proportional tube arrays determine the particle energy from the relativistic increase in the specific ionization, and for Lorentz factors, $\gamma = E/mc^2 > 500$, from transition radiation signals. The tube signals also provide an accurate determination of the trajectory of each particle through the instrument.

1. Data Analysis and Results

After the particle trajectories are reconstructed and the scintillator and Čerenkov signals corrected for zenith angles and spatial non-uniformity in response, the nuclear charge, Z, is determined. The dynamic range available for the signal readout of the tubes limits the current measurement to the charge range from oxygen ($Z = 8$) to iron ($Z = 26$). The further data analysis is aided by extensive Monte Carlo calculations of all details of the detector response based on the GEANT 4 code. Wherever possible, the simulations are verified with data from flight or from accelerator calibrations. Some details are described by Gahbauer et al. (this conference). Figure 2 illustrates the simulated response of the pro-

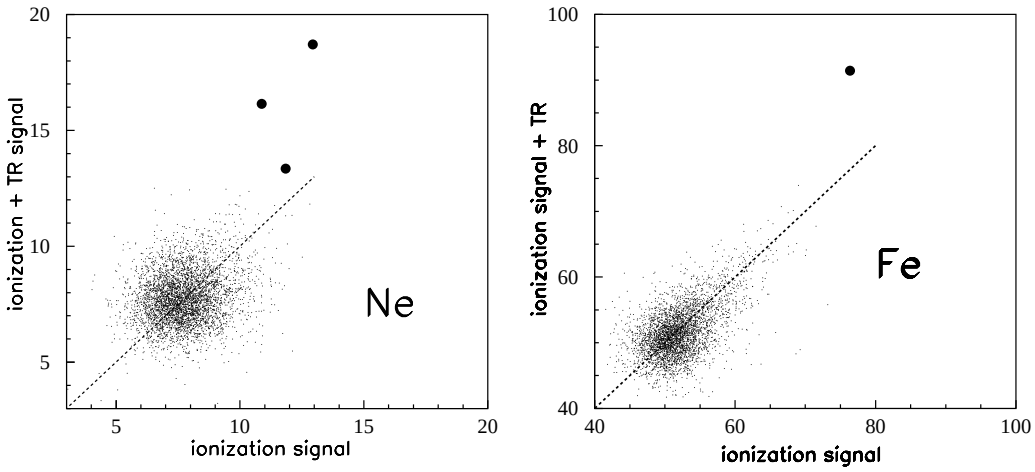

Fig. 3. Identification of highest energy events from the flight. Neon (left) and iron (right).

portional tube arrays for a power law energy spectrum of incident Fe-nuclei. The signals in the TRD-tubes (measuring specific ionization with TR superimposed) are plotted versus those in the upper tube layers that measure specific ionization only (*ionization signal*). The bulk of the particles are minimum ionizing, but the signal increases with energy for both tube arrays in the same proportion, until the onset of TR production leads to significantly larger signals in the TRD system only. This figure clearly illustrates not only the average trend of the signals with energy, but also the fluctuation levels.

Figure 3 shows measured cosmic-ray data for two primary nuclear species. The short duration of the test flight led to a small yield of nuclei at very high energies. Nevertheless, the lack of background in these satter-plots makes possible a clean identification of even a few high-energy particles.

Finally, we obtain absolute particle intensities at the top of the atmosphere after corrections for detector inefficiencies and for losses due to interactions in the atmosphere or in the detector material, and after deconvolving the non-linear energy response of the detector. These results are shown in Figure 4, in comparison to results previsouly reported from the CRN instrument on the Space Shuttle [1], and from measurements on the HEAO-3 satellite [2]. Within the statistical uncertainties, we notice good agreement between the three data sets, even though the instruments are significantly different. For the spectrum of iron nuclei, Figure 4 also includes a prediction of possible spectra for different galactic propagation models [3]. The available data cannot discriminate between these different possibilities, but improved statistics from long-duration flights should

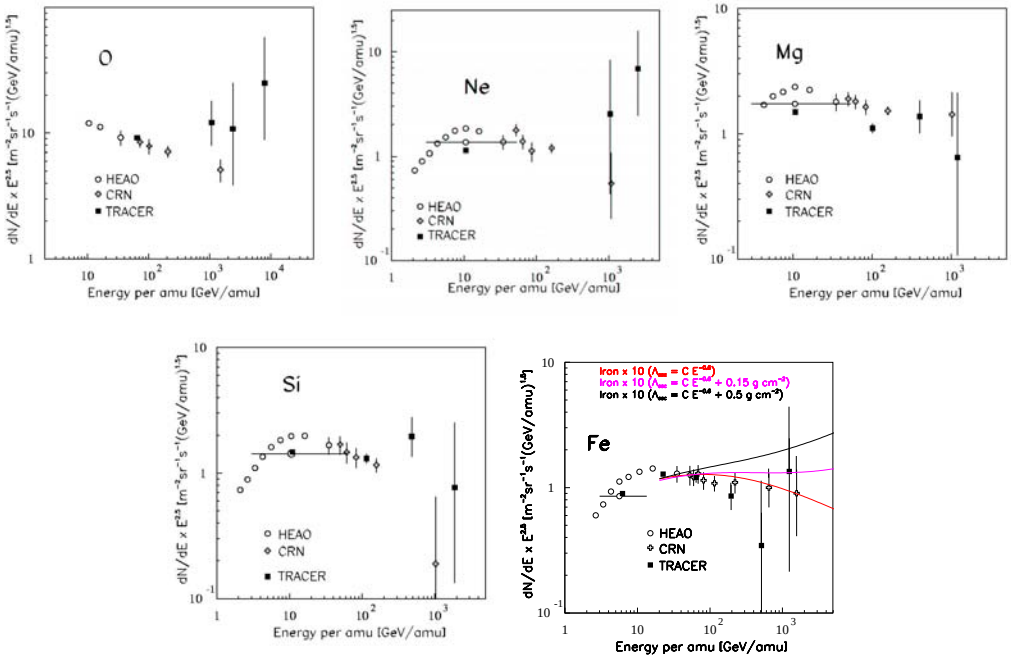

Fig. 4. Spectra for O, Ne, Mg, Si, Fe

lead to meaningful constraints on models such as those illustrated in Figure 4.

Conclusion

The TRACER instrument is different in many design details and response characteristics from previous detectors such as CRN. In particular, the use of proportional tube arrays represents a new approach that makes the use of a pressurized gondola unnecessary. The test flight of TRACER verifies the design, provides new cosmic-ray data in an important energy regime that agree with previous measurements, and gives confidence towards a significantly extended energy coverage in the upcoming long-duration flight.

1. Müller, D., Swordy, S. P., Meyer, P., L'Heureux, J., Grunsfeld, John M. 1991, ApJ 374, 356
2. Engelmann, J. J., Ferrando, P., Soutoul, A., Goret, P. Juliosson, E., Koch-Miramond, L., Lund, N., Masse, P., Peters, B, Petrou, N., Rasmussen, I.L. 1990, A&Ap 233, 96
3. Swordy, S. P., L'Heureux, J., Meyer, P., Müller, D. 1993, ApJ 403, 658

Time structure of the shower front as measured at Haverah Park above 10^{19} eV

M. Ave[1,2], J. Knapp[1], M. Marchesini[1], M. Roth[1,3] and A. A. Watson[1]
(1) Dept. of Physics and Astronomy, University of Leeds, Leeds, LS2 9JT, UK
(2) Center for Cosmological Physics, University of Chicago, Chicago, USA
(3) Inst. für Kernphysik, Forschungszentrum, D-76021 Karlsruhe, Germany

Abstract

The time structure of the air shower front observed with any particle detector is largely defined by the development of the shower in the atmosphere. Shower front structure can thus be correlated with the mass of the initiating primary particle. We have extended previous work on this topic, using the Haverah Park array, to explore these features in events of mean energy 2×10^{19} eV. We compare the measurements with Monte Carlo calculations made using the CORSIKA/QGSGET model. Data and simulations show clear azimuthal asymmetries in the time structure, which relate to the cosmic ray mass composition. The observed time structure can be best understood if iron primaries are dominant at these energies, but this conclusion is model dependent.

1. Introduction

Although the Haverah Park array was closed in 1987, the database has continued to be a rich source for new insights into the properties of high-energy cosmic rays [3,4]. In part, this is because of the availability of increased computational power and improved shower models. In [4] we showed how these resources could be used to infer the mass composition from 2×10^{17} to 3×10^{18} eV from accurate measurements of the lateral distribution of signals in large area water-Cherenkov detectors. An additional mass sensitive parameter that was measured at Haverah Park was the thickness of the shower front observed at the four central 34 m^2 detectors. With these detectors, the first evidence of shower-to-shower fluctuations was obtained [10] and later, using an improved recording system, detailed measurements on over 7000 showers led to an inference of the elongation rate above 3×10^{17} eV [9].

Here we describe an extension of the earlier work on the shower front, focusing on the highest energy events. The parameter measured was the 10-50% risetime ($t_{1/2}$), as before, but, to obtain a consistent data set, all the pulse shapes were remeasured for events $>10^{19}$ eV and zenith angle $<45°$, from a set of records made with a single recording system, as used in [10]. The integrated signals from

pp. 1–??

each 34 m^2 detector were recorded photographically from an oscilloscope. The signal at 1029 m from the core of a shower of 6×10^{19} eV is shown in figure 1A. A total of 266 pulses from 100 showers were measured. At 1000 m from the core of a 10^{19} eV event from near the vertical, a typical risetime is ~250 ns. The risetimes can be measured to ±4 ns: details of the procedure will be given elsewhere.

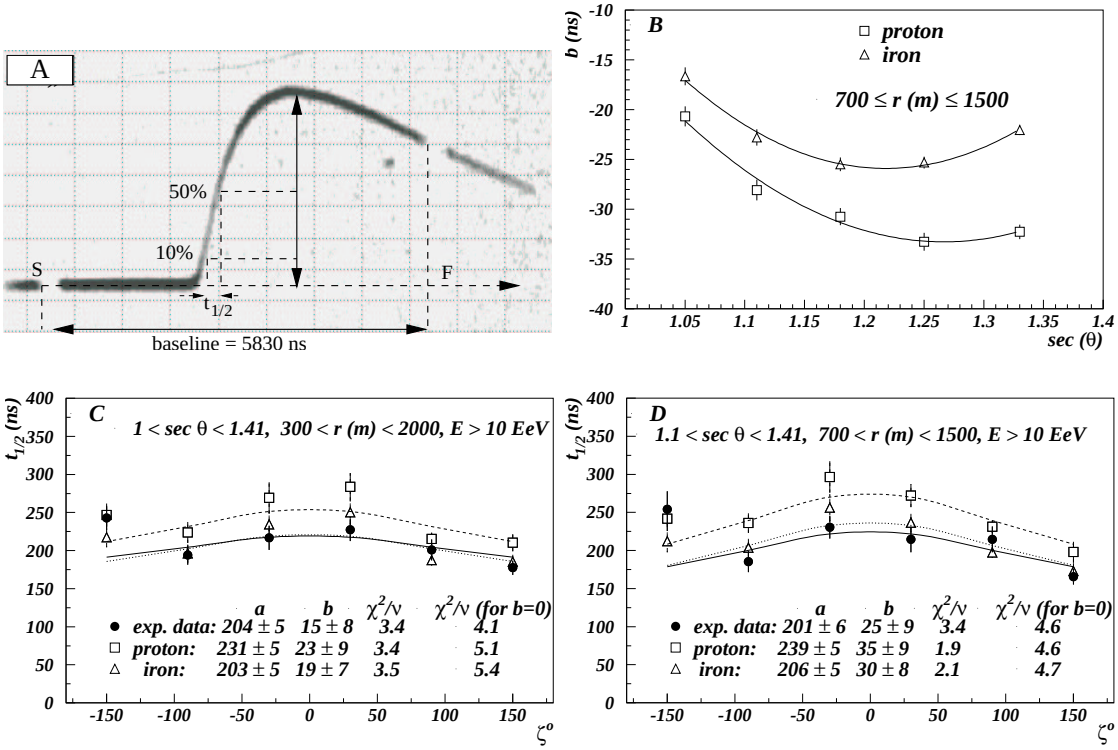

Fig. 1. A: pulse of a typical event recorded at the Haverah Park array: E = 6×10^{19} eV, $\rho \simeq 18$ m^{-2}, $\theta = 30°$ and $t_{1/2} = 260$ ns. The 10% and the 50% levels of the pulse are shown along with the start (S) and the finish (F) of pulse of a defined 5830 ns baseline.
B: variation of b as function of sec θ for core distance range 700 ≤ r ≤ 1500 m.
C: $t_{1/2}$ vs ζ for experimental data (266 pulses) and Monte Carlo.
D: same as C but with 700 ≤ r ≤ 1500 m and 1.1 ≤ sec θ ≤ 1.4 in both data (60 pulses) and Monte Carlo.

2. Results of the measurements

The measurements were parameterised as a function of core distance, r and zenith angle, θ. The shower-to-shower differences were explored using the analysis of variance, as in the original work [10]. This analysis showed that shower-to-shower differences are larger than can be accounted for by experimental uncertainties. The experimental uncertainties in the risetime measurements come

from the measurement uncertainty mentioned above, and from the sampling of the shower front by detectors of finite size. For a density of $\sim$2 m^{-2} in a near vertical shower at 1000 m, the sampling uncertainty, even on a 34 m^2 detector, is $\sim$28 ns, very much larger than the measurement error. The overall uncertainty is so large that, for the small sample of events available, it is only meaningful to work with average values.

3. Comparison of average values of risetimes with shower models

It has been known for many years that asymmetries can arise in the density distribution of air showers because of the magnetic field [1,2,3,5]. In addition, at Haverah Park, attenuation of the density signal as the shower crossed the array was observed in a small number of events with well-located cores [7]. More recently, within the Auger Collaboration, considerable attention has been given to asymmetries, both because of their importance in the reconstruction of the parameter from which the primary energy is derived and because the magnitude of the time asymmetry predicted for various descriptors of the shower front thickness is sensitive to the mass composition [6].

It is convenient to group the pulses for which there are measurements as a function of r, θ, E and ζ, the azimuthal angle in the shower plane, where $\zeta = 0^\circ$ is chosen to lie in the direction of the incoming shower. A detector lying at $\zeta = 180^\circ$ will record signals from a part of the shower that has travelled through more atmosphere than one at $\zeta = 0^\circ$. A suitable parameterisation of $t_{1/2}$ for real data and for Monte Carlo predictions, as a function of ζ is given by $t_{1/2} = a + b \cos \zeta$. The behaviour of the average $t_{1/2}$ for the 266 measurements is shown in figure 1C.

Since the data set is sparse and compiled from a range of r, θ, E and ζ, comparison of it with the Monte Carlo results, which are made for showers of specific energy, zenith angle and mass, is not straightforward. We have used the CORSIKA code with QGSJET01 [8] with proton and iron primaries for the simulations. Then we have parameterised the coefficients a and b, from the simulations, as a function of r, θ, E and ζ, so that the comparisons with the data sample can be done as exactly as possible. In figure 1B a typical variation of b with sec θ is shown and similar interpolations have been formed for a and b with the other variables. It is thus possible to make a prediction of $t_{1/2}$, for p and Fe primaries, using a simulated set of pulses that has identical r, θ, E and ζ to that of the events. Additionally, the choice of binning to maximise the possibility of observing an asymmetry in ζ can be guided by these interpolations. In figure 1C, the comparison of all data with the Monte Carlo results is displayed. In figure 1D, a comparison between data and simulations for a restricted range of angle and distance (60 pulses) is made.

The first point to note is that the predicted average properties of the shower

pulses are clearly different for p and Fe showers at the large distances used here. This is in contrast to the conclusion in [4] where for the relevant distance range, $250 < r < 500$ m the sensitivity of the risetime technique for the extraction of mass information was shown to be rather limited. However, as pointed out there, the technique is expected to have promise for mass separation when used at larger r, as demonstrated here. Secondly, it is clear from figures 1C and 1D that the data are better described using Fe primaries. However, before claiming this as a firm conclusion, it is necessary to explore the sensitivity of it to the choice of different shower models. As noted before, the data are too sparse to make use of fluctuations, as was possible for the lateral distribution work at lower energy [4].

We look forward to seeing this technique developed, with high statistics, using the data expected from the Pierre Auger Observatory.

Acknowledgements

MM is grateful to the University of Leeds for the William Wright Scholarship and MR is grateful to the Humboldt Foundation for support. Our work is supported by PPARC through PPA/G/S/1998/0453 and PPA/Y/S/1999/00276.

4. References

1. D. Andrews et al., Proc 12th ICRC (Hobart 1971) 3 995
2. E. E. Antonov et al., JETP Letters 68 (1998) 185
3. M. Ave et al., Physical Review Letters 85 (2000) 2244
4. M. Ave et al., Astroparticle Physics 19 (2003) 61
5. P. Chaloupka and V. Petrzilka, Czech. J. Phys. 4 (1954) 508, 5 (1954) 286
6. M. T. Dova, for the Pierre Auger Collaboration: this conference
7. C. D. England, PhD Thesis, University of Leeds (1984)
8. D. Heck et al. (1998) FZKA6019 (Forschungzentrum Karslruhe,Germany) and Proc. 27th ICRC (Hamburg 2001) 233
   N. N. Kalmykov et al. Phys. Atom. Nucl. 56 (1993) 346
   and Nucl. Phys. B (Proc.Suppl.) 52B (1997) 17
9. R. Walker and A. A. Watson, J. Phys. G., 7 (1981) 1297
10. A. A. Watson and J. G. Wilson, J. Phys. A. 7 (1974) 1199